PEGMATITIC GRANITES OF THE WINNIPEG RIVER AREA, SOUTHEASTERN MANITOBA

by

BRUCE ELLIOTT GOAD

Faculty of Graduate Studies
Department of Earth Sciences
University of Manitoba
Winnipeg, Manitoba

April 11, 1984

Submitted as partial fulfillment of

requirements for MSc.

PEGMATITIC GRANITES OF THE WINNIPEG RIVER AREA, SOUTHEASTERN MANITOBA

by

Bruce Elliot Goad

A thesis submitted to the Faculty of Graduate Studies of the University of Manitoba in partial fulfillment of the requirements of the degree of

MASTER OF SCIENCE

ACKNOWLEDGEMENTS

The writer wishes to thank his advisor, Dr. Petr Černý, for his continued interest, support, discussions, enthusiasm and patience during the seemingly endless production of this thesis. He always knew it was coming (but he didn't quite know when it would arrive).

Dr. F. Hawthorne nursed most of the garnet data out of the department's microprobe.

B.J. Paul and W.C. Hood provided interesting discussions and able assistance in the field.

Special thanks are extended to the readers of this thesis, Drs. A.C. Turnock and D.L. Trueman, and especially to my wife, Nancy, who, like Petr, knew the document was coming but didn't know when. Her expert editing and typing was greatly appreciated.

NOTICE/AVIS

PAGE(S) iii IS/ARE EST/SONT color photo

PLEASE WRITE TO THE AUTHOR FOR INFORMATION, OR CONSULT THE ARCHIVAL COPY HELD IN THE DEPARTMENT OF ARCHIVES AND SPECIAL COLLECTIONS, ELIZABETH DAFOE LIBRARY, UNIVERSITY OF MANITOBA, WINNIPEG, MANITOBA, CANADA, R3T 2N2.

VEUILLEZ ECRIRE A L'AUTEUR POUR LES RENSEIGNEMENTS OU VEUILLEZ CONSULTER L'EXEMPLAIRE DONT POSSEDE LE DEPARTEMENT DES ARCHIVES ET DES COLLECTIONS SPECIALES, BIBLIOTHEQUE ELIZABETH DAFOE, UNIVERSITE DU MANITOBA, WINNIPEG, MANITOBA, CANADA, R3T 2N2.

FRONTISPIECE

Greer Lake pegmatitic granite on the Winnipeg River

ABSTRACT

Late- to post-tectonic stocks and plugs of pegmatitic granites were intruded along partly dilated fault systems in the Archean Bird River greenstone belt of the English River subprovince in southeastern Manitoba. Each intrusion consists of four phases: (1) fine-grained leucogranite locally grading into (2) interlayered sodic aplite and (3) potassic pegmatite, and (4) pegmatitic leucogranite that also contains bands and lenses of potassic pegmatite. This last phase carries occasional Li-, Be-, Nb,Ta-, As-, P-, B-, F- and Zn-bearing minerals. Textural and compositional relationships suggest separation of supercritical fluids from volatile-oversaturated melt as the primary cause of internal diversity. Bulk compositions are silicic, poor in Ca, Fe and Mg and highly fractionated in terms of K/Rb, K/Cs, K/Ba, Ca/Sr, Rb/Sr, Th/U, Mg/Li and Al/Ga. The rocks are peraluminous, as indicated by 0.1 to 5.0% of normative corundum (CIPW) and by the presence of muscovite, garnet, tourmaline, gahnite and cordierite. From fine-grained leucogranites through sodic aplites and pegmatitic leucogranites to potassic pegmatites, the peraluminous character increases and Σ REE contents decrease. The genetic evidence available, including REE abundances and oxygen isotope ratios, is inconclusive: juvenile origin of parent

melts modified by subsequent fractionation and by reaction with greenstone belt metasediments is possible, as well as shallow anatexis of greenstone belt lithologies followed by igneous fractionation and reaction with host rocks. Loss of fluids to the country rocks probably contributed to the enhanced peraluminous character of pegmatitic fractions and to the depletion of their Σ REEs.

TABLE OF CONTENTS

FIGURES

TABLES

APPENDICES

Chapter 1

INTRODUCTION

A. GENERAL INTRODUCTION

The Winnipeg River area of southeast Manitoba contains abundant pegmatitic intrusions. An earlier study of the pegmatites in the Bird River greenstone belt indicates that they can be divided into distinctly separate groups depending on their location and mineralogy (Černý and Turnock, 1971). On a closer examination of their location it can be observed that most of the swarms of pegmatites are adjacent to small, very coarse-grained granitoid rocks containing local mineralized facies which resemble, both mineralogically and texturally, the closest adjacent pegmatite intrusions.

This close spatial association could possibly indicate a genetic linkage between the pegmatites and the adjacent coarse-grained granites otherwise known as pegmatitic granites. To this point, little work has been devoted to these bodies of pegmatitic granites; consequently, little more than their existence and a very brief description has been reported in the literature.

1. Statement of Problem

The purpose of this thesis is to study the mineralogy, geochemistry, petrology, and origin of the four main intrusions of pegmatitic granite in the Bird River greenstone belt in order:

a) to establish the general characteristics of these rocks;

b) to establish any petrological and/or geochemical similarities or differences among the individual intrusions mutually, and between the pegmatitic granites and associated pegmatites;

c) to characterize the petrologic evolution of each individual intrusion;

d) to detect possible links between the pegmatitic granites and the plutonic granitoids in the area and also between the pegmatitic granites and the adjacent pegmatite groups.

2. Location

The Winnipeg River pegmatite district is located approximately one hundred and eighty kilometres east-northeast of Winnipeg (Figure 1) and is contained within townships 16 and 17, Range 16 and 17 East in the southeastern part of Manitoba. The N.T.S. co-ordinates for this area are 50° 20' to 50° 28' latitude and 95° 24' to 95° 10' longitude.

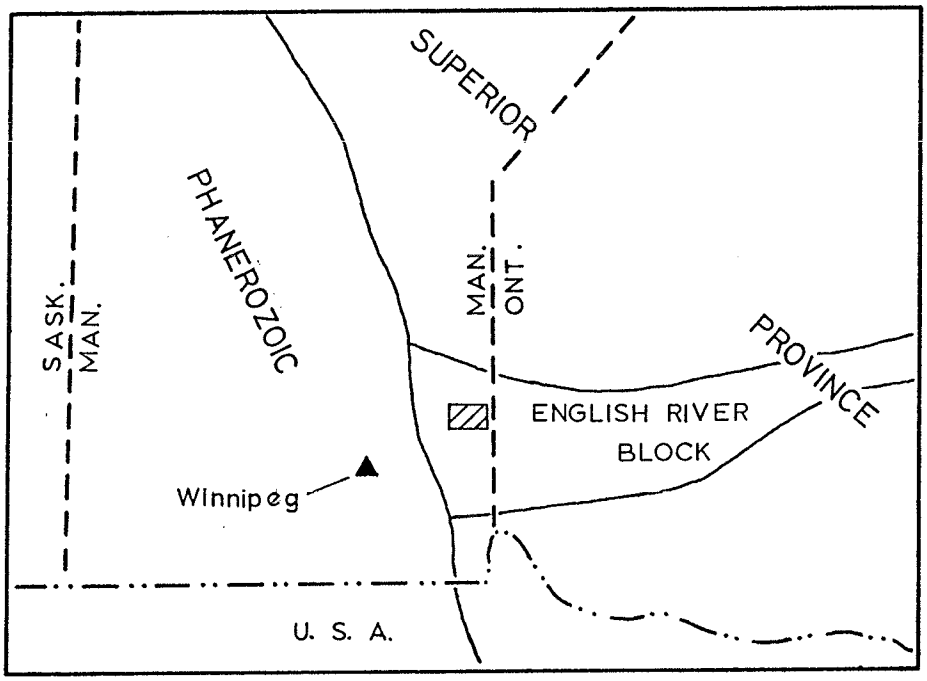

Figure 1. Location map of the Winnipeg River pegmatitic granites in southeastern Manitoba.

3. Access

Four main bodies of pegmatitic granite exist (Figure 2).

Two of the bodies are south of the Winnipeg River in the Whiteshell Provincial Park. One of these (GL) is due north of Greer Lake while the other (ENL) is northwest of Eaglenest Lake. Access to both of these bodies is from Pointe Du Bois via boat or aircraft. The remaining two bodies of pegmatitic granite are located north of the Winnipeg River in the Nopiming Provincial Park. The first of these (TNL) is adjacent to Tin Lake while the other (OL) spans the area between Osis, Booster, and Summerhill Lakes. Access to these northern bodies is south off Provincial Highway 315 at Bird Lake and onto a network of logging roads opened by Abitibi Pulp and Paper of Pine Falls, Manitoba.

A fifth intrusion of pegmatitic granite (AX) is located north of the Winnipeg River and southeast of Birse Lake. Access is gained by traversing 2.5 kilometres north from the Winnipeg River. This body of pegmatitic granite is small (200-300 metres in diameter), extremely homogeneous, and poorly exposed; consequently, it was not included in this study.

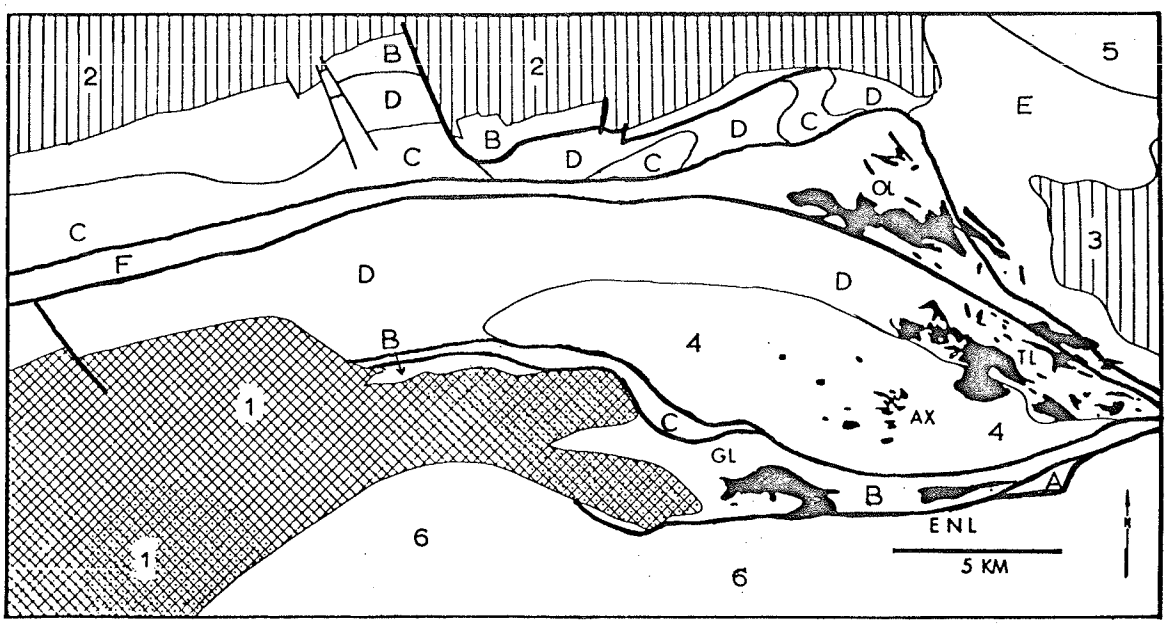

Figure 2. Location of the Winnipeg River pegmatitic granites (GL, ENL, OL, TL, AX) along the east-west fault systems in the Winnipeg River pegmatite district. Faults indicated by heavy lines. (1) Lac du Bonnet batholith, (2) Maskwa Lake intrusion, (3) Marijane Lake intrusion, (4) Birse Lake sub-volcanic tonalite, (5) Manigotagan-Ear Falls gneiss belt, (6) Winnipeg River batholithic belt. (A) Eaglenest Lake formation, (B) Lamprey Falls formation, (C) Peterson Creek formation, (E) Flanders Lake formation, (F) Booster Lake formation.

B. PREVIOUS WORK

Initial work pertaining to the geology of the Bird River area was reported by Tyrell (1900) and Moore (1913). They were studying the regional stratigraphy and correlated the units in the Bird River area to the rocks of the Rice Lake group at Bissett. Cooke (1922) and Wright (1926, 1932) brought attention to mineralization in the Bird River area, both Cu/Ni mineralization at Cat Lake and to the existence of several rare metal-bearing pegmatites. These initial reports created an interest in the area and subsequent prospecting led to the discovery of more pegmatites: the tin-bearing pegmatite of Shatford Lake in 1924 (Springer, 1949); the lithium pegmatite (Silverleaf) at Greer Lake in 1924 (Springer, 1950), Bernic Lake in 1929 (Davies, 1955), Rush Lake in 1928 and 1930; and lithium at the Buck Claim pegmatite on the east end of Bernic Lake in 1934 (Davies, 1955). Further discoveries were made in the Rush Lake area in 1940 (Davies, 1955).

The Superior Province of the Canadian Shield was first dated at 2,500 million years using uranite from the Huron Claim pegmatite (DeLury and Ellsworth, 1931 and Ellsworth, 1932). Subsequent dating using K_{40}/Ar_{40} and Sr/Rb of the adjacent Silverleaf pegmatite was in agreement with this date (Cummings et al., 1955 and Davies et al., 1962).

DeLury (1926, 1930) and Bateman (1943) documented

the beryl and tin pegmatites in Manitoba while detailed accounts of the lithium pegmatite localities were written by Derry (1931), Wright (1932), Stockwell (1933), and Rowe (1956). Portions of Ellsworth's (1932) and Mulligan's (1957, 1961, 1965, 1968, 1975) reports point out the lithium, cesium, and tin potential of the pegmatites in the Bird Lake-Winnipeg River area.

The second world war caused an increase in attention to the tin-bearing pegmatites in the area (Springer, 1949, 1950 and Davies, 1952, 1955, 1956a, 1957). Mapping of the area by Davies coincided with an increase in interest in the lithium potential of southeast Manitoba.

Although the existence of chromium in the Bird River sill was known since 1942, and Cu/Ni has been produced from the Dumbarton Mine at Bird Lake until 1979, the only mine presently (1980) operating is on the Tantalum Mining Corporation of Canada's Ta-(Sn, Li, Cs, Be, and Nb) bearing pegmatite (TANCO) at Bernic Lake.

Davies (1954, 1956a, 1956b, 1957, 1958), Davies et al. (1962), and more recently McRitchie (1971), Janes (in prep.), and Trueman (1980) reported on more regional mapping of the Bird River greenstone belt. Eckelmann et al. (1958) looked specifically at the Greer Lake pegmatitic granite; however, their work was published only as a brief abstract.

Mulligan (1957) notes that the Li-bearing Silverleaf

pegmatite south of the Winnipeg River is adjacent to a large body of pegmatitic granite; however, any genetic interpretation can only be inferred by the reader. Springer (1949) and Davies (1956b) also mention the existence of pegmatitic granite in their reports; however, no genetic connection is discussed between the pegmatitic granite and the pegmatites.

More recently, classification of the pegmatites in the Bird Lake-Winnipeg River area was attempted by Černý and Turnock (1971) and the possibility of genetic relationships between the pegmatites and other late potassic intrusions, including the pegmatitic granites, was suggested by Černý and Trueman (1977, 1978).

C. PRESENT STUDY

This thesis represents a portion of the Pegmatite Mineral Evaluation Project contracted to the Centre for Precambrian Studies, Department of Earth Sciences, University of Manitoba by the Manitoba Department of Mines, Resources, and Environmental Management under the Canada-Manitoba Subsidiary Agreement on Exploration and Development in Manitoba supervised by the Canada Department of Regional Economic Expansion.

Publication of results of this project is in progress (Černý et al., 1981; Goad and Černý, 1981; and Longstaffe et al., 1981). Information about the pegmatitic granites generated by this thesis has been used in this

project report and conversely data on the other plutonic rocks of the Bird River greenstone belt have been quoted in this thesis for the purpose of comparison with the pegmatitic granite data.

Field work pertaining to this study was conducted during the summer of 1976. Initially three of the four intrusions of pegmatitic granite (GL, ENL, and TNL) were systematically sampled. The fourth was added to the study late in the fall of 1976; consequently, sampling of this body (OL) could not be carried out until the spring of 1977. The sampling was done along a grid that was spread over the areas of pegmatitic granite, with a grid interval of approximately 300 metres. Specimens for whole rock analysis plus samples of individual minerals were collected. Out of the numerous specimens collected the following samples were analyzed: 54 whole rock, 121 blocky K-feldspar, 28 graphic K-feldspar, 64 muscovite, 110 garnet, 21 beryl, 24 Nb,Ta oxide minerals, 4 spodumene, 2 cassiterite, 1 ilmenite, and 1 monazite. This tally includes several samples from the Silverleaf pegmatite which is adjacent to the GL intrusion of pegmatitic granite. It was drilled in the fall of 1977 by the Tantalum Mining Corporation of Canada Limited (TANCO) and the core was made available for use in this study.

Chapter II

EXPERIMENTAL METHODS

A. SEPARATION

The collection of data for this thesis involved the separation and cleaning of large amounts of material.

Three to four kilogram samples of clean representative specimens, free of alterations and fractures, were prepared for whole rock analysis. These samples were reduced to fragment size (approximately 5.0 cm^3) using a heat-tempered hammer. At this size they could be accommodated by a laboratory-size jaw crusher and further reduced to an approximately one cubic centimetre size. The material was then routed to a Bleuler ring shatterbox, and pulverized.

The mineral samples were also selected for their purity, lack of alteration, and representativeness. Because of their coarse-grained size, many minerals could be collected in the field (K-feldspar, plagioclase, beryl, Nb,Ta oxide minerals). This minimized separation procedures in the laboratory to hand separation and cleaning of crushed material under a binocular microscope.

Separation of large amounts (1.5 g) of garnet from rock samples was performed by crushing rock fragments in a ring shatterbox for a period of five seconds. This process shattered the rock to individual mineral grains of one to

two millimetres in size, without crushing them, thus liberating the garnet. The material was then sieved to remove the fine and coarse crystal fractions on either side of the average garnet grain size. The fraction containing the garnet was then put through an elutriation tube (Frost, 1959) using water as a separation medium. The material separated by the elutriation tube was processed through a heavy liquid (bromoform-$CHBr_3$) before a final manual separation under a binocular microscope was carried out.

All minerals were observed under a binocular microscope before crushing to ensure a perfectly clean separate, free of inclusion, veins, and minerals, or alterations along fractures. The final cleaned samples were then pulverized in a mechanical agate mortar and pestle, except the muscovite specimens that were to have their structure determined. These samples were set aside for manual filing since vigorous grinding would affect the polytype of the muscovite crystal structure (Yoder and Eugster, 1955).

B. CHEMISTRY

1. Major, Minor, and Trace Elements

Standard whole rocks and minerals were analyzed in the chemical laboratory of the Department of Earth Sciences, University of Manitoba. Techniques utilized include the following:

X-ray fluorescence spectrometry (Si, Al, Ti, total Fe, K, Ca)

atomic absorption spectrometry (flame-Li, Na, K, Rb, Cs, Ca, Mg, Be, Sr, Pb) (flameless-low Cs, Pb)

combustion (H_2O)

combustion plus acid digestion (CO_2)

titration (FeO)

spectrophotometry (P)

The standards used in analyzing the major and trace elements in the rocks and minerals of the pegmatitic granites are listed in Table 1. The methods, precision, and accuracy for specified concentrations of the relevant oxides and elements in silicate whole rock analyses are listed in Table 2 as quoted by Černý et al. (1981).

In addition to the above elements, Bondar, Clegg, and Company Limited in Ottawa analyzed the following trace elements: Ba, Ga, Sn, Th, U, Y, and Zr using X-ray fluorescence spectrophotometry. Table 2 lists the accuracy of replicate analyses claimed for samples with less than 100 ppm of the above elements.

2. Rare Earth Elements

Neutron activation analyses of rare earth elements (La, Ce, Nd, Sm, Eu, Tb, Dy, Yb, and Lu) were performed by Dr. R.V.G. Hancock at the Department of Chemical Engineering and Applied Chemistry, SLOWPOKE Reactor Facility, University of Toronto. Details of the analytical technique are given

Table 1. Standards used for whole rock and mineral analyses

Whole Rocks		
SiO_2		
TiO_2	X	USGS AGV, GSP
Al_2O_3	R	NBS 70A, 99, 99A
Fe	F	CCRMP SY2, SY3
CaO		ANRT GA, GH, GR
K_2O		
Na_2O		
K_2O	A	USGS GSP-1, BCR
MgO	A	CCRMP B1, B2, SY2, SY3
MnO	S	ANRT GA, GH, GR
CaO		
FeO		
P_2O_5		
CO_2		
Rb		USGS BCR, GSP CCRMP B1, SY2, SY3 ANRT GA, GH, GR
Sr		USGS BCR CCRMP B1, SY2, SY3 ANRT GA, GH, GR
Li		CCRMP B1, SY2, SY3 ANRT GA, GH, GR

Whole Rocks	
Be	CCRMP SY1, SY2, SY3 ANRT GA, GH, GR
Pb	NBS 70a, 99a CCRMP SY2, SY3 ANRT GA, GH
Cs	USGS BCR CCRMP SY3 ANRT GR
K-feldspar	NBS 70a
Beryl	USGS BCR, AGV NBS 27e, 70a, 181, 183 CCRMP B1, B2, SY2 SY3
Micas	USGS AGV, GSP-1, BCR NBS 27e, 70a, 181, 183 CCRMP B2, SY1, SY2, SY3 ANRT GA

Table 2. Methods, precision and accuracy of chemical analyses of silicate rocks

Oxide/ Element	Method(s) Primary	Alternate	Concentration	Instrument precision, σ	Accuracy of Replicates, σ
SiO_2	XRF		59.60 wt.%	0.12	0.20
Al_2O_3	XRF		9.34	0.05	0.13
Fe_2O_3*	XRF	AAS	10.08	0.017	0.03
MgO	AAS		4.04	0.04	0.10
CaO	XRF	AAS	10.22	0.02	0.07
K_2O	XRF	AAS	2.69	0.01	0.01
MnO	XRF	AAS	0.41	0.01	0.01
TiO_2	XRF		0.48	0.02	0.02
Na_2O	AAS		4.20	0.01	0.05
H_2O*	combustion		1.60	0.03	0.06
CO_2	combustion; acid digestion		1.15	0.05	0.12
P_2O_5	spectrophotometry		0.20	0.01	0.01
FeO	titration		10.92		0.04
Zr	XRF		0.027	0.003	0.005
Cs	AAS		820 ppm	5.0	13.0
Cs	AAS flameless		0.95	0.02	0.04
Li	AAS		10.0	0.04	0.05
Pb	AAS flame		34.0	2.0	3.0
Pb	AAS flameless		8.0	0.2	0.1
Rb	AAS		228.0	1.0	2.0
Sr	AAS		260.0	5.0	6.0
Ba	XRF		100.0		10.0
Y	XRF		100.0		1.0
Zr	XRF		100.0		2.0
Sn	XRF		100.0		1.0
U	XRF		100.0		1.0
Th	XRF		100.0		1.5
Ga	XRF		100.0		2.0

* = Total

σ = one standard deviation

in Hancock (1976). The REE data obtained have been normalized to the Leedey chondrite (Masuda et al., 1973; Masuda, 1975; Chou et al., 1977). Table 3 summarizes the accuracy data for the REE determinations in this study.

Concentrations of some low abundance REE's occurred below the quantitative detection limits in several samples; consequently, when plotting the normalized values, the maximum possible content was used. These occurrences are indicated on graphs by a downward pointing arrow to illustrate the uncertainty.

3. Oxygen Isotopes

Dr. F.J. Longstaffe provided the analyses of the oxygen isotope ratios of the pegmatitic granites. The ratios were determined in Dr. K. Muehlenbachs' laboratory at the Department of Geology, University of Alberta, Edmonton as a part of a larger study (Černý et al., 1981). Details of the analytical procedures are given in Clayton and Mayeda (1963).

C. NORM CALCULATIONS

Whole rock compositions of the pegmatitic granites were normalized by two methods. The classic CIPW norm calculation, which does not take into account the biotite content of the rocks, was used to obtain corundum values comparable to those quoted in the literature (cf. Chappell

Table 3. Accuracy of replicate INNA determinations of rare earth elements

Element	Concentration ppm	Accuracy, σ
La	9.8	0.7
	45	1
	82	2
Ce	20	2
	80	4
	140	10
Nd	7	2
	20	3
	60	6
Sm	1.6	0.2
	6.4	0.2
	12.0	0.6
Eu	0.30	0.04
	1.3	0.05
	2.5	0.4
Tb	0.10	0.03
	0.15	0.04
	0.50	0.08
Dy	0.57	0.08
	4.4	0.3
Yb	1.0	0.2
	3.0	0.3
	7.5	0.6
Lu	0.14	0.02
	0.42	0.04
	0.8	0.1
Hf	1	0.1
	6.5	0.5
	9	0.6

and White, 1974). Barth (1959, 1962) suggested that if the amount of K_2O in the biotite structure is neglected, as it is in CIPW norms, the computed composition of the feldspar will differ from that of the actual feldspar composition. Consequently, Barth's mesonorm, as modified by Rogers and le Couter (MESO I program), was used to calculate the original content of the granitic melt. This calculated composition is illustrated by ternary feldspar (Ab-Or-An) and alkali granite (Ab-Or-Qtz) diagrams. Another adjustment in the case of these pegmatitic granites, which are essentially biotite-free but do carry abundant garnet and muscovite, was the calculation of garnet, with a sliding Fe/Mn ratio instead of biotite. Any Al_2O_3 remaining above the feldspar alkali/alumina ratio was assigned to muscovite.

D. ELECTRON MICROPROBE ANALYSES

The MAC-5 electron microscope at the Department of Earth Science, University of Manitoba was used to analyze the garnet, the complex Nb,Ta oxide minerals, and an ilmenite crystal. It operated in the wavelength dispersive method using an acceleration voltage of 20 kV and a sample current of 0.04 μA amps. Standards against which the samples were analyzed are listed in Table 4. Once obtained, the raw data were reduced using the EMPADR VII program of Rucklidge and Gasparrini (1969).

Table 4. Standards used for electron microprobe analyses

Nb,Ta oxide minerals		Garnets	
Nb	Manganotantalite, stibiotantalite, $Ba_2NaNb_5O_{15}$	Mn	spessartine
		Fe	chromite, olivine
Ta	manganotantalite, stibiotantalite	Al	spessartine
Mn	manganotantalite	Si	spessartine
Fe	chromite, olivine	Ca	pyrope
Zr	zircon	Mg	chromite, olivine
Hf	zircon, baddeleyite	Ti	titanite
Sn	cassiterite	Sc	metallic Sc
Ti	titanite, benitoite	Zr	zircon
Ca	titanite, $CaWO_4$	Y	YAG
Al	titanite, chromite		
Y	REE glass, YAG	REE glasses from Dr. D.F. Weill,	
Ce	CeO_2, REE glass	University of Oregon (Drake &	
La	LaB_6, REE glass	Weill, 1972). Metallic U from the	
Sc	metallic Sc	Whiteshell Nuclear Research	
Sb	stibiotantalite	Establishment, AECL, Pinawa. All	
Th	ThO_2	other standards from Charles M.	
U	metallic U	Taylor Co., Stanford.	
Mg	chromite		
Na	albite		

E. X-RAY DIFFRACTION

Standard X-ray powder diffraction techniques were carried out for mineral identification and study. A Philips-Norelco powder X-ray diffractometer was used in conjunction with Philips X-ray powder cameras, a Philips Gandolfi camera, and a fast-scan goniometer chart recording unit. Cu ($K\alpha_1$) radiation was used in all studies and transmitted through a nickel filter. An internal standard of quartz (Frondel, 1962) or annealed fluorite (at 800°C: a = 5.462 Å) was used in studies where an accurate absolute value of 2θ was required. Depending on the mineral species and the data required, different methods and conditions of X-ray analyses were used (Table 5).

1. Potassium Feldspar

K-feldspar samples were divided into two types: blocky K-feldspar and graphic K-feldspar. Only the blocky K-feldspar was studied since this group contained the largest number of samples. Two studies were carried out: the obliquity of the microcline crystals, based on Goldsmith and Laves' method in Orville (1967), and the amount of solid solution of (Ab + An) residual in the K-feldspar phase of microcline-perthite (Orville, 1967). Further details and instrument conditions for these methods are listed in Table 5.

Table 5. Settings and experimental conditions of studied materials

Mineral Species	Amount Separated (σ)	Property Studied	Equipment Used	Radiation/ Filter	c.p.s./Time Const./Zero Suppress.	Scan Speed	Chart Speed

Table 5 Continued..

Mineral Species	Angle of Scan	Internal Standard	Additional Information	Reference

2. Muscovite

Samples of muscovite were filed to produce a powder for X-raying in a 114.6 mm Debye-Scherrer/Straumanis camera. The powder was mounted on a glass spindle in the camera and a photograph was recorded. The photograph was compared to polytype photographs published in Rinaldi et al. (1972) in order to assess the polytype. The films were exposed to Cu/Ni radiation for 2.5 to 3 hours (Table 5).

3. Garnet

Garnet that was analyzed by the classical "wet" chemical methods was also studied to determine unit cell size (a_o) by the X-ray methods described in Nuffield (1966). Quartz was used as an internal standard with the 2θ values published in Frondel (1962). Instrument settings are outlined in Table 5.

4. Nb,Ta Oxide Minerals

In their natural state these minerals were X-rayed to identify the phases present. After heating (at 1000°C ± 50°C for 3 hours in air) they were again X-rayed to observe any phase change. In both cases the diffraction patterns were calibrated with annealed CaF_2 in order to calculate the unit cell dimensions. Instrumentation conditions are listed in Table 5.

5. Amblygonite-Montebrasite

This species was X-rayed following the conditions listed in Table 5 to obtain an indirect measure of the fluorine content using the method of Černá et al. (1973).

6. Gahnite

When sufficient material was available, gahnite was mounted on a glass smear mount and X-rayed under the conditions listed in Table 5. CaF_2 was used as an internal standard. The data produced were used to obtain unit cell dimensions.

7. Ilmenite

An X-ray powder diffraction pattern of ilmenite using CaF_2 as an internal standard was obtained following the conditions listed in Table 5. The resulting data were used to obtain unit cell dimensions.

8. General Identification

The remaining minerals in this study were X-rayed solely for the purpose of positive identification (including sphalerite, molybdenite, arsenopyrite, triphylite-lithiophilite, mangano-sicklerite, apatite, and spodumene). Instrument conditions are listed in Table 5. A Gandolfi photograph was obtained for identification purposes if available material was insufficient for a powder smear mount,

and for minute crystals separated from a thin section.

F. UNIT CELL REFINEMENT

To refine the X-ray data produced for the Nb,Ta oxide minerals, gahnite and ilmenite, the self-indexing computer program of Evans, Appleman, and Handwerker (1963), as modified by Appleman and Evans (1973), was used. It is a least squares refinement of the unit cell dimensions with a weighting factor applied to each reflection depending on its clarity and the degree to which it can be reproduced. Errors quoted in Table 15 are standard errors about the mean. An attempt to keep them less than 0.06 percent has been moderately successful.

G. REFRACTIVE INDICES

Refractive indices were determined using the Becke line method, a sodium light source (filter with wavelength 590.5 nm), a Zeiss transmitting microscope, and a series of prepared immersion liquids in 0.001 increments, which bracket the refractive index to be determined. The fourth decimal point on the refractive index was estimated from the colour, intensity, and motion of the Becke line. After a R.I. of an immersion liquid matched the unknown refractive index of the mineral, the R.I. of the liquid was determined using a Zeiss Refractometer.

The refractive index γ was measured on crushed

plagioclase grains showing equally spaced and equal sized twins and low birefringence (010 cleavage platelets). The n_{ω} refractive index of beryl was obtained from thin crystal fragments showing the least birefringence. The γ' refractive index was also measured on the specimen of amblygonite-montebrasite from the Silverleaf Claim. As discussed in Černá et al. (1973), the true refractive index γ could be distinctly higher since the optical direction, Z, deviates for most compositions of the amblygonite-montebrasite series from the (010) cleavage.

H. DENSITY

Density determinations were obtained using a Berman Torsion Balance and toluene as a displacement liquid. To obtain an accurate reading, two readings per grain were recorded and averaged. In addition to this, the density of four grains per sample was measured and averaged to reduce the influence of possible zonation within a single crystal.

I. THIN SECTION

Two hundred thin sections of all facies in all four intrusions of the pegmatitic granite were studied with particular emphasis on

a) any metasomatic textures;

b) accessory minerals;

c) any variation in accessory mineralogy of one specific facies among all four bodies of pegmatitic granite.

Chapter III

GEOLOGY

A. REGIONAL GEOLOGY

1. Geologic Setting

The Winnipeg River pegmatitic granites are located in the Bird River greenstone belt, a part of the western extension of the English River gneissic belt in the Superior Province of the Canadian Shield. Radiometric dating by Farquharson and Clark (1971), Penner and Clark (1971), and Farquharson (1975) places the age of the greenstone belt into the Kenoran Orogeny (2.7-2.5 b.y.).

This greenstone belt is bound to the north by the Manigotagan-Ear Falls gneissic belt and to the south by the Winnipeg River batholithic belt (Beakhouse, 1977). Major igneous intrusions flanking the central area of interest are the Maskwa Lake batholith to the north, the Marijane Lake batholith to the east, and the Lac du Bonnet batholith to the southwest. The former two batholiths are collectively known as the Great Falls quartz diorite (McRitchie, 1971), and all three consist of older tonalitic and younger granitic components.

The Lac du Bonnet batholith is a postkinematic granite showing little deformation after emplacement. Minor deformation of the host rocks occurred during emplacement.

It is restricted to a reorientation of the layering and foliation, and an imprinting of a hornfels texture on the Bird River greenstone rocks on the northern and eastern margins of the batholith. This granitic intrusion is bound on the south by the Winnipeg River batholithic belt. The northern contact is intrusive, sharp with the mafic volcanic rocks of the Bird River greenstone belt, and locally diffuse showing "lit par lit" texture and stoping in the clastic rocks of the same belt. Chronologically, the Lac du Bonnet granite and the pegmatitic granites are presumed to be roughly contemporaneous, intruding along regional fault systems and resulting dilation zones. This event was followed only by the intrusion of the pegmatites, which makes them the youngest rock type in the Bird River greenstone belt.

2. Stratigraphy

The rocks of the Bird River greenstone belt belong to the Rice Lake group and have been subdivided into six formations (Trueman, 1980). Chronologically, from oldest to youngest, they are: the Eaglenest Lake formation, the Lamprey Falls formation, the Peterson Creek formation, the Bernic Lake formation, the Flanders Lake formation, and the Booster Lake formation (Figure 3).

a) Eaglenest Lake Formation. This is the oldest of the rock units observable in the Bird River greenstone

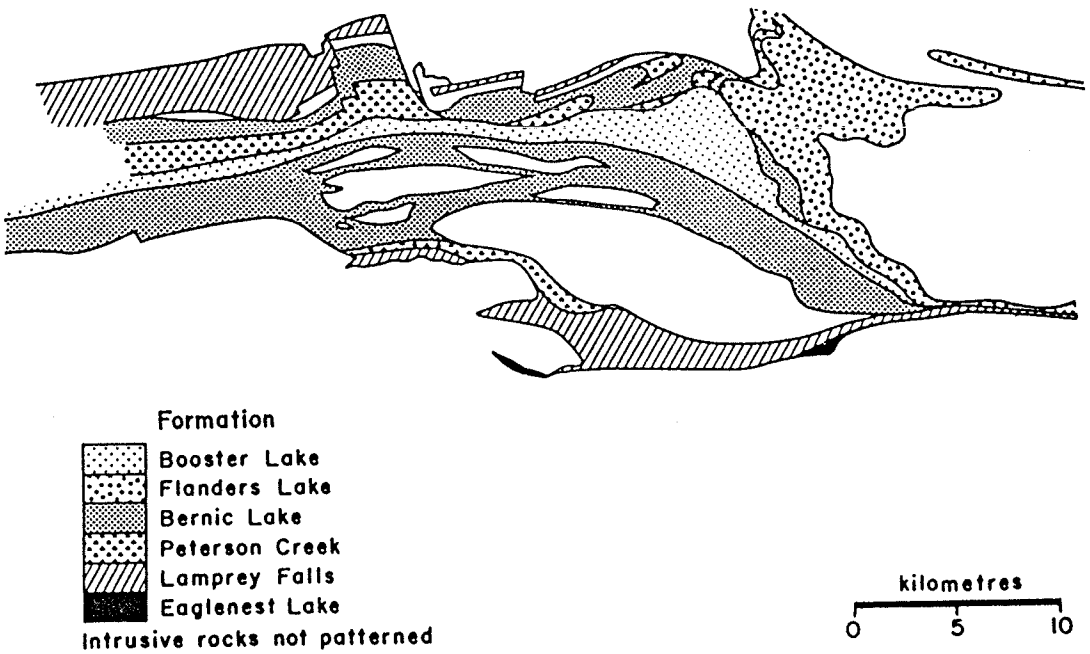

Figure 3. Stratigraphic subdivision of the metavolcanic and metasedimentary rocks of the Bird River area (Trueman, 1980).

belt. It consists mainly of fine to coarse clastic metasedimentary rocks derived from pre-existing volcanic units. The rocks of the formation have been metamorphosed to greenstone facies during several periods of deformation. The formation is probably fault-bound on the south to the Winnipeg River batholithic belt and on the north to the younger Lamprey Falls formation.

b) Lamprey Falls Formation. It consists mainly of pillowed metabasalts and their hypabyssal intrusive equivalents including the chromite-bearing Bird River sill. Extensive iron formation also occurs throughout. The rocks of this formation are in the amphibole hornfels and greenschist metamorphic facies. Contacts of the unit in the southern part of the greenstone belt are fault-bound. To the south, the Lamprey Falls formation is in contact with the Eaglenest Lake formation and the Winnipeg River batholithic belt; to the north, it is in fault contact with the quartz diorite located between Bird Lake and the Winnipeg River, centred at Birse Lake. The northern exposure of the unit is the only unit in contact with the Maskwa Lake batholith.

c) Peterson Creek Formation. It is composed of metarhyolites and their volcaniclastic and epiclastic derivatives (tuff, lapillistones, etc.). This forma-

tion shows an increased metamorphic grade of greenschist to amphibolite facies. The rocks have suffered several deformational periods and have infolded with the younger Bernic Lake formation with which they are in unconformable stratigraphic contact.

d) Bernic Lake Formation. As mentioned above, it lies unconformably above the older units and forms the core of the synclinorium formed by the greenstone belt. These units are infolded with the rocks of the Peterson Creek formation. Rock types within this formation include metamorphosed basalt, andesite, dacite, rhyolite, iron formation, and derived sedimentary rocks such as conglomerates, volcanic wackes, and volcanic sandstones. The iron formation interlayered throughout the Bernic Lake formation is the Algoman type with both oxide (magnetite) and sulfide (pyrrhotite) facies present.

e) Flanders Lake Formation. This unit also forms an unconformable contact with the older Bernic Lake formation and the younger Booster Lake formation. Rocks of the Flanders Lake formation include the metamorphic equivalents of conglomerate interbedded with lithic and pebbly arenites. This formation has also undergone several deformational periods and the units are infolded with both the Bernic Lake

formation and the Peterson Lake formation.

Metamorphism of the Flanders Lake formation has reached amphibolite facies. This is the highest metamorphic grade attained by any rocks in the Bird River greenstone belt.

f) Booster Lake Formation. It is the final and youngest formation of the greenstone belt. The rocks are mainly greywackes and mudstones (illustrating classical Bouma series turbidite sedimentation) with interlayered iron formations. Only one folding event is evident in the rocks and they have been metamorphosed to lower amphibolite facies.

All rocks of the above six formations can be grouped into five structural units (Trueman, 1980) as shown in Figure 4. Major east-west trending faults divide the structure and lithology within the greenstone belt, thus allowing its subdivision into five subareas. Subarea 1 corresponds to the Eaglenest Lake formation. The Lamprey Falls formation is equivalent to Subarea 2 which hosts the two southern intrusions of pegmatitic granite (ENL and GL). Subarea 3 is more complex, consisting of portions of three formations - Peterson Creek, Bernic Lake and Flanders Lake. Subarea 4, which also hosts an intrusion of pegmatitic granite (TNL), contains rocks of the Bernic Lake formation. The final subarea, Subarea 5, hosts the most northern intrusion of the four pegmatitic granites in this study (OL) and

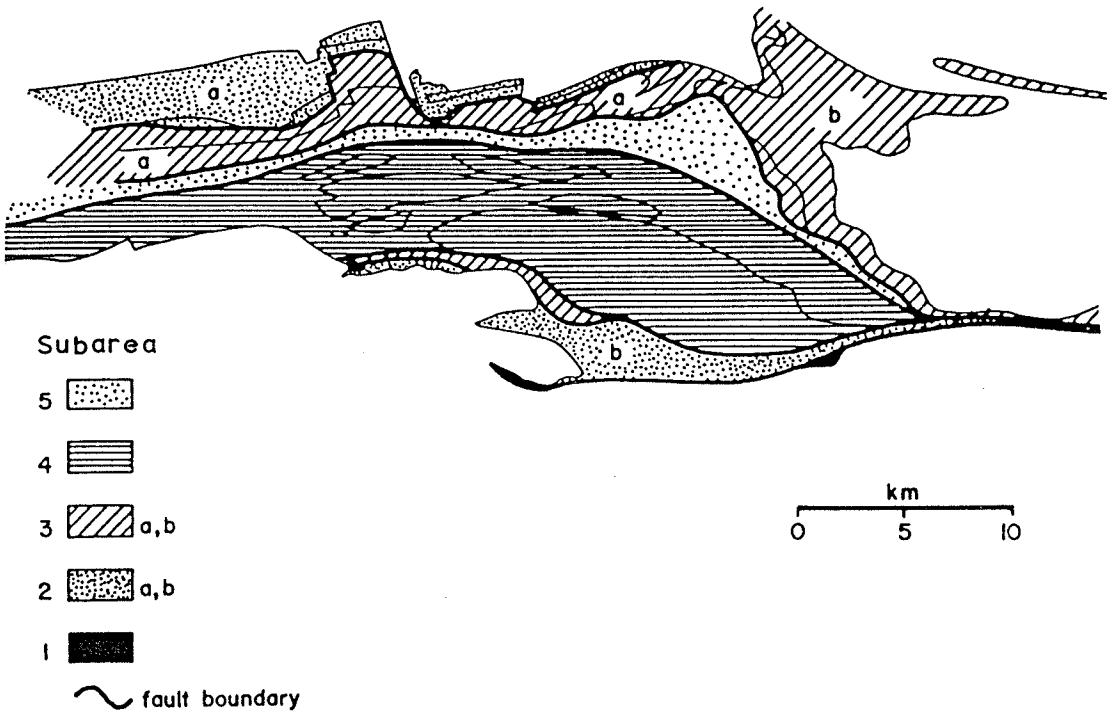

Figure 4. Subdivision of the Bird River greenstone belt into structural subareas (Trueman, 1980).

is composed of rocks of the Booster Lake formation.

The metamorphic history of the greenstone belt has been described by Trueman (1980), and a summary, based on the metamorphic minerals and the facies classification of Winkler (1967), follows below. The relative position of each facies to the subareas is shown in Figure 5.

A1.1 Quartz-albite-muscovite-biotite-chlorite subfacies. This subfacies of the Bird River greenstone belt rocks includes parts of the Lamprey Falls, the Peterson Creek and Bernic Lake formations plus the Bird River sill. For the rocks located north of the Bird River, the A1.1 subfacies is bound on the east by the fault designated NW in Figure 5.

A1.2 Quartz-andalusite-plagioclase-chlorite subfacies. This subfacies of rocks is confined to the fault-bound segment of the Bernic Lake formation which forms structural Subarea 4 (Figure 4) and the Eaglenest Lake formation (Figure 3). Rocks of the A1.2 subfacies carry both actinolite-tremolite and hornblende, the co-existence of which is indicative of the particular subfacies (Winkler, 1967).

A2.1 Andalusite-cordierite-muscovite subfacies. The A2.1 subfacies encompasses parts of the Booster Lake, Flanders Lake, Bernic Lake, Peterson Creek, and Lamprey Falls formations, the Bird River sill, and as far to the east as the sillimanite-andalusite

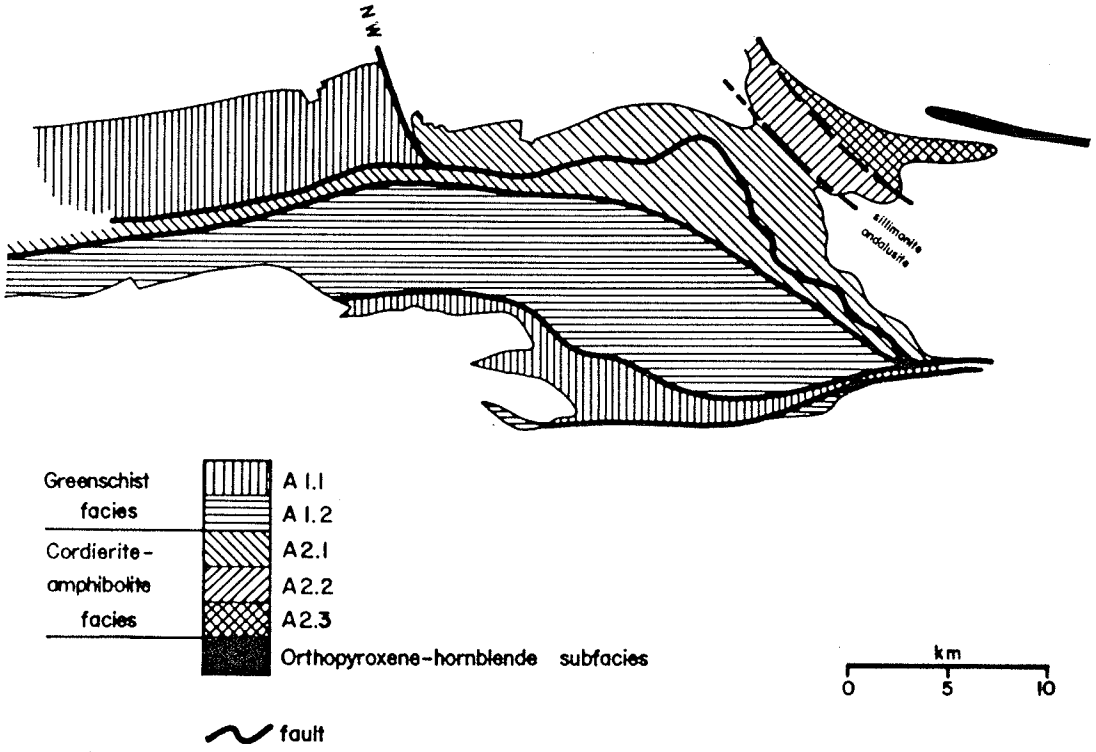

Figure 5. Subdivision of the Bird River greenstone belt into metamorphic subareas (Trueman, 1980).

boundary (Figure 5).

A2.2 Sillimanite-cordierite-muscovite-almandine subfacies. This subfacies is bound to the southwest by the sillimanite isograd and to the north by the A2.3 subfacies rocks. Rocks of this group include those in the Flanders Lake formation, the Peterson Creek formation, and the mafic to intermediate rocks of the Bernic Lake formation.

A2.3 Sillimanite-cordierite-orthoclase-almandine subfacies. The A2.3 subfacies boundary is located in Figure 5 on the basis of the appearance of granitic leucosome intercalated in the meta-arenites of the Flanders Lake formation, the disappearance of muscovite, and the appearance of potassium feldspar.

A2.4 Orthopyroxene-hornblende subfacies. Finally, to the east, rocks of the Flanders Lake formation correlate with orthopyroxene-bearing rocks (Trueman, 1976) which are considered to be part of the Manigotagan gneiss belt of McRitchie (1971). This area belongs to the orthopyroxene-hornblende subfacies.

The overall metamorphic history of the Bird River greenstone belt is summarized in Table 6. This, in general, is the environment into which the pegmatitic granites of the Winnipeg River area have intruded.

Table 6. Table of formations in the Bird River area, Manitoba (Trueman, 1980)

Formation	Dominant lithology	Intrusive rocks	Metamorphic rocks	Metamorphism	Deformation	Structure	Planar fabric
		pegm. granites pegmatites Lac du Bonnet monzogranite inconnu granite Black River Suite granodiorite tonalite		M_3	D_3	F_4 F_3	
			migmatite-complex				
		Great Falls QD	paragneiss	M_2	D_2	F_2	S_2
Booster Lake	metamorphosed greywacke-mudstone						
		UNCONFORMITY					

B. LOCAL GEOLOGY AND INTRUSIVE STYLE OF THE PEGMATITIC GRANITES

The four stocks of pegmatitic granite are mutually quite similar in their geological setting and intrusive style. All intrusions are late to post-tectonic and have ascended along major structural breaks within the greenstone belt. These granites are either intruded within or directly adjacent to the early subvertical major east-west trending faults which separate the five subareas of Trueman (1980) (Figure 5).

As documented below, the intrusion took place during regional dilation along these pre-existing fault systems, and in some of the intrusions it was followed by just slight shearing and displacement (TNL and GL).

Several large rafts of the hosting metabasalts are included and randomly oriented within several of the pegmatitic granites but stoping, is probably of secondary importance. Extensive evidence which would support this mechanism as an important component of intrusive style is lacking in most intrusions.

1. Tin Lake Intrusion

The Tin Lake (TNL) pegmatitic granite (Figure 6) is the more southern intrusive of the two pegmatitic stocks north of the Winnipeg River. Its shape is that of a circular plug that has been bisected laterally, in an east-

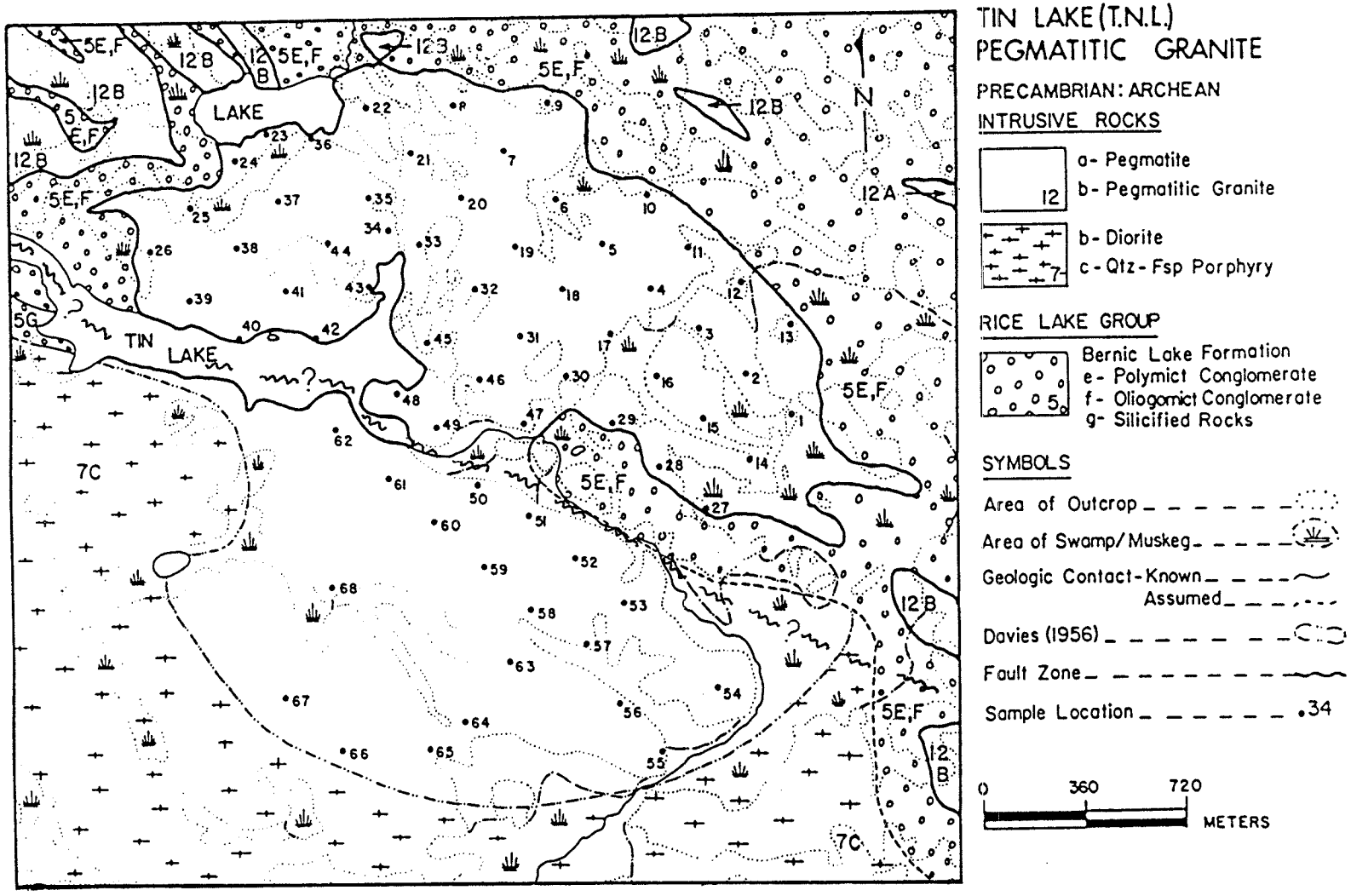

Figure 6. Geology and sampling locations of the Tin Lake pegmatitic granite. Geology after Davies (1955, 1957) and Trueman (1980).

west direction, into two lobes by a cataclastic shear zone passing under Tin Lake. This shear relates to the northern boundary of the subvolcanic quartz-feldspar porphyry (diorite) centred around Birse Lake, between Bird (Oiseau) Lake and the Winnipeg River (Trueman, 1980).

The northern lobe of the granite is extremely homogeneous, medium coarse-grained (0.5-1.0 cm) and overall reddish in colour. Garnet is a very common accessory mineral. Inclusions of units of the hosting Bernic Lake formation are absent.

Toward the western contact of the northern lobe, the granite tends to become coarser-grained up to pegmatitic. Smaller stocks of pegmatitic granite track east-southeast, north of the shear zone towards Ryerson Lake; however, these were not studied as extensively as the main intrusion of granite north of Tin Lake.

This eastern extension of the Tin Lake intrusion (Appendix 10) is very similar to the eastern portion of the northern lobe of TNL, except that it is finer-grained (0.3-0.5 cm) and appears to have a slightly lower garnet concentration. The contacts are sharp with no apparent alteration of the wall rocks, assimilation, or deformation of the original structure of the Bernic Lake formation. No connection between the individual lenses of granite is visible on the surface; however, a similar grain size, texture, mineralogy, and colour would support a possible connection at depth.

Smaller stocks of pegmatitic granite also extend in a west-northwest direction from the main northern lobe. Progressively along this direction, the size of these pegmatitic granite stocks decreases until they are essentially concordant pegmatitic sills streaming off from the end of the pegmatitic granite. Although no sharp boundary exists, this is the area marking a transition into the Birse Lake pegmatite group (Černý et al., 1981).

The Tin Lake granite is late to post-tectonic with no evidence of faulting, shearing, or straining within the northern lobe of the granite intrusion. Irrefutable evidence supporting the existence of the east-west trending fault proposed to underlie Tin Lake and transecting the intrusion into the northern and southern lobes is available. However, three facts indicate its presence: the significant change in rock type across Tin Lake, a distinct topographic low, and the position which is on strike with the fault that separates the subvolcanic quartz-feldspar porphyry centred around Birse Lake from the Bernic Lake formation. The intrusion of the pegmatitic granite was evidently related to this fault.

The southern lobe of the Tin Lake pegmatitic granite is very different from the northern lobe. Inclusions of metabasalts and metasediments are extremely abundant in places, up to a point where inclusions (up to 100 m^2) compose 70 percent of the outcrop surface. All inclusions are random

with respect to orientation and rock type. This breccia is cemented by a white granite phase which is, on average, slightly less garnetiferous than in the northern lobe. This phase is medium-grained (0.4 cm) in areas of abundant inclusions; however, in the rare homogeneous portions where no inclusions are present, the granite does become distinctly pegmatitic. In many locations the inclusions have been assimilated; growth of garnets and porphyroblasts of large K-feldspar (2-3 cm) is quite common. The contacts of this lobe with the enclosing subvolcanic quartz-feldspar porphyry could not be studied because of low topography, vegetation, and muskeg.

2. Eaglenest Lake Intrusion

The Eaglenest Lake pluton (Figure 7) is elongated (2.5 km by 0.5 km) parallel to the east-west layering and foliation of the host metabasalts of the Lamprey Falls formation. The total outcropping area is approximately 1.25 km^2. No inclusions were noted in this stock and the external contacts, where visible on the western and southern sides, are sharp and show no deformation of the hosting metabasalts. Unlike the other contacts of this intrusion, the eastern end does not have a sharp contact but interfingers in a "lit par lit" style with the hosting Lamprey Falls formation metabasalts. The Eaglenest Lake stock is not truely fault-bound; however, it could have ascended

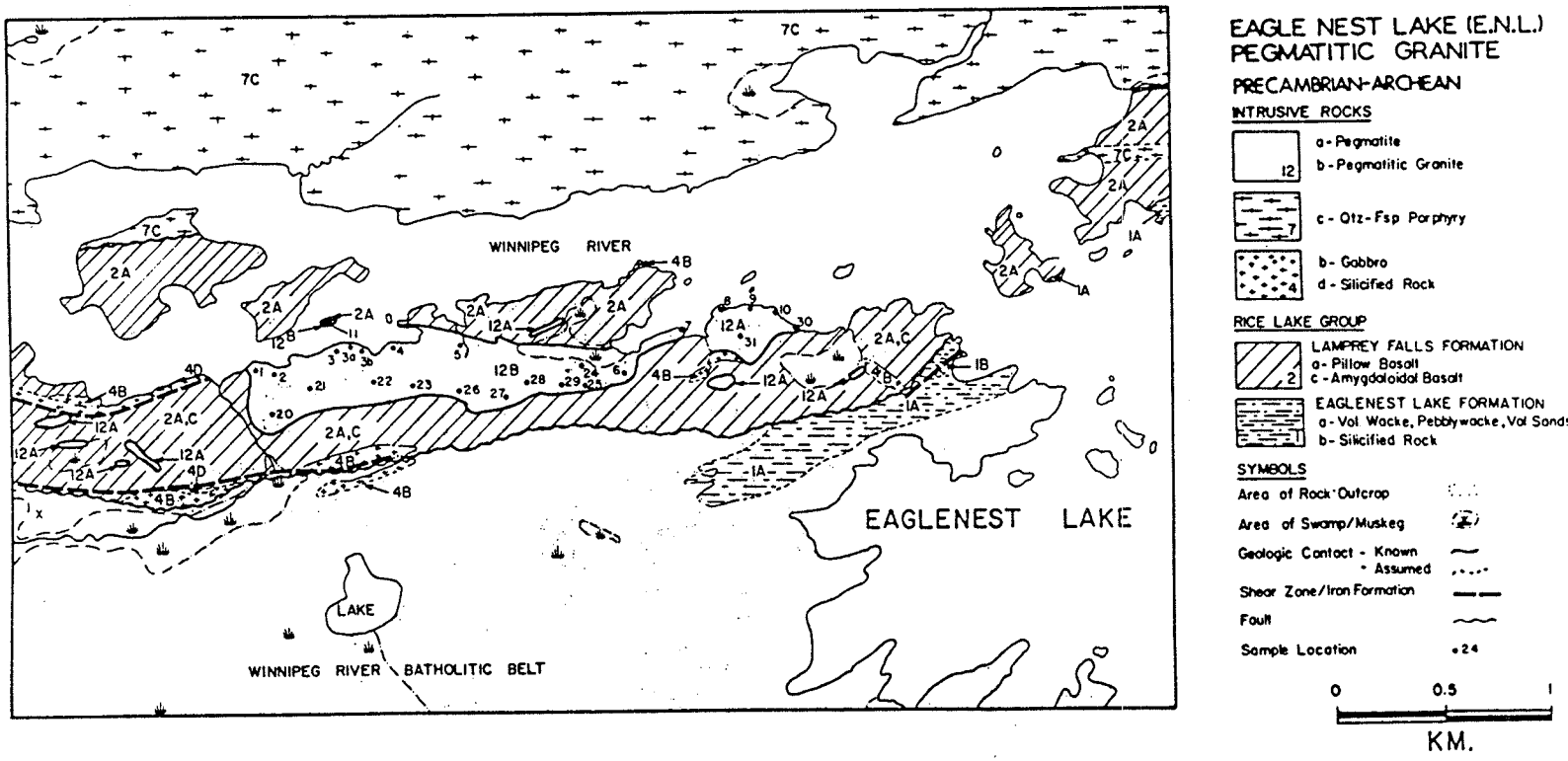

Figure 7. Geology and sampling locations of the Eaglenest Lake pegmatite granite. Geology after Davies (1955, 1957) and Trueman (1980).

tension fractures generated during the period of tectonic instability which created the two major east-west faults that parallel the contacts of the pluton. One of the faults located 200 metres south of the intrusive contact marks the faulted southern contact of the Lamprey Falls formation with the Winnipeg River batholithic belt. The second fault forms the northern contact of the Lamprey Falls formation with the subvolcanic quartz diorite-quartz feldspar porphyry and is located approximately 400 metres north of the northern contact of the Eaglenest Lake pegmatitic granite (Figure 7). All large-scale tectonic displacement within the greenstone belt occurred before emplacement of this and all other stocks of pegmatitic granite since no evidence of late deformation exists.

3. Osis Lake Intrusion

The northernmost stock of pegmatitic granite, Osis Lake (OL), is located between Summerhill, Booster and Osis Lakes (Figure 8) and is possibly the most interesting intrusion structurally. It is situated just north of the major east-west fault that separates Trueman's (1980) Subareas 4 and 5, in the metaturbidites of the Booster Lake formation (Subarea 5). This intrusion outcrops sporadically in an area covering approximately 25 km^2.

The eastern half of the intrusion is composed of isolated lenses (possibly apophyses protruding from a large

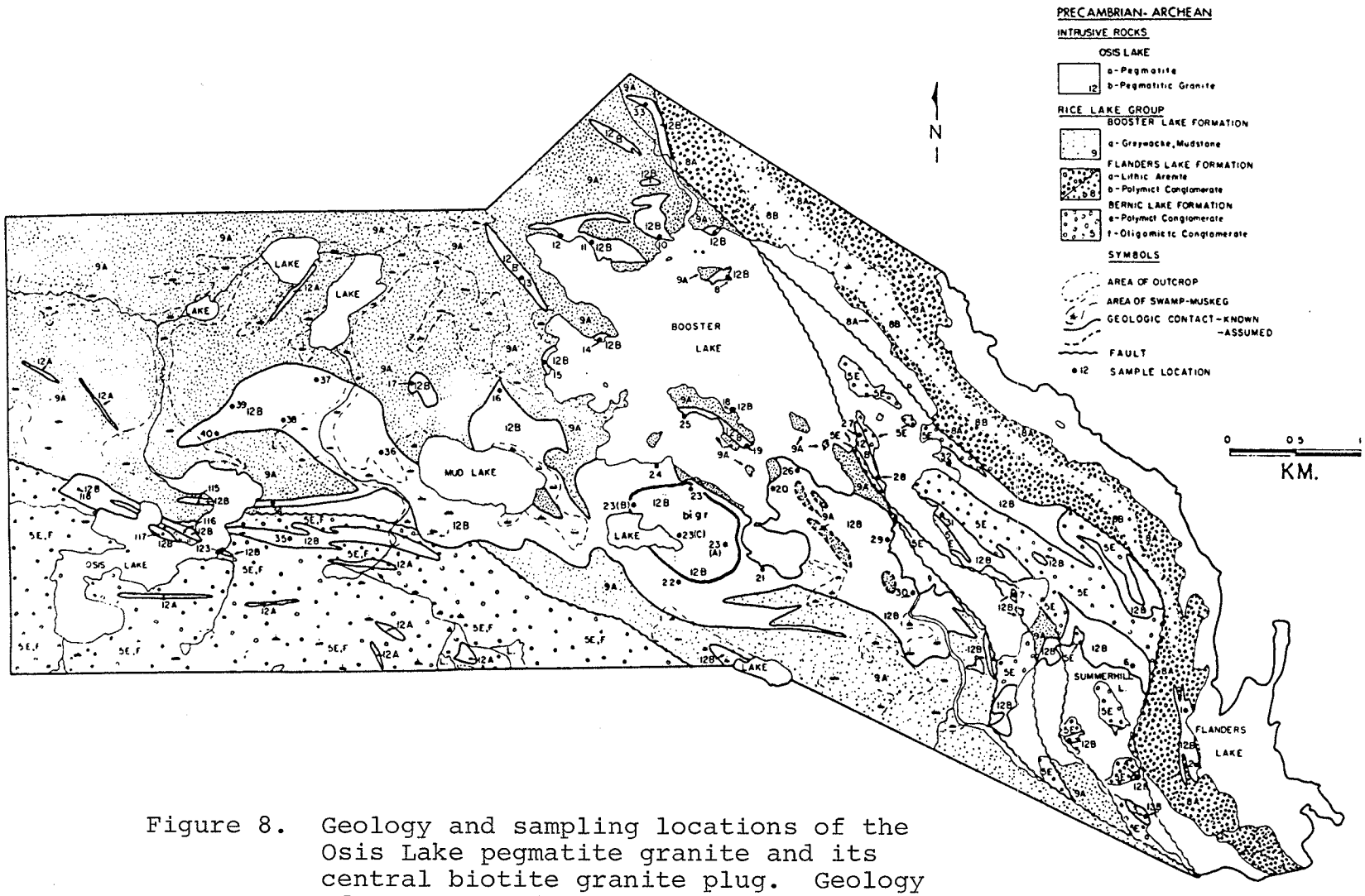

Figure 8. Geology and sampling locations of the Osis Lake pegmatite granite and its central biotite granite plug. Geology after Davies (1955, 1957) and Trueman (1980).

intrusion of pegmatitic granite at depth) intruded into the hosting Booster Lake formation sediments. In most locations the contacts are very sharp causing no alteration or structure deformation in the host rocks. However, along the southern end of the intrusion, the sediments are locally folded and contorted suggesting that this area was subjected to forceful intrusion (Figure 9).

Further west, in the central area of the intrusion, the granite exposed on the surface becomes more continuous and covers a larger percentage of outcrop. Contacts with the sediments are still sharp. In this central area the petrography of the intrusion changes quite dramatically from pegmatitic granite to fine-grained biotite granite. The contact between these two phases of the granite has been eroded; consequently, it is covered mostly by swamp, soil, and vegetation. Despite the limited exposure, there is some evidence of a gradational, continuous contact between the two phases and, in addition, a set of fractures striking at 90° to the contact area. These fractures show minor evidence of shearing and have been filled with fibrous muscovite, possibly after sillimanite, ± tourmaline knots. Slight shearing is also evident parallel to this contact. Parallel to these fractures and crossing the contact zone are pegmatitic stringers probably emanating from the peripheral pegmatitic granite and injected into the central plug of biotite granite. This plug is approximately 0.5 kilometres

NOTICE/AVIS

PAGE(S) 46 IS/ARE EST/SONT black + white photo

PLEASE WRITE TO THE AUTHOR FOR INFORMATION, OR CONSULT THE ARCHIVAL COPY HELD IN THE DEPARTMENT OF ARCHIVES AND SPECIAL COLLECTIONS, ELIZABETH DAFOE LIBRARY, UNIVERSITY OF MANITOBA, WINNIPEG, MANITOBA, CANADA, R3T 2N2.

VEUILLEZ ECRIRE A L'AUTEUR POUR LES RENSEIGNEMENTS OU VEUILLEZ CONSULTER L'EXEMPLAIRE DONT POSSEDE LE DEPARTEMENT DES ARCHIVES ET DES COLLECTIONS SPECIALES, BIBLIOTHEQUE ELIZABETH DAFOE, UNIVERSITE DU MANITOBA, WINNIPEG, MANITOBA, CANADA, R3T 2N2.

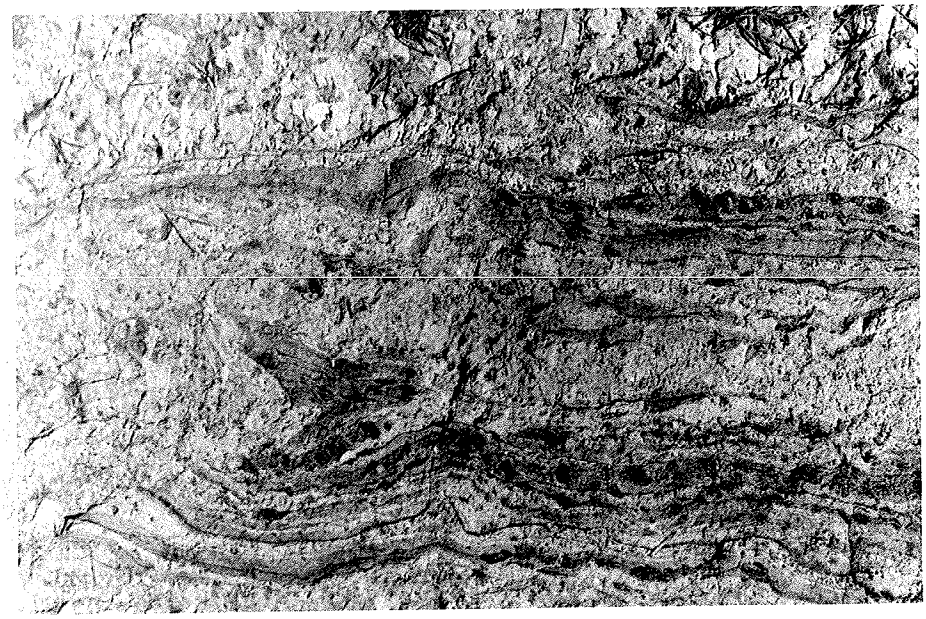

Figure 9. Warping and contortion of metapelites in the southeastern tip of the Osis Lake pegmatitic granite body, suggestive of forceful intrusion of the latter; the shorter edge of the photograph is about 70 cm long.

by 0.75 kilometres in size and carries no inclusions.

Westward from the western contact of this central plug of biotite granite, the grain size of the pegmatitic granite becomes progressively coarser and a slight change in mineralogy occurs (Table 24).

The most exotic portion of the whole intrusion is that lying west of Mud Lake (Figure 8). The grain size is extremely coarse here (3-200 cm), and the mineralogy and alteration of the hosting metaturbidites (tourmalinization) become more extensive. Inclusions varying in size from centimetres to tens of metres in diameter have increased to the point where they occupy 50 percent of the outcrop surface in the western tip of the intrusion (Figure 8). The pegmatitic granite here resembles a series of parallel en echelon dikes intruding along the layering and foliation of the hosting Booster Lake turbidites. In this area there is much evidence of passive intrusion of granite along tension fractures (Figure 10) but also ptygmatic folding of the granite (Figure 11) in the sediments suggesting compression and a locally plastic state of the hosting turbidites at the time of intrusion of the pegmatitic granite.

Alteration of the host sediments in this area is extensive. This western end, unlike the eastern end of the intrusive, is discontinuous. It more resembles an injection or fingering out of the pegmatitic granite into the layering and foliation of the turbidites of the Booster Lake formation.

NOTICE/AVIS

PAGE(S) 48+49 IS/ARE EST/SONT color photos

PLEASE WRITE TO THE AUTHOR FOR INFORMATION, OR CONSULT THE ARCHIVAL COPY HELD IN THE DEPARTMENT OF ARCHIVES AND SPECIAL COLLECTIONS, ELIZABETH DAFOE LIBRARY, UNIVERSITY OF MANITOBA, WINNIPEG, MANITOBA, CANADA, R3T 2N2.

VEUILLEZ ECRIRE A L'AUTEUR POUR LES RENSEIGNEMENTS OU VEUILLEZ CONSULTER L'EXEMPLAIRE DONT POSSEDE LE DEPARTEMENT DES ARCHIVES ET DES COLLECTIONS SPECIALES, BIBLIOTHEQUE ELIZABETH DAFOE, UNIVERSITE DU MANITOBA, WINNIPEG, MANITOBA, CANADA, R3T 2N2.

Figure 10. The Osis Lake pegmatitic granite filling-in dilation fractures in the metapelites of the Booster Lake formation. This is very characteristic of the western portion of the intrusion. Note the near perfect match of the metapelite slabs across the separating pegmatitic granite (25 cm wide).

Figure 11. Ptygmatic folding of pegmatitic granite stringers typical of some metapelite rafts in the western extremity of the Osis Lake intrusion. Note the tourmalinization of the host sediments adjacent to the intrusion. Lens cap is 53 mm in diameter.

4. Greer Lake Intrusion

The Greer Lake (GL) pegmatitic granite extends in an east-west direction along the south shore of the Winnipeg River for a distance of four kilometres and outcrops to the south in an area covering four square kilometres. It has intruded into a narrow fault-bound slice of the Lamprey Falls formation which consists mainly of metabasalts. This intrusion is apparently controlled on the south by the major fault running under Greer Lake which separates the Bird River greenstone belt from the Winnipeg River batholithic belt (Figure 12). The few outcrop areas of contact with the hosting metabasalts on the southwestern and eastern edge of the pluton are extremely sharp, cutting both the layering and foliation with no visible deformation of either. Stoping along the northern contact of this pluton is suggested by the presence of several large, randomly oriented blocks of the hosting metabasalts.

Within this pegmatitic granite is a narrow shear zone paralleling the southern contact and transecting the southern part of the Greer Lake intrusion (Figure 12). An iron formation unit extended along the shear zone within the pegmatitic granite appears to be continuous with the iron formation which occurs east, south, and west of the Greer Lake pegmatitic granite. This unit can be followed further eastward and correlates to the iron formation that passes south of the Eaglenest Lake pegmatitic granite (Figure 7). The preservation of this iron formation within the

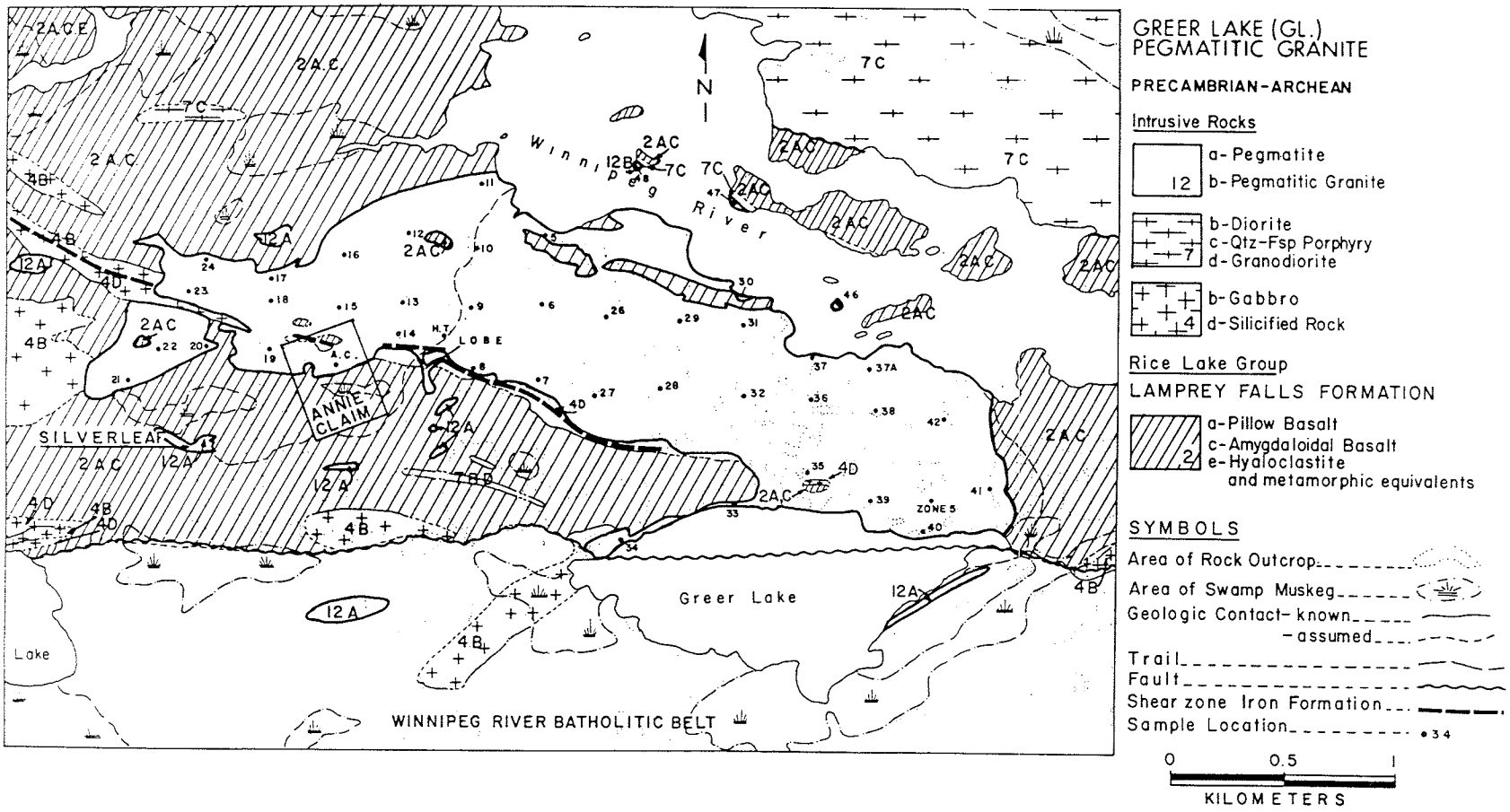

Figure 12. Geology and sampling locations of the Greer Lake pegmatitic granite. Geology after Davies (1955, 1957) and Trueman (1980).

pegmatitic granite supports the suggestion that stoping occurred during intrusion of the granitic mass.

C. EXOMORPHISM

Reaction of the pegmatitic granites with the enclosing rocks varies with the composition of both the intrusion and host. Along the meager contact exposures of the Greer Lake and Eaglenest Lake intrusions, reaction with metabasalts is restricted to very limited recrystallization of hornblende in the metabasalts, and moderate biotitization. In the southern lobe of the Tin Lake intrusion, small inclusions of the tonalite and metavolcanics tend to develop prophyroblastic garnet, and only in the northeastern extremity where this intrusion is in contact with Booster Lake metaturbidites, altered cordierite is found in fine-grained leucogranites. In contrast, the tourmaline-bearing Osis Lake intrusion has reacted extensively with the metaturbidites of the Booster Lake formation: tourmalinization of the latter (Figure 13, 14), coupled with growth of albitic plagioclase and locally muscovite, is ubiquitous, particularly in thin splinters and screens (Figure 15) and on the surface of larger rafts (Figure 16). Thin screens may become completely digested by the pegmatitic granite (Figure 33).

Exomorphic influence of the pegmatitic granites is probably much more pronounced than the effects observed along the immediate intrusive contacts. Post-tectonic growth

NOTICE/AVIS

PAGE(S) 53 IS/ARE EST/SONT color photo

PLEASE WRITE TO THE AUTHOR FOR INFORMATION, OR CONSULT THE ARCHIVAL COPY HELD IN THE DEPARTMENT OF ARCHIVES AND SPECIAL COLLECTIONS, ELIZABETH DAFOE LIBRARY, UNIVERSITY OF MANITOBA, WINNIPEG, MANITOBA, CANADA, R3T 2N2.

VEUILLEZ ECRIRE A L'AUTEUR POUR LES RENSEIGNEMENTS OU VEUILLEZ CONSULTER L'EXEMPLAIRE DONT POSSEDE LE DEPARTEMENT DES ARCHIVES ET DES COLLECTIONS SPECIALES, BIBLIOTHEQUE ELIZABETH DAFOE, UNIVERSITE DU MANITOBA, WINNIPEG, MANITOBA, CANADA, R3T 2N2.

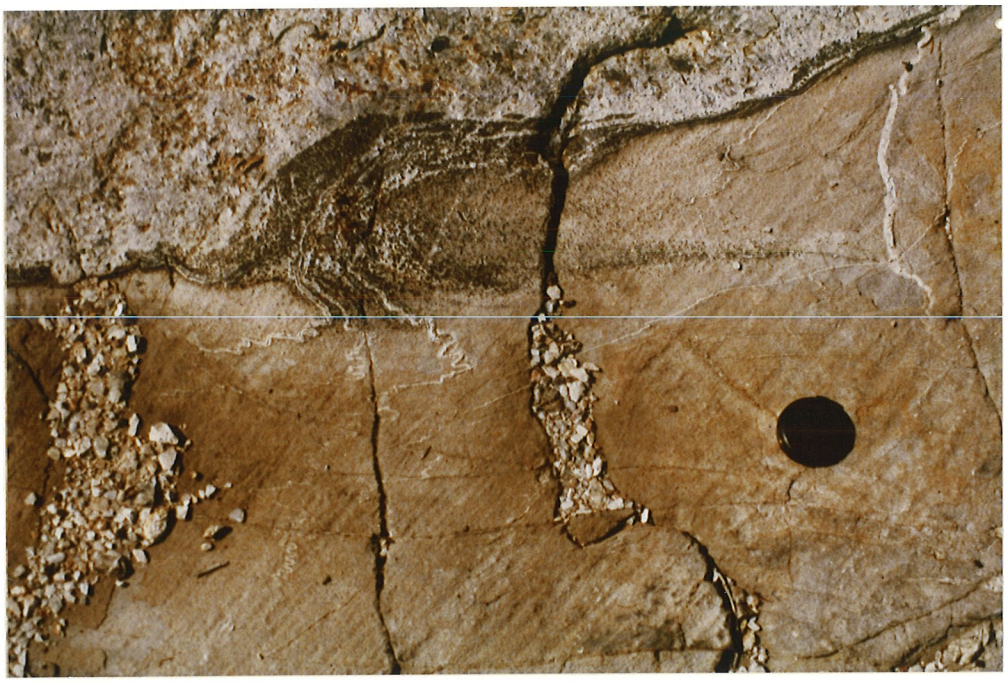

Figure 13. Tourmalinization along the edges of metapelite rafts and within rafts along fractures. This is only observed in the western end of the Osis Lake intrusion.

NOTICE/AVIS

PAGE(S) 54 IS/ARE EST/SONT black + white photo

PLEASE WRITE TO THE AUTHOR FOR INFORMATION, OR CONSULT THE ARCHIVAL COPY HELD IN THE DEPARTMENT OF ARCHIVES AND SPECIAL COLLECTIONS, ELIZABETH DAFOE LIBRARY, UNIVERSITY OF MANITOBA, WINNIPEG, MANITOBA, CANADA, R3T 2N2.

VEUILLEZ ECRIRE A L'AUTEUR POUR LES RENSEIGNEMENTS OU VEUILLEZ CONSULTER L'EXEMPLAIRE DONT POSSEDE LE DEPARTEMENT DES ARCHIVES ET DES COLLECTIONS SPECIALES, BIBLIOTHEQUE ELIZABETH DAFOE, UNIVERSITE DU MANITOBA, WINNIPEG, MANITOBA, CANADA, R3T 2N2.

Figure 14. Tourmalinization (darkest brown) along the edges and in thin fragments of a metapelitic raft, in the western part of the Osis Lake pegmatitic granite body. Hammer is 34 cm long.

NOTICE/AVIS

PAGE(S) 55 + 56 IS/ARE EST/SONT color photos

PLEASE WRITE TO THE AUTHOR FOR INFORMATION, OR CONSULT THE ARCHIVAL COPY HELD IN THE DEPARTMENT OF ARCHIVES AND SPECIAL COLLECTIONS, ELIZABETH DAFOE LIBRARY, UNIVERSITY OF MANITOBA, WINNIPEG, MANITOBA, CANADA, R3T 2N2.

VEUILLEZ ECRIRE A L'AUTEUR POUR LES RENSEIGNEMENTS OU VEUILLEZ CONSULTER L'EXEMPLAIRE DONT POSSEDE LE DEPARTEMENT DES ARCHIVES ET DES COLLECTIONS SPECIALES, BIBLIOTHEQUE ELIZABETH DAFOE, UNIVERSITE DU MANITOBA, WINNIPEG, MANITOBA, CANADA, R3T 2N2.

Figure 15. A thin screen of largely tourmalinized metapelitic schist separating aplitic and pegmatitic crystallization regimes in the western end of the Osis Lake pegmatitic granite intrusion (Černý et al., 1981).

Figure 16. A thin, largely tourmalinized screen of metapelitic schist serving as a substrate for oriented growth of club-shaped (partly graphic) K-feldspar crystals of the Osis Lake pegmatitic granite. Note the accumulation of muscovite books along the screen (Černý et al., 1981).

of biotite, muscovite, gedrite, and chlorite is characteristic of most of the greenstone belt lithologies (A.C. Turnock, pers. comm. 1980), suggestive of widespread alkali metasomatism. Extensive dispersion haloes of K, Li, Rb, and Cs can be expected in the schists hosting the pegmatitic granites, as documented for analogous rocks in the Cat Lake and Lilypad Lake areas (W.C. Hood, pers. comm. 1980; Goad and Černý, 1981).

Chapter IV

PETROGRAPHY

A. FACIES

Initially, the pegmatitic granite intrusions were all tentatively subdivided into four facies according to textures observed in the field. Subsequent examination of the mineralogy and geochemistry of these facies has verified their existence; consequently, they have been defined in the following manner:

1. Leucogranite

Leucogranite (Figure 17) is a fine to medium-grained (< 0.5 cm) hypidiomorphic granular facies containing perthitic microcline, quartz, plagioclase (An < 10), muscovite ± biotite, ± garnet, ± apatite. This facies is massive and very homogeneous with respect to its mineral distribution; however, as discussed below, some variation is evident.

2. Sodic Aplite

This is a fine-grained (< 0.2 cm) equigranular facies containing predominantly sodium plagioclase (An < 10) + quartz ± garnet, ± muscovite. The latter two minerals, when present, are usually aligned along subparallel planar surfaces which give the rock a banded appearance when seen in two-dimensional sections (Figure 18).

NOTICE/AVIS

PAGE(S) 59+60 IS/ARE EST/SONT color photos

PLEASE WRITE TO THE AUTHOR FOR INFORMATION, OR CONSULT THE ARCHIVAL COPY HELD IN THE DEPARTMENT OF ARCHIVES AND SPECIAL COLLECTIONS, ELIZABETH DAFOE LIBRARY, UNIVERSITY OF MANITOBA, WINNIPEG, MANITOBA, CANADA, R3T 2N2.

VEUILLEZ ECRIRE A L'AUTEUR POUR LES RENSEIGNEMENTS OU VEUILLEZ CONSULTER L'EXEMPLAIRE DONT POSSEDE LE DEPARTEMENT DES ARCHIVES ET DES COLLECTIONS SPECIALES, BIBLIOTHEQUE ELIZABETH DAFOE, UNIVERSITE DU MANITOBA, WINNIPEG, MANITOBA, CANADA, R3T 2N2.

Figure 17. Radial (plumose) aggregate of muscovite + quartz in the slightly albitic matrix of the Eaglenest Lake leucogranite (ENL-3). In 3-dimensions, this muscovite forms a conical aggregate with a garnet crystal at the apex. In the Osis Lake intrusion, this configuration has also been noted radiating from a tourmaline crystal. Radial muscovite has only been found in the leucogranite and pegmatitic leucogranite.

Figure 18. Banded garnetiferous sodic aplite which parallels the contact of the Eaglenest Lake intrusion (ENL-8). Towards the centre of the intrusion sodic aplite is in contact with the potassic pegmatite facies. Contact is sharp and note in the centre of the photograph where the bands of sodic aplite are cut off by the potassic pegmatite. Although garnet is present, banding in the ENL intrusion is predominantly due to muscovite bands.

The leucogranite apparently grades into the sodic aplite facies with an increase in the muscovite and/or garnet, an increase in the amount of albitic plagioclase, and the alignment of the feldspar laths parallel to the layering of garnet and/or muscovite. As the transition progresses, the tabular form of the plagioclase in sodic aplite becomes more equant, thus changing the texture from a somewhat pseudo-trachytic appearance to hypidiomorphic granular. The final stage of the transition from leucogranite to sodic aplite is a gradual disappearance of potassium feldspar. Accessory minerals that occur in the sodic aplite facies include apatite, gahnite, monazite, and Nb,Ta oxide minerals (in order of decreasing abundance).

3. Potassic Pegmatite

This coarse-grained ($\rangle$ 2.0 cm) potassium-rich facies is commonly (but not exclusively) intimately associated with, and adjacent to, the sodic aplite facies (Figure 19). The potassic pegmatite facies is defined by the presence of coarse blocky (or partly graphic) potassium feldspar, quartz, and muscovite in pods or bands adjacent to the sodic aplite or within the pegmatitic leucogranite facies. Frequently these minerals have crystallized in concentric zoned patterns. Granular and/or cleavelandite-type albite may appear, especially in the geochemically more fractionated locations. These potassic pegmatite pods or bands appear to

NOTICE/AVIS

PAGE(S) 62 IS/ARE EST/SONT color photo

PLEASE WRITE TO THE AUTHOR FOR INFORMATION, OR CONSULT THE ARCHIVAL COPY HELD IN THE DEPARTMENT OF ARCHIVES AND SPECIAL COLLECTIONS, ELIZABETH DAFOE LIBRARY, UNIVERSITY OF MANITOBA, WINNIPEG, MANITOBA, CANADA, R3T 2N2.

VEUILLEZ ECRIRE A L'AUTEUR POUR LES RENSEIGNEMENTS OU VEUILLEZ CONSULTER L'EXEMPLAIRE DONT POSSEDE LE DEPARTEMENT DES ARCHIVES ET DES COLLECTIONS SPECIALES, BIBLIOTHEQUE ELIZABETH DAFOE, UNIVERSITE DU MANITOBA, WINNIPEG, MANITOBA, CANADA, R3T 2N2.

Figure 19. An excellent example of potassic pegmatite facies. Club-shaped K-feldspar crystals growing at right angles to sodic aplite-potassic pegmatite interface. ENL-10 location.

alternate rhythmically with the sodic aplite facies (Figure 20). The boundary between the two facies may be gradual (Figure 21); however, more often it is extremely sharp with the blocky potassium feldspar crystal "clubs" growing at 90° to the facies interface (Figure 18). Accessory mineralization associated with this facies may be beryl, Nb,Ta oxide minerals, triphylite (mostly altered into ferrisicklerite), arsenopyrite, tourmaline, apatite, molybdenite, and sphalerite. These minerals are usually (but not exclusively) found in the central quartz-rich areas of the pods (Figure 22(a) and (b)).

4. Pegmatitic Leucogranite

This is usually the most dominant and voluminous facies of the pegmatitic granites (Figure 23). The most notable feature of this facies is the megacrystic graphic potassium feldspar plus quartz crystals (5-200 cm). These megacrysts are suspended in a medium to coarse-grained quartz + muscovite + plagioclase (An < 10) ± tourmaline ± garnet matrix (Figure 24). The potassium feldspar crystals are usually euhedral and club-shaped (Figure 23, 24); however, they have been observed to be slightly corroded by the groundmass (Figure 25). In most of the pegmatitic granites, local clots of plumose or radial muscovite and quartz intergrowths are contained within this groundmass. In three dimensions these intergrowths are cone-shaped with a garnet

NOTICE/AVIS

PAGE(S) 64+65 IS/ARE EST/SONT color photos

PLEASE WRITE TO THE AUTHOR FOR INFORMATION, OR CONSULT THE ARCHIVAL COPY HELD IN THE DEPARTMENT OF ARCHIVES AND SPECIAL COLLECTIONS, ELIZABETH DAFOE LIBRARY, UNIVERSITY OF MANITOBA, WINNIPEG, MANITOBA, CANADA, R3T 2N2.

VEUILLEZ ECRIRE A L'AUTEUR POUR LES RENSEIGNEMENTS OU VEUILLEZ CONSULTER L'EXEMPLAIRE DONT POSSEDE LE DEPARTEMENT DES ARCHIVES ET DES COLLECTIONS SPECIALES, BIBLIOTHEQUE ELIZABETH DAFOE, UNIVERSITE DU MANITOBA, WINNIPEG, MANITOBA, CANADA, R3T 2N2.

Figure 20. Alternating bands of sodic aplite and potassic pegmatite in the Osis Lake intrusion (OL-13). Hammer is 45 cm long.

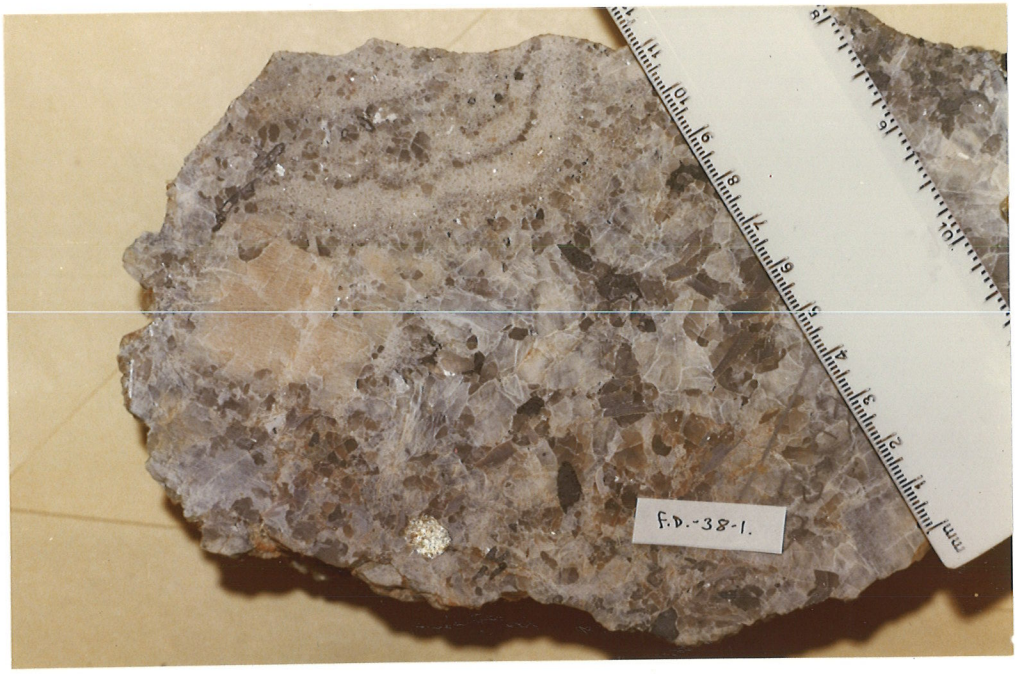

Figure 21. Gradual transition from sodic aplite facies to pegmatitic leucogranite in the Osis Lake pegmatitic granite (OL-38). Note abundance of honey-coloured matrix muscovite and black tourmaline in pegmatitic leucogranite.

NOTICE/AVIS

PAGE(S) 66 IS/ARE/EST/SONT black+white photo

PLEASE WRITE TO THE AUTHOR FOR INFORMATION, OR CONSULT THE ARCHIVAL COPY HELD IN THE DEPARTMENT OF ARCHIVES AND SPECIAL COLLECTIONS, ELIZABETH DAFOE LIBRARY, UNIVERSITY OF MANITOBA, WINNIPEG, MANITOBA, CANADA, R3T 2N2.

VEUILLEZ ECRIRE A L'AUTEUR POUR LES RENSEIGNEMENTS OU VEUILLEZ CONSULTER L'EXEMPLAIRE DONT POSSEDE LE DEPARTEMENT DES ARCHIVES ET DES COLLECTIONS SPECIALES, BIBLIOTHEQUE ELIZABETH DAFOE, UNIVERSITE DU MANITOBA, WINNIPEG, MANITOBA, CANADA, R3T 2N2.

Figure 22(a). Potassic pegmatite facies consists of blocky, or partly graphic, K-feldspar commonly in concentric zoned patterns. Platy muscovite, granular albite, beryl, Nb,Ta oxide minerals, garnet, apatite, tourmaline, arsenopyrite and/or triphylite, in this case altered to ferrisicklerite, occur sporadically in the central parts of the potassic pegmatite bands. Photo from the Osis Lake intrusion (OL-40).

NOTICE/AVIS

PAGE(S) 67-70 ~~IS~~/ARE ~~EST~~/SONT color photos

PLEASE WRITE TO THE AUTHOR FOR INFORMATION, OR CONSULT THE ARCHIVAL COPY HELD IN THE DEPARTMENT OF ARCHIVES AND SPECIAL COLLECTIONS, ELIZABETH DAFOE LIBRARY, UNIVERSITY OF MANITOBA, WINNIPEG, MANITOBA, CANADA, R3T 2N2.

VEUILLEZ ECRIRE A L'AUTEUR POUR LES RENSEIGNEMENTS OU VEUILLEZ CONSULTER L'EXEMPLAIRE DONT POSSEDE LE DEPARTEMENT DES ARCHIVES ET DES COLLECTIONS SPECIALES, BIBLIOTHEQUE ELIZABETH DAFOE, UNIVERSITE DU MANITOBA, WINNIPEG, MANITOBA, CANADA, R3T 2N2.

Figure 22(b). Potassic pegmatite pod containing a large dark tourmaline crystal, whitish ferrisicklerite (#1), blue green apatite crystals (#2), and a bladed Nb,Ta oxide crystal (#3). Sample was obtained from the western end of the Osis Lake intrusion (OL-40).

Figure 23. Pegmatitic leucogranite of the Osis Lake intrusion. This facies is volumetrically the most dominant in all intrusions except TNL, and consists of megacrystic K-feldspar (5-200 cm) usually somewhat intergrown with quartz, and suspended in a medium to coarse-grained albite + muscovite + quartz ± garnet and/or tourmaline groundmass. Hammer is 45 cm long. The larger crystals are usually more corroded.

Figure 24. Pegmatitic leucogranite from the Osis Lake intrusion. Pink subhedral K-feldspar with graphic quartz in a groundmass of albite + quartz + muscovite ± garnet and tourmaline. Pen is 15 cm long.

Figure 25. Plumose (radial) aggregates of muscovite + quartz in the white albite + quartz matrix (with large pink K-feldspar crystals) of the pegmatitic leucogranite facies of the Osis Lake intrusion. Note large crystals of tourmaline and slight bleaching of sediments adjacent to the granite contact. Shot gun shell is 6 cm long.

or tourmaline crystal (depending on the intrusion) at the apex. These intergrowths are evenly distributed throughout the quartz + muscovite + plagioclase matrix (Figure 26); however, occasionally their number increases locally which gives the impression of a late replacement assemblage (e.g., at location ENL-3).

This facies develops locally into the potassic pegmatite facies by the disappearance of quartz from graphic potassium feldspar, accumulation of the potassium feldspar at the expense of the quartz + muscovite + plagioclase matrix (up to its complete disappearance), and gradation into blocky potassium feldspar zones surrounding lenticular or pod-like masses of quartz.

Contacts among the four facies may be either extremely sharp or they may be gradational.

The only facies observed illustrating definite crosscutting relationships with respect to the other facies of the pegmatitic granites, indicating that they were the last to solidify, is the potassic pegmatite facies (Figure 19). Narrow dikelets or stringers (3-5 cm wide) of potassium feldspar phenocrysts + quartz + muscovite (potassic pegmatite facies) crosscutting the other three facies (especially the leucogranite and the sodic aplite facies) are relatively common (Figure 27).

NOTICE/AVIS

PAGE(S) 72+73 IS/ARE EST/SONT color photos

PLEASE WRITE TO THE AUTHOR FOR INFORMATION, OR CONSULT THE ARCHIVAL COPY HELD IN THE DEPARTMENT OF ARCHIVES AND SPECIAL COLLECTIONS, ELIZABETH DAFOE LIBRARY, UNIVERSITY OF MANITOBA, WINNIPEG, MANITOBA, CANADA, R3T 2N2.

VEUILLEZ ECRIRE A L'AUTEUR POUR LES RENSEIGNEMENTS OU VEUILLEZ CONSULTER L'EXEMPLAIRE DONT POSSEDE LE DEPARTEMENT DES ARCHIVES ET DES COLLECTIONS SPECIALES, BIBLIOTHEQUE ELIZABETH DAFOE, UNIVERSITE DU MANITOBA, WINNIPEG, MANITOBA, CANADA, R3T 2N2.

Figure 26. Typical occurrence of radial muscovite in the pegmatitic leucogranite facies of the Osis Lake intrusion (OL-13). Single cones such as in the right central part of the photograph tend to grow together forming muscovite clots (top centre) more so in this intrusion than in the ENL or GL intrusions.

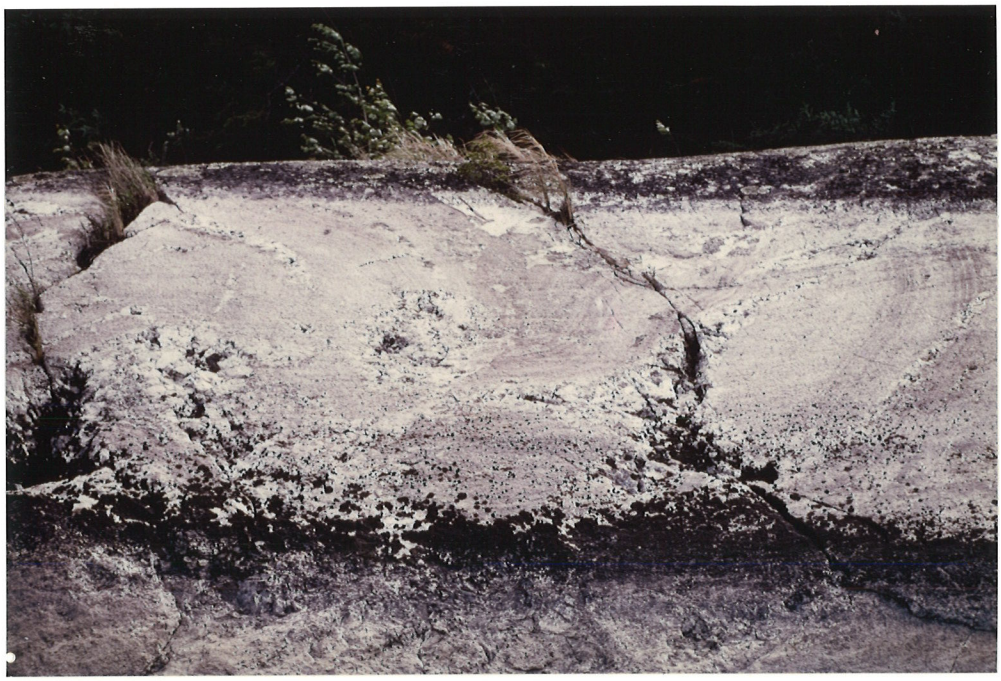

Figure 27. Pods of potassic pegmatite which coalesced within leucogranite (ENL-3). Note crosscutting relationships of potassic pegmatite with banded leucogranite (Figure 28).

B. FACIES DISTRIBUTION WITHIN THE INDIVIDUAL INTRUSIONS

In order to discuss more specifically the facies distribution within each intrusive stock, a detailed examination of each individual intrusion of pegmatitic granite is required.

1. Tin Lake Intrusion

The facies relationships of the Tin Lake intrusion are the least variable of all four stocks of pegmatitic granite in this study. The northern lobe is mainly composed of the leucogranite facies, up to approximately 90 percent (by area). This facies carries two micas, mainly biotite but also minor muscovite, and a relatively high concentration of garnet (as compared to the other leucogranite facies in the other intrusions). The sodic aplite is absent in the east and the few locations where it was observed were in the western end which suggests a possible increase in a western direction. Where the sodic aplite was observed its extent was very localized ($< 1\ m^2$) and internal banding was due to the presence of garnet. The potassic pegmatite facies is also extremely rare. It is also absent in the east and where it occurs in the west it is associated with the sodic aplite facies. No accessory mineralization is associated with this potassic pegmatite facies except in the extreme western side of the northern lobe where a crystal of molybdenite (1 cm^3 in size) was observed. The pegmatitic

leucogranite facies parallels the trends of the sodic aplite and the potassic pegmatite facies; that is, it is absent in the east and becomes more common in a westerly direction. A large area just east of Tin Lake is the point where this facies first appears. Except for a single crystal of tourmaline, no other accessory mineralization was noted in this facies. This tourmaline occurrence is approximately 200 metres northwest of the east end of Tin Lake and from this location to the west, coarse pegmatitic leucogranite becomes increasingly dominant until the intrusion fingers out into the Birse Lake pegmatite group of Černý et al. (1981). Tourmaline content dramatically increases, then rose quartz, and subsequently beryl crystals appear in the pods of potassic pegmatite as the transition progresses into the Birse Lake pegmatite group.

The small stocks of pegmatitic granite south and east of the northern lobe were studied in much less detail than the northern lobe itself; however, a brief description of their facies composition is warranted. This is the eastern extension of the northern lobe of the Tin Lake pegmatitic granite and is composed mostly of a hybrid facies transitional between leucogranite and the sodic aplite. It is medium-grained (0.2-0.3 cm), hypidiomorphic granular and garnetiferous; however, no evidence of banding of the garnet or alignment of any other mineral is evident. Contained within this facies are small areas of pegmatitic leucogranite.

Occasionally these grade into small pods of potassic pegmatite which can have very minor sodic aplite associated with them. As in the other areas of the Tin Lake intrusion, no accessory mineralization was observed to be associated with any of these facies. However, adjacent to the contact of the intrusion with the sediments of the Booster Lake formation, distinct crystals of altered cordierite appear in the granite.

The granite of the southern lobe of the Tin Lake intrusion is composed almost entirely of a white leucogranite facies. Its average grain size (0.4 cm) is smaller than that of the northern lobe (0.5-1.0 cm) and garnet mineralization is not quite as abundant. The remaining three facies do exist but their total area when compared to the area covered by the leucogranite is insignificant. No accessory mineralization is associated with any of the four facies in the southern lobe.

2. Eaglenest Lake Intrusion

The facies relationships in the Eaglenest Lake pegmatitic granite are slightly more complex than those in the Tin Lake intrusion; however, they are still relatively simple. There is very little leucogranite, as it has been previously defined; instead, a transitional facies between leucogranite and the sodic aplite facies (Figure 28) is widespread, as well as that between pegmatitic leucogranite

NOTICE/AVIS

PAGE(S) 77 IS/ARE EST/SONT color photo

PLEASE WRITE TO THE AUTHOR FOR INFORMATION, OR CONSULT THE ARCHIVAL COPY HELD IN THE DEPARTMENT OF ARCHIVES AND SPECIAL COLLECTIONS, ELIZABETH DAFOE LIBRARY, UNIVERSITY OF MANITOBA, WINNIPEG, MANITOBA, CANADA, R3T 2N2.

VEUILLEZ ECRIRE A L'AUTEUR POUR LES RENSEIGNEMENTS OU VEUILLEZ CONSULTER L'EXEMPLAIRE DONT POSSEDE LE DEPARTEMENT DES ARCHIVES ET DES COLLECTIONS SPECIALES, BIBLIOTHEQUE ELIZABETH DAFOE, UNIVERSITE DU MANITOBA, WINNIPEG, MANITOBA, CANADA, R3T 2N2.

Figure 28. Faint banding of the leucogranite in the Eaglenest Lake intrusion is indicative of an incipient transition of the leucogranite to a sodic aplite. Late crystallizing potassic pegmatite crosscuts the leucogranite structure (ENL-3). Compass is 10 cm long.

and leucogranite. This latter facies appears to be highly potassic, containing abundant, randomly oriented muscovite. In the former facies, muscovite tends to be slightly to distinctly aligned. Thin section observation indicates no evidence of metamorphic deformation to cause this alignment. The leucogranite is accompanied by the distinct conical (plumose) form of muscovite (Figure 17).

The most dominant facies is the pegmatitic leucogranite. The large potassium feldspar megacrysts (20-30 cm) do not, on average, attain the dimensions reached in the pegmatitic leucogranite facies of the other (especially OL and GL) intrusions; however, no systematic data were taken to accurately compare the grain size of feldspars among the intrusions. Very coarse biotite (2-3 cm) is present along with the plumose muscovite + quartz intergrowths. Sodic aplite is well represented in the ENL intrusion; however, it tends to be located mainly near and parallel to the contacts of the intrusions (Figure 18). The central area of the stock hosts very little sodic aplite or potassic pegmatite facies and it is mostly composed of the pegmatitic leucogranite, leucogranite, or their hybrid forms. The sodic aplite appears to be relatively potassium-rich, contains abundant muscovite, and often is hybridized, containing a relatively abundant concentration of potassium feldspar crystals. The sodic aplites of this intrusion are unique in that they contain few garnet crystals. Banding in these

aplites results from alignment of the muscovite, not garnet crystals (Figure 18).

The potassic pegmatite facies forms pods and bands adjacent to sodic aplite. Figure 19 illustrates an excellent example of the sodic aplite to potassic pegmatite facies relationship. The club-shaped potassium feldspar crystals grow from the sodic-potassic interface. Thin section observation suggests that this is an abrupt contact (Figure 29) where crystal growth within sodic aplite at the sodic aplite-potassic pegmatite interface has not been terminated but has continued at a greatly increased rate as a result of changing external stimuli and fluid composition.

The potassic pegmatite facies illustrates cross-cutting relationships with respect to the other facies indicating that it crystallized last (Figure 27, 28). No accessory mineralization was observed to be associated with this or any other facies within this intrusion.

3. Osis Lake Intrusion

The facies composition of the Osis Lake pegmatitic granite is substantially more complex than those of the previous two intrusions. It is quite spectacular with respect to intrusion style, the interrelationships of the four facies, the east-west regional zonation within the intrusion, and its variation in colour and mineralization.

Although all outcrops of the pegmatitic granite are

NOTICE/AVIS

PAGE(S)/IS/ARE/EST/SONT 80 color photo

PLEASE WRITE TO THE AUTHOR FOR INFORMATION, OR CONSULT THE ARCHIVAL COPY HELD IN THE DEPARTMENT OF ARCHIVES AND SPECIAL COLLECTIONS, ELIZABETH DAFOE LIBRARY, UNIVERSITY OF MANITOBA, WINNIPEG, MANITOBA, CANADA, R3T 2N2.

VEUILLEZ ECRIRE A L'AUTEUR POUR LES RENSEIGNEMENTS OU VEUILLEZ CONSULTER L'EXEMPLAIRE DONT POSSEDE LE DEPARTEMENT DES ARCHIVES ET DES COLLECTIONS SPECIALES, BIBLIOTHEQUE ELIZABETH DAFOE, UNIVERSITE DU MANITOBA, WINNIPEG, MANITOBA, CANADA, R3T 2N2.

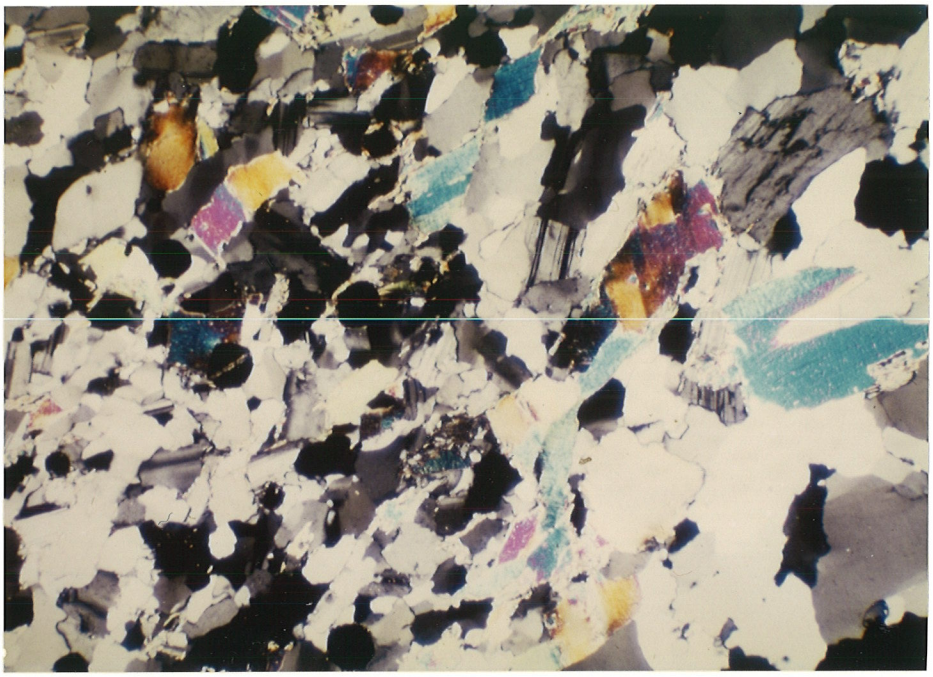

Figure 29. Photomicrograph of the contact of sodic aplite with potassic pegmatite in Figure 36. Note the contact shows no crosscutting relationships; crystals grow directly from the surface of pre-existing minerals.

discontinuous at the present erosional level, they all contain identical mineralogy and texture. The eastern portion is predominantly a white to pink massive medium to coarse-grained (0.5-1.0 cm) muscovite leucogranite containing no inclusions. The leucogranite is a hypidiomorphic granular granite with 5 percent coarse pegmatitic pods containing blocky K-feldspar + muscovite + quartz (potassic pegmatite facies). The sodic aplite facies is quite rare. Garnet and tourmaline are noticeably absent. In the eastern extremities very minor biotite accompanies the muscovite, and arsenopyrite is a common accessory mineral throughout this intrusion. This coarse-grained leucogranite is the predominant facies in the east; however, the sodic aplite and potassic pegmatite facies become increasingly abundant in a westward direction.

At the position just west of the western shore of Booster Lake (sample locations 23, 23(a), 23(b), and 23(c), Figure 8), a facies unique to the Osis Lake pegmatitic granite appears. It is a central plug of grey, biotitic granite illustrating classic subsolvus granitic hypidiomorphic granular texture (Figure 30). It is extremely homogeneous with random orientation of all minerals. The grain size is approximately 0.3 cm. Minor amounts of apatite are observed in thin section; tourmaline and garnet are absent. A fibrous muscovite (possibly after sillimanite) plus minor tourmaline occur in the contact zone (Figure 31).

NOTICE/AVIS

PAGE(S) 82+83 IS/ARE EST/SONT color photos

PLEASE WRITE TO THE AUTHOR FOR INFORMATION, OR CONSULT THE ARCHIVAL COPY HELD IN THE DEPARTMENT OF ARCHIVES AND SPECIAL COLLECTIONS, ELIZABETH DAFOE LIBRARY, UNIVERSITY OF MANITOBA, WINNIPEG, MANITOBA, CANADA, R3T 2N2.

VEUILLEZ ECRIRE A L'AUTEUR POUR LES RENSEIGNEMENTS OU VEUILLEZ CONSULTER L'EXEMPLAIRE DONT POSSEDE LE DEPARTEMENT DES ARCHIVES ET DES COLLECTIONS SPECIALES, BIBLIOTHEQUE ELIZABETH DAFOE, UNIVERSITE DU MANITOBA, WINNIPEG, MANITOBA, CANADA, R3T 2N2.

Figure 30. Fine-grained biotite leucogranite which forms the central plug of the Osis Lake pegmatitic granite (OL-23). This central plug is unique to the Osis Lake intrusion.

Figure 31. Radiating fractures at the edge of the central biotite granite of the Osis Lake intrusion (OL-23). These fractures are usually filled with muscovite and some carry tourmaline (dark crystal aggregate in the centre of the vein).

West of this central plug towards Mud Lake through a gradational contact, the pegmatitic leucogranite facies begins to become quite dominant. Sodic aplite and potassic pegmatite facies also occur more frequently and eventually replace the fine-grained leucogranite facies westward.

Also located here in the coarser-grained leucogranite is a pod of potassic pegmatite containing a second occurrence of fibrous muscovite (Figure 32). An analysis of this mineral is in Appendix 4 (muscovite sample OL-16). It is apparently secondary after an original accessory mineral of the potassic pegmatite facies possibly spodumene or sillimanite. The presence of remaining relicts of the primary mineral could not be confirmed by X-ray diffraction.

Also in this area, west of the central plug, a dramatic change in mineralogy of the intrusion occurs. Tourmaline appears first as a trace mineral and increases westward until, in the western tip of the intrusion, it becomes a subordinate but decidedly rock-forming mineral of the pegmatitic leucogranite facies (Figure 21). Garnet tends to parallel this westward increase but not to such extremes. Grain size also increases until, in the western tip, potassium feldspar blocks reach sizes up to 200 cm (Figure 23). West of sample location 38 (Figure 8) the pods of potassic pegmatite in the pegmatitic leucogranite show signs of more extreme enrichment. Mineralization in excess of the usual K-feldspar + muscovite + quartz appears.

NOTICE/AVIS

PAGE(S) 85 IS/ARE/EST/SONT color photo

PLEASE WRITE TO THE AUTHOR FOR INFORMATION, OR CONSULT THE ARCHIVAL COPY HELD IN THE DEPARTMENT OF ARCHIVES AND SPECIAL COLLECTIONS, ELIZABETH DAFOE LIBRARY, UNIVERSITY OF MANITOBA, WINNIPEG, MANITOBA, CANADA, R3T 2N2.

VEUILLEZ ECRIRE A L'AUTEUR POUR LES RENSEIGNEMENTS OU VEUILLEZ CONSULTER L'EXEMPLAIRE DONT POSSEDE LE DEPARTEMENT DES ARCHIVES ET DES COLLECTIONS SPECIALES, BIBLIOTHEQUE ELIZABETH DAFOE, UNIVERSITE DU MANITOBA, WINNIPEG, MANITOBA, CANADA, R3T 2N2.

Figure 32. Fibrous muscovite occurring in the centre of a potassic pegmatite pod in the Osis Lake intrusion. This is the only occurrence noted throughout all intrusions and is suspected to be secondary after spodumene (?) or sillimanite (OL-36).

Notably present is ferrisicklerite - $Li(Fe,Mn)PO_4 \cdot nFe^{+3}PO_4$ (an alteration product of triphylite - $Li(Fe,Mn)PO_4$ (Figure 22(a), (b)) and rare blades of Nb,Ta oxide minerals. In addition to these two accessory minerals, the quartz pods become faintly pinkish.

The sodic aplite in this area of the intrusion is quite abundant and, as in all the Winnipeg River pegmatitic granites, it is associated with areas of potassic pegmatite within the pegmatitic leucogranite. The sodic aplite is still banded; however, now the banding is a result of either garnet and/or tourmaline alignment.

As mentioned earlier, alteration of the hosting sediments becomes quite extreme as the intrusion begins to finger out into the metasediments as dike-like apophyses in the western tip. Figure 33 illustrates the dilated metasediments tourmalinized along the boron-rich pegmatitic granite.

4. Greer Lake Intrusion

The most extensively studied of the four intrusions is the Greer Lake pegmatitic granite. The leucogranite facies is situated throughout the intrusion in pod-like accumulations. It tends to be coarser-grained (0.5-1.0 cm) than the same facies in the other intrusions and it grades directly into the pegmatitic leucogranite facies. It is garnetiferous, contains no biotite, and hosts occurrences of the plumose form of muscovite that is common in the Osis

NOTICE/AVIS

PAGE(S) 87 IS/~~ARE~~ EST/~~SONT~~ color photo

PLEASE WRITE TO THE AUTHOR FOR INFORMATION, OR CONSULT THE ARCHIVAL COPY HELD IN THE DEPARTMENT OF ARCHIVES AND SPECIAL COLLECTIONS, ELIZABETH DAFOE LIBRARY, UNIVERSITY OF MANITOBA, WINNIPEG, MANITOBA, CANADA, R3T 2N2.

VEUILLEZ ECRIRE A L'AUTEUR POUR LES RENSEIGNEMENTS OU VEUILLEZ CONSULTER L'EXEMPLAIRE DONT POSSEDE LE DEPARTEMENT DES ARCHIVES ET DES COLLECTIONS SPECIALES, BIBLIOTHEQUE ELIZABETH DAFOE, UNIVERSITE DU MANITOBA, WINNIPEG, MANITOBA, CANADA, R3T 2N2.

Figure 33. Symmetrical zoning of a potassic pegmatite band, confined by tourmalinized schist screens on the left-hand side of the photograph, extends to the right where the screens have been reduced to barely visible trains of tourmaline crystals. Note exfoliation of tourmalinized metasediments. Photograph from western end of the Osis Lake intrusion.

Lake intrusion. The pegmatitic leucogranite contains large megacrysts (5-100 cm) of graphic K-feldspar + quartz in the quartz + muscovite + plagioclase matrix. The muscovite in this facies, as a rule, is both the platy and plumose type. There appears to be no regularity in the distribution of the potassium leucogranite and the leucogranite facies within the Greer Lake stock. No accessory minerals have been observed in either facies.

The sodic aplite facies is randomly oriented throughout the intrusion. These rhythmic bands of plagioclase and garnet are in contact with the potassic pegmatite facies. The sodic aplite bands vary in size from one centimetre to several metres in length and can be continuous over this distance or they can be fragmented (Figure 34). This facies occasionally hosts gahnite and/or Nb,Ta oxide minerals as accessory minerals but not in any significant proportions ($<$ 0.001 percent). Different stages in the formation of the sodic aplite facies can be observed. An incomplete separation of the sodic and potassic phases is common; crystallization results in an impure (potassic) sodic aplite (Figure 35) where potassium feldspar phenocrysts are situated within the incipient sodic aplite facies. The rate of crystallization apparently was too rapid, preventing complete segregation of the sodic and potassic phases.

As observed, the potassic pegmatite facies is not always completely separated from the sodic aplite facies.

NOTICE/AVIS

PAGE(S) 89+90 ~~IS~~/ARE ~~EST~~/SONT color photos

PLEASE WRITE TO THE AUTHOR FOR INFORMATION, OR CONSULT THE ARCHIVAL COPY HELD IN THE DEPARTMENT OF ARCHIVES AND SPECIAL COLLECTIONS, ELIZABETH DAFOE LIBRARY, UNIVERSITY OF MANITOBA, WINNIPEG, MANITOBA, CANADA, R3T 2N2.

VEUILLEZ ECRIRE A L'AUTEUR POUR LES RENSEIGNEMENTS OU VEUILLEZ CONSULTER L'EXEMPLAIRE DONT POSSEDE LE DEPARTEMENT DES ARCHIVES ET DES COLLECTIONS SPECIALES, BIBLIOTHEQUE ELIZABETH DAFOE, UNIVERSITE DU MANITOBA, WINNIPEG, MANITOBA, CANADA, R3T 2N2.

Figure 34. Bands of garnetiferous sodic aplite broken and cemented by impure potassic pegmatite facies from the Greer Lake intrusion. This indicates that the potassic pegmatite facies was the last to solidify. See Figure 28 also.

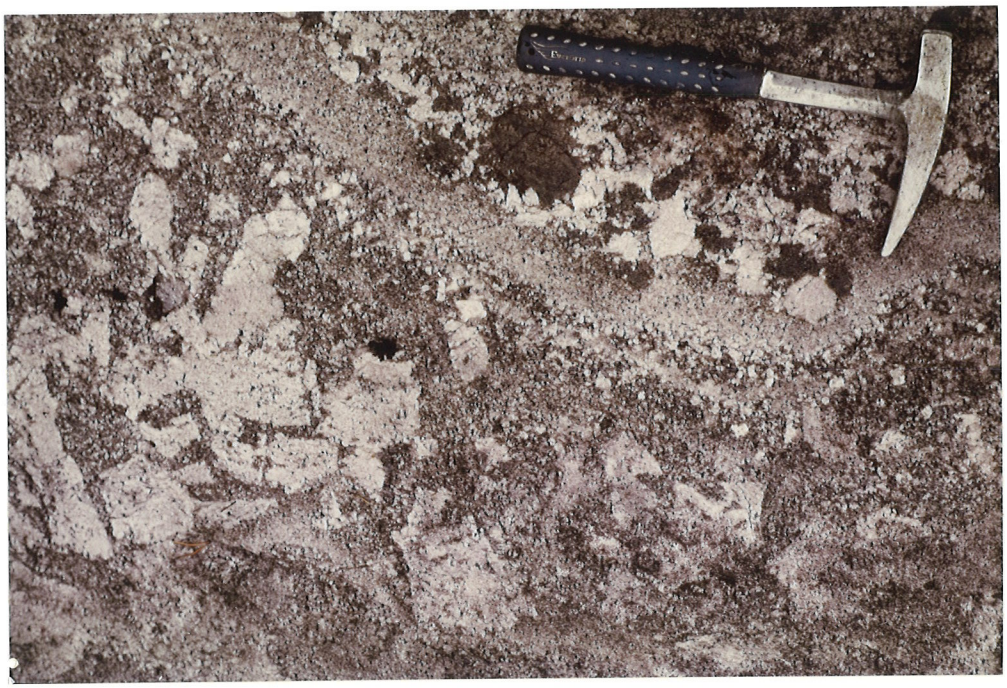

Figure 35. Incomplete segregation of the sodic aplite and potassic pegmatite facies. Small K-feldspar crystals are seen on the top side of the band of predominantly albite + garnet. Several crystals can still be seen within the incipient sodic aplite (GL-9).

It most commonly occurs as pods within the leucogranite and/or pegmatitic leucogranite or as bands adjacent to the sodic aplite facies. Figure 36 indicates the sharp contact between these two facies while Figure 29 is a microphotograph of the same contact illustrating that the potassic pegmatite facies begins continuous crystallization directly onto pre-existing crystals of the sodic aplite and vice versa.

The potassic pegmatite facies of this intrusion tends to be considerably enriched in accessory minerals with respect to the same facies in any of the other three intrusions. Accessory beryl, gahnite, and Nb,Ta oxide minerals are relatively common in the quartz-rich centres of the pods or bands. Three occurrences of these mineralized pods are quite unique as discussed below.

C. MINERALIZED POTASSIC PEGMATITE PODS

Several occurrences of mineralized potassic pegmatite pods are known, and all are located within the Greer Lake stock. The mineralogy contained in these pods suggests a high concentration of rare elements (Li, Rb, Cs, Be, Nb,Ta, etc.) and volatile agents (F, H_2O), and more advanced fractionation trends than those of the potassic pegmatite facies in other locations (either within this intrusion or in the other three stocks of pegmatitic granite). Besides several minor occurrences along the northern margin and inside the GL intrusion, the three most diversified pods are located in

NOTICE/AVIS

PAGE(S) 92 IS/ARE EST/SONT color photo

PLEASE WRITE TO THE AUTHOR FOR INFORMATION, OR CONSULT THE ARCHIVAL COPY HELD IN THE DEPARTMENT OF ARCHIVES AND SPECIAL COLLECTIONS, ELIZABETH DAFOE LIBRARY, UNIVERSITY OF MANITOBA, WINNIPEG, MANITOBA, CANADA, R3T 2N2.

VEUILLEZ ECRIRE A L'AUTEUR POUR LES RENSEIGNEMENTS OU VEUILLEZ CONSULTER L'EXEMPLAIRE DONT POSSEDE LE DEPARTEMENT DES ARCHIVES ET DES COLLECTIONS SPECIALES, BIBLIOTHEQUE ELIZABETH DAFOE, UNIVERSITE DU MANITOBA, WINNIPEG, MANITOBA, CANADA, R3T 2N2.

Figure 36. Sharp contact between banded garnetiferous aplite and potassic pegmatite (GL-20); note the growth fabric in the K-feldspar + quartz + muscovite assemblage normal to the boundary.

the south. Two of these localities are the Annie Claim (AC-1,2 and 3) and the Lobe occurrences. Both these showings are located along the southern margin of the intrusion, the former on the Annie Claim and the latter on the Rapid Claim. A third showing is the Silverleaf occurrence (Figure 12), located on the Silverleaf Claim approximately 500 metres south of the western end of the Greer Lake intrusion. This pod could be described as a distinctly separate pegmatite dike; however, since its location, intrusive style, mineralogy, texture, and geochemistry relate very closely to the main Greer Lake intrusion and its contained AC-3 pod, it is considered to be an apophyse of this main mass of pegmatitic granite.

1. GL-30

This is a potassic pegmatite pod on a small island in the Winnipeg River approximately five metres from the north shore (and assumed contact) of the Greer Lake pegmatitic granite (Figure 12). It is thought to be an apophyse extending from the main intrusion into the Lamprey Falls metabasalts. There are several reasons for this interpretation. There is no connection of the GL-30 location with the main Greer Lake intrusion at the present erosional surface. The mineral geochemistry of this location and that of the Greer Lake intrusion will be shown to be virtually identical. This location hosts the only blue beryl minerali-

zation of the Greer Lake pegmatitic granite (Figure 37, 38). It also hosts abundant Nb,Ta oxide mineralogy and possibly minor lithian muscovite surrounding these beryl crystals. This muscovite could not be separated and cleaned, thus no analysis was obtained.

2. GL-37

This location is in the main Greer Lake intrusion adjacent to the northern contact (Figure 12). It is not a particularly highly enriched pod of potassic pegmatite, as it contains only minor beryl; however, it hosts the only occurrence of garnet + biotite + chlorite pseudomorphing cordierite (Figure 57) found in the northern half of the Greer Lake intrusion.

3. Zone-5

Zone-5 (as designated by Dalhart Beryllium's 1958 survey of the pegmatites in the Greer Lake area) is located near the southwest corner of the Greer Lake intrusion 100 metres north of the shear zone that passes along the southern contact of the intrusion (Figure 12). Mineralogically, it is not significant containing only K-feldspar + quartz + muscovite (curved) ± cleavelandite with no evidence of accessory rare element mineralization. It is noteworthy because it is an unusually large (10 to 15 m^2) area of coarse-grained (0.5 to 1.0 m) potassic pegmatite containing

NOTICE/AVIS

PAGE(S) 95+96 IS/ARE EST/SONT color photos

PLEASE WRITE TO THE AUTHOR FOR INFORMATION, OR CONSULT THE ARCHIVAL COPY HELD IN THE DEPARTMENT OF ARCHIVES AND SPECIAL COLLECTIONS, ELIZABETH DAFOE LIBRARY, UNIVERSITY OF MANITOBA, WINNIPEG, MANITOBA, CANADA, R3T 2N2.

VEUILLEZ ECRIRE A L'AUTEUR POUR LES RENSEIGNEMENTS OU VEUILLEZ CONSULTER L'EXEMPLAIRE DONT POSSEDE LE DEPARTEMENT DES ARCHIVES ET DES COLLECTIONS SPECIALES, BIBLIOTHEQUE ELIZABETH DAFOE, UNIVERSITE DU MANITOBA, WINNIPEG, MANITOBA, CANADA, R3T 2N2.

Figure 37. GL-30 pegmatite pod on the north side of the Greer Lake intrusion. Note the abundant beryl mineralization which has been slightly to completely altered to muscovite zinnwaldite. Nb, Ta oxide mineralization (columbite-tantalite) is evident. Albitization at this locality is fairly intense (Figure 38).

Figure 38. Albitization at the GL-30 location. Blocky K-feldspar (pink) crystal is being corroded by albite + quartz which hosts the beryl and Nb,Ta oxide mineralization. Note alteration of beryl.

abundant curved muscovite ± cleavelandite. This zone is slightly more fractionated than the average potassic pegmatite facies of the intrusion as reflected by the mineral chemistry.

4. Lobe

The Lobe area on the Rapid Claim is a small apophyse of pegmatitic granite extending from the main body of the Greer Lake granite south into the basalts of the Lamprey Falls formation (Figure 12). This area is slightly enriched mineralogically and geochemically, relative to the main intrusion of pegmatitic granite to the north. It exhibits mainly the pegmatitic leucogranite facies; however, areas of sodic aplite (10 to 20 percent) and an above-average number of contained potassic pegmatitic pods exist. In these pods, beryl and Nb,Ta oxide minerals are commonly found. This is also one of the few locations in all four intrusions in the potassic pegmatitic facies where pseudomorphs after cordierite are found (Figure 39). The sodic aplite is highly garnetiferous. It contains rare Nb,Ta oxide minerals but no Li mineralization; however, the zinc spinel, gahnite, is present.

5. Annie Claim

The Annie Claim locations are approximately 300 metres west of the Lobe area within the Greer Lake pegmatitic granite on the extreme southern side (Figure 12). This

NOTICE/AVIS

PAGE(S) 98 IS/ARE EST/SONT color photo

PLEASE WRITE TO THE AUTHOR FOR INFORMATION, OR CONSULT THE ARCHIVAL COPY HELD IN THE DEPARTMENT OF ARCHIVES AND SPECIAL COLLECTIONS, ELIZABETH DAFOE LIBRARY, UNIVERSITY OF MANITOBA, WINNIPEG, MANITOBA, CANADA, R3T 2N2.

VEUILLEZ ECRIRE A L'AUTEUR POUR LES RENSEIGNEMENTS OU VEUILLEZ CONSULTER L'EXEMPLAIRE DONT POSSEDE LE DEPARTEMENT DES ARCHIVES ET DES COLLECTIONS SPECIALES, BIBLIOTHEQUE ELIZABETH DAFOE, UNIVERSITE DU MANITOBA, WINNIPEG, MANITOBA, CANADA, R3T 2N2.

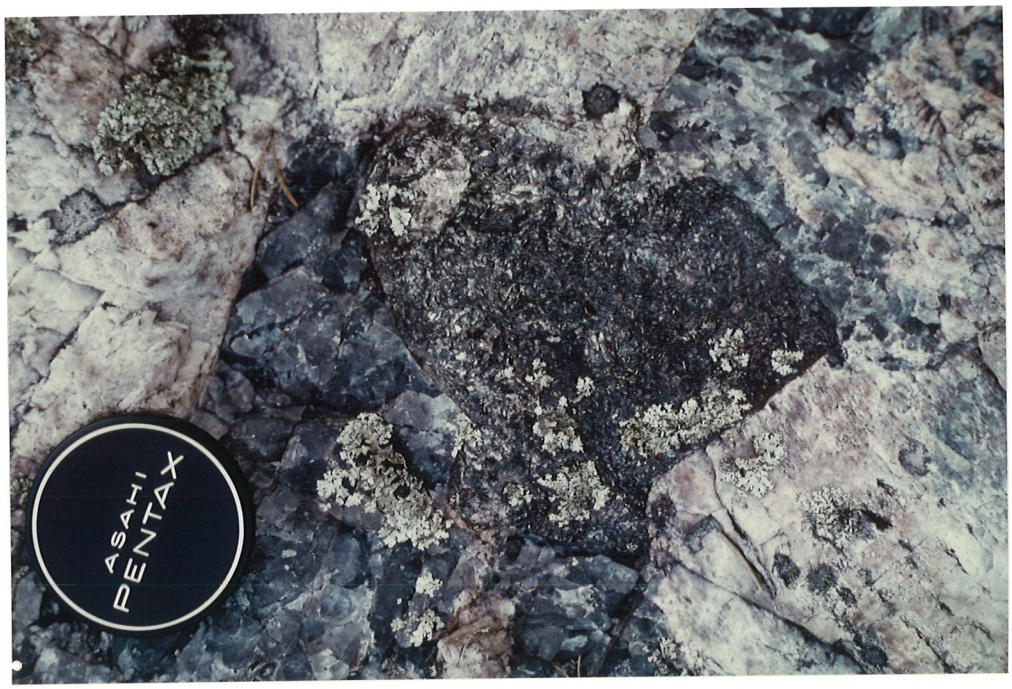

Figure 39. Cordierite pseudomorph from a potassic pegmatite pod from the Lobe location of the Greer Lake pegmatitic granite. See Figure 57 also.

Claim consists of four pods (GL-4, AC-1, 2, and 3). Contacts of these blebs of potassic pegmatite with the enclosing pegmatitic granite are gradational (Figure 40) and evolve through an increase in grain size and a decrease in the amount of muscovite. The textures of this transitional zone suggest a slow gradual crystallization from the surrounding pegmatitic granite inwards. The pods suggest a geochemical enrichment westward (GL-4 → AC-1 → AC-2 → AC-3). GL-4 is an area of mostly garnetiferous aplite with very minor beryl and Nb,Ta oxide mineralization. AC-1 contains more potassic pegmatite facies with minor Nb,Ta oxide minerals, beryl, and smoky quartz. AC-2 hosts late curvilamellar lithian muscovite, beryl, sphalerite, Nb,Ta oxide minerals, and dark smoky quartz. AC-3 is the most enriched pod. It contains the mineral assemblage listed in Table 7 including abundant curvilamellar lithian muscovite, green and purple lithian muscovite, and cleavelandite. The distance from GL-4 through AC-1 and AC-2 to AC-3 is approximately 30 metres. Consequently their locations are shown collectively in Figure 12 as location AC.

6. Silverleaf

The Silverleaf occurrence is located approximately 500 metres southwest of the Annie Claim. It has been described (Wright, 1932; Stockwell, 1933; Davies, 1957; Černý and Turnock, 1971) as consisting mainly of garneti-

Table 7. Mineralogy of the Winnipeg River pegmatitic granites

	K-Feldspar-Microcline	Plagioclase-Albite	Cleavelandite	Quartz	Biotite	Muscovite	Li-Muscovite (curved)	Green	Purple	Spodumene	Cordierite	Garnet	Schorl	Topaz	Zircon	Apatite	Ilmenite	Gahnite	Cassiterite	Columbite/Tantalite	Pseudoixiolite	Wodginite	Microlite	Monazite	Molybdenite	Sphalerite	Arsenopyrite	Beryl	Triphilite/Lithiophilite	Amblygonite/Montebrasite	Spodumene + Quartz
GL	+	+		+		+					(0)	A			X			X		X				X				X			
GL-30	+	+		+		+						A			X					X								X			
Lobe	+	+		+		+					(0)	A			X					X								X			
GL-4	+	+		+		+						A			X			X		X								X			
AC-1	+	+		+		+	X					A			X					X								X			
AC-2	+	+	+	+		+	A					A			X					X	0	0				0		X			
AC-3	+		+	+		+	A	A	A			A			X				[0]	X								X			
Silverleaf	+		+	+		+	A		A	A		A	X	0	X		0	X	X	X				X				X	X	X	X
ENL	+	+		+		+						A			X			X													
ENL-11	+	+		+		+						A			X			X		X											
TNL-main	+	+		+	+	A					(X)	A	0		X	0									0						
TNL-south	+	+		+	+	A						A			X																
TNL-east	+	+		+	A	+						X			X																
OL-east	+	+		+	A	+						X	X		X	X											X				
OL-west	+	+		+		+						A	A		X	0		0		0							X		X		

Rock-forming - +; accessory - A; rare - X; singular occurrence - 0;
pseudomorph - ( ); reported - [ ].

NOTICE/AVIS

PAGE(S) 101 IS/ARE EST/SONT color photo

PLEASE WRITE TO THE AUTHOR FOR INFORMATION, OR CONSULT THE ARCHIVAL COPY HELD IN THE DEPARTMENT OF ARCHIVES AND SPECIAL COLLECTIONS, ELIZABETH DAFOE LIBRARY, UNIVERSITY OF MANITOBA, WINNIPEG, MANITOBA, CANADA, R3T 2N2.

VEUILLEZ ECRIRE A L'AUTEUR POUR LES RENSEIGNEMENTS OU VEUILLEZ CONSULTER L'EXEMPLAIRE DONT POSSEDE LE DEPARTEMENT DES ARCHIVES ET DES COLLECTIONS SPECIALES, BIBLIOTHEQUE ELIZABETH DAFOE, UNIVERSITE DU MANITOBA, WINNIPEG, MANITOBA, CANADA, R3T 2N2.

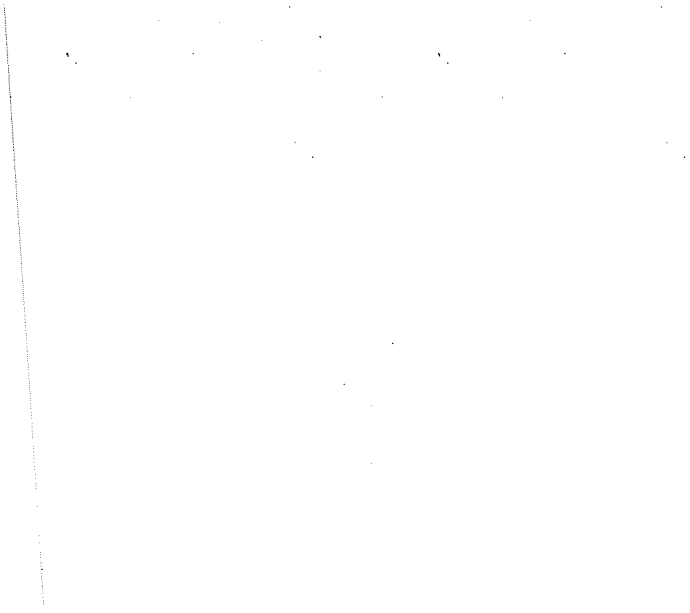

Figure 40. Gradual transition from the pegmatitic leucogranite facies in the lower right of the photograph, into the mineralized pod of potassic pegmatite facies of AC-2. This pod contains garnet, beryl, and Nb,Ta oxide minerals including the only known occurrence of wodginite. Located on the Annie Claim-Greer Lake pegmatitic granite.

ferous sodic aplite containing a large pod of Li-Rb-Mn-Nb-Ta-Sn-enriched pegmatitic assemblages. It exhibits a distinct vertical zoning. The lower portion of the stock is banded garnetiferous sodic aplite with a coarse potassium feldspar, cleavelandite, lithium silicate and phosphate zone; above this there is a coarse quartz, cleavelandite, and muscovite zone, capped in turn by the sodic aplite.

The Silverleaf intrusion is remote from the main GL pegmatitic granite at the present erosional level and appears to be a subvertical dike, crosscutting the vertically foliated east-west trending metavolcanics of the Lamprey Falls formation. A coarse-grained Li-enriched core is surrounded by fine-grained aplite. The mineralogy known from the Silverleaf pegmatitic bleb is listed in Table 7.

Chapter V

DESCRIPTIVE MINERALOGY

A. GENERAL INTRODUCTION

Detailed mineralogical studies were not carried out since this was not the purpose of the present study. However, the mineralogical data discussed here were obtained to allow comparison of compositional and structural data on the mineral species among the individual intrusions of pegmatitic granite, and with characteristics of the same minerals in their respective pegmatite aureoles. These latter data have been previously reported by Černý et al. (1981).

B. ROCK FORMING MINERALS

1. Blocky K-Feldspar

a) Occurrence. Blocky K-feldspar, K(Na,Rb,Cs,Ca)$AlSi_3O_8$, is the coarse (> 3 cm) potassium feldspar found only in the potassic pegmatite facies of all Winnipeg River pegmatitic granites. Except the ubiquitous perthitic albite, this K-feldspar usually shows only very minor plagioclase in veinlets or as isolated grains.

b) Chemistry. One hundred and twenty seven samples of blocky K-feldspar from all four intrusions were analyzed for Li, Na, K, Rb, Cs, Ca, and Pb. The

analyses are tabulated in Appendix 2. The calculated arithmetic means of contents and ratios of geochemically significant elements in the blocky K-feldspar are listed in Table 8. Figure 41 is an Ab-Or-An plot based on K, Na, Rb, and Ca, recalculated on the assumption of ideal stoichiometry to Ab + Or + An = 100, which illustrates the composition of the K-feldspar within each intrusion.

c) X-ray Studies. The obliquity was determined by the relative position of the (131) and $(1\bar{3}1)$ feldspar diffractions as related by the following equation:

$$\text{Obliquity} = 12.5\ (d(131) - d(1\bar{3}1))$$

In this equation obliquity is the measure of the degree of deviation of the feldspar structure from monoclinic symmetry. The two extreme measures of obliquity are 0 and 1. Therefore, when the obliquity = 0, the feldspar crystal has a monoclinic structure; when it is = 1, the feldspar has the largest triclinic deviation from monoclinic symmetry. This change in the structure from monoclinic to triclinic is caused by the ordering of the Si and Al in the tetrahedral sites. The obliquity values for the blocky K-feldspar of the pegmatitic granites are listed in Table 9 and plotted in Figure 42.

Microcline solid solution studies were also

Table 8. Calculated averages of the blocky K-feldspar analyses and significant geochemical ratios

	Eaglenest Lake	Greer Lake	Osis Lake	Tin Lake	Tin Lake E. Ext'n	GL Mineralized Pods
K_2O	12.02	11.89	12.15	12.06	12.70	12.86
Na_2O	3.13	3.05	2.97	2.96	2.92	2.69
CaO	0.06	0.03	0.09	0.08	0.05	0.03
Rb_2O	0.22	0.21	0.08	0.07	0.08	0.60
Cs_2O	0.0073	0.0045	0.0022	0.0012	0.0029	0.0167
Li_2O	0.0079	0.0058	0.0036	0.0041	0.0026	0.0062
PbO	0.0039	0.0034	0.0029	0.0034	0.0043	0.0016
K	9.98	9.88	10.09	10.01	10.50	10.70
Na	2.32	2.26	2.20	2.20	2.17	1.85
Ca	0.04	0.02	0.07	0.06	0.04	0.02
Rb	0.202	0.188	0.072	0.066	0.076	0.547
Cs	0.0068	0.0042	0.0020	0.0012	0.0027	0.0157
Li	0.0037	0.0026	0.0017	0.0019	0.0012	0.0029
Pb	0.0036	0.0032	0.0027	0.0032	0.0040	0.0015
K/Rb	50	53	140	151	138	20
Rb/Cs	30	21	36	55	28	35
K/Cs	1455	2352	5045	8342	3889	628

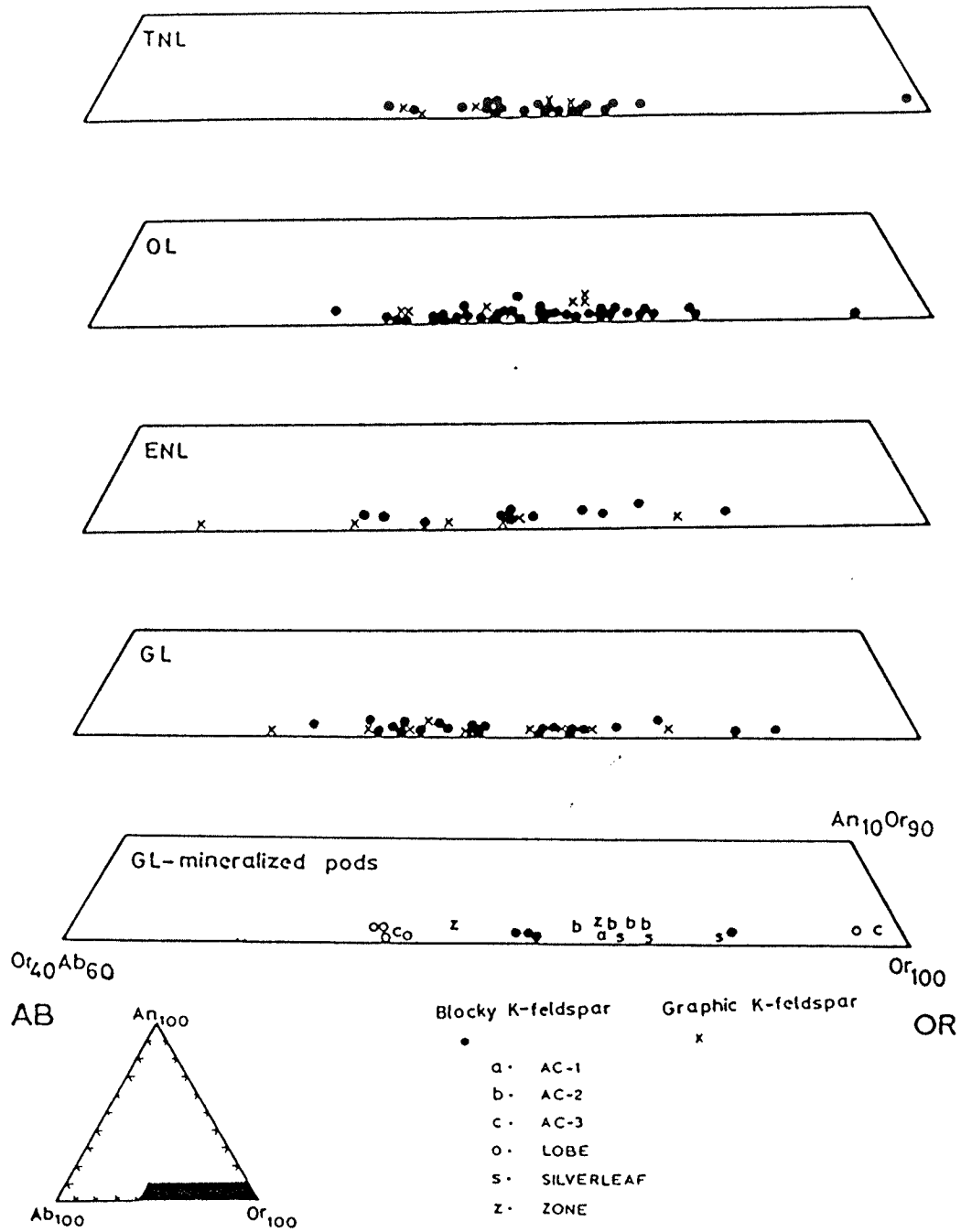

Figure 41. Ab-Or-An diagrams of blocky and graphic K-feldspar from all intrusions. All samples are from the potassic pegmatite facies. Samples from the mineralized pods of the Greer Lake intrusion are from pods of potassic pegmatite containing accessory beryl, Nb,Ta oxide mineralization etc.

Table 9. Obliquity - blocky K-feldspars

Sample No.	Obliquity	Sample No.	Obliquity	Sample No.	Obliquity
TNL-1	0.99	OL-25	0.93	GL-15	0.98
TNL-4	0.98	OL-27	0.81	GL-17(b)	1.00
TNL-6	0.90	OL-28	0.65	GL-19	0.96
TNL-8	0.91	OL-30	0.83	GL-19-1	0.95
TNL-10	0.93	OL-31	0.84	GL-19-2	1.00
TNL-12	0.96	OL-32	0.94	GL-19-3	0.94
TNL-14	0.98	OL-33	0.95	GL-20(a)	0.98
TNL-16	1.00	OL-34	1.00	GL-21	0.98
TNL-18	1.00	OL-35	0.90	GL-22(a)	0.95
TNL-23	0.94	OL-36	0.88	GL-24	1.00
TNL-26	1.00	OL-37	0.90	GL-26	0.99
TNL-29	0.95	OL-38	0.81	GL-28	0.94
TNL-30	0.95	OL-39	0.90	GL-30-1	0.95
TNL-32	0.99			GL-30-2	0.96
TNL-35	0.94	Average	0.89	GL-32	0.94
TNL-37	1.00			GL-35(c)	0.96
TNL-38	0.95			GL-36(b)	0.99
TNL-40	0.96	ENL-1	0.96	GL-37(d)	0.98
		ENL-2	1.00	GL-38	0.98
Average	0.97	ENL-3(a)-1	0.86	GL-41	0.94
		ENL-5	0.96	GL-46(b)	0.94
		ENL-6	0.94		
OL-1	0.94	ENL-7	0.96	Average	0.97
OL-4	0.89	ENL-9	0.96		
OL-5	0.99	ENL-10-3	0.95		
OL-6	0.78	ENL-10-6	0.99	AC-1	1.00
OL-7	0.95	ENL-10-9	0.94	AC-2(a)	0.93
OL-8	0.91	ENL-22(d)	0.98	AC-2(b)	0.96
OL-9	0.94	ENL-23(d)	0.99	AC-2(c)	0.98
OL-11	0.86	ENL-27(a)	0.95	AC-2(d)	0.99
OL-12	0.91	ENL-31(a)	0.94	AC-3(a)	1.00
OL-13	0.89			AC-3(b)	0.95
OL-14	0.83	Average	0.96	Average	0.99
OL-15	0.78				
OL-16	0.83			GL-4(f)	0.95
OL-17	0.83	GL-6	1.00		
OL-18	0.81	GL-9	0.95	Zone-5-4	1.00
OL-19	0.84	GL-11(e)	0.91	Zone-5-5	1.00
OL-20	1.00	GL-12	0.93	Average	1.00
OL-21	0.74	GL-13	0.96		
OL-22	0.93	GL-14	0.99	Lobe-5	1.00
OL-24	0.98			Lobe-11	0.95
				Lobe-13	0.96
				Lobe-17	0.95
				Average	0.97

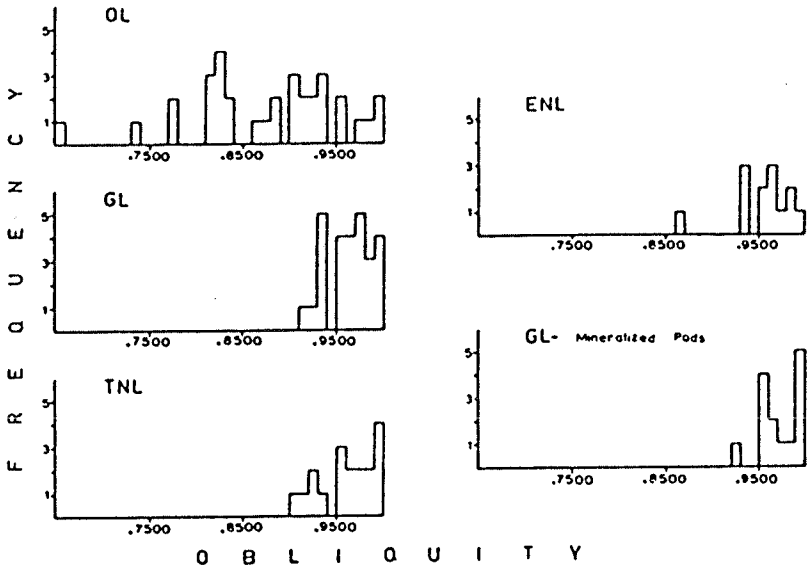

Figure 42. Obliquity of blocky K-feldspar from the potassic pegmatite facies of the four intrusions of pegmatitic granite.

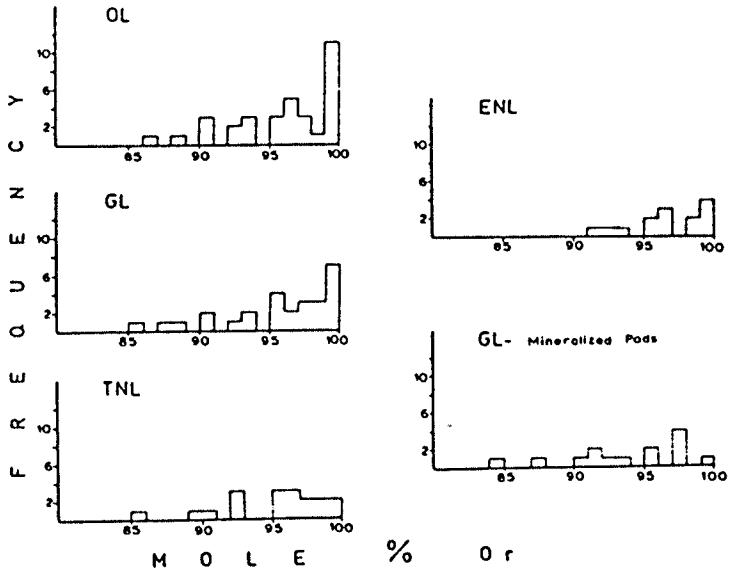

Figure 43. The Or content, indicative of the residual (Ab + An) solid solution, in the K-feldspar phase of microcline - perthite in the four intrusions of pegmatitic granite in the Winnipeg River area.

undertaken to determine the amount of plagioclase solid solution (Ab + An) residual in the K-feldspar phase of microcline-perthite. The $KBrO_3$ method of Bowen and Tuttle in Orville (1967) was used to estimate the amount (mole percent) of the Or molecule in the microcline structure. Results are shown in Figure 43.

2. Graphic K-Feldspar + Quartz

a) Occurrence. Graphic K-feldspar occurs only in the pegmatitic leucogranite facies of the Winnipeg River pegmatitic granites. It is found as coarse euhedral blocks (3-200 cm) of graphic K-feldspar + quartz intergrowths in a quartz + plagioclase + muscovite matrix. There is no significant alteration of this feldspar. The size of the quartz rods varies directly with the size of the hosting feldspar crystal, ranging from 1.0 mm to 1.5 cm.

b) Chemistry. Twenty eight samples of graphic K-feldspar + quartz were analyzed for the alkali elements, plus Ca and Pb. The analyses are listed in Appendix 3. Using this data, the weight percent of the Ab, Or, and An molecules was calculated assuming ideal feldspar stoichiometry. This allowed the calculation of the weight percent of quartz in the graphic intergrowth; therefore, recalculation of the

weight percent of Ab, Or, and An to 100 percent was relatively simple. This data, plus the graphic K-feldspar + quartz analyses recalculated to quartz-free K-feldspar are listed in Table 10.

The Ab-Or-An composition of the recalculated graphic K-feldspar is plotted in Figure 41 for comparison with other blocky K-feldspar from the same intrusion.

3. Plagioclase Feldspar

a) Occurrence. The plagioclase feldspars have been subdivided into five different types (depending on the facies in which each has crystallized) to determine if there is a compositional difference among the different facies.

i) Type A. This plagioclase is associated with muscovite + quartz which forms the matrix of the pegmatitic leucogranite facies.

ii) Type B. This plagioclase is that from the leucogranite facies.

iii) Type C. This is any fine-grained ($<$ 1 cm) plagioclase in the potassic pegmatite facies.

iv) Type D. This type is the rare coarse ($>$ 1 cm) plagioclase in the potassic pegmatite pods (found only in one location).

Table 10. Recalculated quartz-free K-feldspar from graphic intergrowths of K-feldspar + quartz

Sample No.	Recalculated Wt. %				Total	%
	Or	Ab	An	K-Fsp.		Quartz
TNL-1	73.72	25.55	0.55	0.18	100.00	31.50
TNL-4	74.81	24.52	0.46	0.21	100.00	28.62
TNL-18	70.79	28.56	0.43	0.22	100.00	18.77
TNL-24	67.93	31.09	0.38	0.60	100.00	13.15
TNL-26	67.83	31.44	0.39	0.34	100.00	23.04
OL-2	75.12	23.96	0.69	0.23	100.00	29.05
OL-6	74.83	24.43	0.59	0.15	100.00	22.22
OL-10	71.05	28.10	0.65	0.20	100.00	25.97
OL-13	71.74	27.70	0.14	0.41	99.99	29.61
OL-22	72.19	27.16	0.47	0.17	99.99	30.05
OL-28	74.85	23.55	1.36	0.24	100.00	28.66
OL-36	67.98	31.27	0.48	0.26	99.99	31.89
OL-40	68.29	31.29	0.19	0.24	100.01	19.46
ENL-2	65.87	33.28	0.31	0.54	100.00	27.89
ENL-3(b)	71.83	27.37	0.33	0.47	100.00	26.21
ENL-21(e)	78.87	20.16	0.36	0.62	100.01	15.68
ENL-23(d)	72.51	26.63	0.40	0.46	100.00	24.15
ENL-10-3-G	59.10	39.67	0.44	0.79	100.00	24.37
ENL-10-6-G	69.65	29.16	0.29	0.90	100.00	23.19
GL-12(c)	66.78	32.38	0.32	0.53	100.01	25.87
GL-22(b)	73.03	25.84	0.19	0.94	100.00	26.47
GL-23(b)	62.47	36.66	0.33	0.54	100.00	26.36
GL-24(b)	70.68	28.32	0.30	0.70	100.00	25.86
GL-26(a)	68.01	31.05	0.28	0.65	99.99	22.07
GL-32(b)	68.85	30.45	0.44	0.26	100.00	24.47
GL-34(c)	75.74	23.41	0.45	0.40	100.00	27.38
GL-37(a)	79.27	19.82	0.58	0.33	100.00	21.79
GL-38(c)	74.88	24.35	0.46	0.30	99.99	17.87

v) Type E. This is the saccharoidal plagioclase within the sodic aplite facies.

At each sampling station as many of these five types as possible were sampled close to the contacts of different rock types (facies), mostly within an area of 1 m^2, to make possible compositional differences among the different plagioclase types more meaningful.

b) Optical Studies. The γ' refractive index in the (001) cleavage plane was measured on these five types of plagioclase using the Becke line method. The graphs of Morse (1968) were used to approximate the An content of the plagioclase crystals occurring within each of the facies of the pegmatitic granite.

4. Muscovite

a) Occurrence. Three distinct morphological forms of muscovite can be distinguished in all pegmatitic granites of the Winnipeg River area of southeastern Manitoba.

i) Coarse Platy (book) Muscovite (Figure 22(a)). This occurs as transparent to translucent sheets of yellow to yellowish-brown books of muscovite in or near the coarse quartz core of the potassic pegmatite facies. The size of these muscovite books generally range from 2.0 to 10.0 cm^2.

ii) Plumose (radial) Muscovite (Figure 17). It is abundant in GL, ENL and OL (western half), while its occurrence is quite rare in TNL and the eastern half of OL. Morphologically, it occurs as a conical intergrowth of muscovite + quartz which radiates out from the apex where a garnet (or tourmaline) crystal is usually located. The plumose muscovite is usually 5 to 8 cm in diameter. Genetically, it appears to be simultaneous with the albite + quartz assemblage which hosts it, but possibly secondary to potassium feldspar, which it corrodes.

iii) Matrix Muscovite. This is a fine to medium-grained (< 1.0 cm^2) primary muscovite. Two subtypes were arbitrarily selected depending in which facies they occurred: those which occur in the pegmatitic leucogranite facies (Figure 21) and matrix muscovite which occurs in the leucogranite facies. Both types occur as yellow to yellowish-brown flakes intimately associated with the other minerals (e.g. plagioclase, quartz, etc.) occurring in each type's respective facies.

In addition to these three types of muscovite common to all four intrusions of pegmatitic granite, three other muscovite types were observed and found

to be associated with only the more complex pods of potassic pegmatite in the Greer Lake stock (AC-2, AC-3 and the Silverleaf pod).

iv) Curvilamellar. This muscovite has a dish-shaped form, 1.0 to 5.0 cm in diameter and is usually found adjacent to blocky potassium feldspar crystals in textures that suggest simultaneous growth. It occurs as crystals curved immediately at the point of origin adjacent to the potassium feldspar crystal, or in the form of small (< 0.5 cm) flat muscovite plates (samples AC-2(k) and (m)) which only begin to curve as the crystal size increases (samples AC-2(k)-1 and (m)-1). The colour is usually a translucent yellow to yellowish-brown up to a silver-white.

v) Green Curvilamellar Muscovite. This type was observed in one location only (samples AC-3(r) and (s)). Textures suggest it to be a primary phase occurring as small, (< 1.0 cm) curved, green crystal aggregates within smoky-grey quartz pods of AC-3.

vi) Purple Muscovite. A purple variety of muscovite was found in two potassic pegmatite pods along the southern margin of the Greer Lake intrusion (AC-3 and the Silverleaf locality) (Figure 44). It appears to have a curvilamellar crystal form,

NOTICE/AVIS

PAGE(S) 115 IS/ARE/EST/SONT color photo

PLEASE WRITE TO THE AUTHOR FOR INFORMATION, OR CONSULT THE ARCHIVAL COPY HELD IN THE DEPARTMENT OF ARCHIVES AND SPECIAL COLLECTIONS, ELIZABETH DAFOE LIBRARY, UNIVERSITY OF MANITOBA, WINNIPEG, MANITOBA, CANADA, R3T 2N2.

VEUILLEZ ECRIRE A L'AUTEUR POUR LES RENSEIGNEMENTS OU VEUILLEZ CONSULTER L'EXEMPLAIRE DONT POSSEDE LE DEPARTEMENT DES ARCHIVES ET DES COLLECTIONS SPECIALES, BIBLIOTHEQUE ELIZABETH DAFOE, UNIVERSITE DU MANITOBA, WINNIPEG, MANITOBA, CANADA, R3T 2N2.

Figure 44. Pods of purple Li-muscovite in cleavelandite from the Silverleaf offshoot of the Greer Lake intrusion. Amblygonite and triphylite-lithiophylite were also reported from here (Černý, pers. comm. 1978).

both in the larger (2 cm) crystal sizes found in the Silverleaf pod and the small (< 1.0 cm) aggregates within K-feldspar in the AC-3 locality. It is mostly associated with cleavelandite in aggregates replacing blocky K-feldspar and quartz (Figure 45).

vii) Two other types observed only in the Silverleaf potassic pegmatite pod adjacent to the Greer Lake intrusion include a greyish-brown plumose form which is secondary, forming as a fracture-filling muscovite. The other type is a fine flaked purple variety similar to type iv above but finer-grained. It has formed by replacement of K-feldspar. Neither type occurs in significant amounts; consequently, they will not be discussed further.

b) Chemistry. Sixty four samples of fresh muscovite were separated and analyzed for K, Li, Rb, Cs, Ca, Mg, Be, Mn, and total Fe (Fe^{++}+ Fe^{+++}) content. The analyses are listed in Appendix 4. The arithmetic means of the contents and of calculated ratios of geochemically significant elements are listed in Table 11. This table compares the different types of muscovite in one intrusion and illustrates variations in the composition of muscovite types among individual intrusions.

Table 11. Calculated averages of the platy, radial, and matrix muscovite analyses from the Winnipeg River pegmatitic granites

	OL Platy	OL Radial	OL Matrix	TNL Platy	GL Platy	GL Radial	GL Matrix
K_2O	9.03	9.23	9.70	8.84	8.56	8.80	9.25
Na_2O	0.85	0.66	0.71	0.69	0.84	0.63	0.65
CaO	0.046	0.026	0.018	0.027	0.019	0.024	0.013
Rb_2O	0.134	0.082	0.104	0.117	0.42	0.21	0.31
Li_2O	0.041	0.055	0.029	0.110	0.155	0.112	0.145
Cs_2O	0.0077	0.0019	0.0073	0.0130	0.008	0.0046	0.0038
MgO	0.39	0.43	0.60	0.43	0.14	0.25	0.22
K	7.50	7.66	8.05	7.34	7.11	7.30	7.68
Na	0.63	0.48	0.53	0.51	0.62	0.46	0.48
Ca	0.034	0.019	0.013	0.019	0.013	0.017	0.009
Rb	0.124	0.075	0.095	0.109	0.38	0.19	0.26
Li	0.019	0.026	0.014	0.052	0.072	0.056	0.069
Cs	0.0072	0.0018	0.0068	0.012	0.0075	0.0043	0.0037
Mg	0.24	0.26	0.30	0.26	0.085	0.15	0.13
Fe	1.49	1.39	1.82	3.08	2.44	2.50	2.43
Be	0.0004	0.0001	0.0008	0.0007	0.0008	0.0007	0.0019
K/Rb	60	102	85	67	19	38	30
K/Cs	1042	4256	1183	612	948	1698	1969
Rb/Li	6.5	2.9	6.8	2.1	5.3	3.4	3.8
Rb/Cs	17.2	41.7	14.0	9.1	50.7	44.2	70.3
Mg/Li	12.6	10.0	21.4	5.0	1.2	2.7	1.9

Table 11 Continued...

	ENL Platy	ENL Radial	ENL Matrix	Mineralized Pods SF Platy	AC Platy	Lobe Platy	Zone Platy	GL
K_2O	8.88	9.15	9.13	9.34	9.43	8.80	9.18	8.72
Na_2O	0.72	0.64	0.61	0.49	0.31	0.82	0.44	0.69
CaO	0.026	0.020	0.014	0.014	0.039	0.021	0.002	0.015
Rb_2O	0.33	0.19	0.34	1.48	1.37	0.38	0.89	0.61
Li_2O	0.24	0.20	0.24	2.19	1.08	0.177	0.41	0.253
Cs_2O	0.0094	0.0048	0.0079	0.122	0.088	0.0067	0.039	0.028
MgO	0.196	0.175	0.235	0.123	0.033	0.193	0.056	0.11
K	7.37	7.59	7.58	7.81	7.83	7.31	7.62	7.24
Na	0.54	0.47	0.45	0.36	0.23	0.61	0.32	0.52
Ca	0.019	0.014	0.010	0.013	0.028	0.015	0.015	0.010
Rb	0.30	0.17	0.31	1.35	1.25	0.34	0.81	0.560
Li	0.11	0.09	0.11	1.02	0.50	0.066	0.19	0.117
Cs	0.0089	0.0045	0.0075	0.116	0.081	0.0061	0.036	0.026
Mg	0.117	0.100	0.14	0.073	0.002	0.117	0.033	0.07
Fe	2.27	2.30	2.20	2.10	2.85	2.70	4.09	3.25
Be	0.0011	0.0008	0.0021	0.0035	0.0028	0.0009	0.0014	0.0022
K/Rb	25	45	24	7	6	22	9	13
K/Cs	828	1687	1011	67	97	1198	212	278
Rb/Li	2.7	1.9	2.8	1.3	2.5	5.2	4.3	4.8
Rb/Cs	33.7	37.8	41.3	11.6	15.4	55.7	22.5	21.5
Mg/Li	1.1	1.1	1.3	0.1	0.004	1.8	0.2	7.6

NOTICE/AVIS

PAGE(S) 119 IS/~~ARE~~ EST/~~SONT~~ color photo

PLEASE WRITE TO THE AUTHOR FOR INFORMATION, OR CONSULT THE ARCHIVAL COPY HELD IN THE DEPARTMENT OF ARCHIVES AND SPECIAL COLLECTIONS, ELIZABETH DAFOE LIBRARY, UNIVERSITY OF MANITOBA, WINNIPEG, MANITOBA, CANADA, R3T 2N2.

VEUILLEZ ECRIRE A L'AUTEUR POUR LES RENSEIGNEMENTS OU VEUILLEZ CONSULTER L'EXEMPLAIRE DONT POSSEDE LE DEPARTEMENT DES ARCHIVES ET DES COLLECTIONS SPECIALES, BIBLIOTHEQUE ELIZABETH DAFOE, UNIVERSITE DU MANITOBA, WINNIPEG, MANITOBA, CANADA, R3T 2N2.

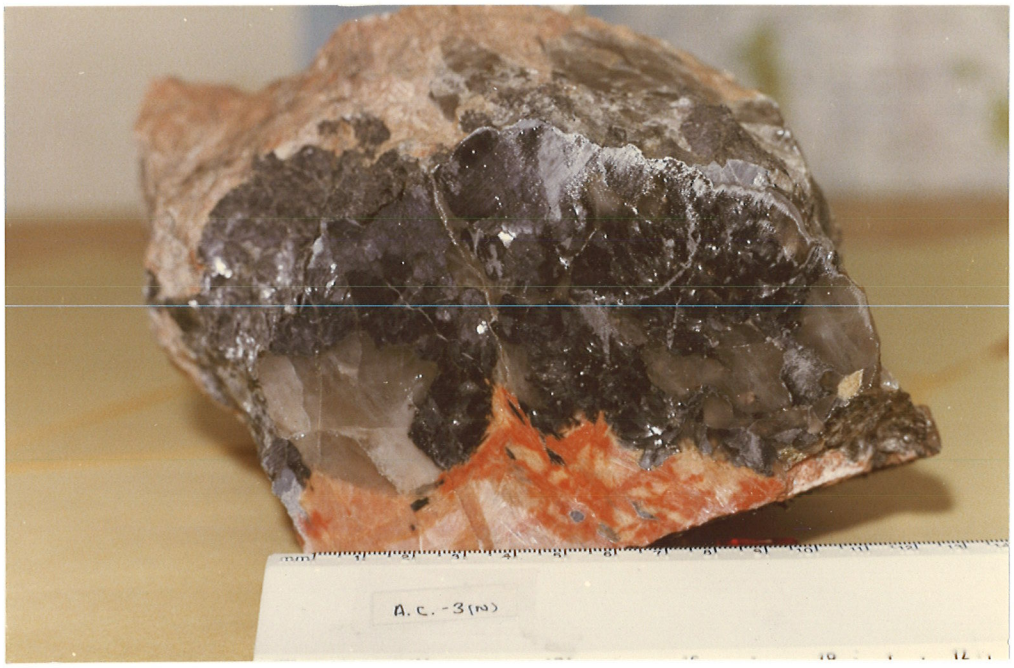

Figure 45. Cut slab of potassic pegmatite showing K-feldspar (pink) being corroded by cleavelandite (red-orange) which in turn is being corroded by curved green, Li-enriched muscovite (AC-3(n)). This muscovite is straight/platy adjacent to the cleavelandite. Outward (towards the top) the grain size increases and the crystals become curved. No variation in chemistry or polytypism was observed.

c) X-ray Studies. X-ray diffraction photographs were taken of all samples of muscovite to determine their structure polytype. All samples had $2M_1$ structures as indicated by the $(\bar{1}14)$, (006), and (114) reflections; however, several samples from the AC-3 and Silverleaf locations (GL) produced additional weak reflections $(\bar{1}12)$, (003), and (112). These indicate the presence of subordinate amounts of the 1M polytype admixed to the predominant $2M_1$ muscovite. These muscovites with a subordinate 1M polytype are those containing increased amounts of Li_2O. The results are listed in Table 12.

5. Garnet

a) Occurrence. Garnet is found throughout the pegmatitic granites. In some facies (e.g. sodic aplite) its abundance approaches an estimated 2-3 percent of the rock, whereas in other facies it is only an accessory mineral ($< \frac{1}{2}$ percent). Within the pegmatitic granites the garnets have been divided into three types.

i) Type A garnet is a small (< 3.0 mm) euhedral garnet which occurs in the banded fine-grained sodic aplite. Alteration to chlorite and/or biotite along fractures is absent (Figure 46).

ii) Type B garnet occurs in the leucogranite facies

Table 12. Muscovite polytypes

Sample No.	Structure Type	Sample No.	Structure Type
Platy Muscovite		**Radial Muscovite**	
TNL-2	$2M_1$	OL-10	$2M_1$
TNL-9	$2M_1$	OL-14	$2M_1$
TNL-18	$2M_1$		
TNL-25	$2M_1$	ENL-9(c)	
		ENL-13(b)	$2M_1$
OL-BP	$2M_1$	ENL-27(c)	$2M_1$
OL-Grid 2N/OE	$2M_1$	ENL-31(a)	$2M_1$
OL-2-P	$2M_1$	ENL-34(b)	$2M_1$
OL-14-P	$2M_1$		
OL-39	$2M_1$	GL-1	
		GL-3	$2M_1$
ENL-4(f)	$2M_1$	GL-34(b)	$2M_1$
ENL-17(b)	$2M_1$		
ENL-19-3	$2M_1$	**Matrix Muscovite**	
ENL-26(c)	$2M_1$		
ENL-30(a)	$2M_1$	OL-2	$2M_1$
ENL-36(c)	$2M_1$	OL-16	$2M_1$
ENL-HT	$2M_1$		
		ENL-14(d)	$2M_1$
GL-2	$2M_1$	ENL-25(b)	$2M_1$
GL-10-3	$2M_1$		
GL-23(b)	$2M_1$	GL-8(a)	$2M_1$
GL-25(c)	$2M_1$	GL-20(b)	$2M_1$
GL-31(b)	$2M_1$		
		Curvilamellar Muscovite	
Lobe-1	$2M_1$		
Lobe-7 and 10	$2M_1$	AC-3(o)	$2M_1 > 1M_1$
Lobe 17	$2M_1$	AC-3(n)	$2M_1$
		AC-2(m)-1	$2M_1$
AC-2(i)	$2M_1$	AC-2(k)-1	$2M_1$
AC-2(k)	$2M_1$		
AC-2(m)	$2M_1$	Zone-5-4	$2M_1$
AC-3(k)	$2M_1$		
AC-3(r)	$2M_1$	SF-1	$2M_1 >> 1M_1$
AC-3(s)	$2M_1 >>>> 1M_1$	SF-1(a)	$2M_1 = 1M_1$ $2M_1 > 1M_1$
		SF-4	$2M_1$
Zone-5-1	$2M_1$	SF-5	$2M_1 >>> 1M_1$
Zone-5-6	$2M_1$		
Zone-5-9	$2M_1$		
SF-1-64.5	$2M_1$		
SF-2-14.3	$2M_1$		
SF-2-28	$2M_1$		
SF-2-8-10	$2M_1 >>> 1M_1$		

NOTICE/AVIS

PAGE(S) 122 IS/ARE EST/SONT color photo

PLEASE WRITE TO THE AUTHOR FOR INFORMATION, OR CONSULT THE ARCHIVAL COPY HELD IN THE DEPARTMENT OF ARCHIVES AND SPECIAL COLLECTIONS, ELIZABETH DAFOE LIBRARY, UNIVERSITY OF MANITOBA, WINNIPEG, MANITOBA, CANADA, R3T 2N2.

VEUILLEZ ECRIRE A L'AUTEUR POUR LES RENSEIGNEMENTS OU VEUILLEZ CONSULTER L'EXEMPLAIRE DONT POSSEDE LE DEPARTEMENT DES ARCHIVES ET DES COLLECTIONS SPECIALES, BIBLIOTHEQUE ELIZABETH DAFOE, UNIVERSITE DU MANITOBA, WINNIPEG, MANITOBA, CANADA, R3T 2N2.

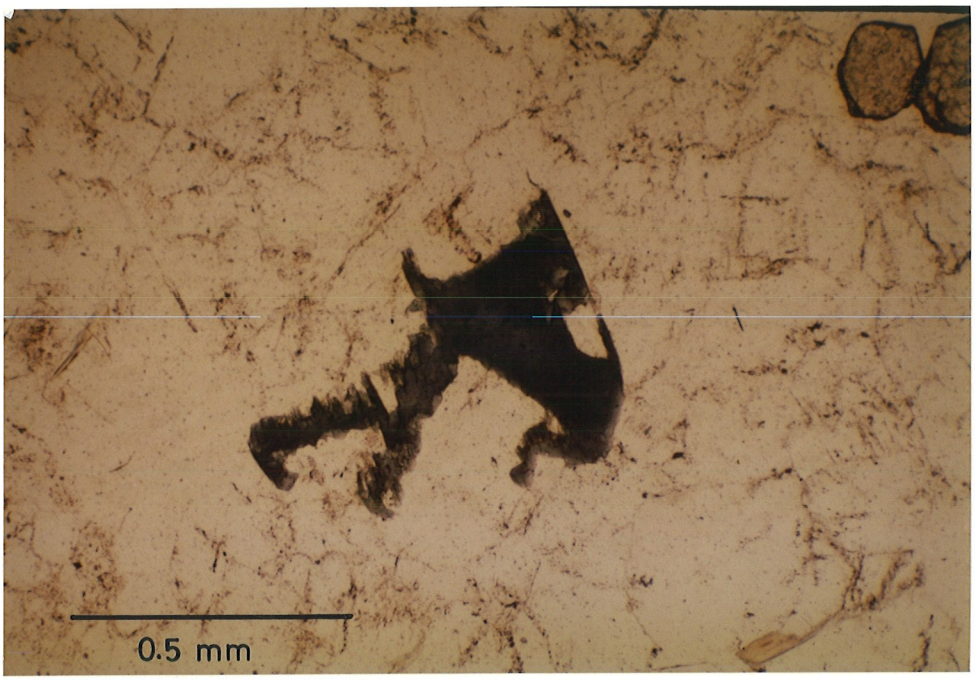

Figure 46. The only tourmaline noted in the pegmatitic granites south of the Winnipeg River was from the sodic aplite of the Silverleaf offshoot of the Greer Lake intrusion. This crystal was adjacent to a green beryl crystal also in the sodic aplite. Note minute Nb,Ta oxide mineralization. Garnet is typical of all sodic aplite; euhedral and lacking alteration and fractures.

or locally in areas of finer-grained pegmatitic leucogranite. The crystals are larger, 3-4 mm, than the A garnet and more fractured. Alteration to chlorite and/or biotite along fractures is widespread (Figure 47).

iii) Type C. C garnet is a coarse-grained (> 4.0 mm) garnet from the potassic pegmatite facies or coarse areas of pegmatitic leucogranite. Again fracturing and alteration is widespread.

b) Chemistry. A total of twenty four samples were separated by elutriation and analyzed for SiO_2, Al_2O_3, Fe_2O_3, Y_2O_3, FeO, MnO, MgO, CaO, and P_2O_5. A second group of eighty eight samples was mounted, polished, and analyzed for SiO_2, TiO_2, Al_2O_3, total $Fe(Fe^{++} + Fe^{+++})$, Y_2O_3, MnO, MgO, CaO, ZrO_2, and HfO_2 on a MAC-5 electron microprobe. These results are listed in Appendix 5.

c) X-ray Studies. The garnet samples separated for "wet" chemical analyses had unit cell dimensions a determined from quartz-calibrated X-ray powder diffraction patterns. The a_o was calculated using the equation

$$d(hkl) = a_o(h^2 + k^2 + l^2) \quad \text{(Nuffield, 1966)}$$

and the (611) garnet peak calibrated by the (1122) quartz reflection, the value of which was taken from

NOTICE/AVIS

PAGE(S) 124 IS/ARE EST/SONT color photo

PLEASE WRITE TO THE AUTHOR FOR INFORMATION, OR CONSULT THE ARCHIVAL COPY HELD IN THE DEPARTMENT OF ARCHIVES AND SPECIAL COLLECTIONS, ELIZABETH DAFOE LIBRARY, UNIVERSITY OF MANITOBA, WINNIPEG, MANITOBA, CANADA, R3T 2N2.

VEUILLEZ ECRIRE A L'AUTEUR POUR LES RENSEIGNEMENTS OU VEUILLEZ CONSULTER L'EXEMPLAIRE DONT POSSEDE LE DEPARTEMENT DES ARCHIVES ET DES COLLECTIONS SPECIALES, BIBLIOTHEQUE ELIZABETH DAFOE, UNIVERSITE DU MANITOBA, WINNIPEG, MANITOBA, CANADA, R3T 2N2.

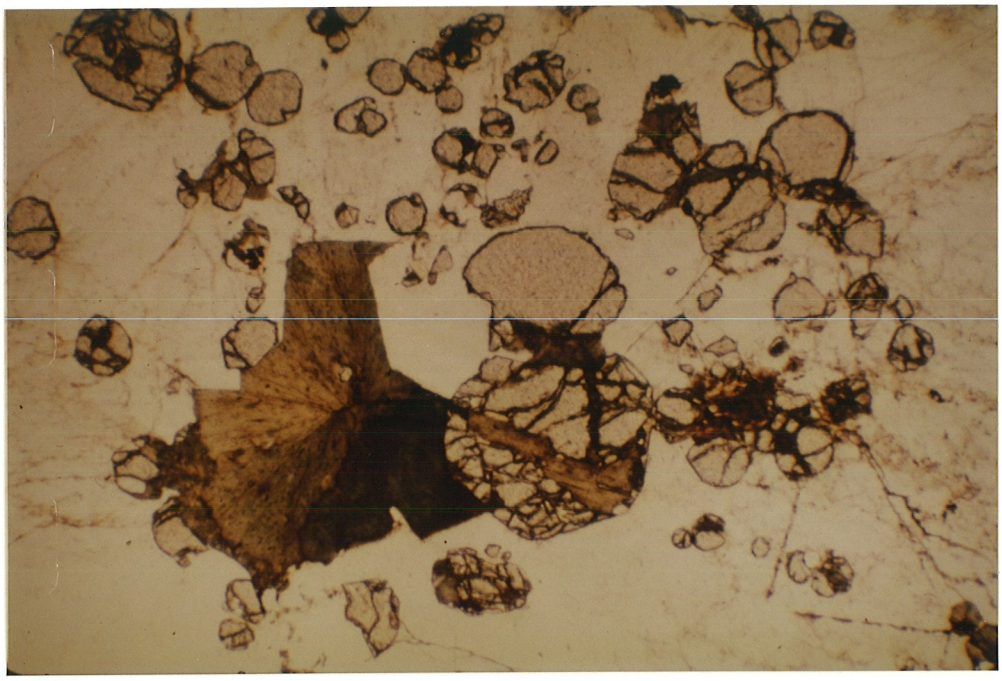

Figure 47. Garnet from the leucogranite facies, Tin Lake intrusion. Generally garnet from this facies in all intrusions is fractured and moderately to heavily chloritized as opposed to sodic aplite garnet which is equant and unaltered. Short edge of photograph is 1 cm.

Frondel (1962). Results are presented in Table 13, Figure 48.

Two special types of garnet were studied: those located at the apex of plumose muscovite upon which the muscovite + quartz crystallization nucleated, and garnet grains seated in pseudomorphs after cordierite (Figure 57). Chemical analyses are listed in Appendix 5 and the calculated a_o dimensions are in Table 13.

C. ACCESSORY MINERALS

1. Niobium, Tantalum Oxide Minerals

a) Occurrence. Most Nb,Ta oxide minerals collected, and all that were analyzed, were from pods of potassic pegmatite in the Greer Lake intrusion (including AC and Silverleaf localities). Several minute crystals were suspected in thin sections of the sodic aplite facies of both the Greer Lake and Eaglenest Lake intrusions (Figure 49); however, the minute size prevented any separation and subsequent analysis.

None of these oxides were located in the Tin Lake intrusion and only one sample was obtained from the Osis Lake intrusion (OL-BP).

b) Chemistry. Twenty samples of Nb,Ta oxide minerals were analyzed on a MAC-5 electron microprobe for Nb, Ta, Mn, Fe, Al, Zr, Sn, Hf, Sc, Ca, Ti, and Na. The

Table 13. Garnet unit cell dimensions calculated by x-ray diffraction methods

Sample No.	*	a_o	Sample No.	*	a_o
TNL-1	P.	11.539	ENL-1(a)	H.	11.551
TNL-15	P.	11.537	ENL-2	P.	11.554
TNL-17	S.A.	11.540	ENL-6(b)	H.	11.545
TNL-20	H.	11.545	ENL-10-1	S.A.	11.545
TNL-37	S.A.	11.540			
			GL-4(a)	H.	11.550
TNL-39	H.	11.544			
			GL-9(d)	S.A.	11.551
OL-2	P.	11.554	GL-11(c)	S.A.	11.534
OL-16 (pink)	P.	11.544	GL-25(d)	P.	11.544
OL-16 (orange)	P.	11.540	GL-36(a)	H.	11.540
OL-18 (pink)	H.	11.545	GL-41(b)	H.	11.535
OL-18 (orange)	H.	11.535			
			Lobe-6	S.A.	11.561
Cord. Pseudo.		11.593			
			AC-3(j)	P.	11.585

*Type of garnet:

P. = in pegmatitic leucogranite

S.A.= in sodic aplite

H. = in leucogranite

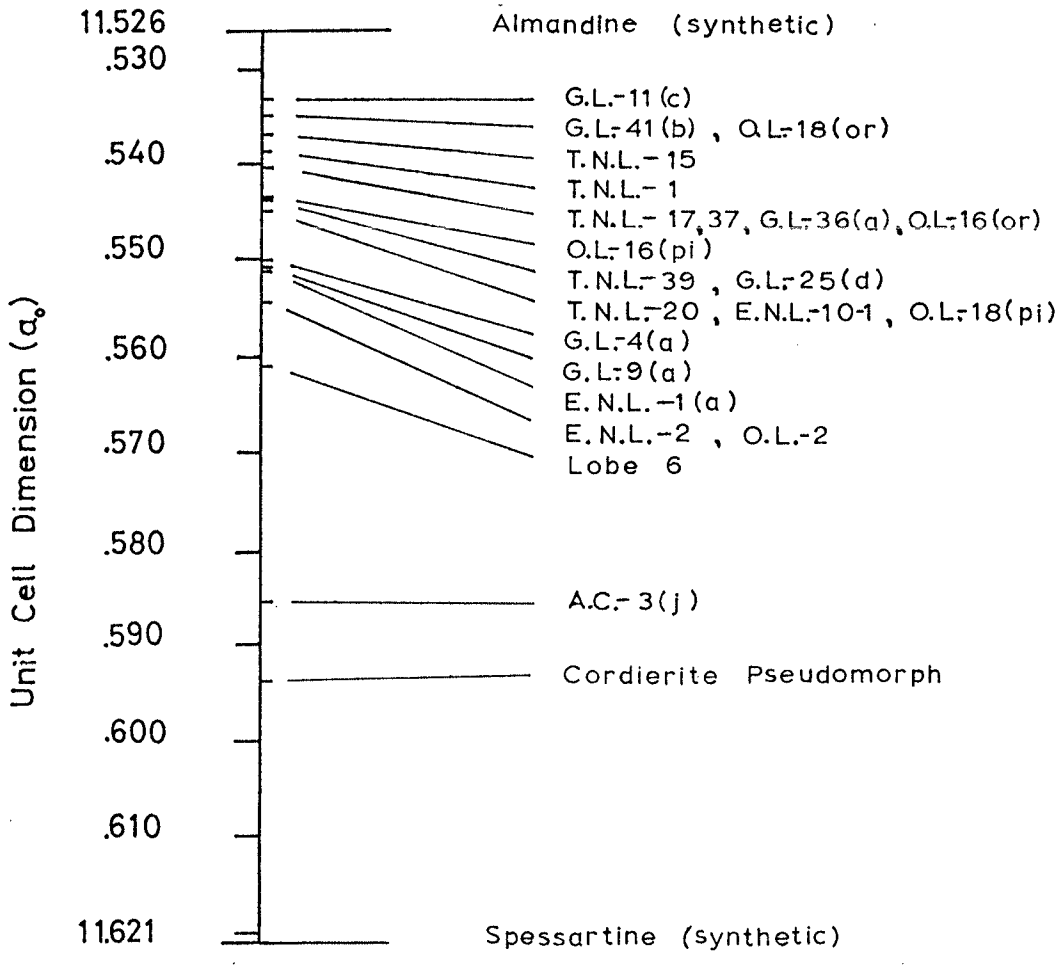

Figure 48. Unit cell dimensions of selected garnet samples determined by X-ray powder diffraction methods. (Or) indicates bright orange garnet, (pi) indicates pink coloured garnet. All remaining samples are reddish. Synthetic end members as reported in Deer, Howie, and Zussman, 1968.

NOTICE/AVIS

PAGE(S) 128 IS/~~ARE~~ EST/~~SONT~~ color photo

PLEASE WRITE TO THE AUTHOR FOR INFORMATION, OR CONSULT THE ARCHIVAL COPY HELD IN THE DEPARTMENT OF ARCHIVES AND SPECIAL COLLECTIONS, ELIZABETH DAFOE LIBRARY, UNIVERSITY OF MANITOBA, WINNIPEG, MANITOBA, CANADA, R3T 2N2.

VEUILLEZ ECRIRE A L'AUTEUR POUR LES RENSEIGNEMENTS OU VEUILLEZ CONSULTER L'EXEMPLAIRE DONT POSSEDE LE DEPARTEMENT DES ARCHIVES ET DES COLLECTIONS SPECIALES, BIBLIOTHEQUE ELIZABETH DAFOE, UNIVERSITE DU MANITOBA, WINNIPEG, MANITOBA, CANADA, R3T 2N2.

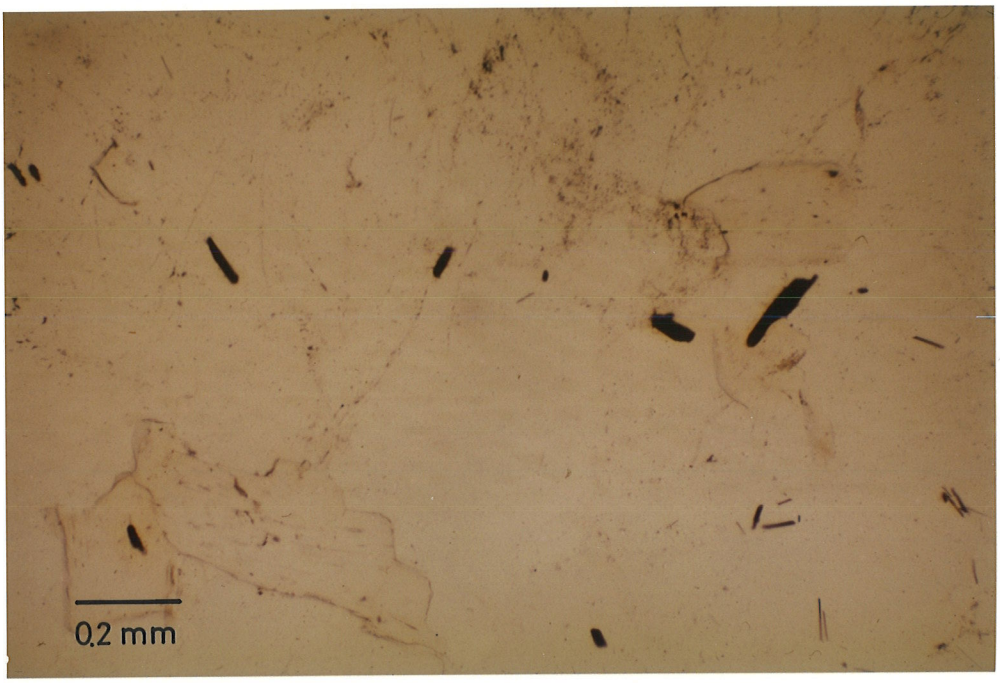

Figure 49. Nb,Ta oxide mineralization in the sodic aplite facies of the Greer Lake intrusion. Although common in this intrusion, the only other location where abundant Nb,Ta oxide minerals were observed was at ENL-11; at the eastern end of the Eaglenest Lake intrusion, also occurring as minute crystals in the sodic aplite facies (Appendix 9).

geochemically significant MnO/(MnO + FeO) and $Ta_2O_5/(Ta_2O_5 + Nb_2O_5)$ ratios were calculated and are listed with the chemical analyses in Appendix 6. The mineral compositions are illustrated on the ternary $(Ta_2O_5 + Nb_2O_5)$-(FeO + MnO)-$(SnO_2 + TiO_2 + ZrO_2 + HfO_2$ + etc.) diagram in Figure 50, and the Ta/(Ta + Nb) vs. Mn/(Mn + Fe) plot in Figure 51.

c) X-ray Studies. Upon heating in air at 800°C ± 50°C for three hours (Nickel et al., 1963; Gouder de Beauregard et al., 1967), disordered minerals of the columbite-tantalite group are reported to undergo a phase change (Nickel et al., 1963); pseudo-ixiolite $((A,B\gg C)_4O_8)$ converts to columbite-tantalite $(A_4B_8O_{24})$ while ixiolite $((A,B,C)_4O_8)$ converts to a wolframite-like phase, wodginite $(A_4B_4C_8O_{32})$ (Foord, 1982) where A = (Fe,Mn), B = (Nb,Ta), and C = (Sn, Ti, Sc, Mg, Ca, Al, Na, Zr). The pseudo-ixiolite:columbite-tantalite transformation involves an ordering of the cation distribution causing a threefold increase in the a unit cell dimension and thus a corresponding tripled unit cell volume. Heating of pseudo-ixiolite also produces a slight decrease in the a and b cell edges and an increase in the c/3 edge (Komkov, 1970). The specimens were X-rayed to calculate and document the above changes and to determine the initial mineral

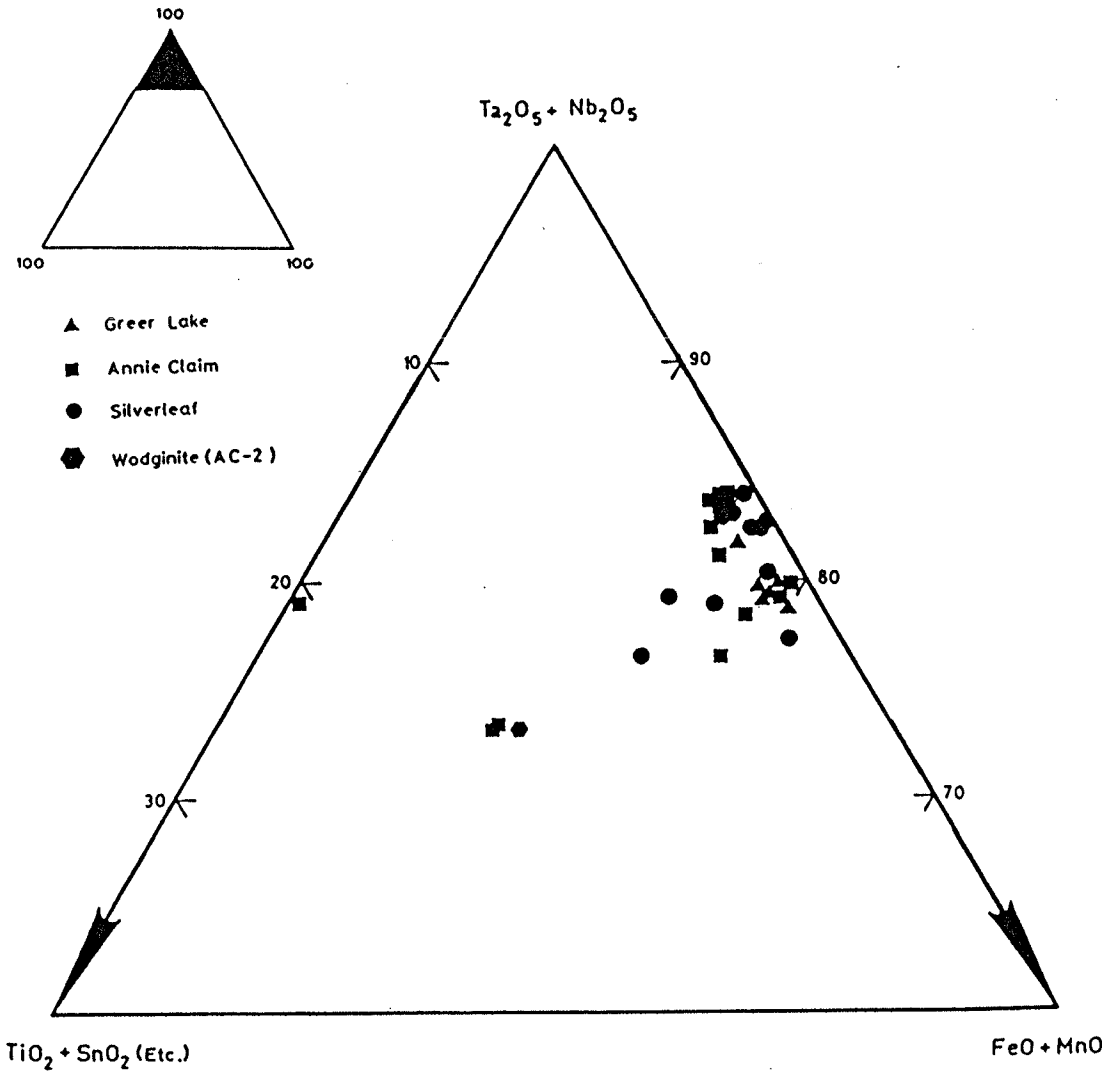

Figure 50. Columbite - tantalite (including wodginite sample from AC-2(o)) of the Winnipeg River pegmatitic granites in the (FeO + MnO)-(Ta_2O_5 + Nb_2O_5)-(TiO_2 + SnO_2 + Sc_2O_3 etc.) triangular plot.

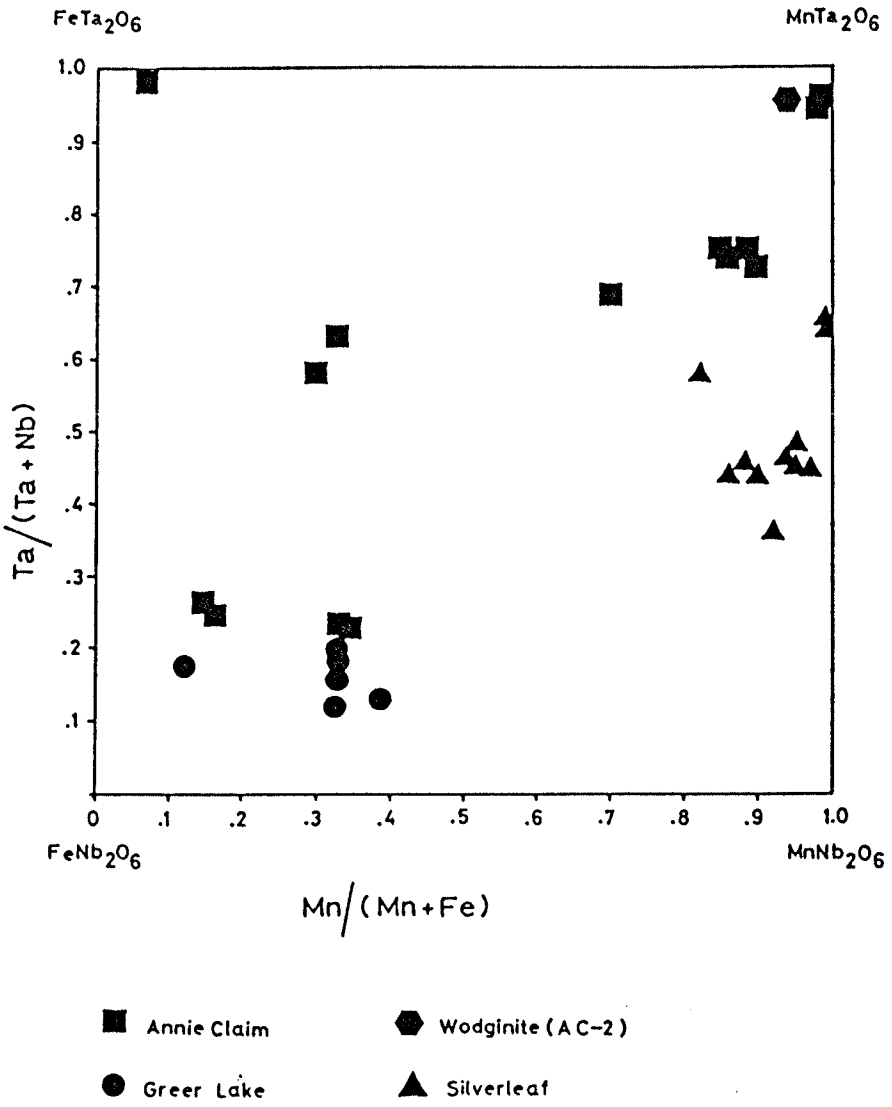

Figure 51. Columbite-tantalite mineralization from the Annie Claim, the Silverleaf offshoot and the main Greer Lake intrusion in the $FeNb_2O_6$ - $FeTa_2O_6$ - $MnNb_2O_2$ - $MnTa_2O_6$ (molecular percent based on Ta_2O_5 and MnO ratios) diagram.

phase present. Results are listed in Table 14. All X-ray powder diffractograms were calibrated (CaF_2) to refine unit cell dimensions of both heated and natural samples. The results obtained on the columbite-tantalite minerals are shown in Table 15, together with several other samples from the Silverleaf Claim previously published by Černý and Turnock (1971).

The compositional and structural data indicate that the studied minerals of the columbite-tantalite group belong predominantly to the strongly to partially disordered columbite-tantalite with a relatively narrow range of Ta/(Ta + Nb) values but broad variations in Mn/(Mn + Fe) ratios. Only a few samples show largely ordered structure and a single sample is wodginite.

2. Beryl

a) Occurrence. Beryl was located only in the Greer Lake pegmatitic granite and the adjacent Silverleaf Claim. It always occurs in the same association. The most common occurrence is with K-feldspar + quartz + muscovite (± Nb,Ta oxide minerals) in or near the coarse cores of the potassic pegmatite facies in the main Greer Lake intrusion. However, in the more mineralogically diversified pods along the southern

Table 14. Results of heating (800°C for three hours) on the ordering of the Nb,Ta oxide crystal structure

Sample Location	Heating	
	Before	After
AC-1(a)		
-light		
-dark		
AC-1(b)		
-light		
-dark		
AC-2-79-1	W	W
AC-3-79-1	C	C
AC-3-79-2	C	C
AC-3-12	P	C
AC-3(i)	C	C
SF-17	P	C
SF-21	P	C
SF-22	P	C
GL-25(d)	P	C
GL-HT		
GL-30(a)-1	P	C
GL-30-1	P	C
GL-30-2	P	C
GL-30-3	P	C
GL-30-4	P	C
OL-BP		
LOBE-(7&10)		
GL-11(a)		
SF-14	P	C
SF-15	P	C
SF-16	P	C
SF-18		
SF-19		

W = wodginite ($A_4B_4C_8O_{32}$)

C = columbite, tantalite ($A_4B_8O_{24}$)

P = pseudoixiolite $(A,B,C)_4O_8$)

In these structures A = (Fe,Mn)
B = (Nb,Ta)
C = (Ti,Sn,Sc,Mg,Ca,Al, etc.)

Table 15. Unit cell dimensions of Na,Ta oxide minerals from the Winnipeg River pegmatitic granite

Sample No.	State	a_o	b_o	c_o	Volume	Direct Cell Standard Error a_o	b_o	c_o
GL-11			Insufficient sample					
GL-25(a)	natural	4.743(0)	5.727(6)	5.070(3)	413.22	0.004	0.014	0.005
	heated		Insufficient sample					
GL-30(a)-1	natural	4.744(4)	5.724(8)	5.081(8)	138.03	0.005	0.007	0.008
	heated	14.280(1)	5.736(3)	5.053(1)	413.92	0.003	0.009	0.004
GL-30-1	natural	4.749(7)	5.728(2)	5.095(2)	138.63	0.002	0.006	0.003
	heated	14.260(7)	5.731(7)	5.060(6)	413.64	0.005	0.012	0.005
GL-30-2	natural	4.746(0)	5.722(9)	5.100(8)	138.54	0.002	0.006	0.003
	heated	14.299(1)	5.735(4)	5.058(2)	414.83	0.001	0.003	0.002
GL-30-3	natural	4.743(5)	5.732(8)	5.098(0)	138.63	0.002	0.003	0.002
	heated	14.282(5)	5.734(0)	5.064(8)	414.79	0.002	0.005	0.003
GL-30-4			Insufficient sample					
Lobe-7-10			Insufficient sample					
AC-1(a)			Insufficient sample					
AC-1(b)			Insufficient sample					
AC-2-79-1	natural	4.756(7)	5.732(9)	5.151(1)	140.49	0.002	0.005	0.002
	heated	14.274(5)	5.747(3)	5.057(0)	414.88	0.009	0.027	0.010
AC-3-79-1	natural	4.741(2)	5.752(2)	5.082(4)	138.61	0.006	0.002	0.003

edge of the Greer Lake stock (AC-3 and Silverleaf), beryl occurs with cleavelandite + quartz (± K-feldspar ± Nb,Ta oxide minerals). The former beryl is always lime-green while the latter is lime-green to white. The crystals display a short prismatic habit (1-4 cm long) and are commonly broken along the basal (001) parting and subsequently healed by quartz. Beryl at the GL-30 location on the north side of the intrusion has an ice-blue colour and it is coated with fine silvery-white muscovite. This was the only alteration of beryl that was noted (Figure 37).

b) Chemistry. Sixteen samples of beryl were analyzed for Na, K, Li, Rb, Cs, Fe, Ca, and Mg. The results are tabulated in Appendix 7. Geochemically significant ratios and the total alkali content (R_2O) are also listed. The composition of the beryl samples is shown in Figure 52.

c) Optical Studies. The refractive index ($n_{\omega r}$) of all beryl specimens was determined by the Becke line method. Figure 53 is a plot of R_2O + CaO vs. refractive index ($n_{\omega r}$) which documents the level of fractionation attained by the beryl in the intrusion.

It should be noted that beryl shows in most of its typical occurrences, and particularly in considerably fractionated pegmatites, a distinct compositional zoning with alkali contents increasing from

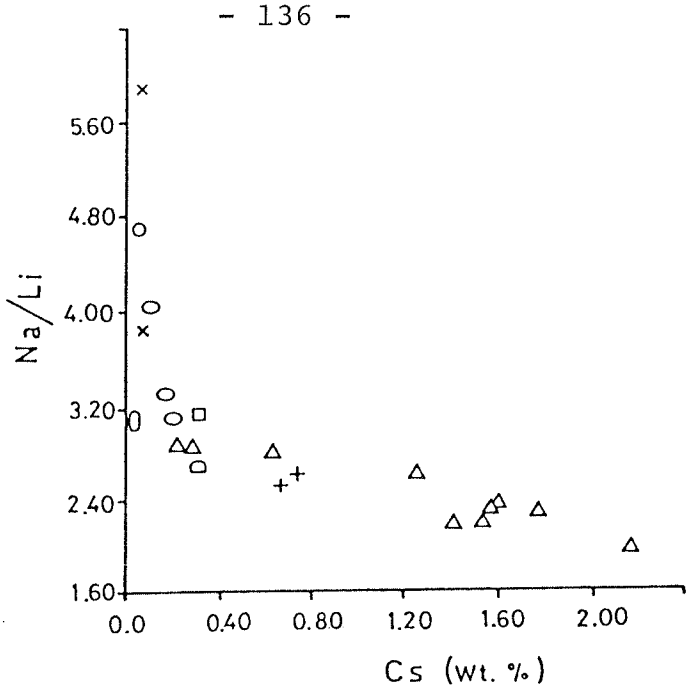

Figure 52. Beryl composition from the mineralized potassic pegmatite pods of the Greer Lake pegmatitic granite. Symbols as follows: Greer Lake potassic pegmatite (x), GL-19 (⊙), GL-30(0), Silverleaf (+), AC-1 (▫), AC-2 (⌓), AC-3 (△), Lobe (o).

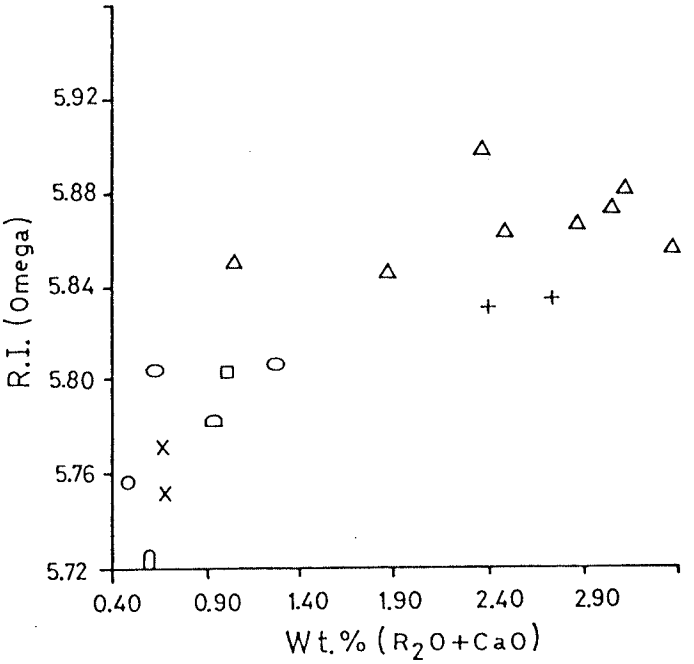

Figure 53. Refractive index vs. alkali content of beryl from the Greer Lake intrusion (potassic pegmatite facies). Symbols as in Figure 52.

the centre of the crystal outwards (Černý and Simpson, 1977). To provide a uniform basis for comparison of all examined specimens, each crystal was sampled at its surface both for n_{Na} determinations and chemical analyses. In several cases this was not possible since the beryl crystals were too small; in situations like this the correlation of refractive indices and chemical compositions deviate from the trend of other specimens. These samples are marked by asterisks (*) in the list of refractive indices (Appendix 6).

D. RARE MINERALS

No genetically significant data have been collected on the mineral species discussed here because of their extreme rarity. Their occurrences are restricted to only some of the pegmatitic granite intrusions and quantities of separable material are commonly negligible.

1. Gahnite

This mineral is relatively common in the two intrusions located south of the Winnipeg River (GL, ENL). Only one crystal was observed north of the river in the western end of the Osis Lake intrusion. This mineral, a zinc spinel ($ZnAl_2O_4$), was separated with the garnet in the elutriation tube. In the Greer Lake and Eaglenest Lake stocks it appears quite commonly in thin section, always

with a muscovite reaction rim surrounding it (Figure 54). Unit cell dimensions were obtained on three samples and these are listed in Table 16.

2. Monazite

Monazite, (Ce, La, Th)PO_4, was also separated out with the garnet in the elutriation tube. It was identified by a Gandolfi single-grain photograph. A monazite was reported (Černý, pers. comm. 1979) from the Silverleaf Claim, adjacent to a Nb,Ta oxide mineral and associated with purple (lithian) muscovite. No chemical analyses of this monazite are available.

3. Spodumene

Spodumene, $LiAlSi_3O_8$, occurs only in the Silverleaf location as a spodumene + quartz intergrowth (Figure 55) suggestive of pseudomorphism after petalite crystals ($LiAlSi_2O_6$) (Černý and Ferguson, 1972). Several analyses of this mineral, both from surface outcrop and from drill core, are presented in Appendix 8.

4. Cassiterite

Cassiterite, SnO_2, is quite common in thin sections of the sodic aplite of the Silverleaf Claim (Figure 56). It has also been reported in the literature from the Annie Claim (Springer, 1950); however, this was not verified during

NOTICE/AVIS

PAGE(S) 139 IS/ARE EST/SONT color photo

PLEASE WRITE TO THE AUTHOR FOR INFORMATION, OR CONSULT THE ARCHIVAL COPY HELD IN THE DEPARTMENT OF ARCHIVES AND SPECIAL COLLECTIONS, ELIZABETH DAFOE LIBRARY, UNIVERSITY OF MANITOBA, WINNIPEG, MANITOBA, CANADA, R3T 2N2.

VEUILLEZ ECRIRE A L'AUTEUR POUR LES RENSEIGNEMENTS OU VEUILLEZ CONSULTER L'EXEMPLAIRE DONT POSSEDE LE DEPARTEMENT DES ARCHIVES ET DES COLLECTIONS SPECIALES, BIBLIOTHEQUE ELIZABETH DAFOE, UNIVERSITE DU MANITOBA, WINNIPEG, MANITOBA, CANADA, R3T 2N2.

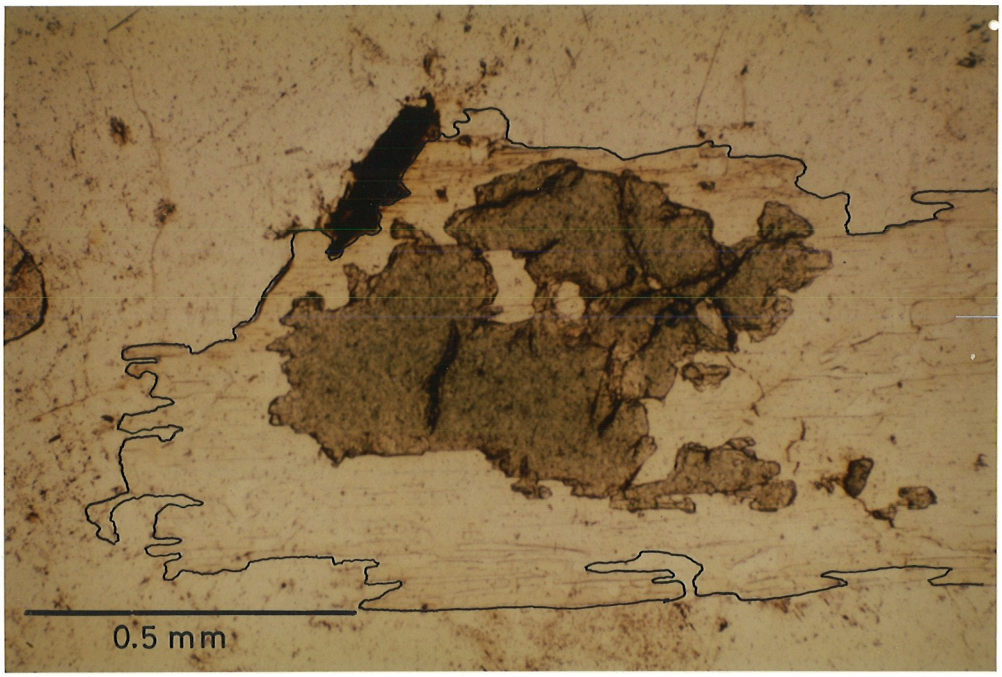

Figure 54. Pale green gahnite (high relief) enclosed in and corroded by muscovite (outlined) with possible opaque blades of Nb,Ta oxide minerals. This mineral is relatively common in the sodic aplite of the Greer Lake and Eaglenest Lake intrusions.

Table 16. Unit cell dimensions of gahnite and ilmenite

Gahnite		
Sample No.	a_o	Volume
GL-6(a)	8.116(8) ±0.002(0)	534.8
GL-41	8.110(6) ±0.001(0)	533.5
ENL-8(d)	8.108(1) ±0.001(3)	533.0
OL-38	8.093(2) ±0.000(0)	530.1

Ilmenite			
Sample No.	a_o	c	Volume
SF-Ti	5.0868 ±0.0008	14.0833 ±0.0050	131.6

NOTICE/AVIS

PAGE(S) 141 - 143 ~~IS~~/ARE ~~EST~~/SONT color photos

PLEASE WRITE TO THE AUTHOR FOR INFORMATION, OR CONSULT THE ARCHIVAL COPY HELD IN THE DEPARTMENT OF ARCHIVES AND SPECIAL COLLECTIONS, ELIZABETH DAFOE LIBRARY, UNIVERSITY OF MANITOBA, WINNIPEG, MANITOBA, CANADA, R3T 2N2.

VEUILLEZ ECRIRE A L'AUTEUR POUR LES RENSEIGNEMENTS OU VEUILLEZ CONSULTER L'EXEMPLAIRE DONT POSSEDE LE DEPARTEMENT DES ARCHIVES ET DES COLLECTIONS SPECIALES, BIBLIOTHEQUE ELIZABETH DAFOE, UNIVERSITE DU MANITOBA, WINNIPEG, MANITOBA, CANADA, R3T 2N2.

Figure 55(a). Mineralogy of the Silverleaf pegmatite - an enriched offshoot of the Greer Lake intrusion. Columnar spodumene + quartz pseudomorphs after petalite in a groundmass of albite + quartz + lithian muscovite.

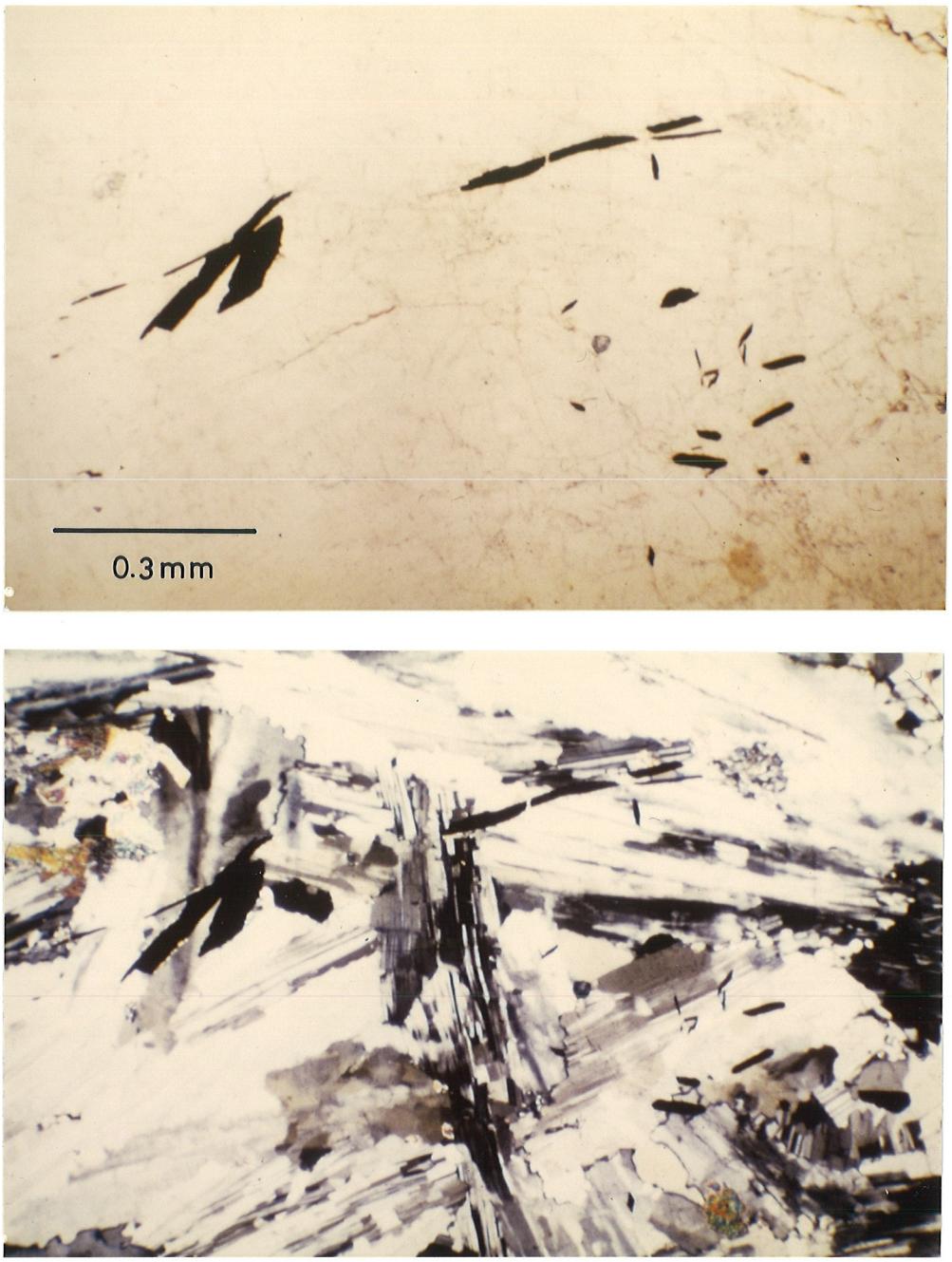

Figure 55(b). Photomicrograph of bladed opaque minerals (probably Nb,Ta oxide phases) in cleavelandite of the Silverleaf offshoot of the Green Lake intrusion (plane polarized light above, crossed polars below). Note typically shaped bluish tourmaline crystal in right central area of photograph.

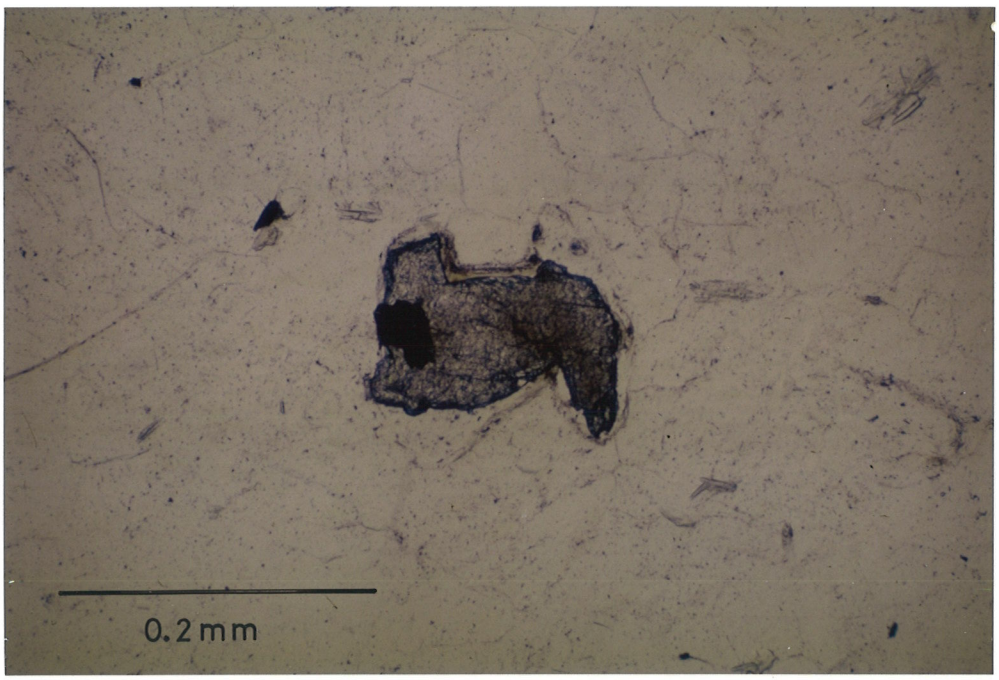

Figure 56. Cassiterite in the sodic aplite facies from the Silverleaf offshoot. Note possible Nb,Ta oxide mineralization (opaque) and reaction rim.

the present study. Microprobe analyses of the Silverleaf cassiterite are listed in Appendix 8.

5. Ilmenite

Ilmenite, $FeTiO_3$, was found in drill core in a quartz + feldspar vein twenty centimetres below the Silverleaf Claim intrusion within the hosting metabasalts. It was analyzed (Appendix 8) to compare its composition to that of a similar occurrence beneath the adjacent Huron Claim pegmatite situated approximately 600 metres to the east (Paul, in prep.). Its density was obtained using a Berman torsion balance (Appendix 8).

6. Amblygonite-Montebrasite

This species, $(Li,Na)AlPO_4(F,OH)$, was reported from the Silverleaf Claim (Černý, pers. comm. 1978) but was not observed during this study; however, a sample was obtained from the mineral collection of Harvard University (Sample No. 101698). The name applied to a particular mineral specimen depends on the OH/F ratio. If OH < F the mineral is amblygonite; if OH > F it is montebrasite. The density and the refractive index (γ') of this specimen were obtained and are listed in Appendix 8. This mineral was X-rayed four times following the method of Černá et al. (1973) to determine the weight percent fluorine in the structure. Consequently, the mineral was classified as montebrasite (Table 17).

Table 17. Fluorine content of amblygonite-montebrasite samples

Sample No.	20131	Wt. % F
SF-1	52.340	3.00
SF-2	52.305	2.55
SF-3	52.285	2.40
SF-4	52.280	2.30

7. Lithiophilite-Triphylite

A salmon pink lithiophilite, $Li(Mn,Fe)PO_4$, was associated with the montebrasite in the above sample (#101689). A positive identification was obtained by X-ray powder diffraction methods. The density was obtained and is listed in Appendix 8.

8. Topaz

Topaz ($Al_2SiO_4(OH,F)_2$) was found only in the Silverleaf pegmatite pod located south of the Greer Lake intrusion of pegmatitic granite. The fluorine content of this species was determined. The method of Ribbe and Rosenberg (1971) was utilized. Reagent grade NaCl was used as an internal standard. Results are listed in Table 18.

9. Other Trace Minerals

Other minerals found in only one location were X-rayed for positive identification. These include molybdenite (MoS_2) from a potassic pegmatite pod in the western end of the Tin Lake intrusion and a sphalerite (ZnS) from the Annie Claim (AC-2) pod.

E. SECONDARY MINERALS

Several secondary minerals whose primary phase can only be assumed were studied.

Table 18. Diffraction peak locations of topaz and reagent grade NaCl. The fluorine content of topaz has been calculated using the graph and equation presented in Ribbe and Rosenberg (1971)

Location	Sample No.	NaCl (200)	Topaz (120)	Change (120)	Wt. % F (graph)	Wt. % F (equation)
Silverleaf Claim	SHEE-2-SE	31.77	27.94	3.83	18.75	18.89
Silverleaf Claim	M16111	31.69	27.87	3.82	19.20	19.34

1. Cordierite Pseudomorphs

These pseudomorphs, characteristic only of the Greer Lake pegmatite group (Černý et al., 1981; Černý and Turnock, 1971) have been observed within the potassic pegmatite facies of the Greer Lake intrusion (Figure 38, 39). Also, where the Tin Lake pegmatitic granite is in contact with the metaturbidites of the Booster Lake formation, altered cordierite pseudomorphs occur in the fine-grained leucogranite facies (Černý, pers. comm. 1978).

Thin section study shows the mineralogy of the pseudomorphs to be, in order of decreasing abundance, green biotite, chlorite, muscovite, garnet, beryl, and possibly small relics of primary cordierite (Figure 57). Textures suggest that biotite and chlorite first formed along parallel parting planes separating basal plates of cordierite (Figure 57). Replacement of the remaining cordierite mass continued by a 3-dimensional layer silicate invasion with flakes oriented subnormal to normal to the basal parting, imparting on the final aggregate a box-like texture when dissected parallel to c (Figure 57). All phases have been identified by X-ray diffraction photographs except the cordierite. It was tentatively identified optically. The garnet has a high spessartine content and its calculated a cell dimension is plotted in Figure 48.

NOTICE/AVIS

PAGE(S) 149 - 152 ~~IS~~/ARE ~~EST~~/SONT color photos

PLEASE WRITE TO THE AUTHOR FOR INFORMATION, OR CONSULT THE ARCHIVAL COPY HELD IN THE DEPARTMENT OF ARCHIVES AND SPECIAL COLLECTIONS, ELIZABETH DAFOE LIBRARY, UNIVERSITY OF MANITOBA, WINNIPEG, MANITOBA, CANADA, R3T 2N2.

VEUILLEZ ECRIRE A L'AUTEUR POUR LES RENSEIGNEMENTS OU VEUILLEZ CONSULTER L'EXEMPLAIRE DONT POSSEDE LE DEPARTEMENT DES ARCHIVES ET DES COLLECTIONS SPECIALES, BIBLIOTHEQUE ELIZABETH DAFOE, UNIVERSITE DU MANITOBA, WINNIPEG, MANITOBA, CANADA, R3T 2N2.

Figure 57(a). It shows one of the larger specimens found (GL-37). Note the large garnet porphyroblasts and the regular crystal outline of the original cordierite mineralization. The cordierite began to alter along the basal portion of the crystal and then worked into the interior, forming planes of biotite + chlorite.

Figure 57(b). Planes of biotite + chlorite (reflecting light) showing parallel orientation.

Figure 57(c). This parallel orientation of biotite + chlorite along cleavage planes which forms "layering" of the pseudomorph is shown as step-like boxwork sandwiching flattened garnet crystals.

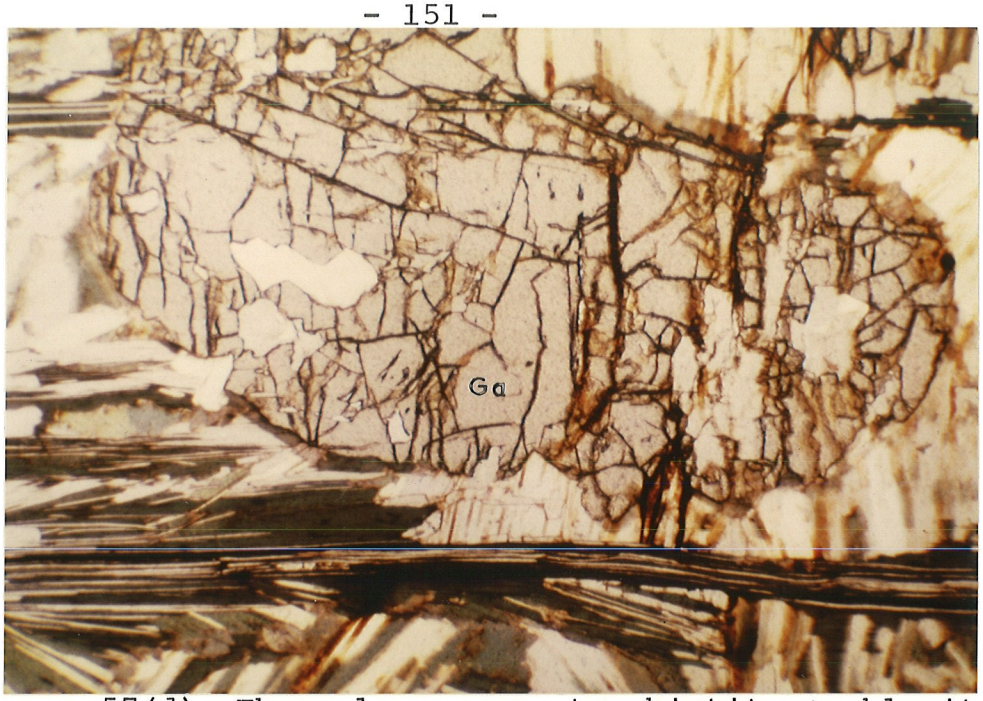

Figure 57(d). These layers are two biotite + chlorite layers (which formed initially along a cleavage plane of the cordierite crystal) enclosing a band of garnet + muscovite + quartz ± biotite ± cordierite ± beryl usually growing perpendicular to the biotite + chlorite layer. Short edge of photo is 1 cm.

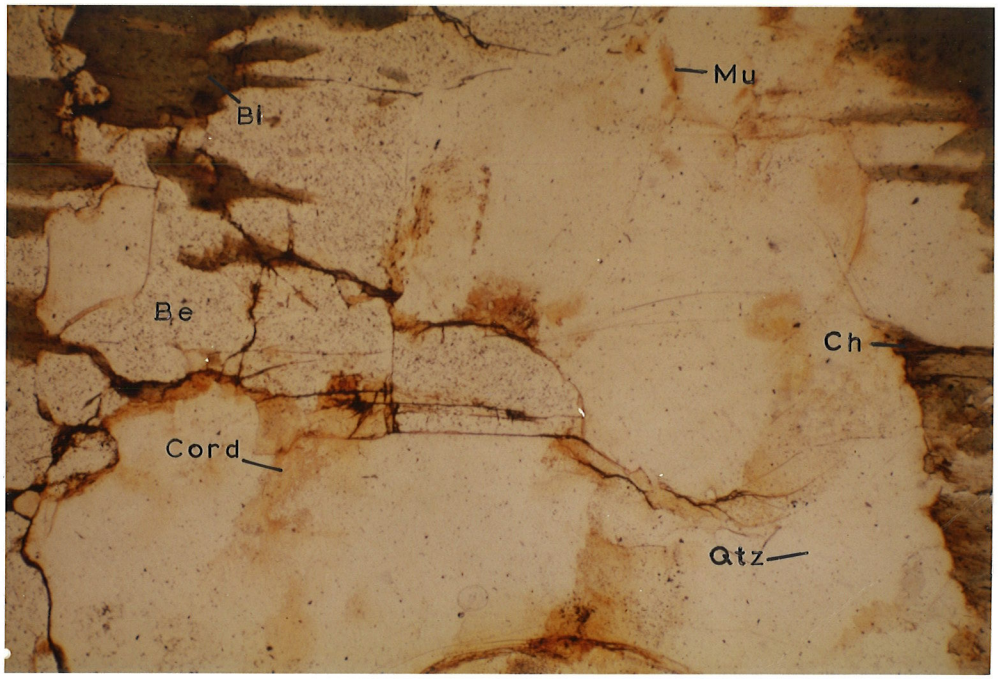

Figure 57(e). It is an enlarged section of the pseudomorph showing biotite (Bi), chlorite (Ch), muscovite (Mu), garnet (Ga), beryl (Be), and relict cordierite - all identified by X-ray diffraction methods. Short edge of photo is 1 cm.

Figure 57(f). Cordierite pseudomorphs were also found in the hosting sediments of the Tin Lake intrusion adjacent to the pegmatitic granite and a lone occurrence (shown) at OL-13 of a more biotite-rich pseudomorph. Unfortunately this one was only noted in the field and thus not available for study. Note the garnet and tourmaline-rich intrusion at this location.

2. Manganoan Sicklerite

This mineral only appears in the western end of the Osis Lake intrusion in the potassic pegmatite facies (Figure 22(a). It forms as an alteration product after lithiophilite-triphylite. This species was identified by X-ray diffraction.

3. Fibrous Muscovite

This alteration was noted only in one location within the Osis Lake intrusion and has been discussed earlier and illustrated in Figure 32.

4. Pseudomorph After Topaz(?)

Two occurrences of a fine muscovite apparently replacing some primary mineral were found in the Tin Lake intrusion. It has been suggested (Černý, pers. comm. 1978) that the original mineral could have been topaz; however, this could not be verified. Thin section and X-ray diffraction illustrated muscovite and epidote to be the only phases present, and the presence of epidote ($CaFeAl_2O.OH[Si_2O_7][SiO_4]$) does not support the idea of topaz ($Al_2SiO_4(OHF)_2$) being the primary phase.

Chapter VI

PETROCHEMISTRY

A. INTRODUCTION

In total, fifty four whole rock samples were analyzed for SiO_2, TiO_2, Al_2O_3, Fe_2O_3, FeO, MnO, MgO, CaO, Na_2O, K_2O, P_2O_5, CO_2, and H_2O. Most of these samples were analyzed for selected minor and trace element content (Li, Rb, Cs, Be, Sr, Ba, Pb, U, Th, Zr, Sn, Y, and F) and several were selected for rare earth element analyses (La, Ce, Nd, Sm, Eu, Tb, Dy, Yb, and Lu). These samples included specimens representative of all four facies within each intrusion of pegmatitic granite.

The purpose of these analyses was to:

a) establish the general compositional characteristics of the pegmatitic granites;

b) compare the bulk chemistry of the individual intrusions of pegmatitic granite among themselves;

c) illustrate fractionation trends within individual intrusions and compare these trends to those of other intrusions of pegmatitic granite in the Winnipeg River area;

d) derive the genesis of the pegmatitic granites in this study.

B. BULK CHEMISTRY

The chemical analyses of the samples covering all facies of the four pegmatitic granites are listed in Appendix 1. These analyses show that the composition of the pegmatitic granites are silicic and carry low amounts of CaO, FeO, and MgO with respect to adjacent batholithic granites (Černý et al., 1981).

CIPW norms were calculated (Table 19) to verify the peraluminous character of these rocks (Figure 58) as suggested by the accessory garnet, muscovite, tourmaline, cordierite, and gahnite of the pegmatitic granites. Values of normative (CIPW) corundum range from 0.0 to 5.4 percent (Figure 58).

The CIPW norm calculation does not calculate values for hydrous minerals (the pegmatitic granites carry accessory to subordinate muscovite). Consequently Barth's mesonorm calculation which allots a portion of the K_2O into biotite and muscovite was used, thus allowing the calculation of a more realistic composition of the pegmatitic granites (Barth, 1966).

The above program was modified to omit muscovite for a better representation of Or in plotting the ternary Ab-Or-An and Ab-Or-Quartz diagrams (Figure 59). The four facies within the pegmatitic granites arrange themselves in these diagrams into trends originating from the leucogranite composition. This is in agreement with textural evidence

Table 19. CIPW normative corundum (or diopside; sodic aplite sample SL-2-18) of all analyzed samples from the four facies of the Winnipeg River pegmatitic granites

Leucogranite	Normative Corundum (CIPW)
TNL-2	0.874
TNL-21	0.519
TNL-27	0.972
TNL-31	0.720
TNL-34	0.958
TNL-39	0.853
TNL-43(HG)	1.341
TNL-54	2.221
TNL-58	0.333
TNL-61	1.618
TNL-65(a)	1.454
TNL-67	1.504
TNL-68	3.866
OL-8	4.522
OL-10	3.167
OL-23	2.620
OL-23(a)	2.319
OL-23(b)	3.144
OL-23(c)	2.300
GL-13(a)	0.131
GL-33(e)	3.106
GL-35(a)	0.615
GL-38(a)	1.270
GL-1002(HG)	3.522
ENL29(c)	2.578
ENL-6(b)	2.100
SR-54-E-2	2.184

Transitional: Sodic Aplite to Pegmatitic Leucogranite	Normative Corundum (CIPW)
ENL-2(a)	2.246
ENL-26(b)	3.195
GL-33(c)	2.296
OL-12	3.474
GL-19(c)	3.827
GL-25(a)	1.721
ENL-25(c)-A	3.166

Sodic Aplite	Normative Corundum (CIPW)
TNL-37(c)	2.038
OL-11	4.930
GL-6(a)-A	1.457
GL-6(d)-A	3.333
SL-1-95	1.871
SL-2-18	-0.024
LOBE-12	3.534
ENL-10-1	0.691
ENL-11(a)	0.969
ENL-20(c)	2.533

Pegmatitic Leucogranite	Normative Corundum (CIPW)
TNL-1006	1.446
OL-1005	2.947
OL-1004	4.641
GL-1003	3.352
GL-1002	4.742
ENL-1001	3.593

Potassic Pegmatite	Normative Corundum (CIPW)
GL-6(a)-P	5.483
GL-6(d)-P	5.199
ENL-25(c)-P	4.279
OL-13(P+SA mix)	5.203

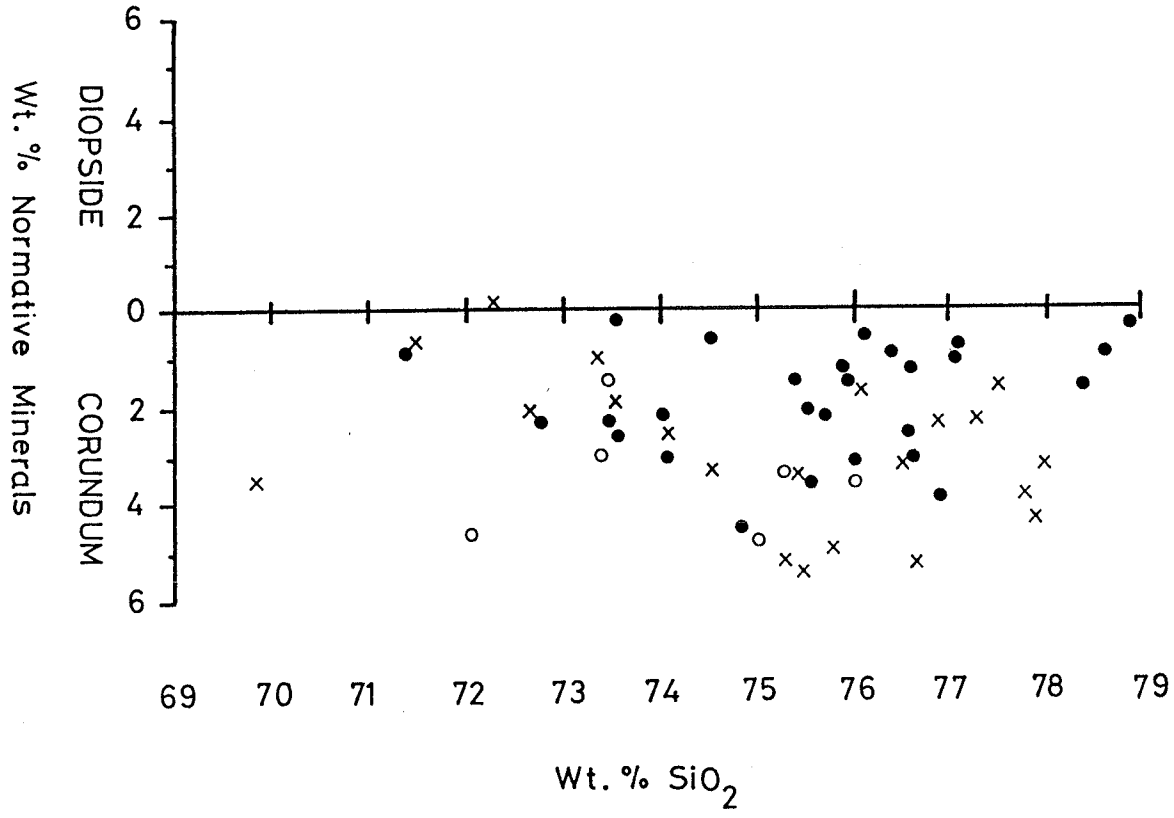

Figure 58. Normative corundum and diopside (CIPW) of the leucogranites (●), the sodic aplites (x), and the pegmatitic leucogranites (o) from all four intrusions of pegmatitic granite in the Winnipeg River area of southeastern Manitoba, plotted against SiO_2.

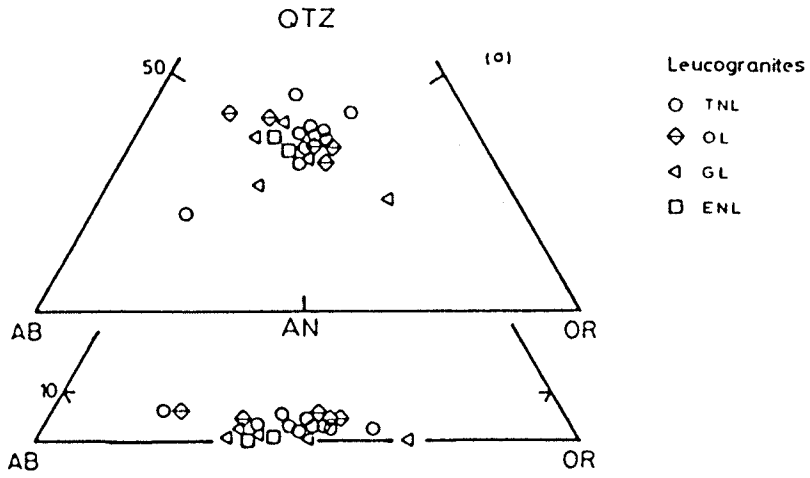

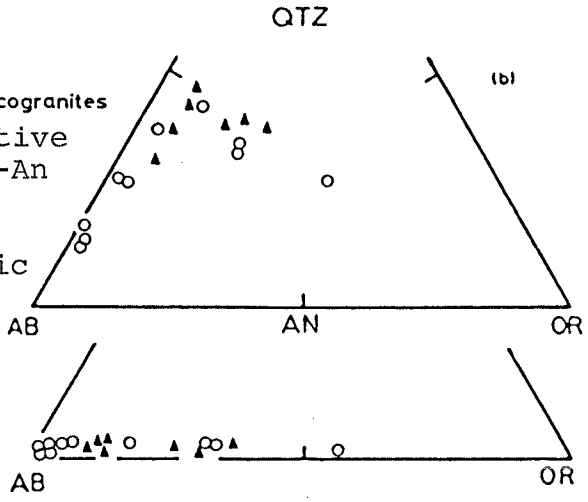

Figure 59. Plots of normative * Ab-Or-Qtz and Ab-Or-An in the fine-grained leucogranites, sodic aplites, and pegmatitic leucogranites of the Winnipeg River pegmatitic granites. *Barth's mesonorm.

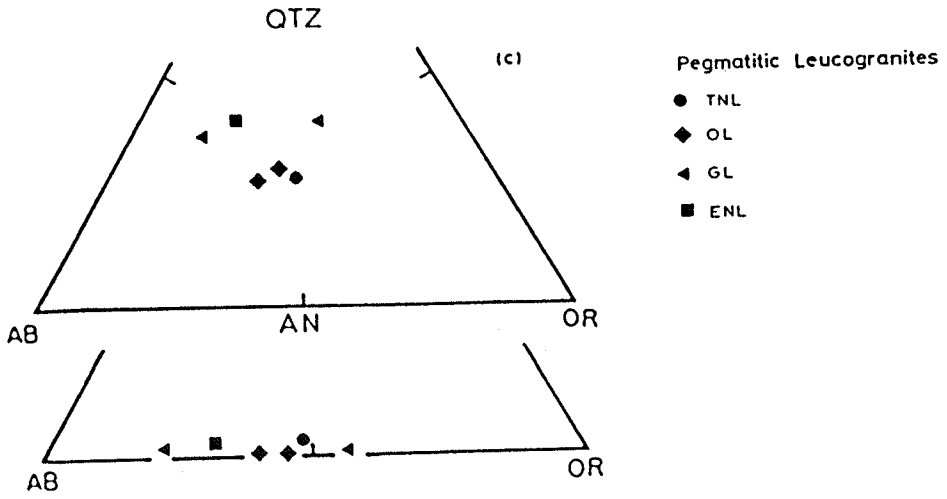

seen both in the field and in thin section. The leucogranites are grouped in the area of Ab_{30-35}-Or_{30-35}-Qtz_{30-38} (Figure 59) within Winkler and Von Platen's (1961) granitic field, on or near the low-pressure granitic minima (Winkler, 1965; Winkler et al., 1975).

The sodic aplite develops from leucogranite by an initial decrease in the K-feldspar (Or) component and a slight increase in quartz. This is followed by a significant decrease in the quartz component and by an increase in the Ab component with further loss of the Or component (Figure 59). The pegmatitic leucogranites are scattered in the area of the granitic minima. This scattering may be due to difficulties encountered in obtaining large samples representative of this facies; however, Orville (1960) and Proctor and El Etr (1968) obtained data on similar rocks in the Black Hills, South Dakota and in Wyoming, showing a similar decrease in SiO_2 and a slightly greater Ab concentration than Or.

Figure 59 also illustrates the normative compositions of the pegmatitic granites in the ternary Ab-Or-An feldspar system. Both the leucogranites and the pegmatitic leucogranites are in, or very near the low-temperature trough discussed in Kleeman (1965). The scattering is again possibly due to sampling problems of the pegmatitic leucogranite, or in the case of the leucogranite, incipient transition toward the Ab-enriched sodic aplite composition. In

Figure 59, the leucogranites of the TNL and OL intrusions reflect a slight increase in the CaO content by a slight, but distinct, enrichment of the An component.

C. TRACE ELEMENTS

An examination of recent literature reveals that most general trace element trends in differentiated igneous rock series are well documented. Rb (Ahrens et al., 1952; Taylor et al., 1956; Dostal, 1975), Cs, Li (Siedner, 1968), and partly Ga (de Albuquerque, 1971) are all concentrated in the late differentiates. Ba decreases more rapidly than Sr as differentiation proceeds (Heier and Taylor, 1959(a) and 1959(b); El Bouseily and El Sokkary, 1975). Ba is concentrated relative to K in early minerals, and therefore the early formed rocks; however, it is not extensively depleted in the magma until the late stages of the differentiation sequence (Nockolds and Allen, 1953; El Bouseily and El Sokkary, 1975).

In the present discussion, several significant geochemical ratios are used to illustrate the fractionation trends of rocks and mineral species. They include K/Rb, K/Cs, Mg/Li, Ca/Sr, Al/Ga, K/Ba, and Rb/Sr. These ratios for each sample are listed in Appendix 1. With respect to the batholithic granites of the Lac du Bonnet intrusion (Černý et al., 1981) the geochemistry of the pegmatitic granites is highly fractionated.

Geochemical traits of the Winnipeg River pegmatitic granites are easily demonstrated graphically. The low concentration of U and Th resulting from outward diffusion is illustrated in Figure 60. The composition of the pegmatitic granites fall into the field of Bailey's (1977) stanniferous granites where the F/(Sn + Li) ratio is lower than the same for normal granites. The Sn/Li ratio of the pegmatitic granites changes as the transition of sodic aplite to leucogranite occurs. In all facies of the pegmatitic granites the F content remains consistently low and mostly contained within muscovite (Figure 61).

Many geochemical relationships were studied and the best chemical trends were distinguished by the following relationships. General fractionation trends common to all four intrusions are suggested by plots of Rb vs. Sr (Figure 62), K/Ba vs. Ba, K/Rb vs. Rb (Figure 63) and Rb vs. Ba (Figure 64). However, several of these relationships and others (Rb vs. Sr, K/Rb vs. Rb, Rb vs. Ba, Mg vs. Li, Ba vs. Sr, Ba/Sr vs. Sr, Mg/Li vs. Li, Al vs. Ga, Al/Ga vs. Ga and K vs. Ba (Figures 62 to 71, respectively) also illustrate a difference in the absolute trace element content and discontinuities between the leucogranite facies of the two pegmatitic granites north of the Winnipeg River and the same facies of the pegmatitic granites south of the river. This type of variation is also apparent between the two intrusions south of the river and also between the two intrusions north

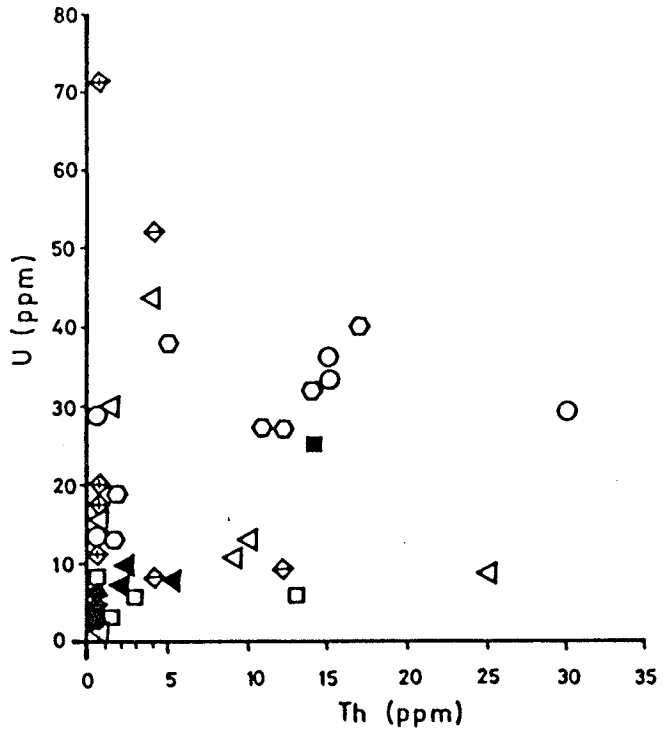

LEUCOGRANITE

- TNL–NORTH
- TNL–SOUTH
- OL (OL-23 ◈)
- GL
- ENL

SODIC APLITE

- TNL–NORTH
- OL
- GL
- ENL

PEGMATITIC LEUCOGRANITE

- TNL–NORTH
- OL
- GL
- ENL

POTASSIC PEGMATITE

- TNL–NORTH
- OL
- GL
- ENL

Figure 60. U vs. Th plot of the leucogranite and pegmatitic leucogranite facies from the pegmatitic granite intrusions. Note the separate fields of each intrusion and low U and Th content of the pegmatitic leucogranite facies.

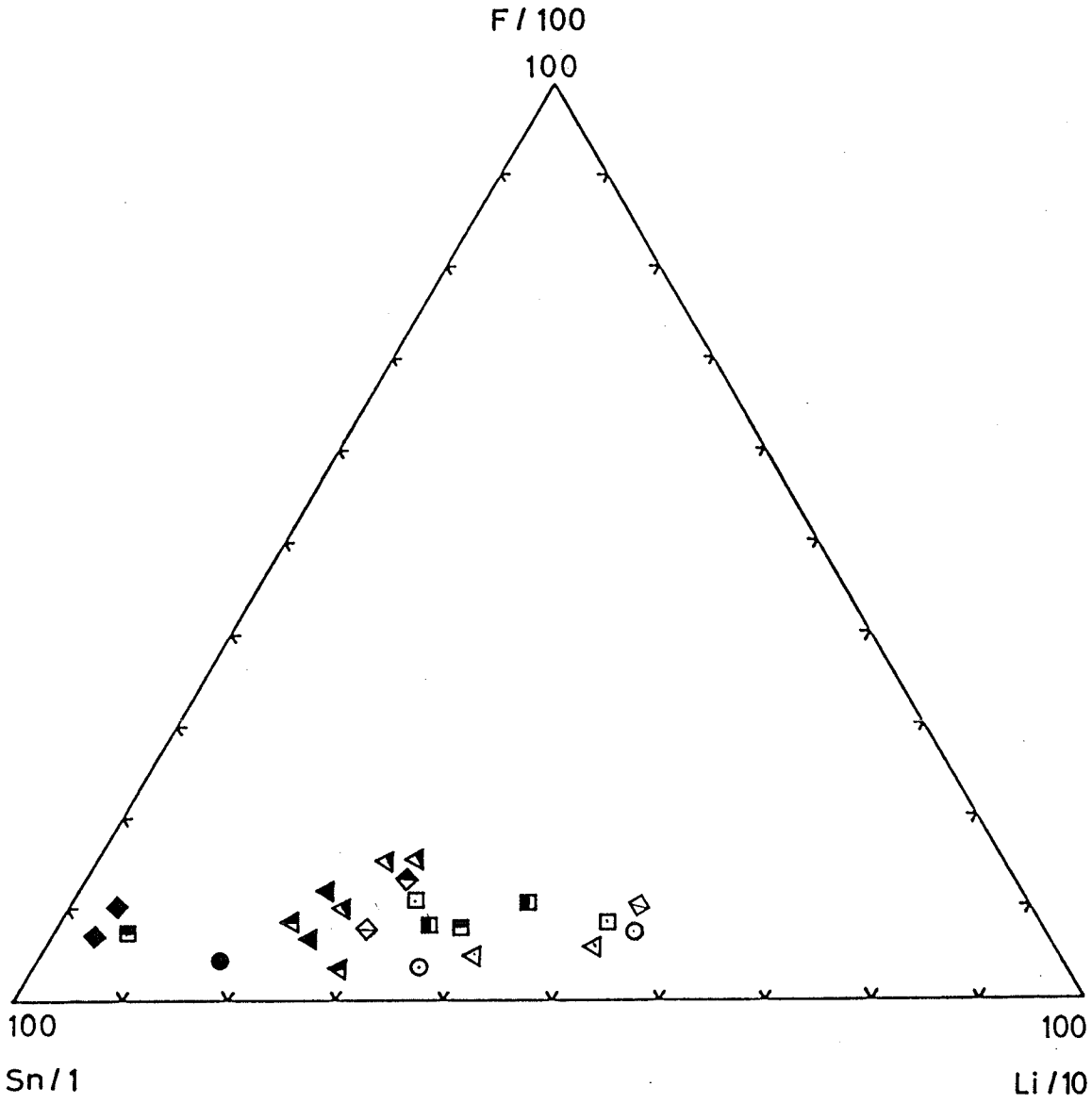

Figure 61. Sn-Li/10-F/100 plot of samples representative of each facies from all intrusions. Symbols as in Figure 60.

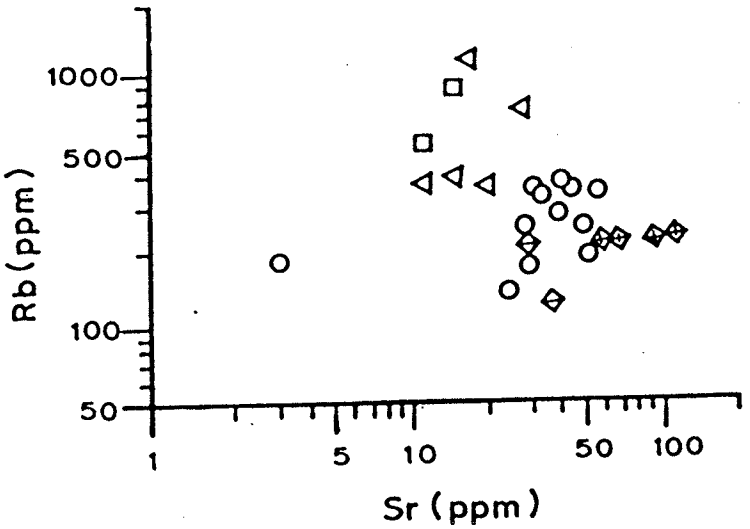

Figure 62. Rb vs. Sr plot of the fine-grained leucogranites from pegmatitic granite intrusions. Symbols as in Figure 60.

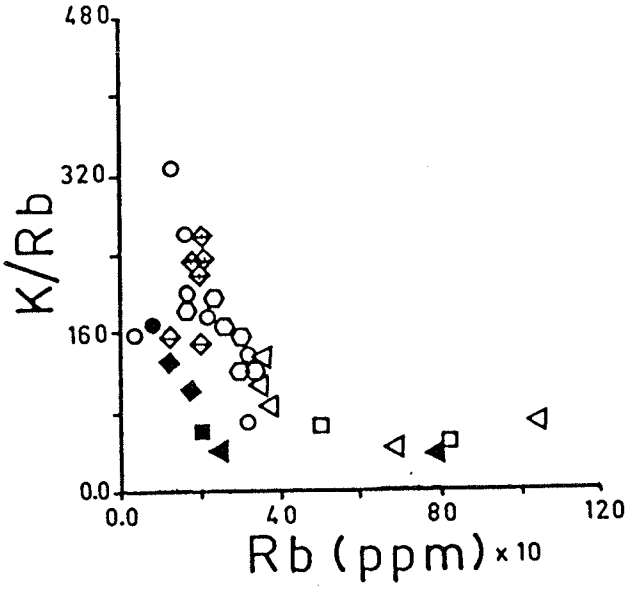

Figure 63. K/Rb vs. Rb plot of the fine-grained and pegmatitic leucogranites from pegmatitic granite intrusions. Note the Rb enrichment in the pegmatitic granites, and in the GL and ENL intrusions in general. Symbols as in Figure 60.

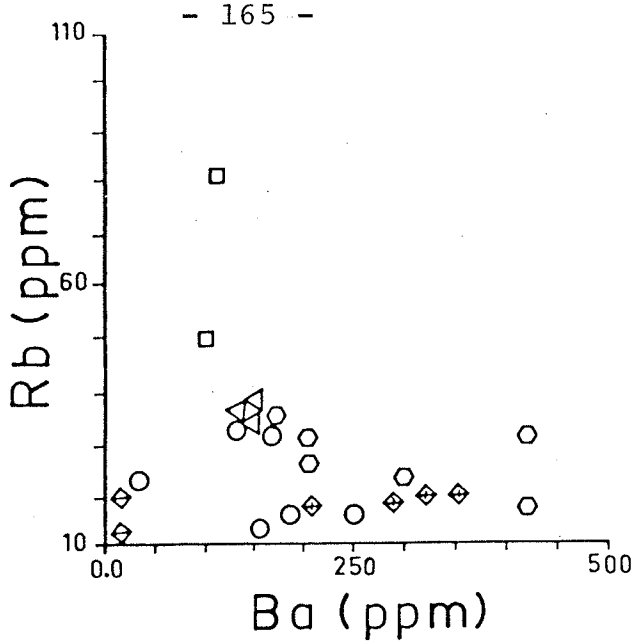

Figure 64. Rb vs. Ba plot of the leucogranite facies in the Winnipeg River pegmatitic granite. Symbols as in Figure 60.

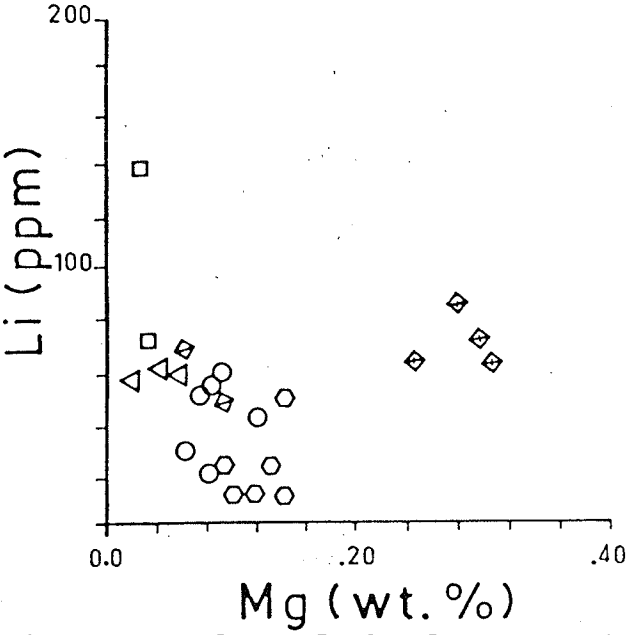

Figure 65. Li vs. Mg plot of the leucogranite facies in each intrusion of pegmatitic granite. Note individual fields of each intrusion and the elevated Li content of the GL and ENL intrusions. Symbols as in Figure 60.

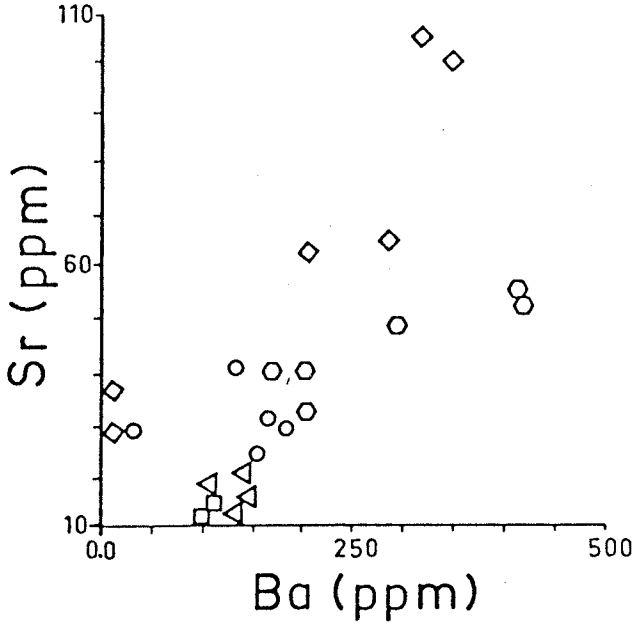

Figure 66. Sr vs. Ba plot of the leucogranite facies within the four intrusions of pegmatitic granite. Symbols as in Figure 60.

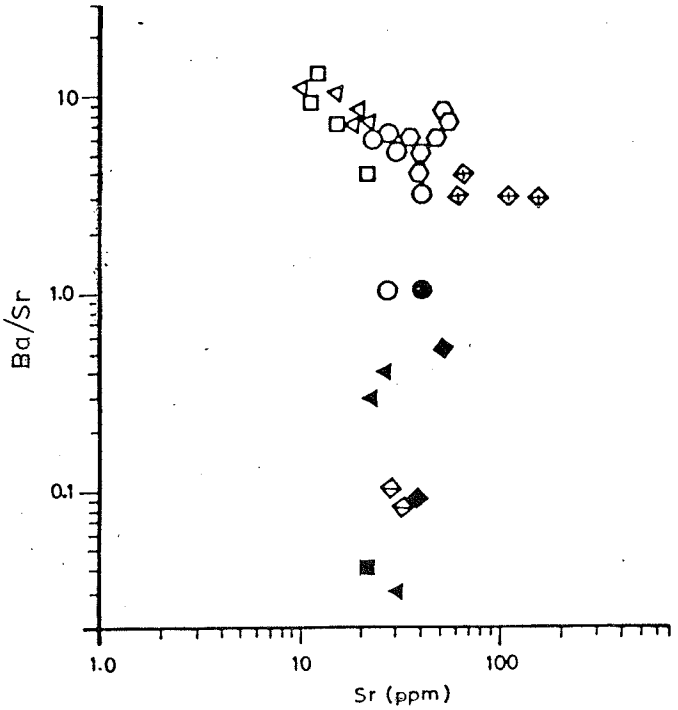

Figure 67. Ba/Sr vs. Sr plot of samples from the leucogranite and pegmatitic leucogranite facies of the pegmatitic granites. Note the fields of each intrusion and the Ba content of the pegmatitic leucogranite facies lower than the corresponding leucogranite facies. Symbols as in Figure 60.

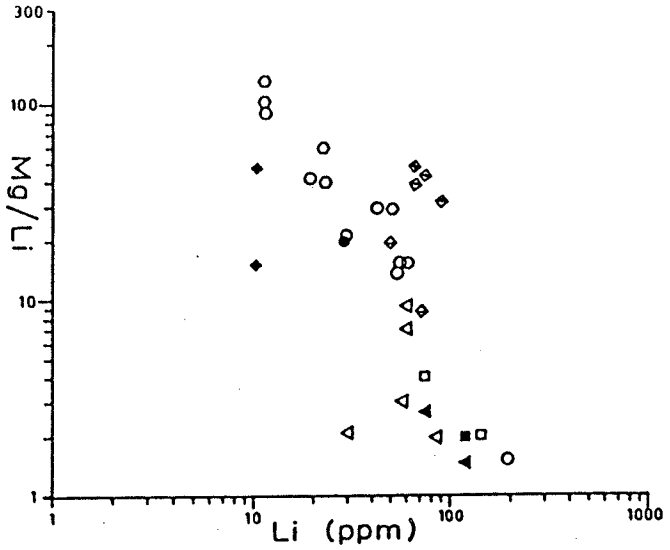

Figure 68. Mg/Li vs. Li plot of the fine-grained and pegmatitic leucogranites from pegmatitic granite intrusions. Note the low Mg/Li values in pegmatitic granites, and the Li enrichment in the GL and ENL intrusions. Symbols as in Figure 60.

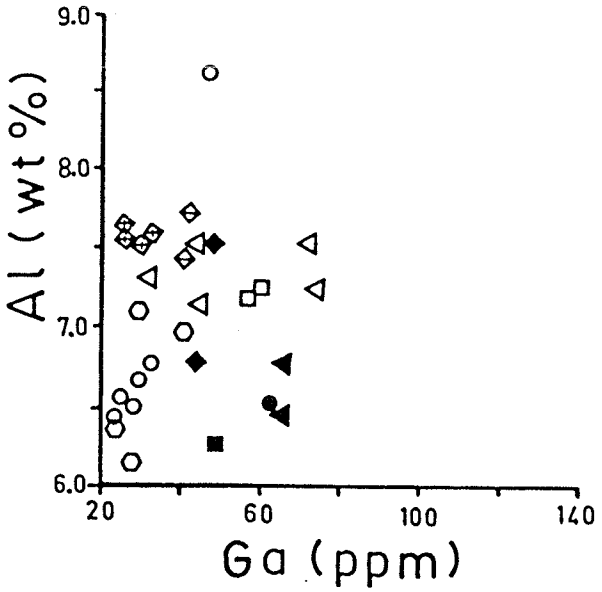

Figure 69. Al vs. Ga plot of the fine-grained and pegmatitic leucogranite from the pegmatitic granite intrusions. Note the high Al and Ga contents of the pegmatitic leucogranites, and the Ga enrichment in the GL and ENL intrusions. Symbols as in Figure 60.

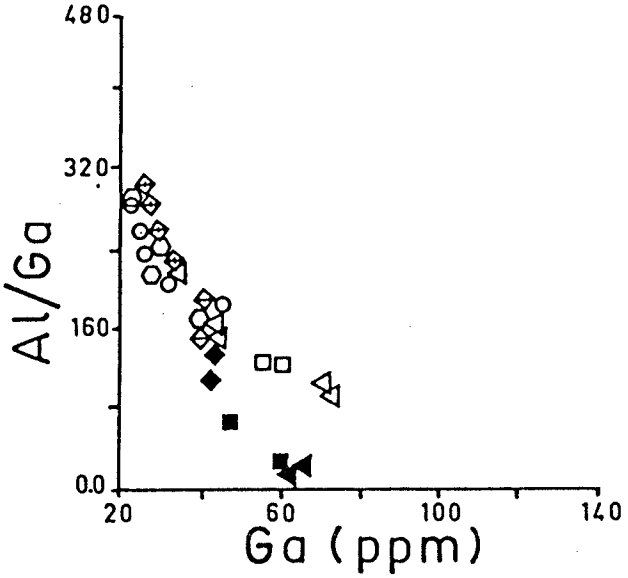

Figure 70. Al/Ga vs. Ga plot of the fine-grained and pegmatitic leucogranites from the pegmatitic granite intrusions. Note the low Al/Ga ratios of the pegmatitic granites and of the GL and ENL intrusions in general. Symbols as in Figure 60.

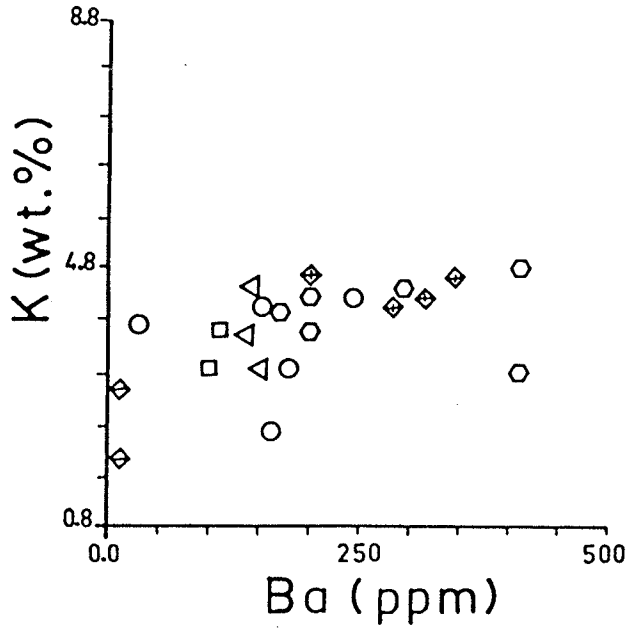

Figure 71. K vs. Ba plot of the leucogranite facies in each intrusion of pegmatitic granite. Note the low Ba content of the OL intrusion compared to OL-23, the central plug of biotite granite. Symbols as in Figure 60.

of the river; however, it is not as pronounced. This feature is suggestive of a relationship which is more complex than a simple continuous differentiation/fractionation link among the four intrusions.

D. RARE EARTH ELEMENTS

REE data for the two predominant rock types of the pegmatitic granites, the leucogranites and the pegmatitic leucogranites, are listed in Appendix 1. All analyses are normalized to the Leedey chondrite (Masuda et al., 1973). These elemental abundances are also listed in Appendix 1. Generally, low total REE content and extreme negative Eu anomalies predominate, flanked by flat LREE and HREE distribution with low normalized Ce/Yb ratios. The only exception is the Osis Lake intrusion (including the central plug of biotite granite) which has a steeper sloping distribution (normalized Ce/Yb > 1) and a moderate Eu anomaly. Within a single intrusion, the REE concentration tends to be slightly, to distinctly, lower in the pegmatitic leucogranites than in the fine-grained leucogranites; however, the REE pattern is identical for both facies. The limited data available for the other two facies indicate that the sodic aplites have REE contents within the limits of the associated fine-grained leucogranites but the REE abundances decrease drastically in the potassic pegmatites (Appendix 1, Figure 71). The REE total also appears to decrease with increasing normative

corundum; however, this trend does show a wide scatter.

The pegmatitic granites follow the general trends listed in Koljonen et al. (1974). The REE content decreases with decreasing K/Rb, K/Cs, and other ratios indicative of progressive fractionation. The negative Eu anomaly increases with progressive fractionation as Eu is incorporated into early phases containing Ca (plagioclase). Koljonen et al. (1974) and Emmermann et al. (1975) both mention the fact that the HREE (Gd to Lu) are commonly depleted relative to the LREE (La to Sm) during the final stages of granitic differentiation. All these trends are shown by the different pegmatitic granites, as illustrated in Figure 72. The TNL and OL REE patterns are not as flat as the REE patterns of the southern intrusions (GL and ENL); in other words the LREE were not depleted as rapidly as the HREE. It has been suggested (Puchelt and Emmermann, 1976; Hanson, 1978) that apatite and biotite (both REE accumulating minerals) show an enrichment of the LREE over the HREE. Consequently, those intrusions carrying either, or both these minerals should show a corresponding LREE-enriched pattern, as is the case in OL and TNL. This is illustrated by Figure 72. Koljonen et al. (1974) state that pegmatites and other highly fractionated SiO_2-rich rocks contain less REE than average granites. The pegmatitic granites have low normalized element/chondrite rare earth ratios (70-10). The REE content is highest in the TNL intrusion which appears to be

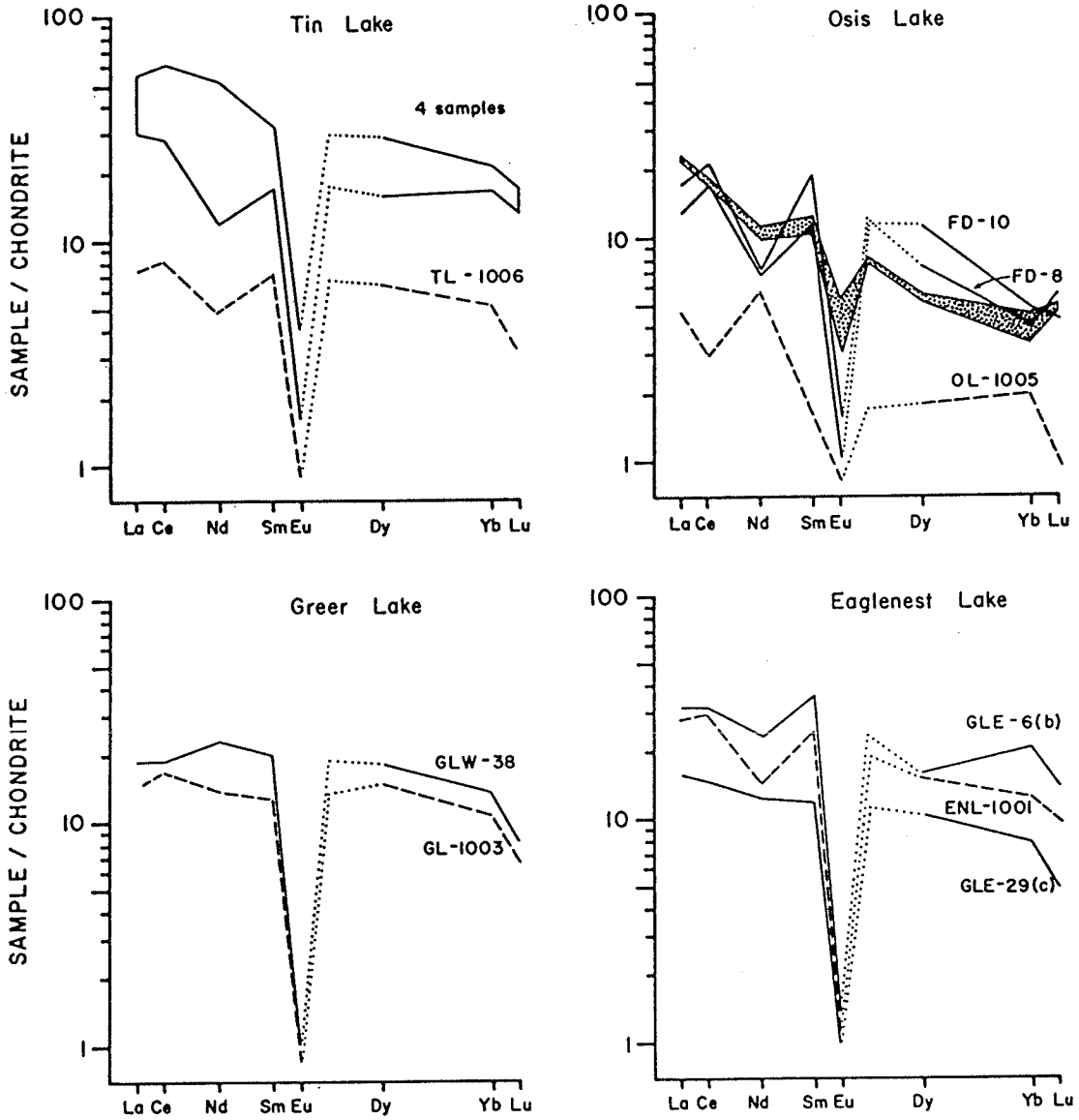

Figure 72. REE abundances in the fine-grained leucogranite (——) and pegmatitic leucogranite (— —) phases of the pegmatitic granite intrusions and in the biotite granite of the Osis Lake intrusion (....) (Goad and Černý, 1981).

the least fractionated (K/Rb=176, K/Cs=6800) and decreases through OL and ENL to the least REE-enriched GL intrusion (K/Rb=27, K/Cs=5108).

The rare earth patterns of the GL, ENL, and TNL intrusions are quite similar; all have the same rate of LREE to HREE depletion (i.e. similar slopes) and the same negative Eu anomaly. The distinctive OL samples will be discussed in chapter IX; however, the location of some of the samples should be noted. OL-1005 is from the coarse B, Li, H_2O-enriched western dike-like area of the intrusion while the other two samples (OL-23(a) and OL-23(b)) are from the homogeneous biotite-bearing central plug within the intrusion.

E. OXYGEN ISOTOPES

Oxygen isotope ratios ($\delta^{18}O$, normalized to SMOW) were determined in several representative rock types within each intrusion (Table 20) and in several minerals in these facies. $\delta^{18}O$ was calculated by:

$$\delta^{18}O = \left[\left(\frac{R(\text{sample})}{R(\text{standard})}\right) - 1\right] \times 1000$$

where $R = (^{18}O/^{16}O)$

The ^{18}O values are plotted in Figure 73 along with the $\delta^{18}O$ values of the enclosing metasedimentary and/or metavolcanic rocks. The oxygen isotope ratios of all facies are quite variable among the four intrusions of pegmatitic granite

Table 20. List of the $\delta^{18}O$ rock and mineral values for the analyzed samples from the Winnipeg River pegmatitic granites

Sample No.	Facies	$\delta^{18}O$ (rock)	$\delta^{18}O$ (quartz)	$\delta^{18}O$ (alk.fsp.)	$\delta^{18}O$ (musc.)	$\delta^{18}O$ (biot.)
GL-38(a)	leucogranite	8.1	10.2	7.5	6.4	3.4
GL-1002	peg. leuco.	8.2	9.8	7.5	6.4	
GL-1003	peg. leuco.	8.4				
GL-6(a)-P	potassic peg.	8.7				
GL-6(d)-P	potassic peg.	8.5				
GL-6(a)-A	sodic aplite	8.3				
GL-6(d)-A	sodic aplite	8.6				
ENL-6(b)	leucogranite	9.3	10.6	7.9	6.3	
ENL-29(c)	leucogranite	9.0				
ENL-1001	peg. leuco.	8.6	10.4	7.7	6.5	3.3
ENL-25(c)-P	potassic peg.	9.1				
ENL-25(c)-A	sodic aplite	9.0				
ENL-10-1	sodic aplite	8.8				
ENL-20(c)	sodic aplite	8.8				
TNL-31	leucogranite	10.9				
TNL-27	leucogranite	10.9				
TNL-34	leucogranite	10.9	12.1	10.1	8.4	5.3
TNL-43-HG	leucogranite	10.7				
TNL-1006	peg. leuco.	10.3	12.0	9.7		4.9
OL-8	leucogranite	11.9				
OL-10	leucogranite	11.8	13.4	11.0	9.6	5.8
OL-23	biot. gran.	11.1				
OL-23(a)	biot. gran.	11.1				
OL-23(b)	biot. gran.	11.2	13.0	11.4	9.5	5.9
OL-23(c)	biot. gran.	11.1				
OL-1004	peg. leuco.	11.7	13.0	10.7		
OL-1005	peg. leuco.	11.7				
OL-11	sodic aplite	11.8				
OL-12	sodic aplite	12.4				

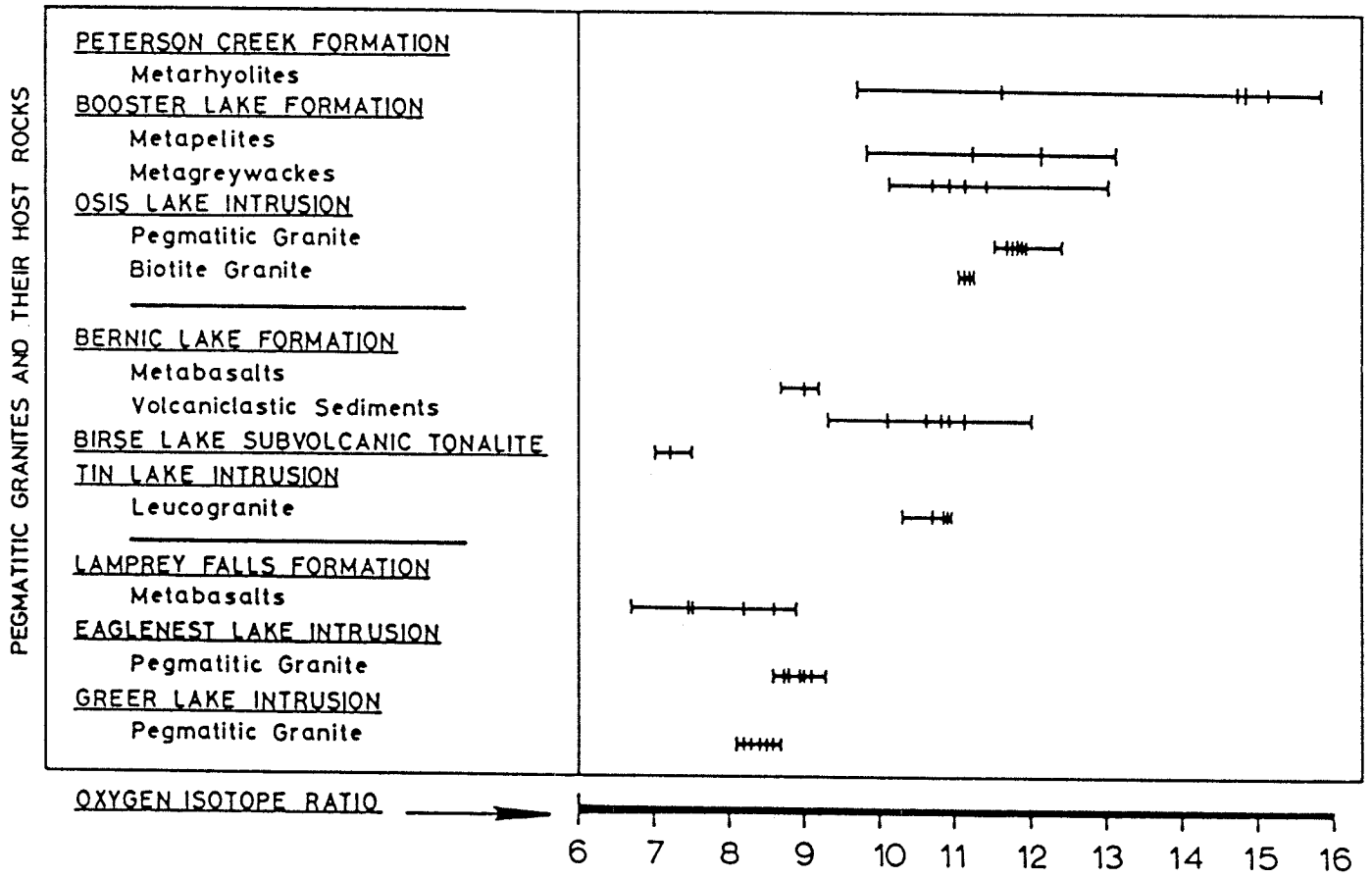

Figure 73. Oxygen isotope ratios in selected facies of the pegmatitic granites and the enclosing host rock of the Bird River greenstone belt. Data have been adapted after Longstaffe et al. (1981).

(Figure 73). Data in Table 21 illustrates the high degree to which the $\delta^{18}O$ values of the pegmatitic granites correlate to the $\delta^{18}O$ of the hosting metasedimentary and/or metavolcanic rocks. This suggests that some equilibration of the $^{18}O/^{16}O$ ratio between the two rock types has occurred. This will be discussed further in Chapter IX.

Table 21. Correlation of the $\delta^{18}O$ values (average) of each intrusion to that of the hosting metasedimentary and/or metavolcanic rocks * range of $\delta^{18}O$ values

Intrusion	$\delta^{18}O$ (average)	Hosting Formation	$\delta^{18}O$ (average)
Greer Lake	8.33 (8.1-8.7)*	Eaglenest Lake formation	7.9
Eaglenest Lake	8.94 (8.6-9.3)	Eaglenest Lake formation	7.9
Osis Lake	11.58 (11.1-12.4)	Booster Lake formation	11.6
Tin Lake	10.74 (10.3-10.9)	Bernic Lake formation	9.4

Chapter VII

INTERNAL INHOMOGENEITIES

A. GENERAL INTRODUCTION

The pegmatitic granites of the Winnipeg River area are not homogeneous. Slight changes in the mineralogy across individual intrusions are reflected by minor changes in the bulk chemistry. Variations in trace element chemistry of whole rocks and individual mineral species are even more conspicuous within these intrusions.

These changes will be documented in order to a suggest a direction of fractionation at the present erosional level across each of the four pegmatitic granites.

B. FIELD INHOMOGENEITIES

1. Tin Lake Intrusion

The Tin Lake intrusion is a rather homogeneous stock of pegmatitic granite in the Winnipeg River area. It is composed almost entirely of medium to coarse-grained (< 2.0 cm) leucogranite which tends to become coarser in a westward direction. Aside from this, several other indications of the intrusion becoming more exotic in a western direction were noted. The occurrences of the sodic aplite and coarse pegmatitic leucogranite facies become more common. Rare appearances of tourmaline, apatite, rose quartz, and

molybdenite in the western portion of the intrusion suggest accumulation of volatiles along this margin of the intrusion. This is supported by the western fingering out of the intrusion into the tourmaline-beryl-rose quartz-(± Nb,Ta oxide) bearing pegmatites of the Birse Lake group (Černý et al., 1981). The final field-observed inhomogeneity is related to the fault which transects the intrusion under Tin Lake. North of this fault the intrusion is relatively homogeneous with the top of the intrusion apparently in the western end. South of this fault the intrusion is fine-grained leucogranite containing many inclusions of the host rock suggesting a lower level section which has been faulted up relative to the northern lobe.

2. Osis Lake Intrusion

The Osis Lake intrusion, like the Tin Lake pegmatitic granite has a general increase in grain size westward, except for the central plug of fine-grained biotite leucogranite which is unique to this pegmatitic granite. This central plug may represent an apex of a larger underlying core of the intrusion. The eastern portion is a fine to medium-grained leucogranite that carries common accessory garnet and apatite. This grades into a coarse tourmaline + garnet (+ triphylite ± rose quartz) pegmatitic granite at the western extremity of the intrusion. The mineralogy in this western portion, the alteration of the hosting

turbidites, and the intrusive style indicate an accumulation of volatiles and suggest that the western area of the pegmatitic granite is the roof portion of the intrusion.

3. Eaglenest Lake Intrusion

This intrusion is composed mainly of medium-grained pegmatitic leucogranite facies throughout. The northern (apparent) contact zone adjacent to the Winnipeg River contains abundant sodic aplite facies which generally parallels the contact. Few internal mineralogically-enriched pods of potassic pegmatite were observed; however, adjacent pegmatites at each end of the intrusion on the northern side were observed to contain beryl or Nb,Ta oxide minerals.

4. Greer Lake Intrusion

This intrusion has well developed areas of all four facies. It shows diversified paragenesis of its potassic pegmatite facies which becomes particularly varied along or near the southern contact. In these locations beryl and Nb,Ta oxide minerals tend to be quite abundant, especially in the potassic pegmatite pods south of the shear zone transecting the intrusion. Included in this position are the Annie Claim and Silverleaf Claim, both of which are highly fractionated, containing cesian beryl, Nb,Ta oxide minerals, Li-micas, and cassiterite.

B. INTERNAL COMPOSITIONAL TRENDS

1. Bulk Composition

a) Tin Lake Intrusion. Bulk composition of the leucogranite is very homogeneous and shows no major geochemical trends across the intrusion. Most indicators of increasing fractionation vary randomly (e.g. K/Ba) over the intrusion. K/Cs (Figure 74) illustrates a general indistinct decrease in value in a western direction across the Tin Lake intrusion. K/Rb values (Figure 75) also suggest an increasing fractionation trend in a western direction; however, this may be due just to a lack of samples. There appears to be no difference in the bulk chemistry between the leucogranites of the northern end and southern lobes. No leucogranite samples from the TNL-eastern extension area were analyzed; therefore, with respect to bulk chemistry of the leucogranites, this area cannot be compared to the main TNL intrusion.

Figures 62 to 71 illustrate the chemistry of the TNL leucogranites and define arbitrary fields of the bulk composition. Figure 64 (Ba vs. Rb) suggests a possible difference between the northern and southern lobes. Ba is quite variable in the intrusion (125-425 ppm) while Rb remains essentially constant. Figure 66 (Ba vs. Sr) is similar to

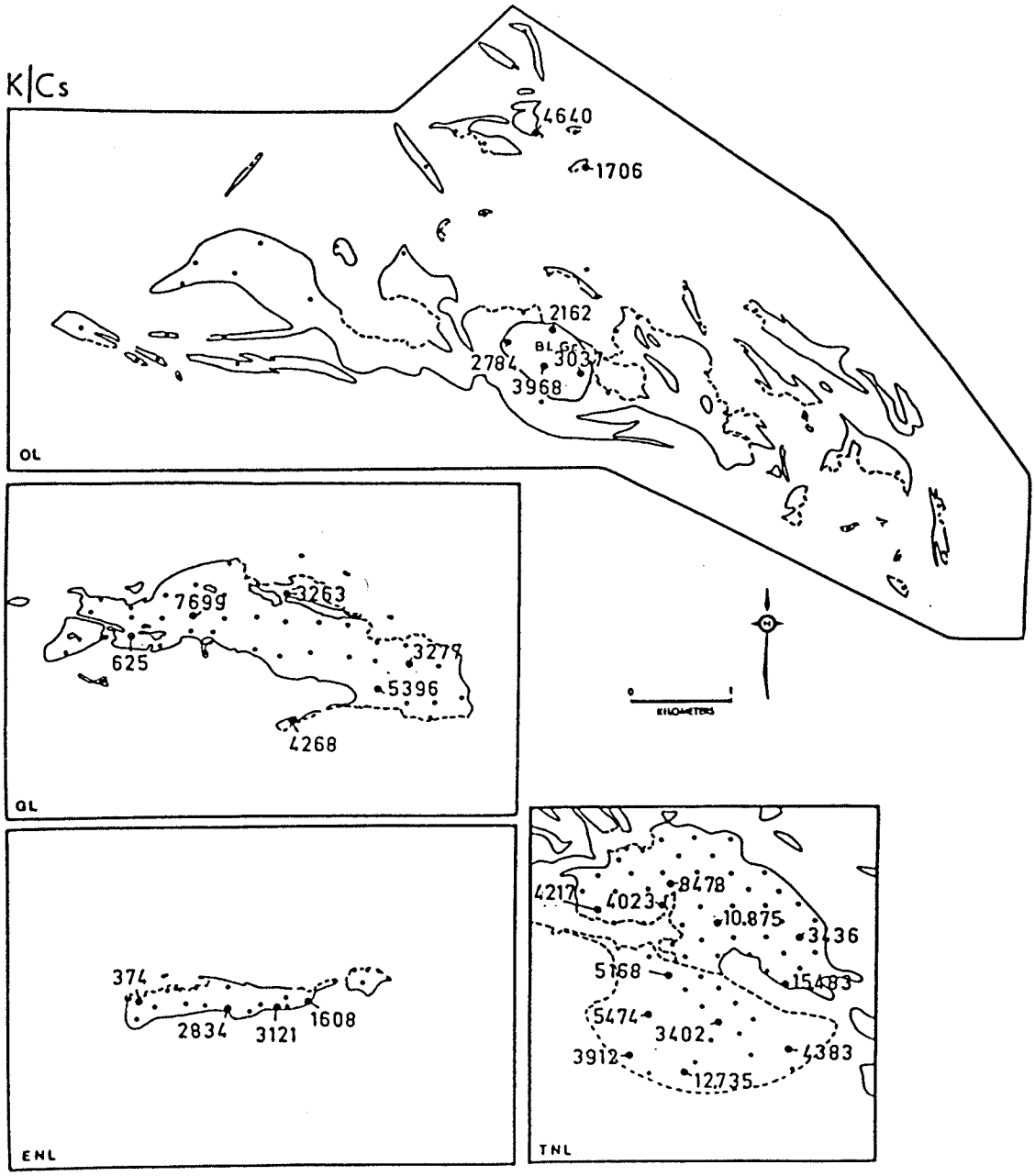

Figure 74. Whole rock K/Cs ratios for the fine-grained leucogranite facies in the four pegmatitic granites studied in the Winnipeg River area of southeastern Manitoba. Closed circles indicate sampling stations and the numbers are the K/Cs values.

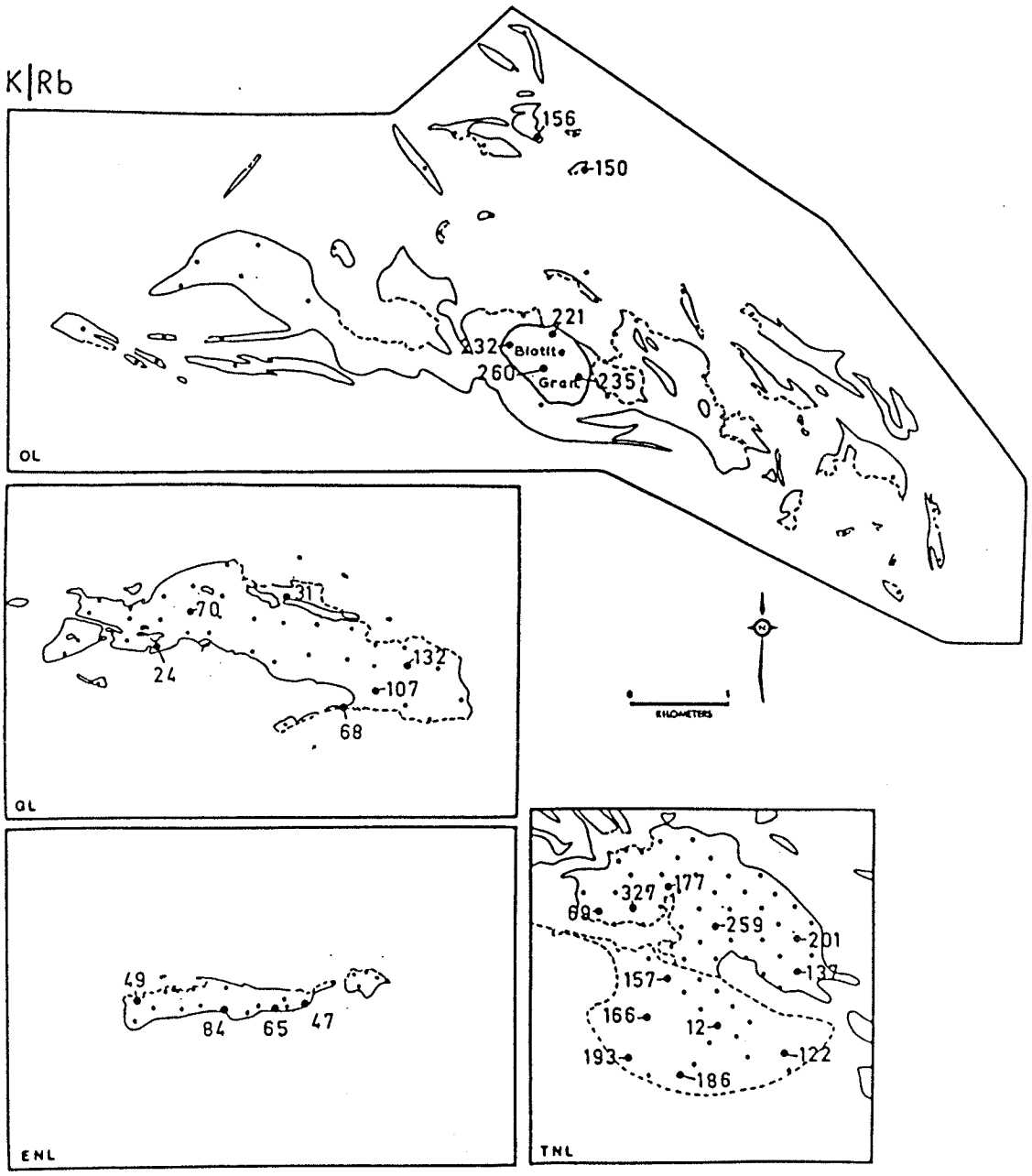

Figure 75. Whole rock K/Rb ratios for fine-grained leucogranites in the four pegmatitic granite intrusions. Closed circles indicate sampling stations and the numbers are the K/Rb values.

Figure 64 (Ba vs. Rb); however, the intrusion has a wider Sr (15-60 ppm) than Rb variation. Figure 71 (K vs. Ba) shows that Ba variation throughout the intrusion is independent of variation in the concentration of its compatible major element, potassium.

Figure 68 demonstrates that there is little variation in the Mg/Li ratio within each lobe of the intrusion; however, the data supports a difference in the chemistry of these two lobes as suggested by Ba vs. Rb.

b) Osis Lake Intrusion. Very minor bulk chemical sampling of the Osis Lake intrusion was undertaken mainly because typical leucogranite facies was scarce and large representative samples of pegmatitic leucogranite were difficult to obtain. The obvious mineralogical changes across the intrusion strongly suggest a definite Li, B, and P content increase westward. K/Rb (Figure 75), K/Cs (Figure 74), and K/Ba values of the leucogranite facies and of the central plug of biotite granite all indicate that the intrusion of pegmatitic granite is more highly fractionated than the central plug of biotite granite.

This difference in chemistry between these two rock types is demonstrated in all geochemical plots

(Figures 64 to 66, 71). The biotite granite is distinctly higher in Sr, Ba, and Mg than the main leucogranite facies.

c) Eaglenest Lake Intrusion. Analysis of bulk samples of the leucogranite facies suggest the existence of fractionation trends within this intrusion. A low sample density will have some effect on the determination and validity of the trends; thus support will be sought from mineral geochemical trends later.

K/Rb (Figure 75) and K/Cs (Figure 74) values both decrease parallel to the long axis towards the eastern and western extremities of the intrusion. This suggests an increasing degree of fractionation outwards from the central area of the intrusion at the present level of erosion. These two trend documentations are not supported by the K/Ba values which decrease (i.e. fractionation increasing) towards the central area of the intrusion. This reverse trend could be only apparent, caused by a lack of analyzed samples across the intrusion. Also, Ba is known to behave much more erratically in acid igneous rocks than other trace elements (Černý et al., 1981).

Figures 62 to 71 show the general composition of the ENL leucogranite; low Ba, Sr concentrations and

Rb much more abundant than Sr as is the Li content versus the Mg content. Little scatter in the composition on the leucogranite is evident; however, this could quite possibly be due to a low number of analyzed samples.

d) Greer Lake Intrusion. Eight samples of the leucogranite facies were analyzed from sites across this intrusion. K/Ba, K/Rb (Figure 75), and K/Cs (Figure 74) values of the leucogranite suggest a northeast to southwest direction of fractionation, increasing diagonally across the intrusion. Trends in the mineral geochemistry as discussed later support this suggestion.

Of the leucogranite samples analyzed, two of them (GL-1002-HG and GL-13(a)) have been discarded since they are not representative. GL-1002-HG is a fine-grained muscovite leucogranite/sodic aplite adjacent to an area of pegmatitic leucogranite and GL-13(a) is a fine-grained ($\sim$ 1 cm) sample of K-feldspar pegmatitic leucogranite. With the elimination of these two samples, the mutual deviation of the chemistry of the leucogranites is quite slight. Rb is moderately enriched over Sr and Ba shows no correlation with K. Li is slightly enriched over Mg.

2. Blocky K-Feldspar

a) Tin Lake Intrusion. Fractionation trends of elemental ratios in the blocky K-feldspar crystals of this intrusion add support to the general western decrease in the K/Rb and K/Cs values of the TNL leucogranite. K/Rb ratios (Figure 76) show the general decreasing values westward across the northern lobe as do the K/Cs values (Figure 77). These both indicate fractionation within the intrusion increasing westward. K/Cs values in the central area of the northern lobe tend to be lower than the K/Cs values from K-feldspar occurring at or near the margin of the intrusion. No samples from the southern lobe were obtained; however, both K/Rb and K/Cs of the K-feldspar in the eastern extension of TNL (Appendix 10) are significantly lower (Table 22, Appendix 2) suggesting a fractionation trend eastward. This is also illustrated in Figure 80. Figure 78 however, does not show any separation of these two parts of the Tin Lake intrusion.

b) Osis Lake Intrusion. K-feldspar from the potassic pegmatite facies of the Osis Lake pegmatitic granite shows very distinct geochemical trends. Both K/Cs (Figure 77) and K/Rb (Figure 76) ratios decrease significantly in a western direction parallel to the east-west axis of the intrusion and also in a north-

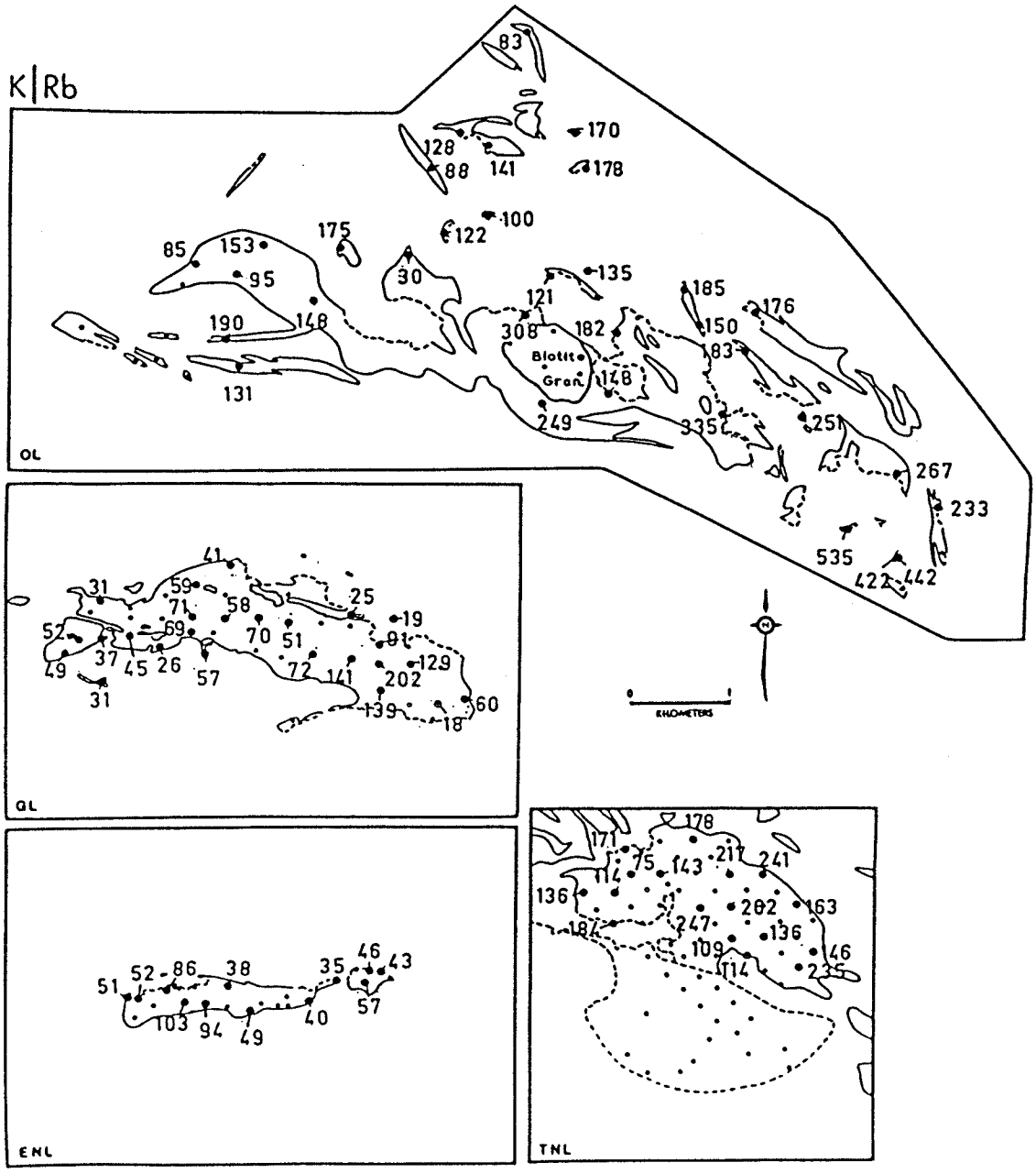

Figure 76. K/Rb ratios in blocky K-feldspars of the potassic pegmatite phase in the four intrusions of pegmatitic granites. Closed circles indicate sampling stations and the numbers are the K/Rb values.

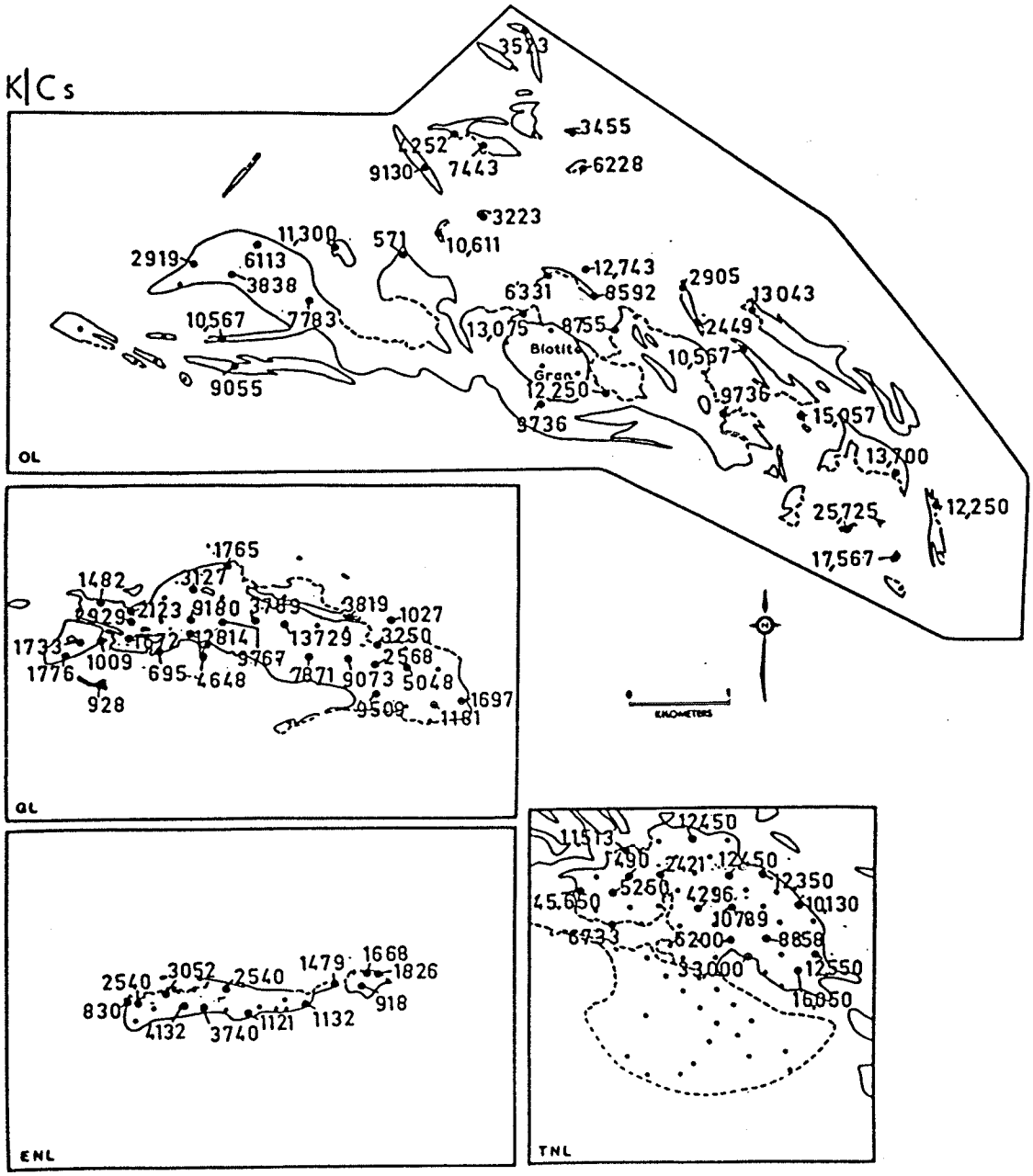

Figure 77. K/Cs ratios in the blocky K-feldspars of the potassic pegmatite phase in the four intrusions of pegmatitic granites. Closed circles indicate sampling stations and the numbers are the K/Cs values.

Table 22. Arithmetic means of contents (weight percent) and ratios of geochemically significant elements in blocky K-feldspars from potassic pegmatite bands of the four major intrusions of pegmatitic granites

	K_2O K	Na_2O Na	CaO Ca	Rb_2O Rb	Cs_2O Cs	Li_2O Li	PbO Pb	K/Rb	K/Cs	Rb/Cs
Greer Lake	11.89	3.05	.031	.21	.0045	.0058	.0034			
	9.88	2.26	.022	.188	.0042	.0026	.0032	69	4475	68
Eaglenest Lake	12.02	3.13	.059	.221	.0073	.0079	.0039			
	9.98	2.32	.042	.202	.0068	.0037	.0036	56	1982	35
Tin Lake	12.06	2.96	.082	.072	.0025	.0029	.0034			
	10.01	2.20	.059	.066	.0022	.0013	.0032	170	12048	79
Osis Lake	12.15	2.97	.091	.078	.0022	.0036	.0029			
	10.09	2.20	.065	.072	.0020	.0017	.0027	180	8920	52

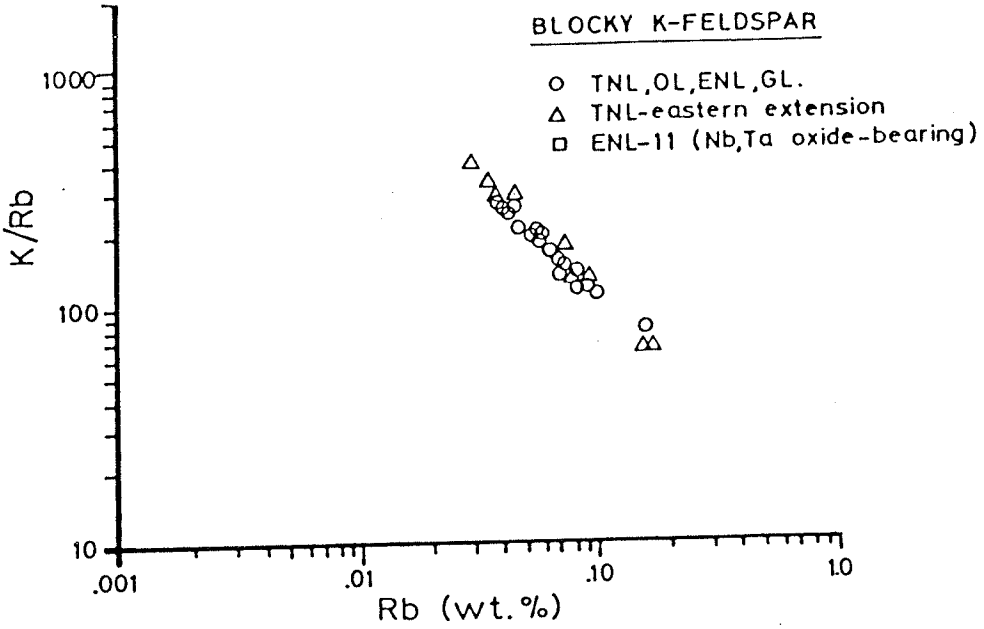

Figure 78. K/Rb vs. Rb plots showing the composition of the blocky K-feldspar from the potassic pegmatite facies of the Tin Lake intrusion.

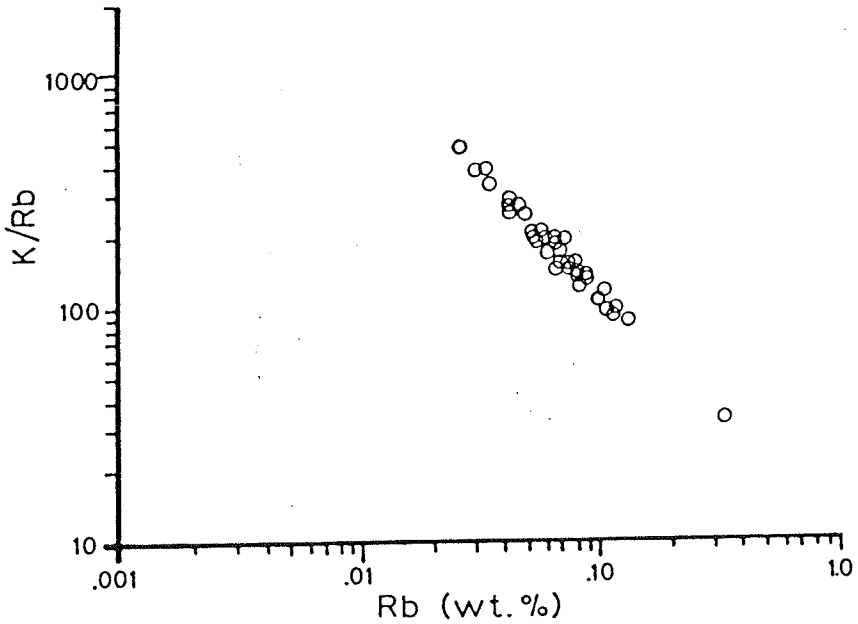

Figure 79. K/Rb vs. Rb plots showing the composition of the blocky K-feldspar from the potassic pegmatite facies of the Osis Lake intrusion. Symbols as in Figure 78.

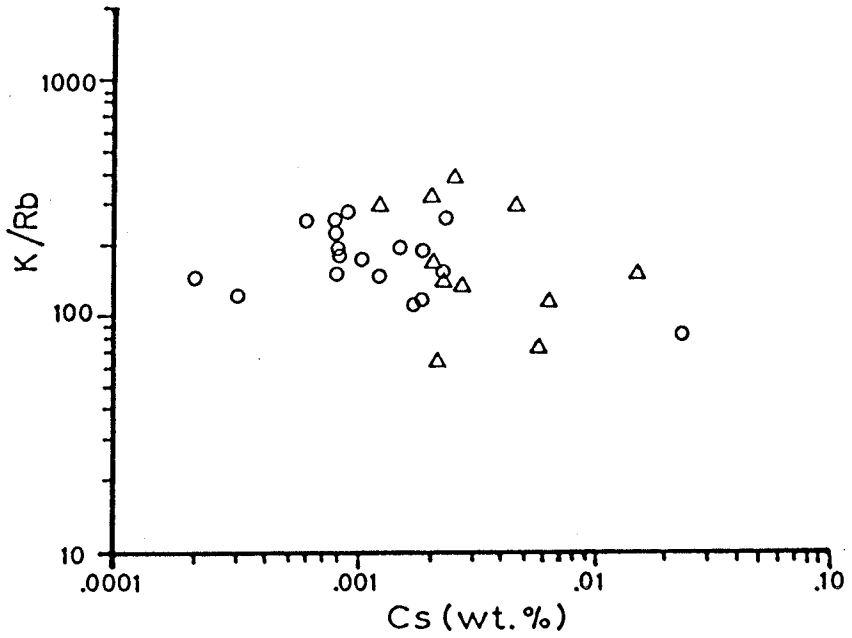

Figure 80. K/Rb vs. Cs plots showing the composition of the blocky K-feldspar in the potassic pegmatite facies of the Tin Lake intrusion. Symbols as in Figure 78.

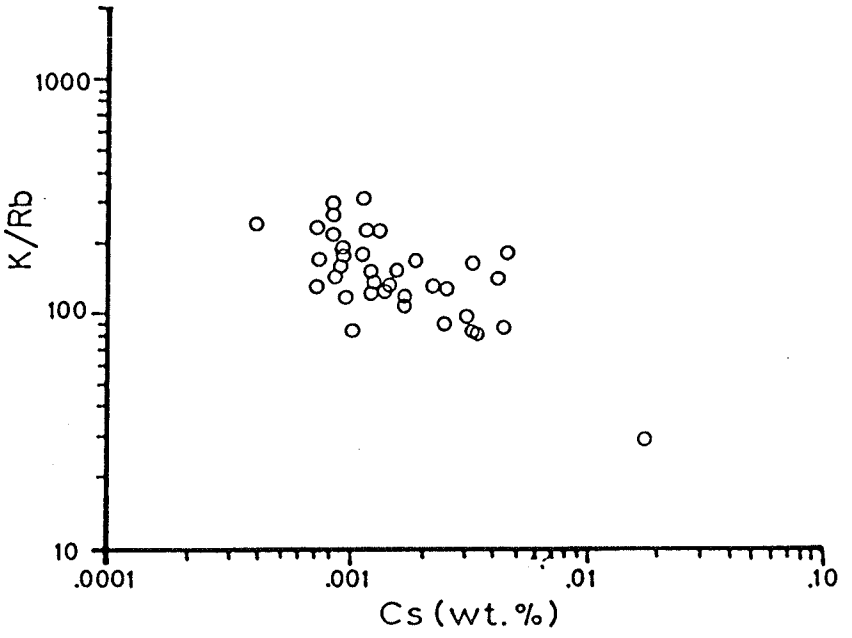

Figure 81. K/Rb vs. Cs plots showing the composition of the blocky K-feldspar in the potassic pegmatite facies of the Osis Lake intrusion. Symbols as in Figure 78.

western direction. The eastern exposed extremities of the intrusion are markedly less fractionated than either the western or northern areas of the pegmatitic granite.

Plots of K/Rb vs. Rb and K/Rb vs. Cs showing the relative positions of individual K-feldspar samples and the overall field covered by the Osis Lake intrusion are shown in Figures 79 and 81, respectively. The average K-feldspar composition has been listed in Table 22.

c) Eaglenest Lake Intrusion. K/Rb (Figure 76) and K/Cs (Figure 77) ratios of the K-feldspar from the potassic pegmatite facies of the Eaglenest Lake pegmatitic granite follow the same trend demonstrated by the bulk leucogranite K/Rb and K/Cs values. This intrusion appears to attain a higher degree of fractionation outwards from the exposed central area toward both the eastern and western extremities.

Figures 82 and 84 illustrate the mutual relationships of the ENL blocky K-feldspar and the field of K/Rb vs. Cs and K/Rb vs. Rb, respectively. In both cases the compositions vary but little. The three isolated samples with a higher K/Rb ratio are all from the central area of the intrusion. Location ENL-11 is a Nb,Ta-bearing pegmatite in the river adjacent to the northwest tip of the intrusion. Two

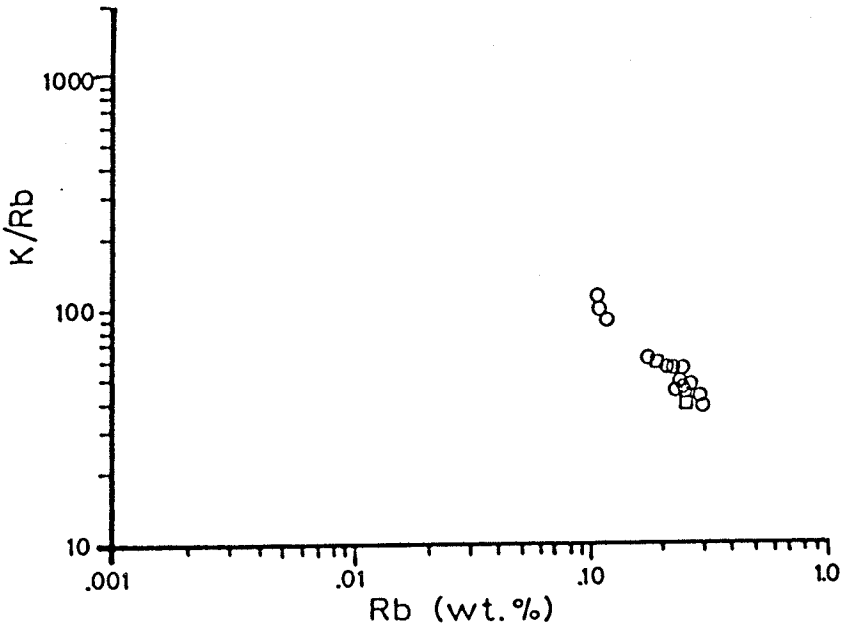

Figure 82. K/Rb vs. Rb plot of the blocky K-feldspar composition in the Eaglenest Lake intrusion. Symbols as in Figure 78.

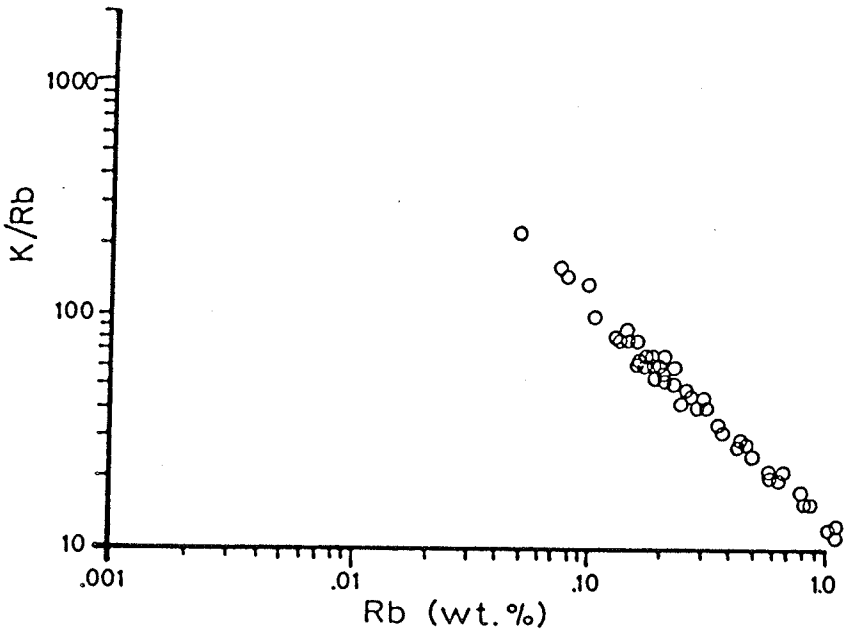

Figure 83. K/Rb vs. Rb plot of the blocky K-feldspar composition in the Greer Lake intrusion. Symbols as in Figure 78.

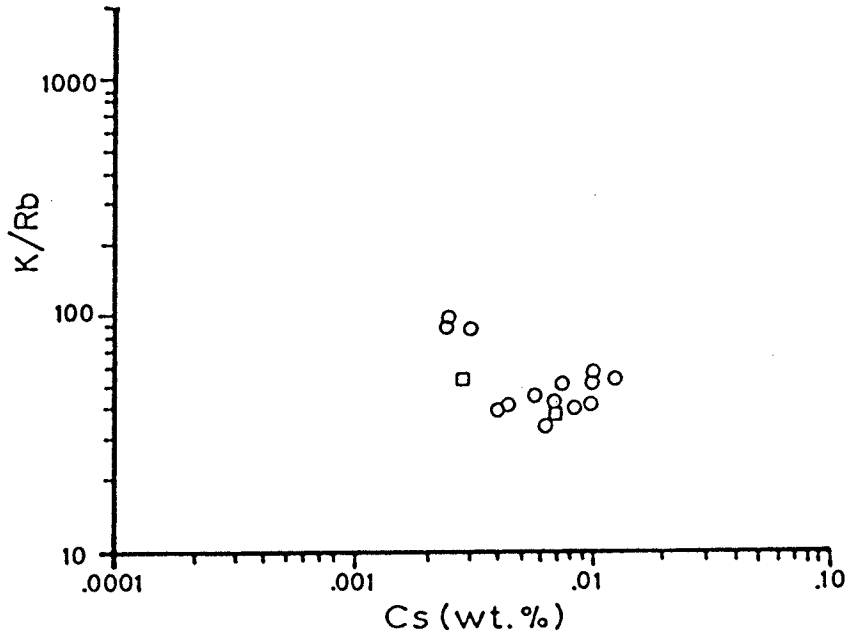

Figure 84. K/Rb vs. Cs plot of the blocky K-feldspar composition in the Eaglenest Lake intrusion. Symbols as in Figure 78.

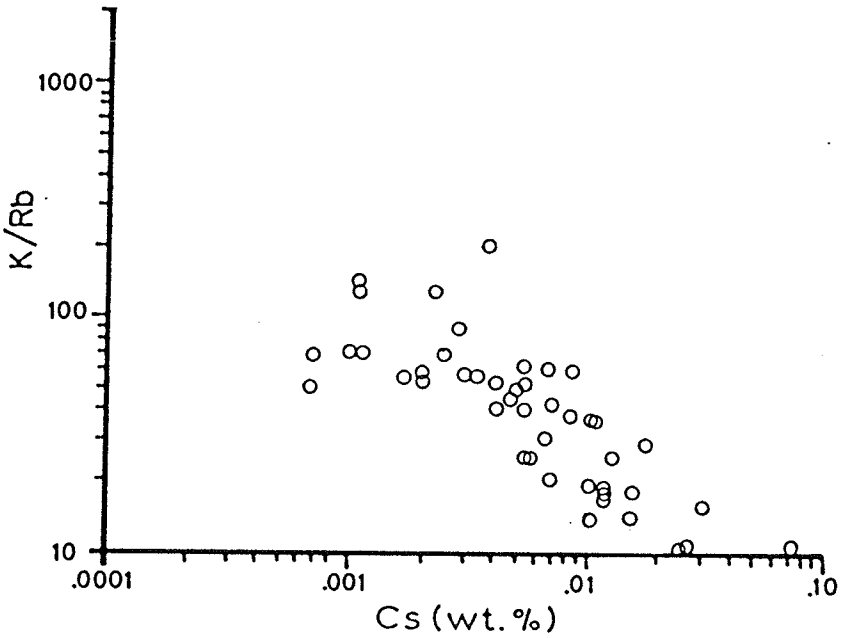

Figure 85. K/Rb vs. Cs plot of the blocky K-feldspar composition in the Greer Lake intrusion. Symbols as in Figure 78.

samples from this location do not deviate from the field of the remaining ENL samples.

d) Greer Lake Intrusion. Examination of the geochemistry of the K-feldspar illustrates the same general northeast to southwest increasing fractionation trend as demonstrated by the Greer Lake leucogranite; however, there are some variations. K/Rb values of the blocky K-feldspar define a less fractionated (K/Rb:91-202) area in the eastern half of the intrusion (Figure 76). The K/Rb values decrease outwardly from this area in a southeasterly, northwesterly, and westerly direction toward sample locations Zone-5, GL-30, and AC, Lobe, and Silverleaf, respectively. All these areas are known to be mineralogically more diversified with respect to the surrounding pegmatitic granite. Their geochemistry will be discussed below.

K/Cs values of the K-feldspar (Figure 77) are also lower at the east and west extremities in the areas of enriched potassic pegmatite pods mentioned above. However, a more noticeable trend is the higher K/Cs values in the central area of the intrusion. These values tend to decrease toward the margins of the intrusion especially towards the southwest contact.

This increased fractionation within the intrusion is well illustrated by the K/Rb vs. Rb and K/Rb vs. Cs (Figures 83, and 85, respectively) of the blocky K-feldspar in the potassic pegmatite facies of the Greer Lake intrusion. The compositional fields of the K-feldspar from the normal nonenriched pods of potassic pegmatite are outlined in Figures 83 and 85 with several more fractionated specimens containing significantly higher Cs and Rb concentrations. These enriched pods will be discussed further below.

3. Muscovite

a) Tin Lake Intrusion. Insufficient muscovite samples across the TNL intrusion make any trends shown by the muscovite geochemistry unreliable on their own; however, they appear to be in agreement with trends shown by the analyses of whole rock samples and other minerals. K/Rb (Figure 86), K/Cs, and Mg/Li (Figure 87) values generally decrease in the western part of the northern lobe. The Be (Figure 88) and Na content of the muscovite remains essentially constant throughout. No muscovite samples were analyzed from either the TNL-eastern extension or the southern lobe of the main intrusion.

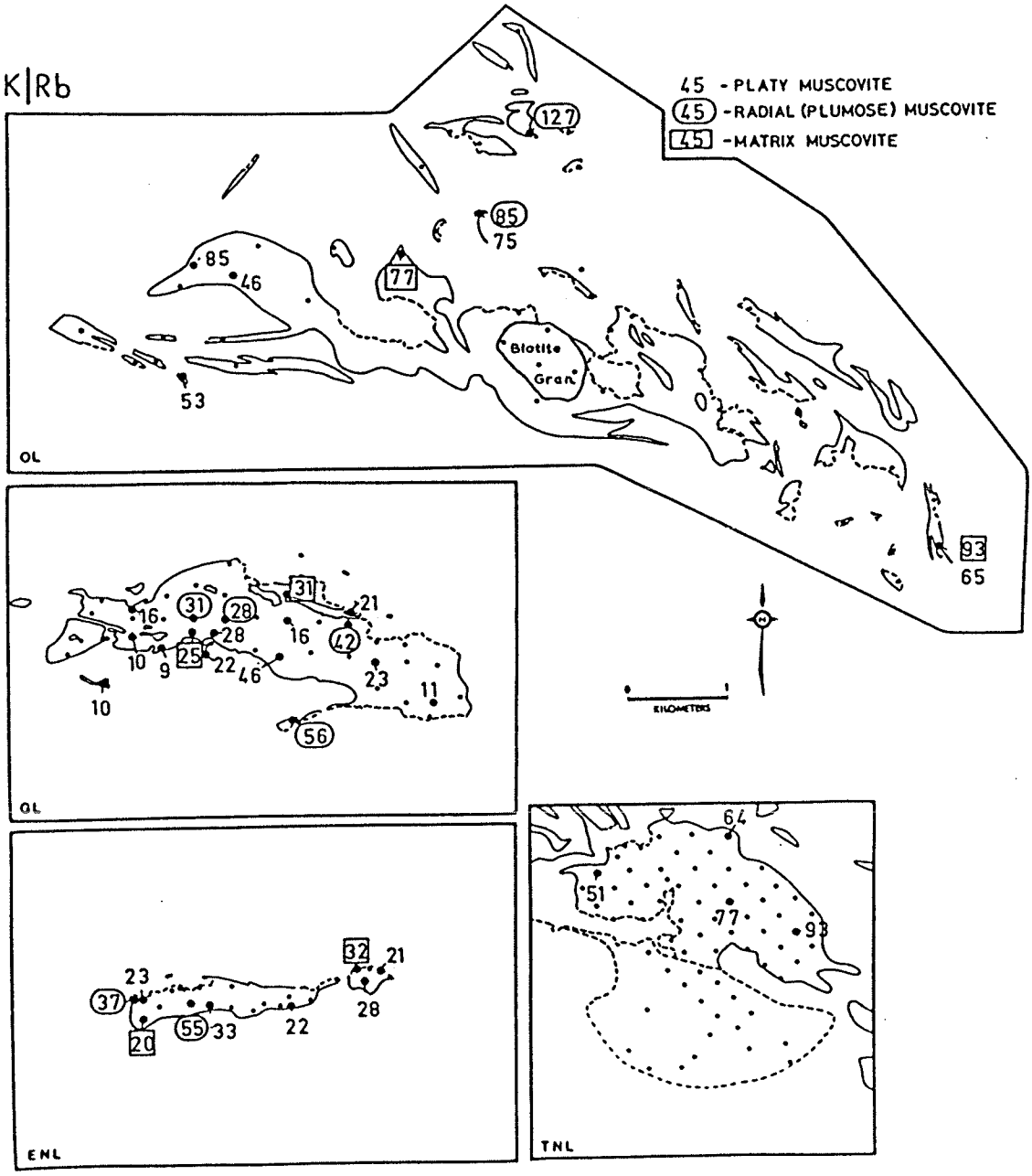

Figure 86. K/Rb ratios in muscovite from the four pegmatitic granite intrusions.

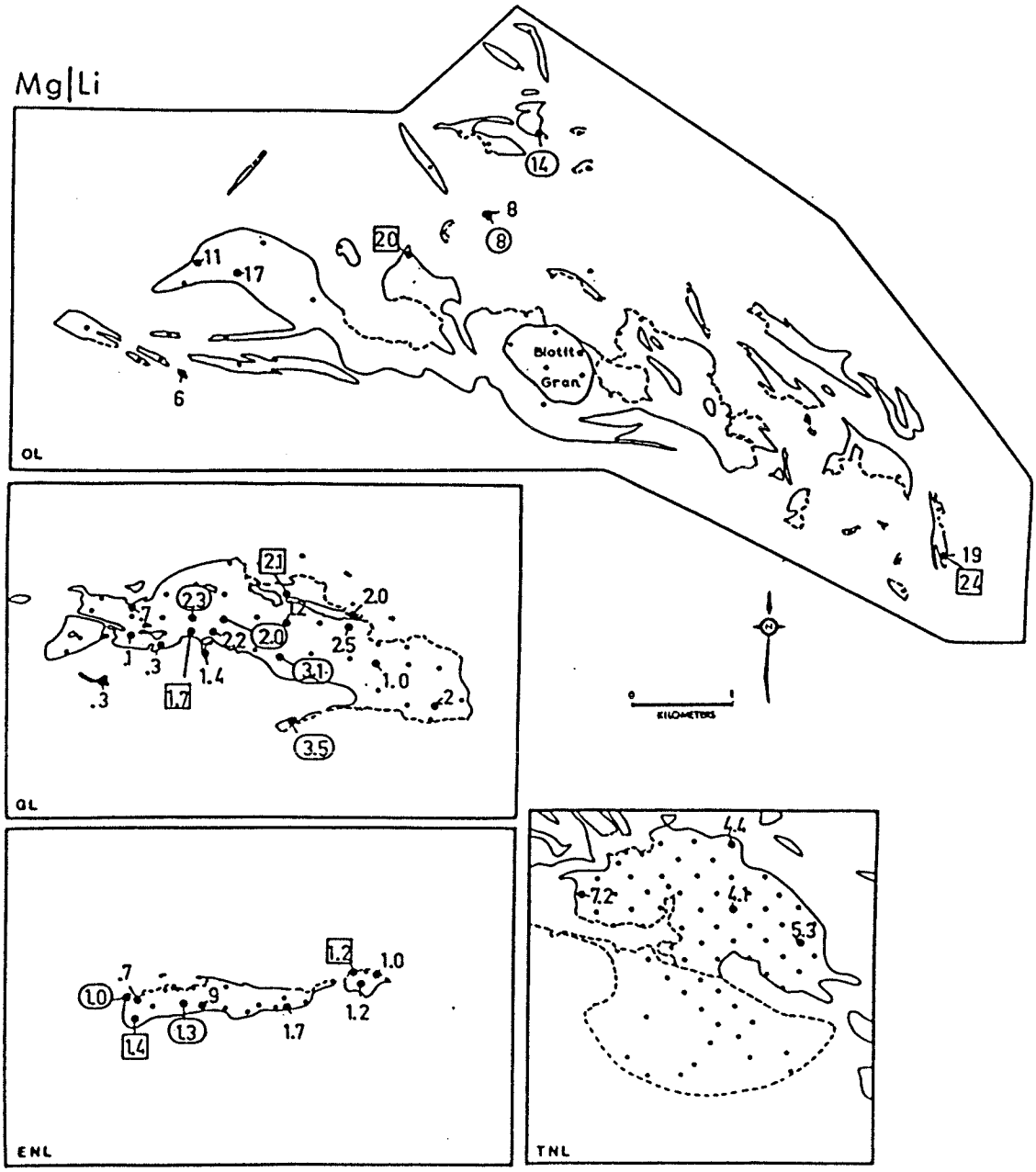

Figure 87. Mg/Li ratios in muscovite of the four pegmatitic granite intrusions. Symbols as in Figure 86.

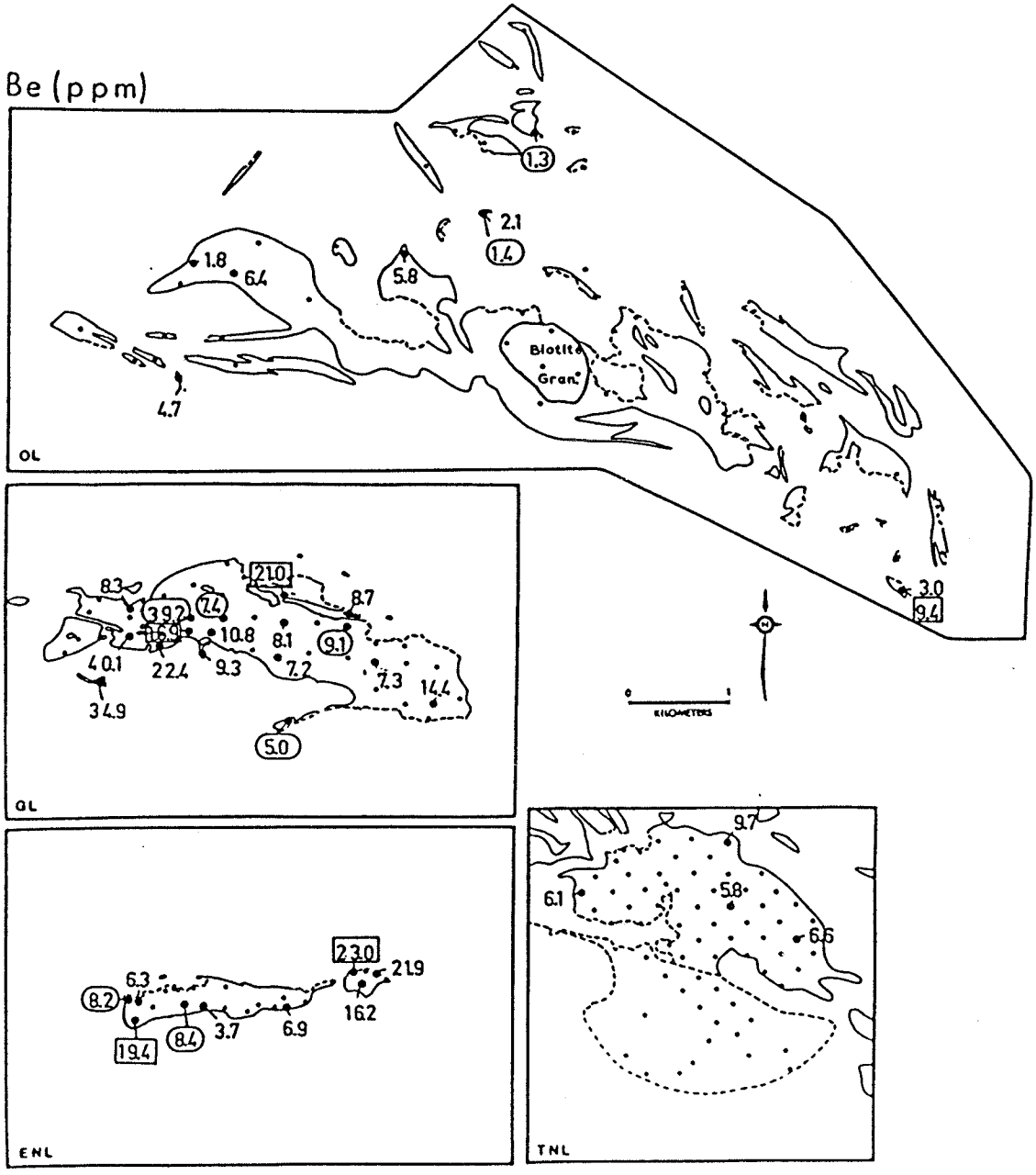

Figure 88. Be contents of muscovite from the four pegmatitic granite intrusions. Symbols as in Figure 86.

Plots of geochemical ratios and elements of Tin Lake muscovite have been selected from a multitude of others which were not so informative and are arranged in Figure 89. These plots show the compositions of individual muscovite samples and compositional fields of the muscovite within the intrusion. Figure 89 covers the platy muscovite. No radial or matrix muscovite was analyzed from the Tin Lake intrusion.

b) Osis Lake Intrusion. Muscovite geochemistry supports the trends indicated by the K-feldspar geochemistry; however, data are based on a very low sampling density. K/Rb values loosely parallel those in K-feldspar, indicating an east to west increase in the degree of fractionation. The northwestern trend is not indicated, resulting from a lack of samples from this area of the intrusion. The Mg/Li ratios (Figure 87) and to a lesser degree the K/Cs ratios follow the suggestion of the westward increase in fractionation. The Be (Figure 88) and the Na content of the muscovite shows minor random variation with a possible increase in the western part of the intrusion. Confirmation of this variation would require more sample analyses from this area.

Compositional fields of the muscovite from all facies of the Osis Lake pegmatitic granite are

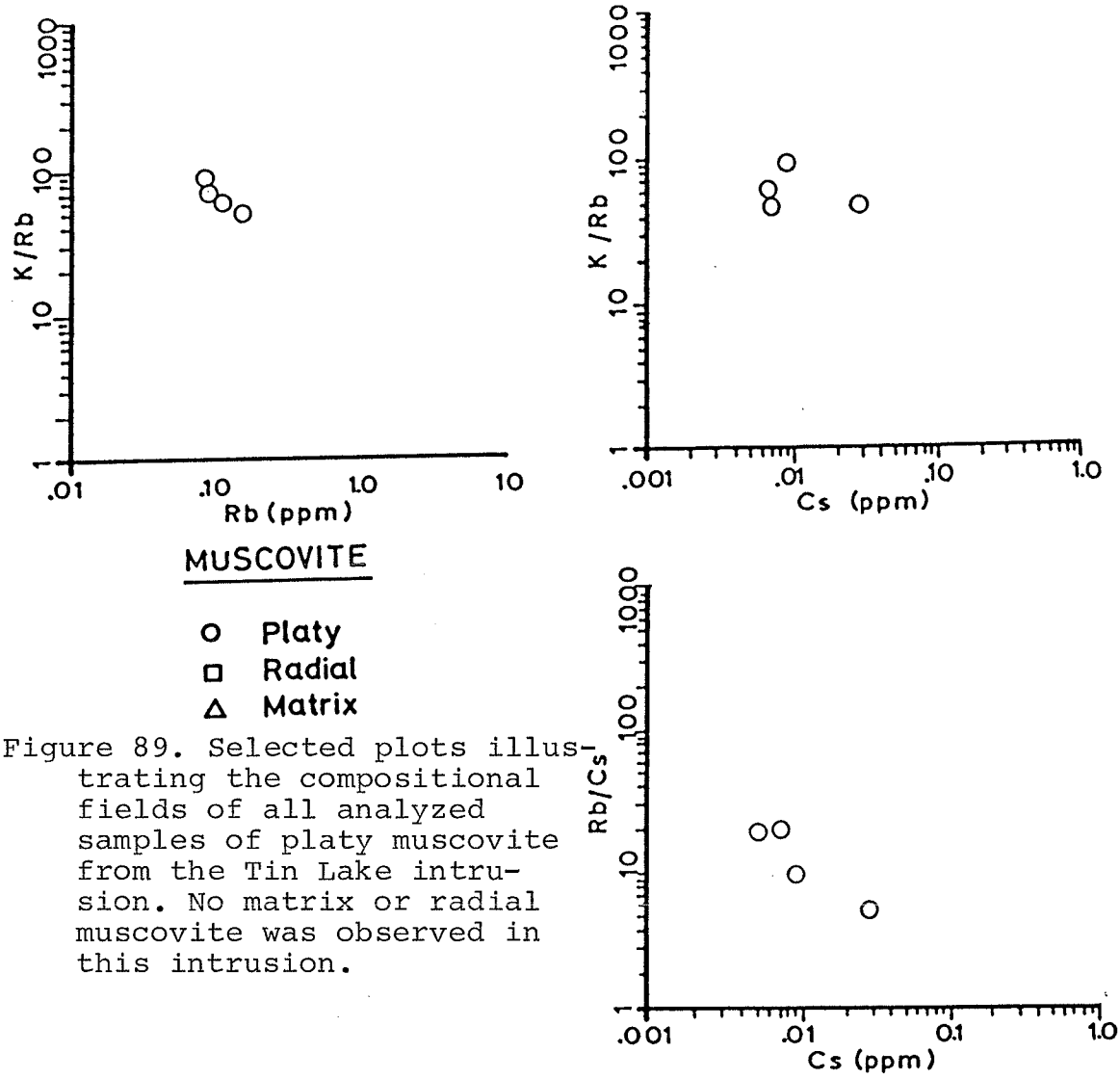

Figure 89. Selected plots illustrating the compositional fields of all analyzed samples of platy muscovite from the Tin Lake intrusion. No matrix or radial muscovite was observed in this intrusion.

illustrated in Figure 90.

c) Eaglenest Lake Intrusion. K/Rb (Figure 86), Mg/Li (Figure 87), and K/Cs ratios from all types of muscovite indicate a general increase in the degree of fractionation in an east-west direction within the Eaglenest Lake intrusion. Be content of muscovite (Figure 88) supports this east-west trend. Na content in the three muscovite types is relatively stable, with a very slight increase eastwards.

Geochemical plots of individual samples and ranges of muscovite compositions within the ENL intrusion are shown in Figure 91. This figure reflects the trends discussed above.

d) Greer Lake Intrusion. Geochemistry of muscovite from the Greer Lake pegmatitic granite adds significant support to the trends suggested by the K-feldspar geochemistry. K/Rb (Figure 86) and K/Cs values of all Greer Lake muscovite types illustrate an overall northeast to southwest increase in the degree of fractionation. Deviations from this trend occur as local pods of fractionated potassic pegmatite are approached. The degree of fractionation of these pods locally is higher than that of the main intrusion.

The Mg/Li ratio (Figure 87), Be (Figure 88) and Na content of muscovite are relatively constant

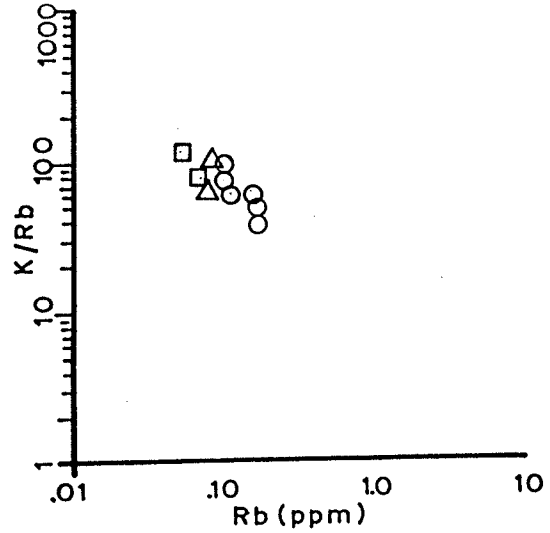

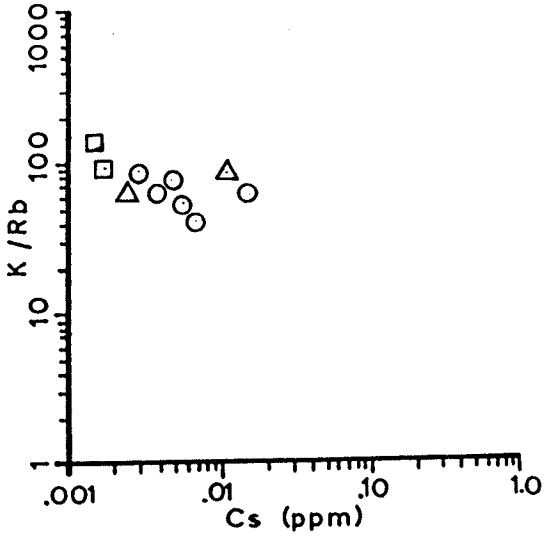

Figure 90. Selected plots illustrating the compositional fields of all analyzed samples of platy, matrix, and radial muscovite from the Osis Lake intrusion. Symbols as in Figure 89.

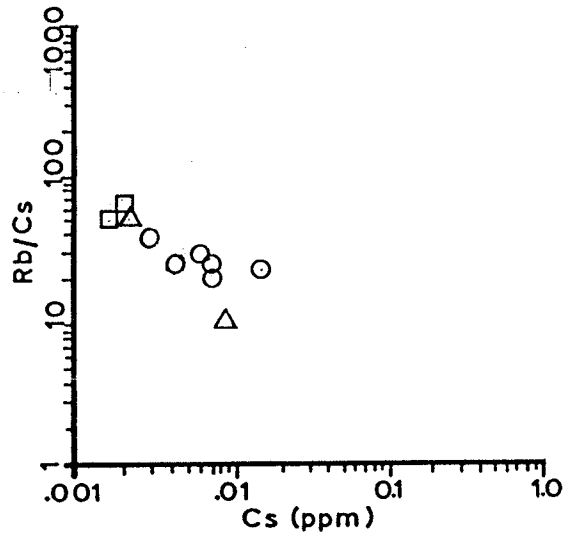

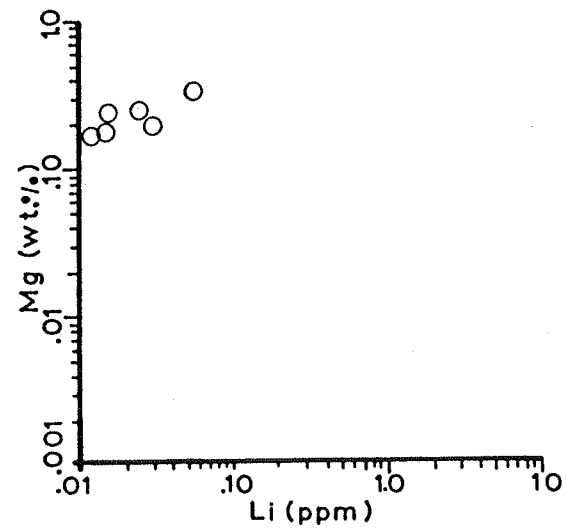

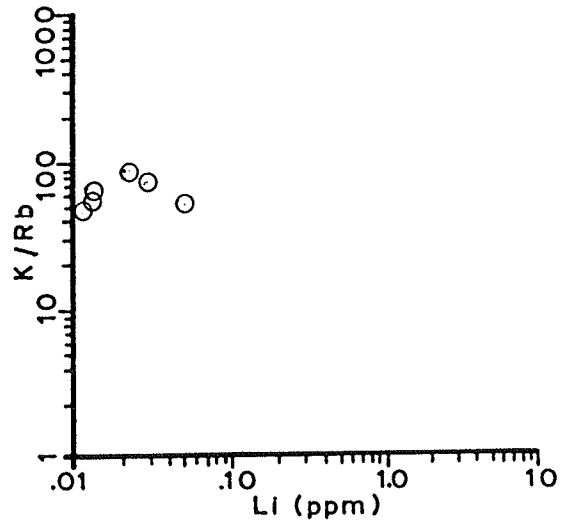

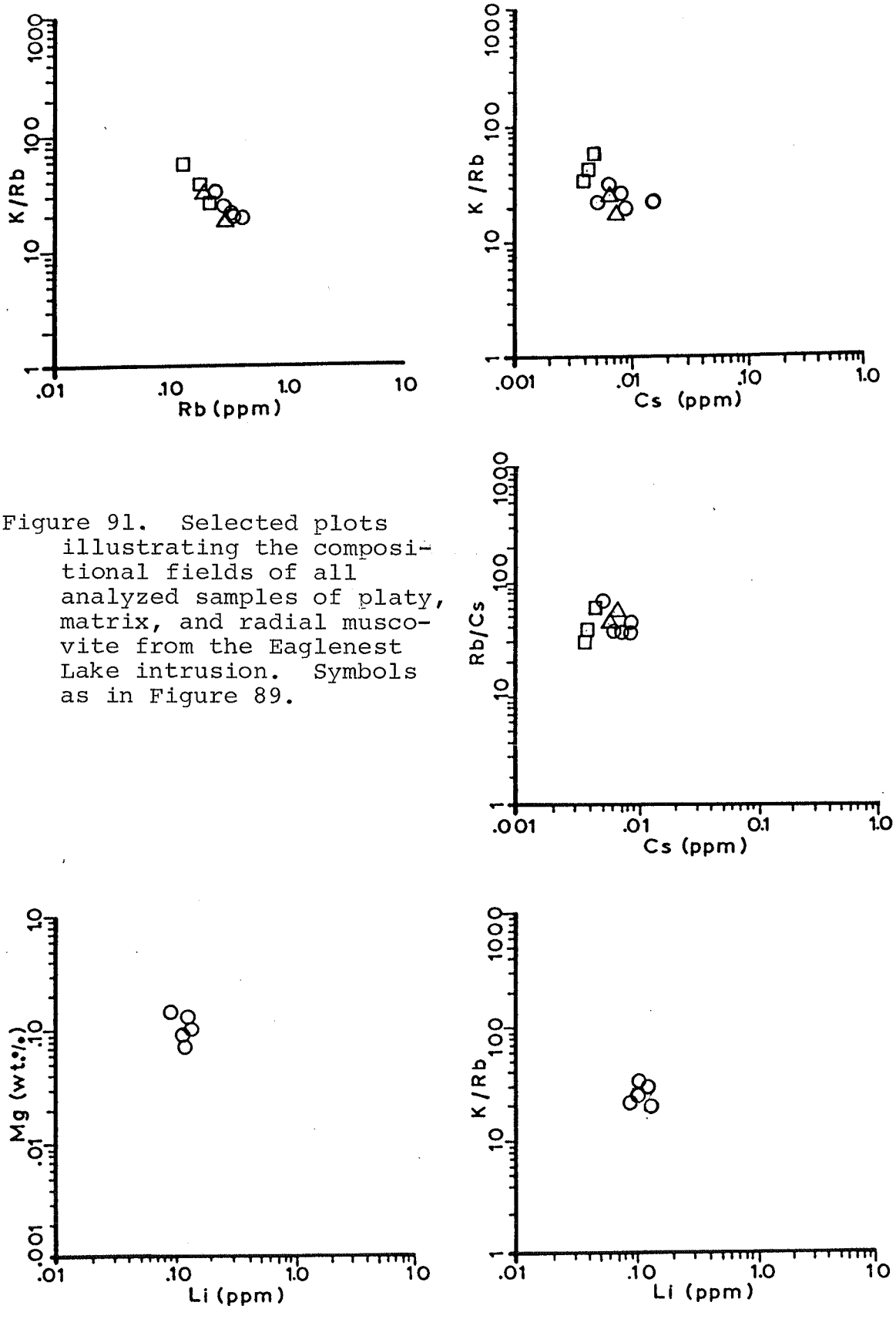

Figure 91. Selected plots illustrating the compositional fields of all analyzed samples of platy, matrix, and radial muscovite from the Eaglenest Lake intrusion. Symbols as in Figure 89.

across the central area of the intrusion; however, these ratios also show local content deviations as the distance from an occurrence of a potassic pegmatite facies with abundant accessory mineralogy (beryl, Nb,Ta oxides) decreases.

Figure 92 illustrates the compositional field covered by the three muscovite types of the Greer Lake intrusion.

4. Garnet

The Mn/(Fe + Mn) x 100 ratio of analyzed garnet was calculated and used as a fractionation indicator characteristic of the parent rock sample.

a) Tin Lake Intrusion. The Mn/(Fe + Mn) x 100 ratio of the garnet in the Tin Lake intrusion (Figure 93) shows no definite direction of increasing fractionation. The values of this ratio in the western half of the northern lobe are slightly higher; however, on their own these data are inconclusive.

b) Osis Lake Intrusion. The Mn/(Fe + Mn) x 100 ratio of garnet from all facies of the Osis Lake intrusion (Figure 93) suggests trends within the intrusion that are consistent with the geochemical trends of the OL minerals, previously discussed. This ratio increases to the north and also to the west indicating increasing fractionation in these directions.

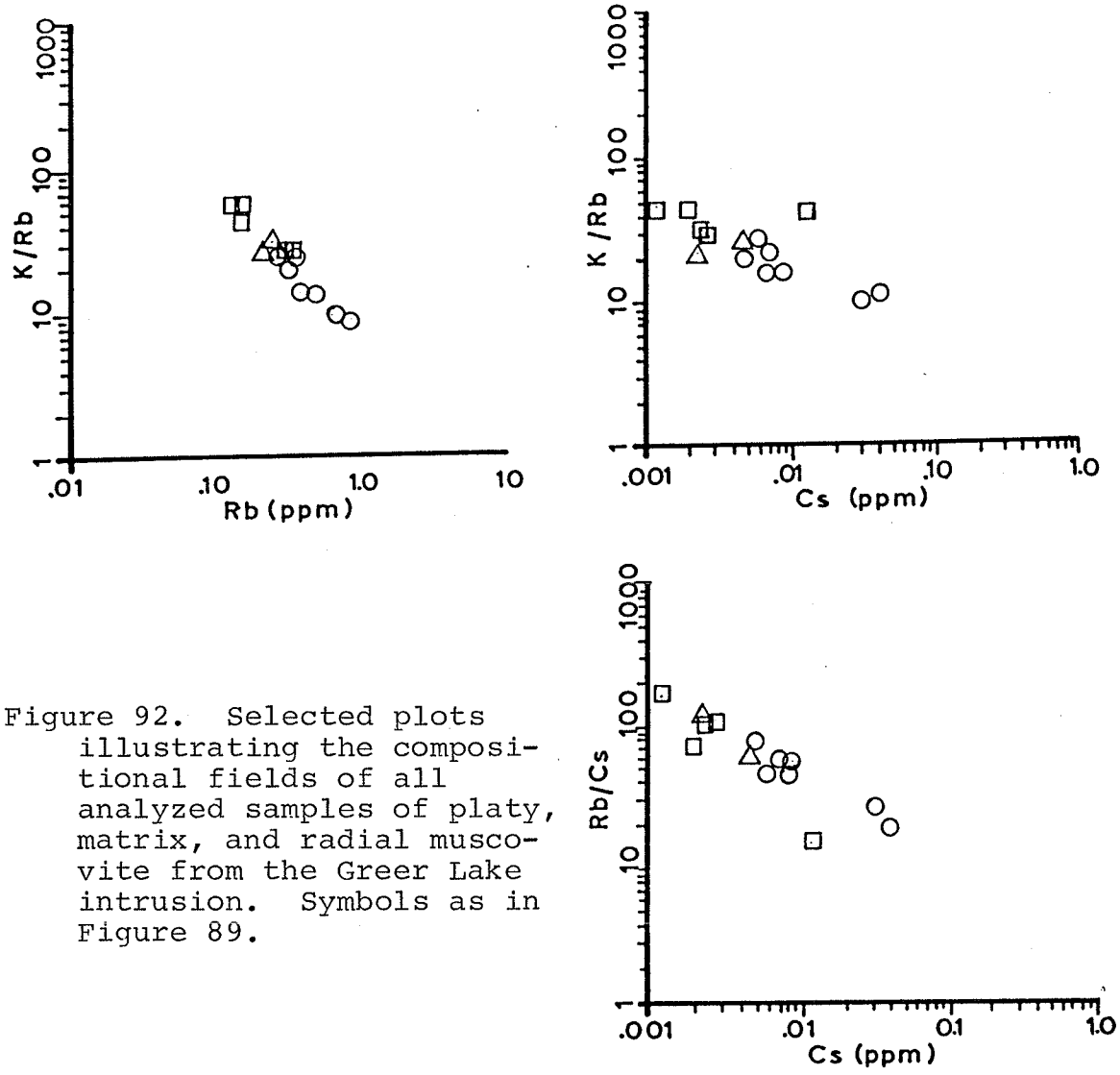

Figure 92. Selected plots illustrating the compositional fields of all analyzed samples of platy, matrix, and radial muscovite from the Greer Lake intrusion. Symbols as in Figure 89.

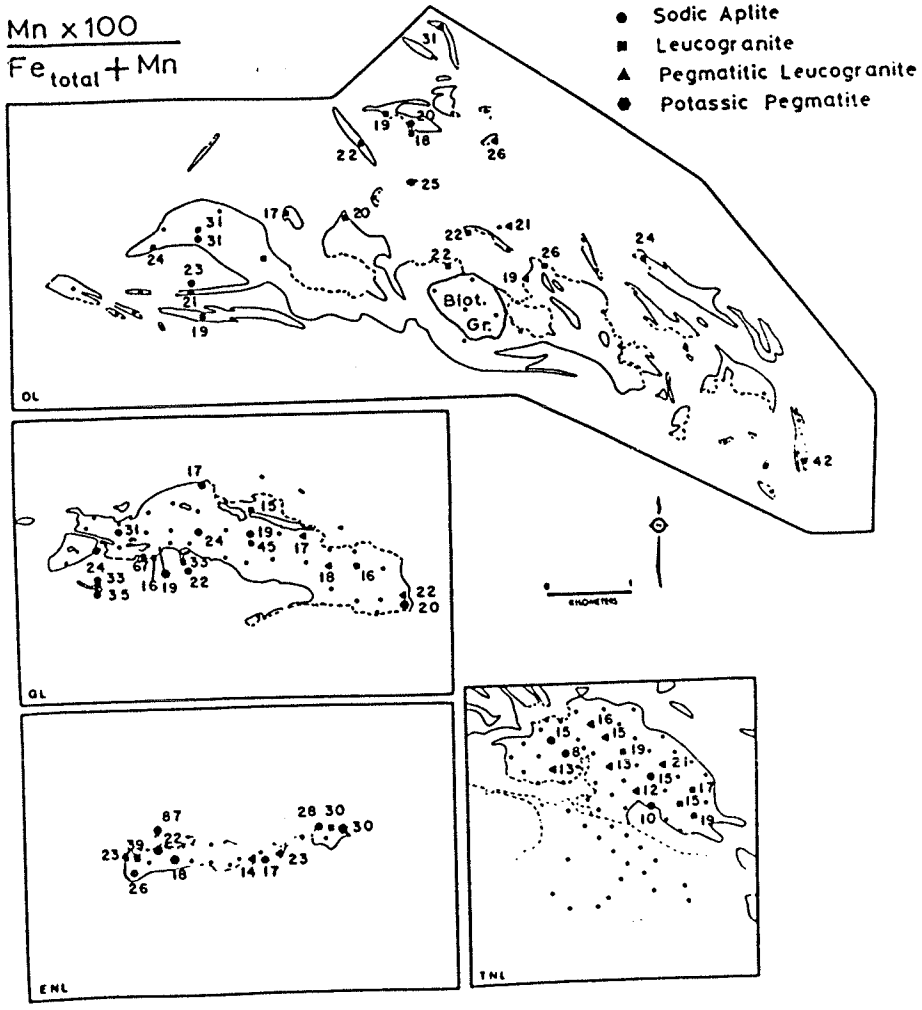

Figure 93. Mn/(Fe + Mn) x 100 ratio of garnet in the four intrusions of pegmatitic granite. The garnet samples were obtained from the indicated facies.

Continuation of the trend of Mn depletion to the eastern portion of the intrusion is uncertain since only one non-representative coarse (5 cm) graphic quartz + garnet intergrowth crystal was located.

c) Eaglenest Lake Intrusion. The Mn/(Fe + Mn) x 100 ratio in garnet from all facies in this intrusion (Figure 93) follow trends parallel to the blocky K-feldspar and muscovite mineralogy. This ratio is low in the central area of the intrusion (~15) and increases, in both an eastern and western direction to values of approximately 30 and 40, respectively.

A single, extremely anomalous sample (ENL-11) with an Mn/(Fe + Mn) x 100 ratio of 89 very strongly suggests that its pegmatitic host is much more highly fractionated than the main ENL intrusion. This and the abundant Nb,Ta oxide minerals present suggest that ENL-11 is, in fact, a separate pegmatite dike which fractionated from the ENL intrusion.

d) Greer Lake Intrusion. The Mn/(Fe + Mn) x 100 of the Greer Lake garnet (Figure 93) follows trends similar to those suggested by the blocky K-feldspar and muscovite mineralogy. This trend is one of increasing fractionation in a west-southwest direction across the intrusion. The GL intrusion is the only one of the four bodies of pegmatitic granite to show

(locally) significantly higher ratios in some garnet from the pods of potassic pegmatite than garnet from an adjacent facies (e.g. GL-6) (Figure 94). Foord (1976) states that the potassic pegmatite garnet should be Mn-enriched over the other facies. Lack of sufficient statistically significant samples would possibly explain why this does not appear to be the usual case in the Winnipeg River pegmatitic granites.

5. Geochemical Trends Towards Enriched Pods of the Potassic Pegmatite Facies

All four intrusions have local pods of the potassic pegmatite (quartz + muscovite + K-feldspar) facies; however, in some areas these pods are unusually highly fractionated with respect to the ubiquitous potassic pegmatite facies widespread in all four intrusions. Consequently, they have concentrated enough rare elements (Be, Nb, Ta, Sn, Li, Rb, Cs, As, Zn, and Mo) to crystallize diversified accessory minerals (beryl, Nb,Ta oxides, Li-micas, etc.).

a) Tin Lake Intrusion. The Tin Lake intrusion was found to be poor in these enriched potassic pegmatite pods. One crystal (1.5 cm) of molybdenite was located in one of these pods on the western end of the northern lobe but this occurrence was too unique to be considered significant. Beryl, tourmaline, and

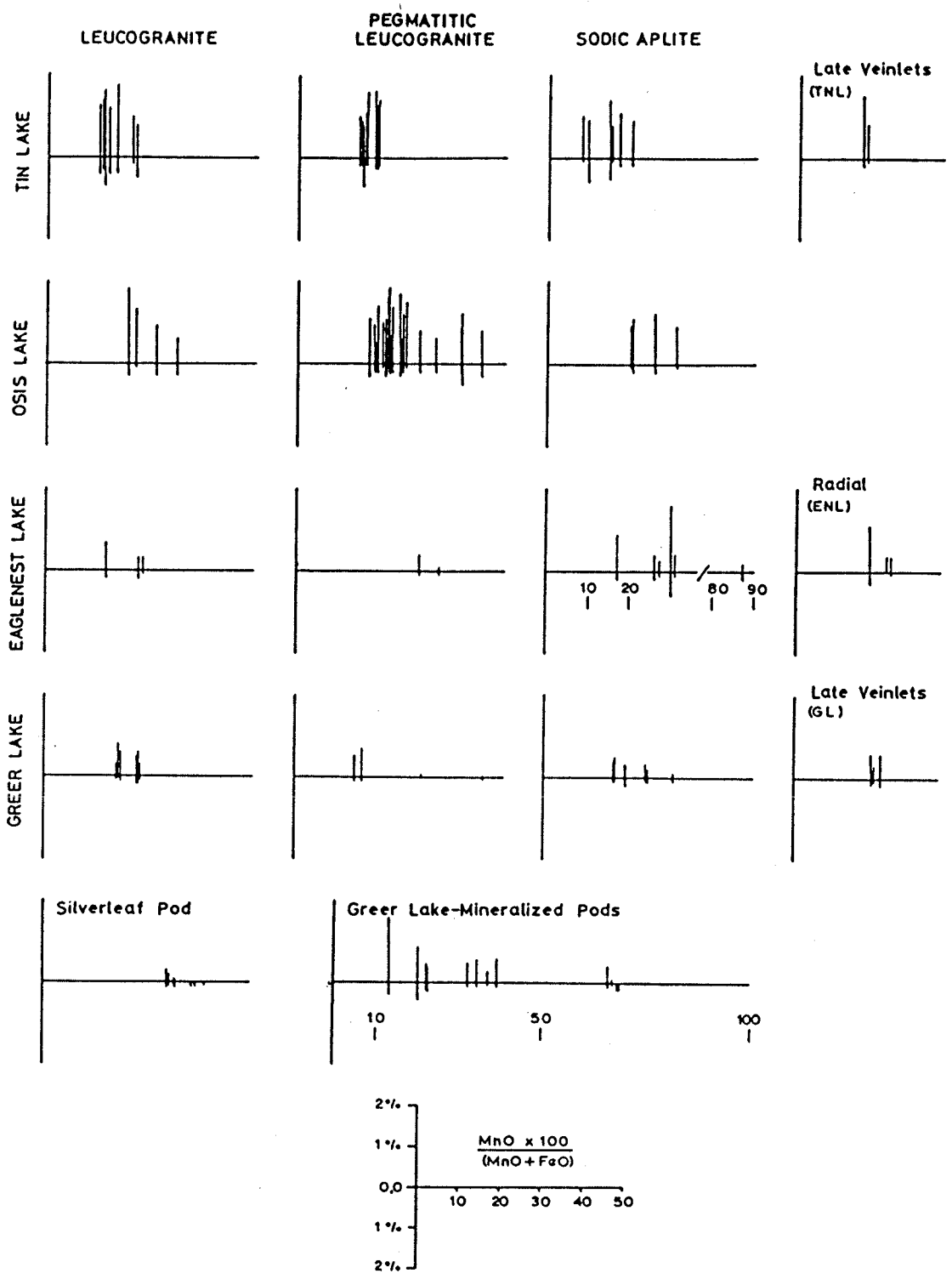

Figure 94. Molecular percentages of spessartine, and weight percentages of MgO and CaO of garnets from various assemblages in the Greer Lake, Eaglenest Lake, Tin Lake, and Osis Lake pegmatitic granites.

Nb,Ta oxide minerals begin to appear in the potassic pegmatite facies as the western contact of the TNL intrusion grades into the Birse Lake pegmatite group (Černý et al., 1981); however, no exotic accessory mineralization is associated with the TNL intrusion as such.

b) Osis Lake Intrusion. The western part of the Osis Lake intrusion has many small potassic pegmatite pods that are diversified (Figure 22(a)) beyond the ubiquitous K-feldspar + quartz + muscovite association of this facies. The enriched pods contain rose coloured quartz, apatite, tourmaline, and alteration products (sicklerite to manganoan sicklerite) of triphylite-lithiophilite, and locally Nb,Ta oxides and arsenopyrite in addition to the usual granitic mineralogy.

The degree of enrichment over the normal pods is very slight. The only usual noticeable change is the occasional occurrence of a triphylite-lithiophilite crystal, as in Figure 22(a). The frequency of this mineralization occurring in the potassic pegmatite pods increases towards the extreme western tip; however, there has been no accumulation in any particular area of potassic pegmatite within the intrusion.

c) Eaglenest Lake Intrusion. The Eaglenest Lake intrusion is relatively barren, not only of enriched locations of the potassic pegmatite facies but of this facies in general. No accessory mineralization was found in this intrusion. Stocks of pegmatite were found adjacent to the main intrusion at the northwest contact on an island in the Winnipeg River (location ENL-11) and also at the eastern contact where the intrusion fingers out into the metavolcanics (Černý et al., 1981). The K-feldspar from the pegmatite located adjacent to the northwest contact has a similar composition to that within the ENL pegmatitic granite (Figure 82, 84); however, the garnet composition is extremely Mn-enriched (Figure 93). A distinct difference between the main intrusion of the ENL pegmatitic granite and this adjacent pegmatite is in the occurrence of Nb,Ta oxide minerals in the sodic aplite facies of ENL-11 (Appendix 9).

d) Greer Lake Intrusion. The GL intrusion is the most mineralogically diversified pegmatitic granite of the Winnipeg River area (followed by OL, then the relatively barren ENL and TNL intrusions). Many relatively small pods of potassic pegmatite which contain beryl, and locally also Nb,Ta oxide minerals, are common throughout this intrusion. Several

occurrences of these pods are quite large (2 to 3 m^2) and host abundant beryl, Nb,Ta oxide minerals plus lesser amounts of Li, Sn, Rb, and Cs-bearing phases. The larger and best developed will be discussed below.

The first two localities differ from the average potassic pegmatite pods only in dimensions but not in geochemistry.

i) GL-30. The composition of blocky K-feldspar (Figure 95) and platy muscovite (Figure 96) from this location is very similar to the minerals in the adjacent main GL intrusion. Fractionation attained the same level as in the Greer Lake intrusion; however, larger quantities of rare elements (Be, Nb, Ta) led to crystallization of greater accumulation of the accessory minerals.

ii) Zone-5. Compositions of Zone-5 blocky K-feldspar and muscovite are within the field defined by other analyzed Greer Lake samples. Only very slight advanced fractionation of specimens from this location is apparent in Figure 95 (blocky K-feldspar) or in Figure 96 (muscovite).

The following pods of mineralized potassic pegmatite in the Greer Lake intrusion are particularly interesting because of their higher fractionation and greater concentration of rare elements

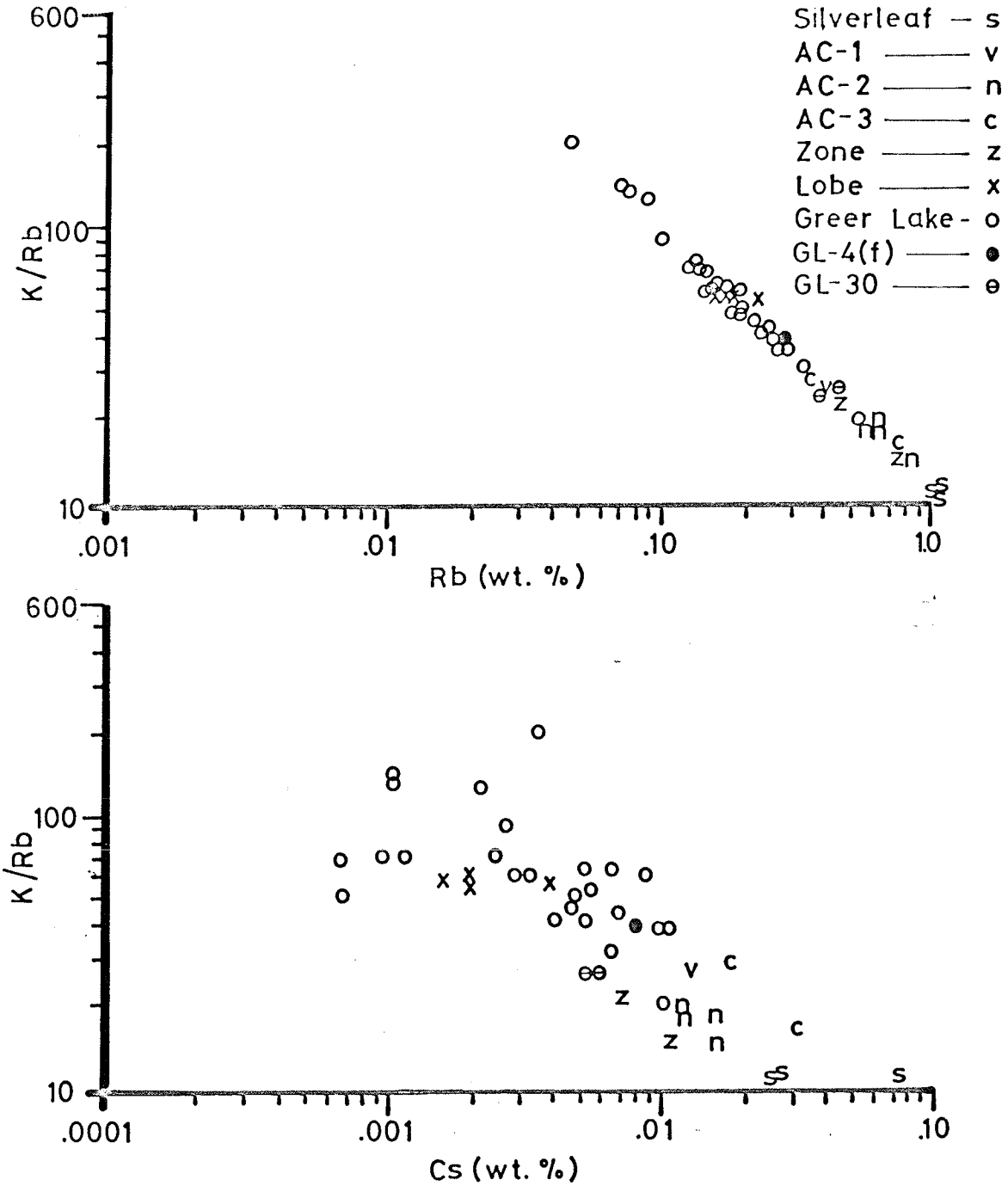

Figure 95. K/Rb vs. Rb and K/Rb vs. Cs plots of the blocky K-feldspar samples from the Greer Lake intrusion and all mineralogically enriched pods of potassic pegmatite associated with this intrusion. GL-4(f) is a pod of potassic pegmatite adjacent to the east side of AC-1.

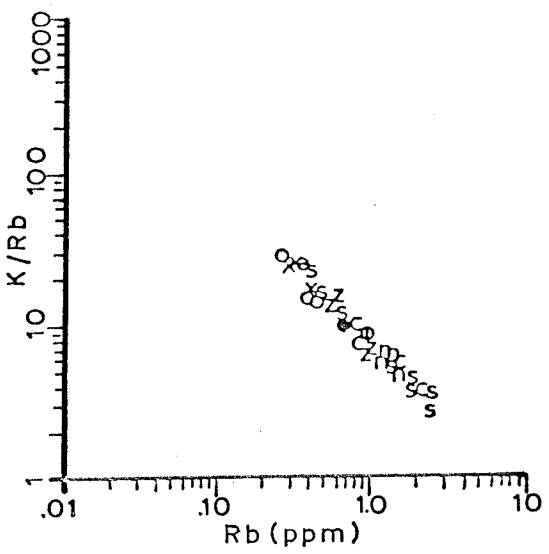

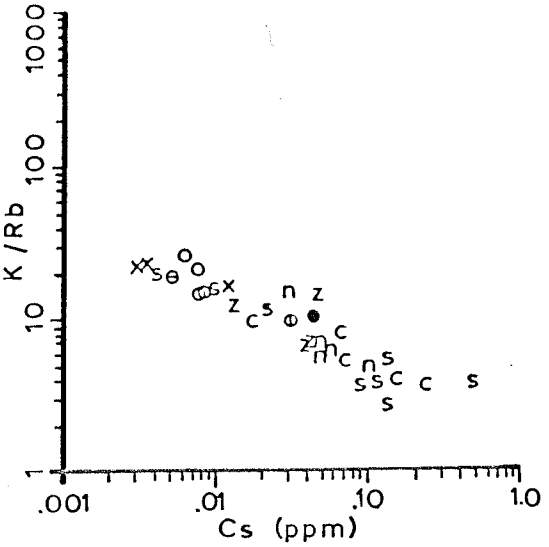

Figure 96. Selected geochemical plots of all platy muscovite samples that were analyzed from the Greer Lake intrusion. G.L.-19-1 is a slightly mineralogically enriched pod of potassic pegmatite containing beryl crystals and coarse, slightly curved muscovite (φ). Symbols as in Figure 95.

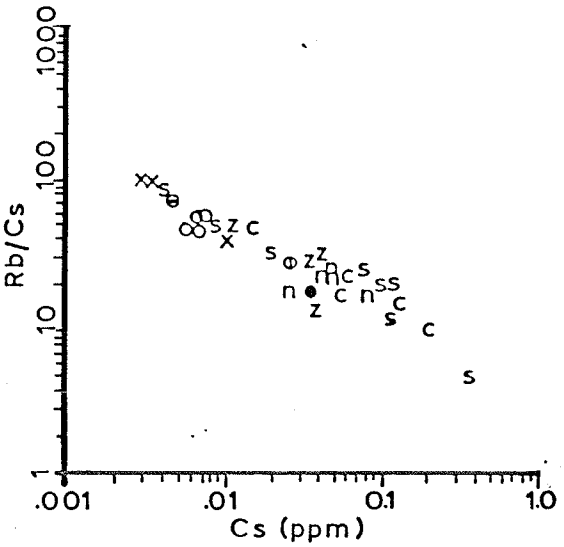

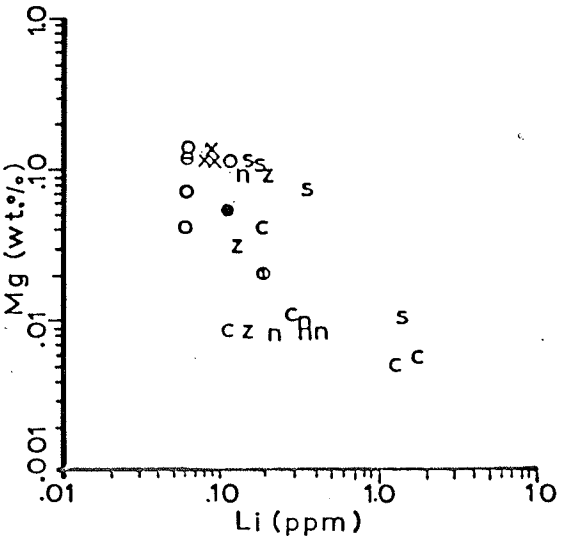

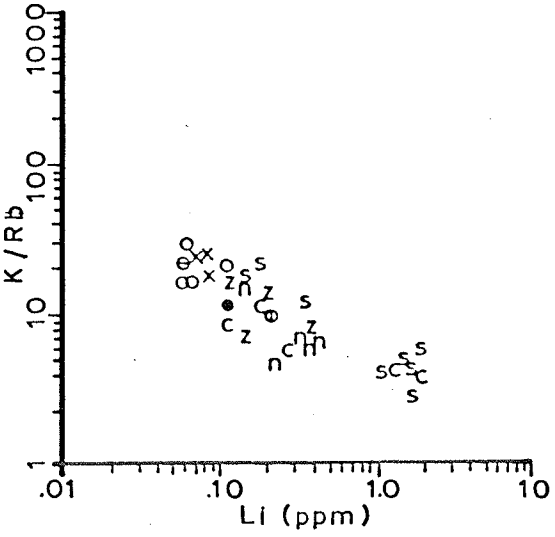

(Li, Be, Nb, Ta, Rb, Cs) than in any other area of potassic pegmatite within the Greer Lake intrusion, or in any other Winnipeg River pegmatitic granite. These pods occur along or adjacent to the southern contact of the Greer Lake intrusion, south of the internal shear zone.

iii) Lobe. The Lobe area commonly contains beryl and very minor Nb,Ta oxide mineralization plus occurrences of garnet + biotite + chlorite pseudomorphing cordierite. Blocky K-feldspar (Figure 95) and muscovite (Figure 96) show some indications of an increased degree of fractionation over the main stock of the Greer Lake pegmatitic granite. The Mn/(Fe + Mn) x 100 ratio of garnet is also slightly elevated (Figure 93, Appendix 5).

West from the Lobe location, along the southern contact, an area is approached that shows enrichment trends above the average composition of the main Greer Lake intrusion.

Four pods of potassic pegmatite, each one progressively more enriched (mineralogically and geochemically) over its eastern neighbour, have been noted.

iv) Annie Claim (AC). GL-4 is the easternmost pod of potassic pegmatite on the Annie Claim and

contains mineralogy mostly equivalent to the main Greer Lake intrusion. Several beryl crystals and one Nb,Ta oxide mineral were found. From this location the mineralogy becomes increasingly varied, and evidence of increased fractionation across the three remaining pods of potassic pegmatite in a western direction (AC-1 → AC-2 → AC-3) is suggested by the geochemistry of the contained minerals.

Blocky K-feldspar from the Annie Claim locations (Figure 95) shows a marked increase in the degree of fractionation over the main Greer Lake intrusion. Fractionation increases progressively from GL-4 → AC-1 → AC-2 → AC-3 and along with this the mineralogy becomes more diversified (Table 23). Muscovite shows parallel trends to the blocky K-feldspar as seen in Figure 96. The lithian muscovites found only in AC-3 have the lowest K/Rb (4) and K/Cs (33) ratios of any Greer Lake muscovite.

The Mn/(Fe + Mn) x 100 ratio of a single garnet from the potassic pegmatite facies on the Annie Claim (AC-3(j)) indicates a high degree of fractionation (Figure 93); however, other samples from AC-3 and AC-2 indicate a slight enrichment over the average Greer Lake garnet composition

Table 23. Paragenesis of the pegmatitic bands and nodules in the southwestern part of the Greer Lake pegmatitic granite

	AC-1	AC-2	AC-3	Silverleaf
Microcline	●	●	x	●
Albite	x	●	●	●
Quartz	●	●	●	●
Muscovite	x	o	x	x
Li-muscovite		o	●	o
Lepidolite			•	•
Spodumene				x
Petalite				(x)
Epidote				•
Garnet	•			x
Schorl			•	
Elbaites			•	•
Topaz				•
Gahnite				•
Beryl				•
Cassiterite			•	•
Columbite-tantalite	•	•	•	•
Apatite		•	•	•
Monazite				•
Triphylite-lithiophilite				•
Amblygonite-montebrasite				•
Sulphides of Zn,Cd			•	

Abundant, rock-forming - ●, subordinate - o, accessory - x rare - •, an early phase which is now totally altered - ( ).

as well (Appendix 5).

The extreme enrichment in a potassic pegmatite pod associated with the Greer Lake intrusion is attained in the pegmatite on the Silverleaf Claim, located southwest of the Annie Claim.

v) Silverleaf (SF). For reasons discussed previously the Silverleaf stock is thought to be an apophysis of the main Greer Lake pegmatitic granite. Mineral compositions indicate a degree of fractionation equal to or greater than that attained by the pegmatitic pods of the Annie Claim. Silverleaf blocky K-feldspar compositions and muscovite compositions are shown in Figures 95 and 96, respectively, in relation to the compositional field covered by the Greer Lake intrusion. Mn/(Fe + Mn) x 100 ratios (Figure 93, Appendix 5) are slightly higher in the garnets of the Silverleaf stock than those in the main Greer Lake intrusion. The mineralogy of the Silverleaf stock is also quite diversified (Table 23).

A trend unique to the Greer Lake intrusion is that of the progressive increase in the Li and Cs content of beryl. Na/Li vs. Cs (Figure 52) demonstrates this increase from the alkali-poor beryl from the potassic pegmatite facies of the main Greer Lake intrusion (e.g. GL-37) through intermediate

compositions (e.g. Lobe-4) to highly alkali-enriched beryl from the AC-3 and Silverleaf pods.

6. K-Feldspar Obliquity

Obliquity of every analyzed blocky K-feldspar sample from all four intrusions was measured (Table 9, Figure 42) and no systematic variation across the intrusions was observed.

7. Microcline Solid Solution

The amount of solid solution of Ab + An residual in the K-feldspar phase of microcline perthite was measured on all analyzed K-feldspar samples from all intrusions of pegmatitic granite (Figure 43); no systematic variations within the intrusions were apparent.

Apparent fractionation directions within the four intrusions of pegmatitic granite as suggested by data in Figures 74-77, 86-88, and 93 are shown by Figure 97.

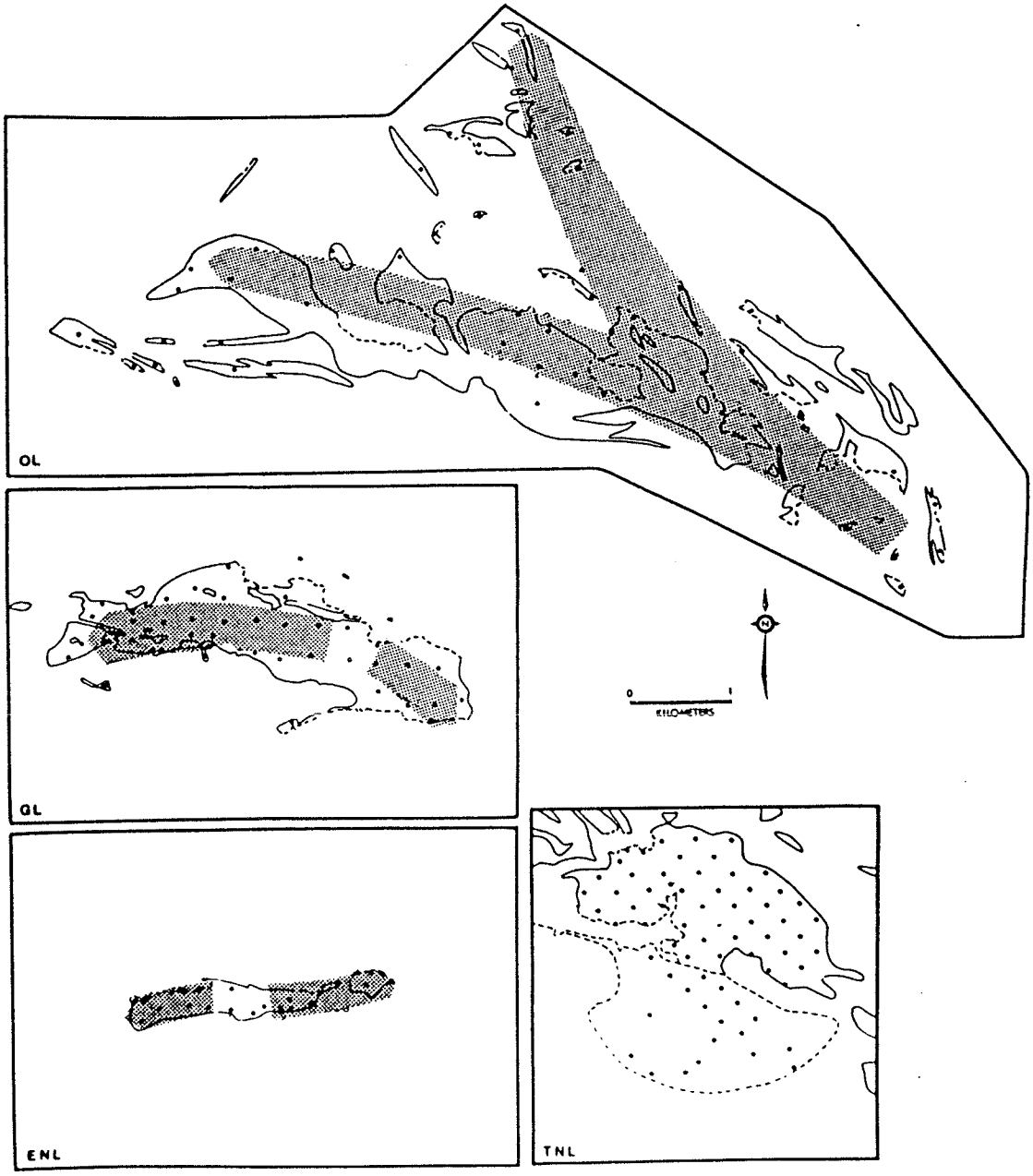

Figure 97. Fractionation directions in the four pegmatitic granites based on whole rock K/Rb and K/Cs, blocky K-feldspar K/Rb and K/Cs, muscovite K/Rb, Mg/Li, and Be and garnet (Mn/(Fe + Mn) x 100).

Chapter VIII

DIFFERENCES AMONG THE INTRUSIONS

A. INTRODUCTION

The following discussion deals with variations among the four intrusions. Many quantitative differences are observed despite the qualitative similarities stressed in the chapters on petrography and petrochemistry.

B. FIELD OBSERVATIONS

All of the intrusions lie along or close to major faults within the Bird River greenstone belt and show only very slight differences in their intrusive style. Intrusion involved minor stoping and extensive dilation of intruded fractures. Plastic deformation of the country rocks is only prominent in the Osis Lake intrusion.

Field observations of the mineralogy of the four pegmatitic granites give the first suggestion that slight variations in the bulk chemical compositions could exist. All of the intrusions contain similar proportions of the major granitic rock-forming minerals (K-feldspar + quartz + plagioclase); however, it is in the type and quantity of the contained accessory minerals that the pegmatitic granites deviate from each other. Table 24 illustrates the mineralogical differences among the intrusions. This table also suggests a more general division of the pegmatitic

Table 24. Accessory minerals in the four major intrusions of pegmatitic granites

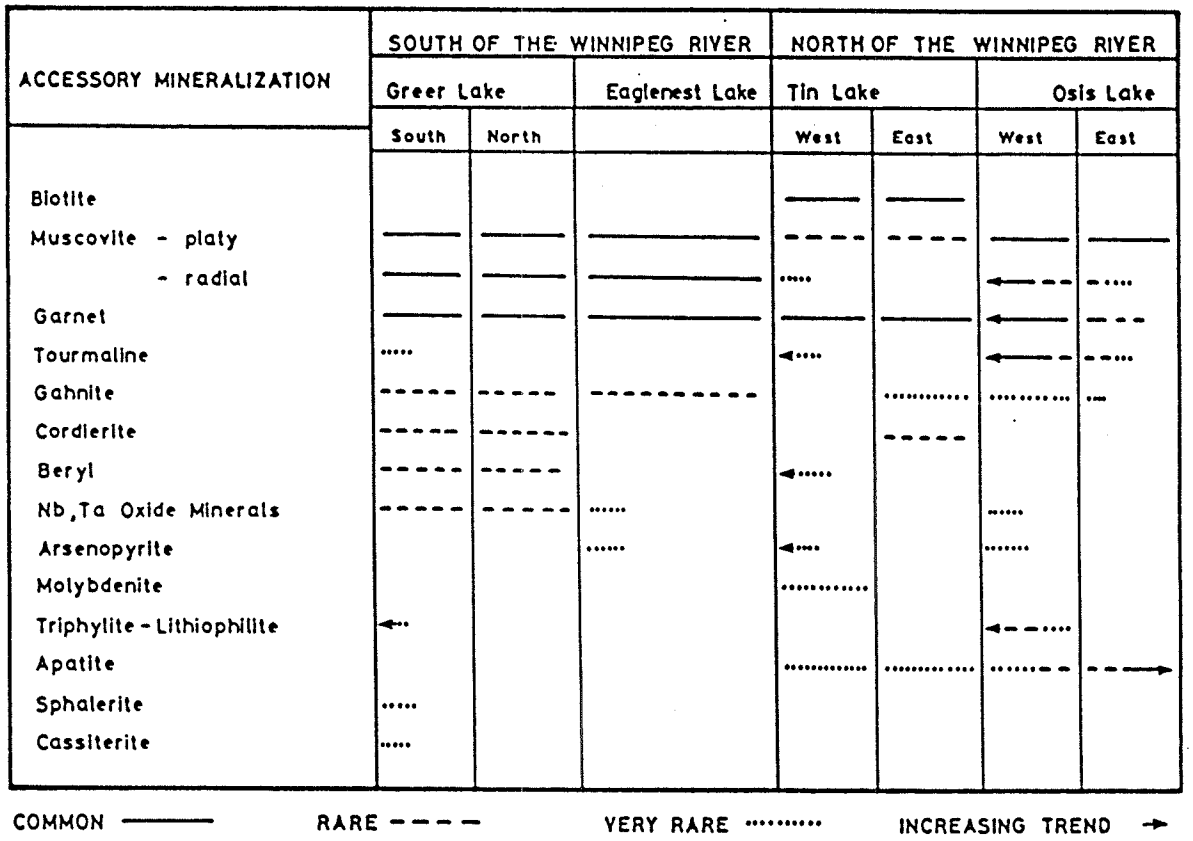

granites into those intrusions located north of the Winnipeg River (OL, TNL) and those south of it (GL, ENL). For example: biotite (Fe, Mg), tourmaline (B), apatite (P), and arsenopyrite (As, S) are not found in the intrusions south of the Winnipeg River while beryl (Be), Nb,Ta oxide minerals, gahnite (Zn ± Al), and garnet + biotite + chlorite pseudomorphing cordierite (Al) are extremely rare or absent in the TNL and OL intrusions north of the river. Bulk and trace element geochemistry confirm compositional variations as suggested by different accessory mineralogy of each intrusion.

C. CHEMISTRY

Significant differences among the four intrusions are evident when the chemistry of each individual granite is compared to that of the other stocks. The northern intrusions tend to have a slight increase in CaO over the leucogranites of the southern intrusions. Examination of Figures 62 to 70 shows that each intrusion has a separate field in each of the plots. The ENL and GL intrusions are somewhat enriched in Rb and depleted in Sr with respect to the northern TNL and OL intrusions. These figures also demonstrate a difference between the trace element composition of the main OL leucogranite and the central biotite leucogranite.

Table 25 lists selected major and trace element relationships in the leucogranite facies of the four intru-

Table 25. Selected major and trace element relationships in fine-grained leucogranites of the four major intrusions of pegmatitic granites

	Greer Lake	Eaglenest Lake	Tin Lake	Osis Lake bio. gr.	Osis Lake fg. lgr.
Li. ppm	58* ±20.2 29-86	79.7 ±56.9 27-140	31.83 ±18.30 11-59	71.5 ±11.1 63-87	63.3 ±14.4 47-74
Rb	562 ±309.7 340-1050	536 ±264 293-817	244.75 ±75.3 128-338	187.5 ±9.8 179-196	137.3 ±48.6 103-193
Cs	8.9 ±3.2 5.1-13.7	12.7 ±10.3 3.8-24	7.24 ±3.22 2.9-11.4	15.6 ±3.4 11.8-20	8.4 ±7.4 3.9-17
Be	3.8 ±3.5 1.2-10	5.6 ±6.5 0.7-13	1.98 ±0.66 1-3	0.73 ±0.34 0.3-1	0.77 ±0.45 0.3-1.2
Sr	18.2 ±6.4 11-28	10.3 ±5. 5-15	35.42 ±14.33 3-55	83.5 ±22.6 63-105	25.7 ±11.7 13-36
Ba	112.4 ±57.05 12-150	70 ±61 0-110	217.3 ±111.6 31-416	287.3 ±61.8 203-347	8 ±8.7 3-18
Ga	53 ±18.1 32-73	58.3 ±2 56-60	30 ±7.7 22-46	28 ±3.2 25-32	48 ±8.2 41-57
U	15 ±9.1 8-30	6 ±2 4-8	28 ±9 13-40	30.2 ±27.4 12-71	23 ±25.1 8-52
	7.4	7	10.3	0	6.7

Hf		±1.3 0.8-3.4	±0.6 3.5-4.6		
Sn	13.6 ±8.5 5-25	13 ±2 11-15	8.7 ±4.1 0.13	4.75 ±3.1 2-9	13 ±2.6 10-15
K/Rb	87.2 ±34.6 42-132	74.7 ±33.6 47-112	176.3 ±67.4 69-327	237 ±16.5 221-260	131.7 ±38 89-156
K/Cs	5108 ±1817 3277-7699	4462 ±3711 1608-8658	6800 ±4113 3402-15483	2988 ±750 2162-3968	2823 ±1587 1706-4640
K/Ba	767 ±939 215-2425	338 325-351	278.7 ±316.6 75-1258	162.5 ±45.3 136-230	5402 ±4612 507-9667
Ba/Sr	7.4 ±4.5 0.43-12.36	8.2 7.3-90	11.7 ±22 1.1-81.3	3.50 ±0.6 3.0-4.36	0.53 ±0.76 0.083-1.4
Rb/Sr	32.1 ±17.4 17.0-61.8	52.8 ±6.8 45.4-58.6	10.9 ±14.3 3.2-56	2.35 ±0.52 1.87-2.84	6 ±2.5 3.2-7.9
Mg/Li	4.68 ±3.36 1.74-9.36	6 ±5.5 1.7-12.2	48.6 ±38.5 13.5-127	39.7 ±6.7 32.03-48.25	11.5 ±6.7 6.7-19.1
Al/Ga	1526 528 990-2284	1258 ±29 1227-1284	2351 ±392 1742-2909	2737 ±310 2372-3060	1674 ±189 1520-1885
Zr/Hf	48.3	32.9 ±26.9 14.1-63.7	30.8 ±1.5 29.3-32.6	47.7 46.8-48.7	24.3

58: arithmetic mean, ±20.2: 1σ, 29-86: range

sions of pegmatitic granite of the Winnipeg River area. It should be noted that each intrusion attained its own particular level of fractionation. In general, the southern intrusions (ENL and GL) have become more highly fractionated.

Direct differentiation relationships among the leucogranite facies of all four intrusions is not suggested by most geochemical data. Plots of K/Rb vs. Rb (Figure 63), Mg/Li vs. Li (Figure 68), Al vs. Ga (Figure 69), Al/Ga vs. Ga (Figure 70) all suggest that fractionation of the four intrusions successively from each other was not possible since each intrusion follows its own distinct trend. These trends may be somewhat parallel as in the case of Al/Ga vs. Ga or they can show no relationship to each other as is the case with K/Rb vs. Rb.

Rb vs. Sr (Figure 62) is one of the few plots that suggests fractionation relationships of the four intrusions of pegmatitic granite since the individual leucogranite fields overlap on a rough Sr depletion and Rb enrichment trend; however, all other data indicate that this is not the case.

Figure 72 illustrates the REE abundances in the fine-grained leucogranites and pegmatitic leucogranites (usually somewhat lower in the latter phase). In general, the Greer Lake, Eaglenest Lake, and Tin Lake intrusions show very low abundances, about equal for all REE's except Eu which displays extreme depletion. The abundances

decrease in these three bodies with Sr and decreasing K/Rb. In contrast to these three intrusions, the Osis Lake body (including its central plug of biotite granite) exhibits low REE abundances despite its high K/Rb ratio, moderate Eu anomaly, and relatively high Ce_N/Yb_N.

Oxygen isotopic compositions of the pegmatitic granites are remarkably homogeneous within individual bodies but widely different among them. Most of the data are correlatable with $\delta^{18}O$ values found for enclosing metasedimentary and/or metavolcanic rocks. In the Greer Lake and Eaglenest Lake intrusions seated in O^{18} - low metabasalts, $\delta^{18}O$ = 8.1 - 8.7 and 8.6 - 9.3, respectively. The $\delta^{18}O$ ranges for the Tin Lake and the Osis Lake intrusions, 10.3 - 10.9 and 11.1 - 12.4, respectively, also closely correspond to those of their metasedimentary hosts.

The REE patterns (Figure 72) and the oxygen isotope composition of the four intrusions support the hypothesis of a largely independent evolution of the pegmatitic granites and rule out a simple and direct fractionation relationship among them. The genetic significance of these data will be discussed in Chapter IX.

1. Mineral Chemistry

Mineral compositions reflect the differences among the four intrusions of pegmatitic granite and also the north-south differences between the Greer Lake-Eaglenest

Lake intrusion pair and Tin Lake-Osis Lake stocks. All the plots in Chapter VII show some degree of separation in the mineral chemistry of the four intrusions and document a more advanced fractionation of the Greer Lake and Eaglenest Lake intrusions. This is best illustrated by the K/Rb vs. Cs plot (Figure 98) of the blocky K-feldspar and any of K/Rb vs. Cs (Figure 99), Mg vs. Li (Figure 100), K/Rb vs. Li (Figure 101) or Rb/Cs vs. Cs (Figure 102) plots of platy muscovite. Both of these mineral species are from the potassic pegmatite facies.

Garnet (Figure 103, 104) compositions among the intrusions also have slight variations in the Mn/(Fe + Mn) x 100 ratio (Appendix 5). Garnet from the Tin Lake intrusion has the lowest Mn content followed by the garnet from the main intrusions of GL and ENL. Osis Lake garnet compositions have the highest Mn content with the exception of three garnet occurrences from the highly fractionated areas of GL (AC-3(j), GL-6(a)) and ENL (ENL-11). These GL occurrences are from bands of potassic pegmatite facies and illustrate that Mn enrichment occurs in garnet from this facies. In the remaining three intrusions (and other localities in GL) garnet compositions from the potassic pegmatite facies overlap with compositions from the other facies. Figures 94, 103 and 104 illustrate that garnet from the northern intrusions (TNL, OL) have CaO and MgO contents that are distinctly higher than those from the southern

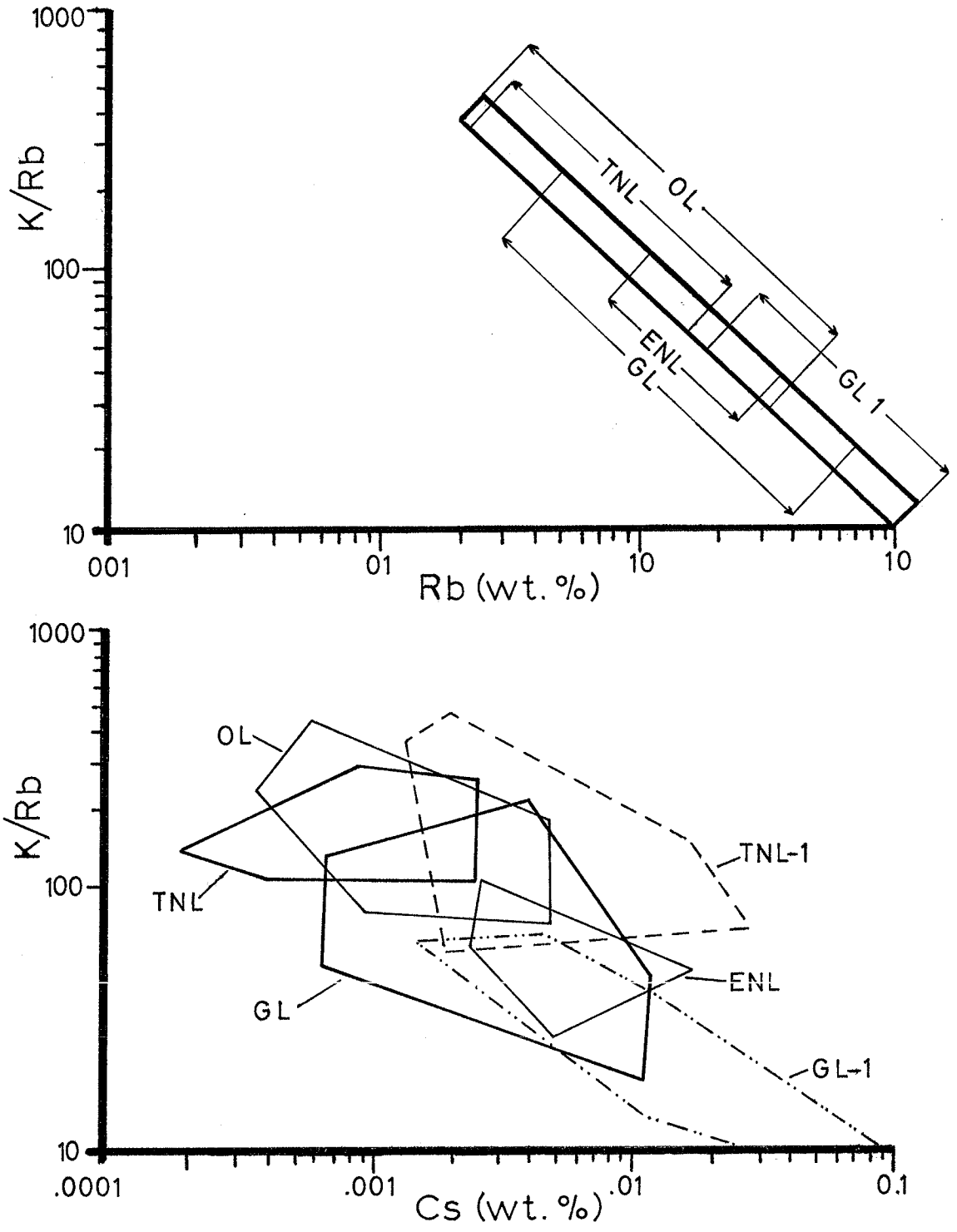

Figure 98. K/Rb vs. Rb and K/Rb vs. Cs compositional fields of blocky K-feldspar from pods of potassic pegmatite facies from all four intrusions. Symbols as follows: Tin Lake (TNL), Osis Lake (OL), Eaglenest Lake (ENL), Greer Lake (GL), Greer Lake - mineralized pods (GL-1), Tin Lake-eastern extension (TNL-1).

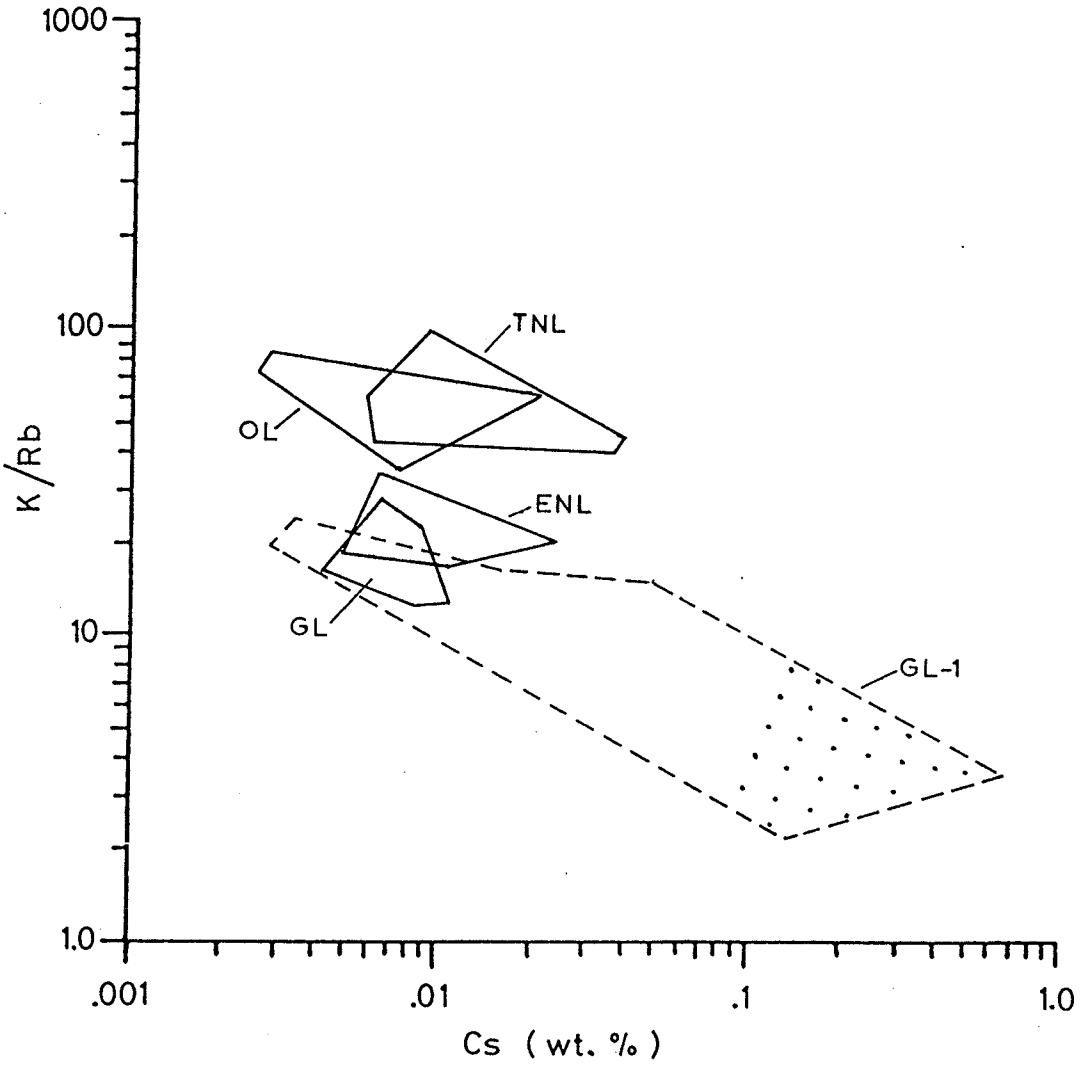

Figure 99. Shown is the area covered by the plot of K/Rb vs. Cs in the platy muscovite from the potassic pegmatite facies of each intrusion of pegmatitic granite. GL-1 covers all the muscovite samples from the mineralized pods of potassic pegmatite within the Greer Lake intrusion. The dotted area corresponds to the samples of purple (Li-enriched) lepidolite from the Annie Claim (AC-3) and Silverleaf Claim pods of potassic pegmatite.

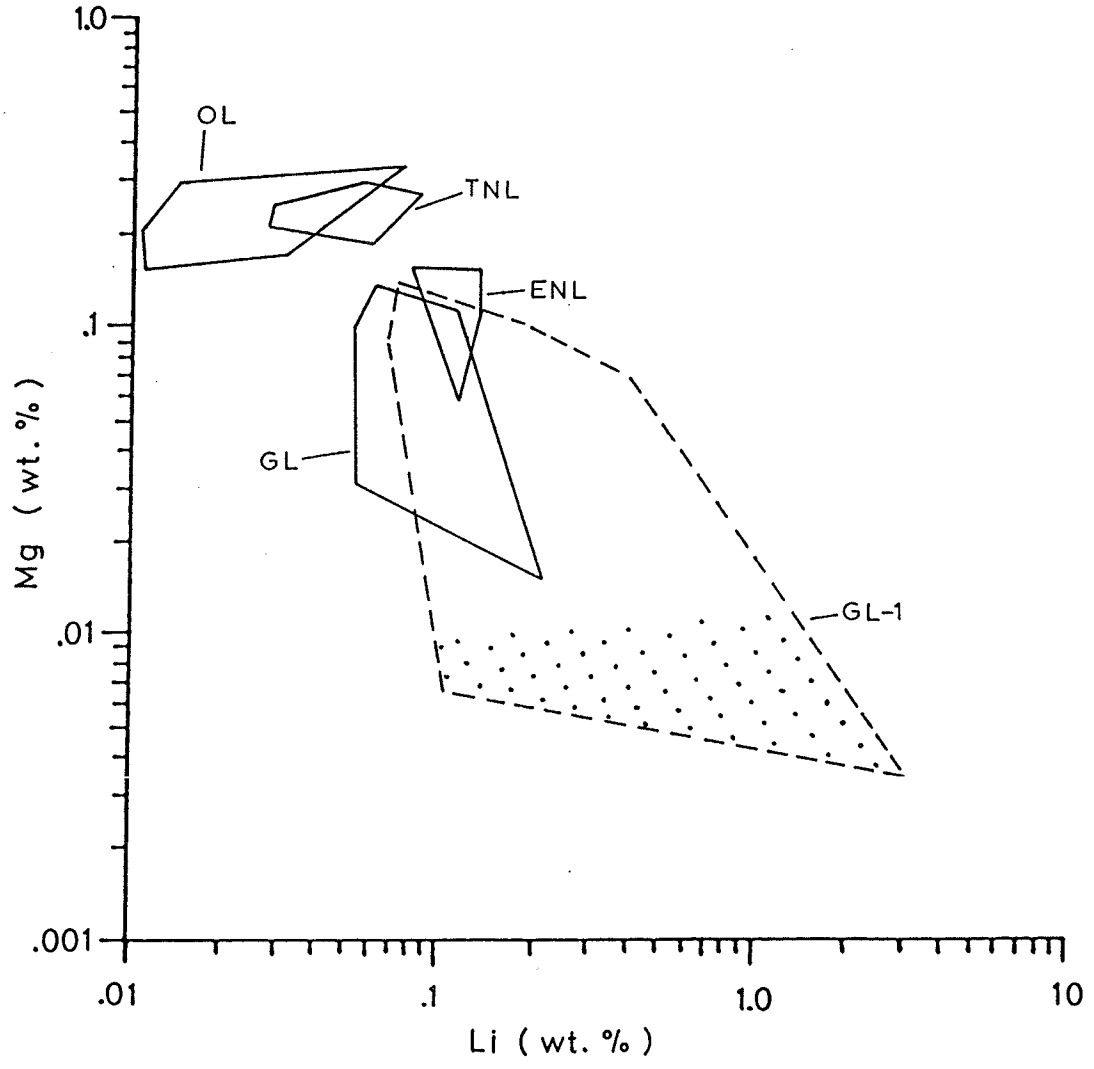

Figure 100. Shown is the area covered by the plot of Mg vs. Li in platy muscovite from the potassic pegmatite facies in each of the four intrusions of pegmatitic granite. Symbols as in Figure 99.

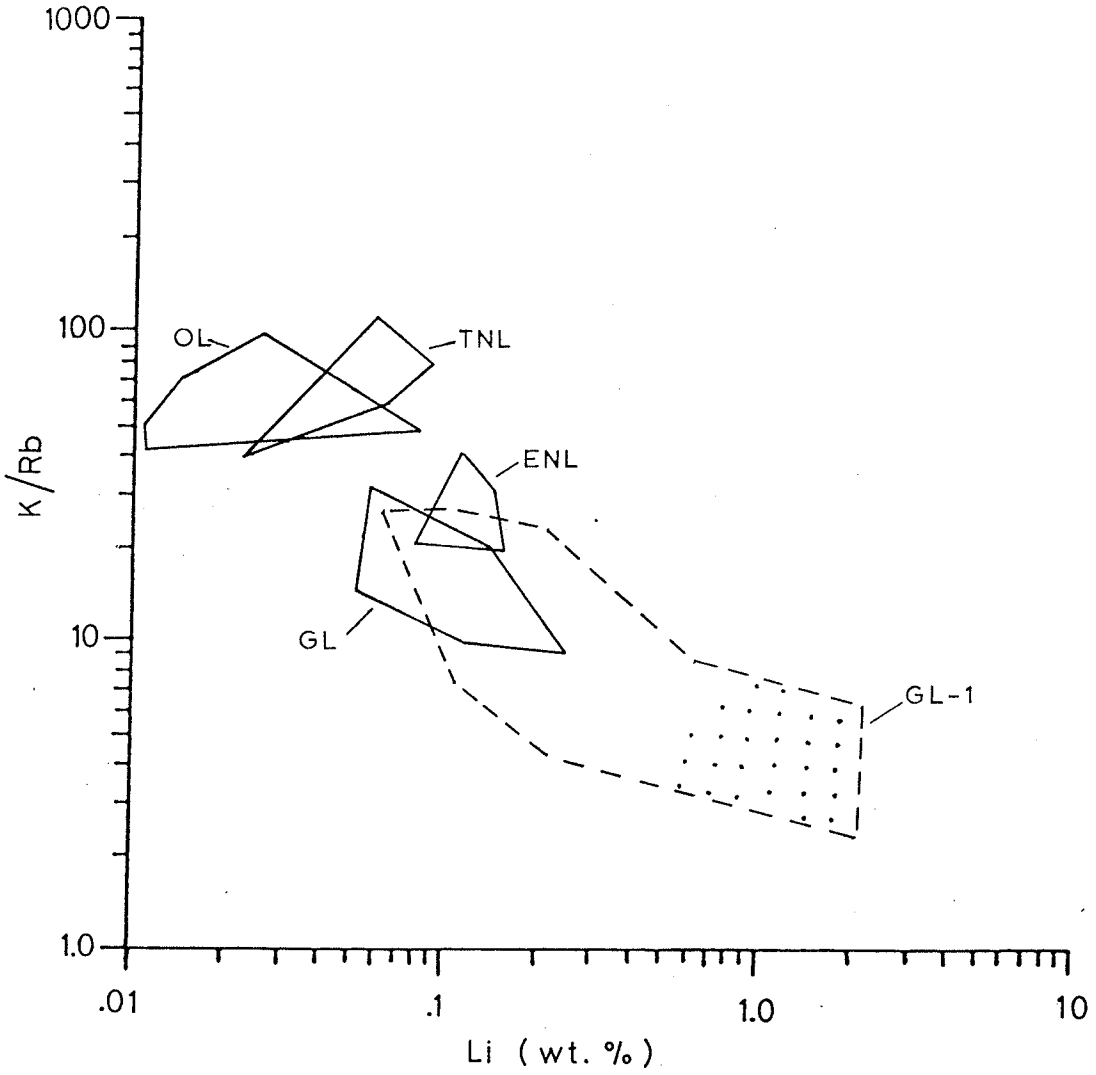

Figure 101. Shown is the area covered by a plot of K/Rb vs. Li in platy muscovite from the potassic pegmatite facies from each of the four intrusions of pegmatitic granite. In Figures 98 to 100 note the distinct separation of the Osis Lake, Tin Lake fields from the Greer Lake, Eaglenest Lake fields. This corresponds to the mineralogical difference between the intrusions north of the Winnipeg River and those south of it (Table 25). Symbols as in Figure 99.

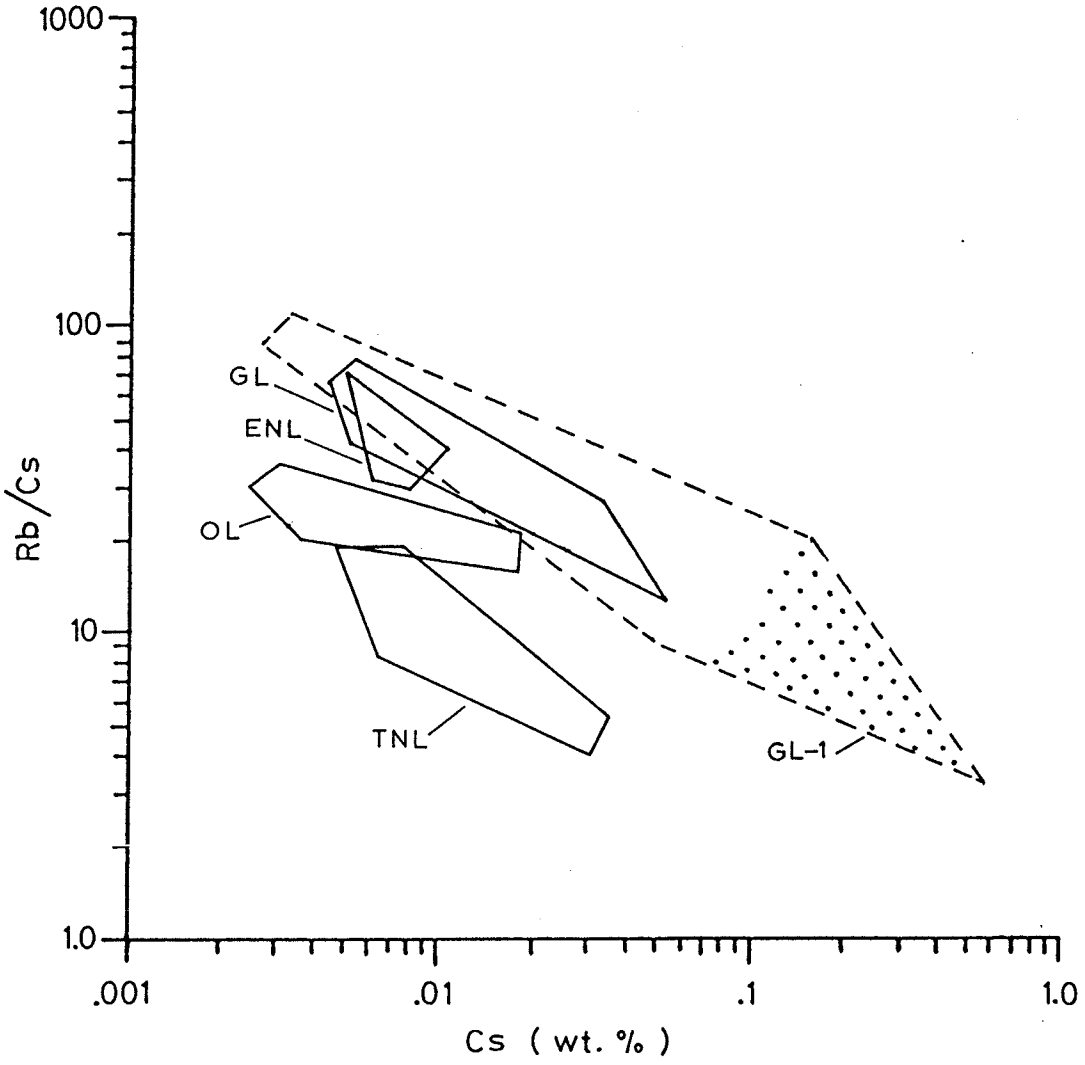

Figure 102. Shown is the area covered by the plot of Rb/Cs vs. Cs in platy muscovite from the potassic pegmatite facies in each of the four intrusions of pegmatitic granite. Symbols as in Figure 99.

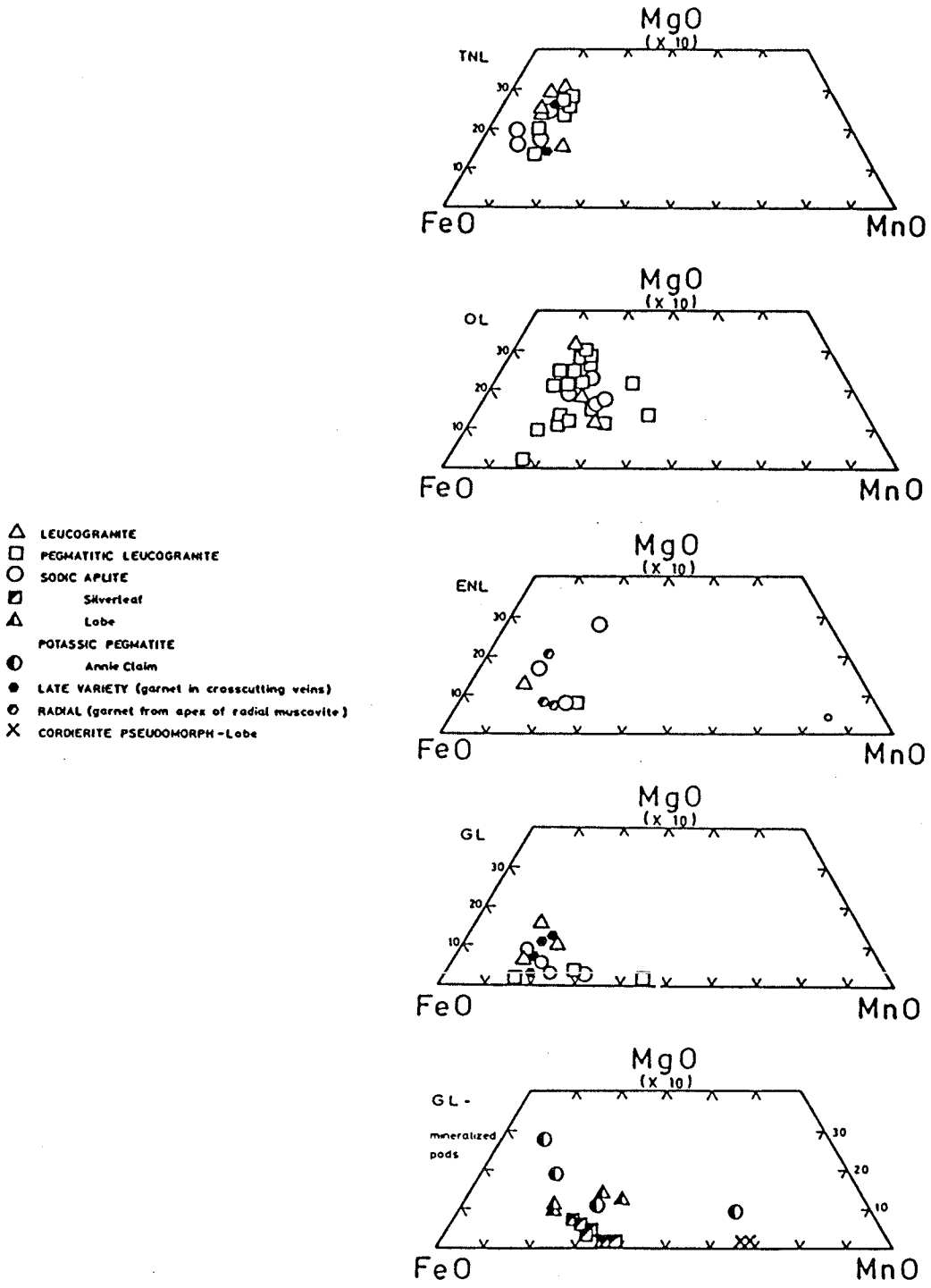

Figure 103. Composition of garnet from the pegmatitic leucogranite facies of all four intrusions of pegmatitic granite (weight percent).

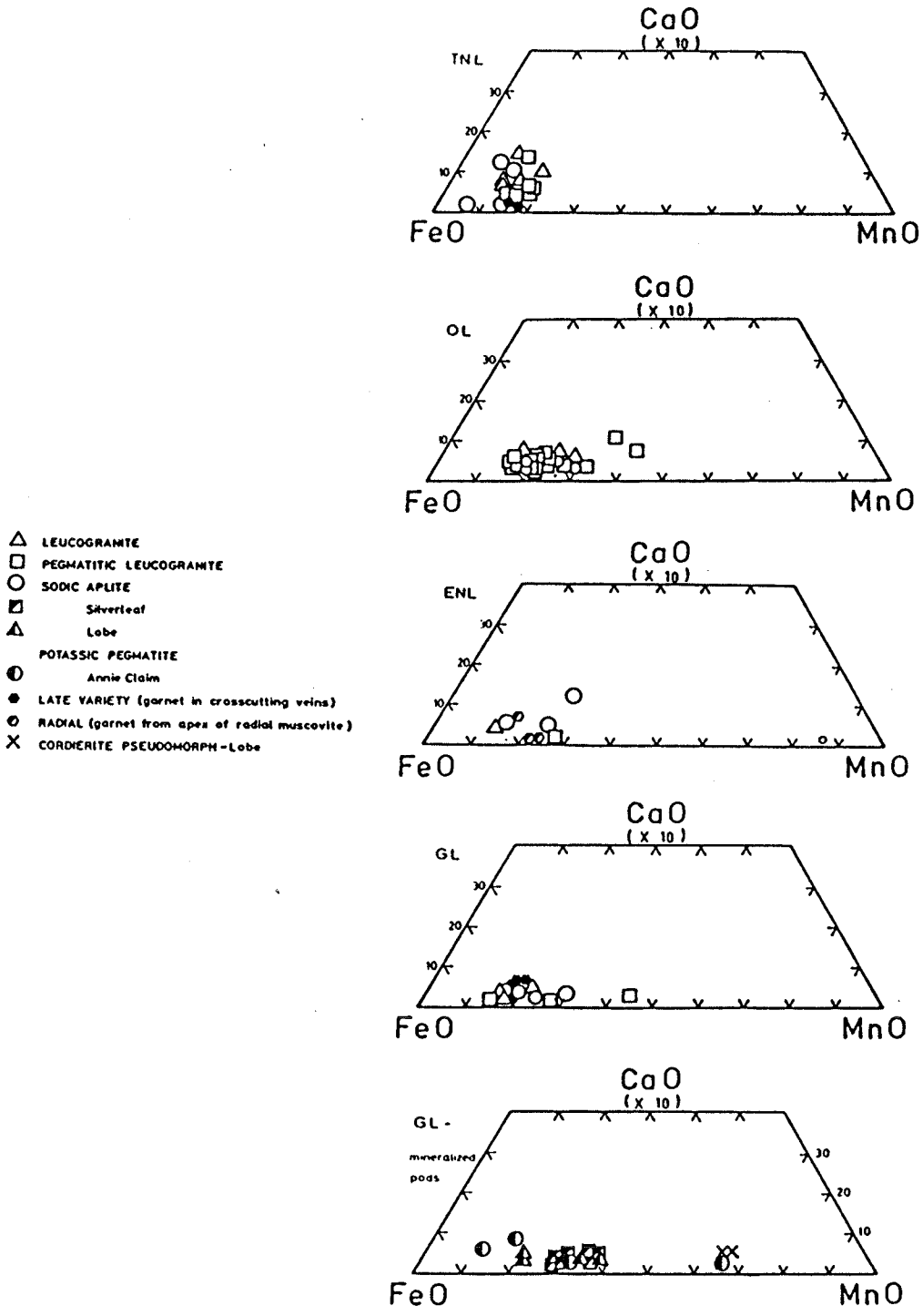

Figure 104. Composition of garnet from the pegmatitic leucogranite facies of all four intrusions of pegmatitic granite (weight percent).

intrusions (GL, ENL).

As can be seen from Appendix 5, the Osis Lake garnet is enriched in P_2O_5 (0.23 weight percent), Tin Lake garnet is slightly enriched in ZrO_2 (average 0.03 weight percent), and the Greer Lake and Eaglenest Lake garnet show slightly elevated Y_2O_3 content (0.10 to 0.25 weight percent).

Chapter IX

GENETIC DISCUSSION

A. INTRODUCTION

In this chapter, the genetic significance of all the observations from field and experimental data, presented in previous chapters will be discussed, as will possible relationships among the four intrusions of pegmatitic granite and the adjacent batholithic intrusions and pegmatite groups. Detailed data pertaining to the batholiths and pegmatites are presented in Černý et al. (1981).

B. PETROLOGY: INTERNAL EVOLUTION OF THE PEGMATITIC GRANITES

Theories suggested for the origin of the pegmatitic granites include late and post-magmatic recrystallization of granites with albitization and other metasomatic processes, low percentage partial melting of supracrustal sources, advanced igneous fractionation of granitoid intrusions, or "in-situ" lateral secretion processes as listed by Jahns (1955). Several interpretations of pegmatitic granites have been discussed in the literature and their origin is still controversial.

Metasomatic recrystallization and albitization of pre-existing granitoids, strongly advocated by Russian authors and applied to "in-situ" lateral secretion processes,

are not considered viable mechanisms for the formation of these granites. Some kind of direct magmatic differentiation as proposed by Jahns and Burnham (1969) is suspected to be a more probable hypothesis. This mechanism is suggested throughout all four intrusions by textural relationships, mineral assemblages, and composition of individual minerals. The major evidence is discussed below.

Differences in the textures, bulk chemistry, and trace elements suggest that the leucogranite crystallized from a relatively dry melt, whereas the pegmatitic leucogranite facies was derived from a more fractionated volatile-oversaturated melt which did not attain large-scale spatial segregation of supercritical fluids from the residual magma. Whenever this occurred, the fine-grained sodic aplite and coarse-grained potassic pegmatite facies have been produced. Pods of potassic pegmatite facies in either the leucogranite or pegmatitic leucogranite facies can be accounted for (Jahns and Burnham, 1969) by concentrations of supercritical fluids accumulated locally in the leucogranite facies. Graphic potassium feldspar + quartz megacrysts in the leucogranite facies may have grown from local concentrations of the supercritical fluid that did not coalesce. These potassic pegmatite bands, that develop locally by gradual or abrupt changes in the mineral assemblages or textures of the pegmatitic leucogranite, correspond to incipient segregation of supercritical fluids into larger pods and

extract preferentially K, Si, and rare elements.

In many locations, the fine-grained leucogranites and, rarely, the pegmatitic leucogranites, grade into the layered assemblages of garnetiferous sodic aplite which alternate with the potassic pegmatite facies. Either of the following interpretations can be inferred from this:

a) the sodic aplite has crystallized from a residual melt which was depleted in silica, potassium, and trace elements by their extraction into a super-critical fluid which concentrated into the potassic pegmatite bands (Jahns and Burnham, 1969).

b) the sodic aplite has a metasomatic orgin similar to saccharoidal albitization fronts in complex pegmatites (Beus, 1961).

On closer examination of textural and mineral composition data, several observations favour the former mechanism.

a) Sodic aplite bands often serve as a substrate for crystallization of the pegmatitic assemblages (Figure 36).

b) The potassic pegmatitic assemblages transect and cement broken bands of sodic aplite (Figure 27, 28) but the reverse was never observed.

c) The An content of albite in the sodic aplite approximates the composition of albite in all other phases of the pegmatitic granite intrusions. If albitization had been a factor, the metasomatic

albite would be extremely An poor.

d) Similarly, a non-metasomatic process is indicated by the Mn content of garnet in the fine-grained and also pegmatitic leucogranite. Had albitization been a factor, Mn enrichment in garnet could have been expected since Fe-Mn fractionation continues as metasomatism proceeds.

e) Finally, had albitization occurred, the composition of individual minerals across facies boundaries would remain constant and not show the enrichment of Rb and Cs that is seen in potassium feldspar and muscovite of the potassic pegmatite facies.

Features of the sodic ablite that suggest that albitization may have occurred are the texture and the presence of accessory minerals (especially niobium, tantalum oxide minerals) which resemble those of many typically albitized units in pegmatites. If the layered albitic assemblages were generated through sodic metasomatism then their textural relationships to the potassic pegmatite facies (mentioned above) would indicate total recrystallization of the original rock type(s). The compositional uniformity of albite, garnet, and muscovite would also suggest a thorough metasomatic reworking of pre-existing lithologies whose only remnants might be represented by the fine-grained leucogranites. Such total metasomatism and recrystallization would suggest an analogy with apogranites of Soviet authors which

are in contrast to the rocks examined here, much more sodic in bulk compositions, extremely enriched in Li, Rb, Cs, Be, and F and not associated with mineralized pegmatite swarms (Beus et al., 1968).

A concept of igneous and supercritical crystallization from melt and fluids, triggered by a pressure quench in dilation zones (as modified by Jahns and Burnham, 1969), is the preferred mechanism for generation of all four facies of the Winnipeg River pegmatitic granite intrusions.

C. ESTIMATES OF PRESSURE AND TEMPERATURE

In principle, the crystallization conditions of the pegmatitic granites can be roughly estimated following the method of Harris (1974) and Castle and Theodore (1972). The intersection of the minimum melting of the granite curve and the muscovite + quartz + potassium feldspar + sillimanite + water curve suggests possible temperature and lower pressure limits. The latter melting curve was adjusted by the above authors to allow for a paragonite component in the muscovite which reacts with quartz before the minimum melting pressure and temperature of the pure muscovite system is reached. In the peraluminous pegmatitic granites studied here, cordierite must also be taken into consideration when estimating the maximum temperature and pressure. Crystallization conditions estimated by Harris (1974) are 2.5-3.5 kb at 600-650°C. These estimates would

be in the crystallization range of the Winnipeg River pegmatitic granites if no other factors were involved.

A further reduction in the melting point would be caused by Li (Wyllie and Tuttle, 1964) and B (Chorlton and Martin, 1978). Fluorine is also recognized for its role in depressing the granitic solidus by allowing more water to be dissolved in the silicate melt (Bailey, 1977; Wyllie, 1979). The Li, B and F contents of the present rock types are not particularly high, but the mineralogy of the pegmatites surrounding the four pegmatitic granites indicates that the original Li, B and F contents of the melts must have been considerable.

Consequently, with all these factors suppressing the crystallization temperature, the pegmatitic granites of the Winnipeg River area should have formed at temperatures slightly lower than those suggested by the SiO_2-Al_2O_3-K_2O-Na_2O-H_2O system alone. This is in agreement with approximate two-feldspar temperatures of 640 - 600°C suggested by Goad and Černý (1981).

The leucogranite facies is the simplest and most primitive rock type of the four facies of the pegmatitic granites; however, its composition has probably been altered slightly from that of the initial composition of the melt since all facies were derived from the same melt. Following the Jahns and Burnham (1969) model, a partial loss of some of the components of the original melt (e.g. alkalis, SiO_2)

b) The low metamorphic grade in the western portion of the Winnipeg River pegmatitic granite district is insufficient to have caused local "sweating-out" at the level within the greenstone belt where the pegmatitic granites were emplaced.

c) A time gap exists between the end of the period of prograde metamorphism and the beginning of the injection of the pegmatitic intrusions. During this gap large-scale regional faulting occurred.

Most authors discussing the origin of highly fractionated, intrusive leucogranites and pegmatitic granites propose either low percentage partial melting of supracrustal sources, or advanced igneous fractionation.

Anatectic origin has been advocated by Dostal (1975) for the Loon Lake pluton located near Bancroft, Ontario (however this was later refuted by Heaman et al., 1982), Didier and Lameyre (1969) for the granitic rocks of the Massif Central, Dickson (1974) for the Herefoss Granite in southern Norway, and Harris (1974) for leucogranite rocks from the Pyrenees. Hauseux (1977) discusses a leucogranite intrusion in Quebec and proposes an even more extreme metasomatic mode of origin.

Igneous differentiation was suggested for the origin of leucogranites studied by Kolbe and Taylor (1966) in Australia and South Africa, Proctor and El Etr (1968) in Wyoming, Taylor et al. (1968) in Australia, McKenzie and

into fluorine-bearing supercritical fluids would cause a deviation of leucogranite composition from the original composition of the melt.

Despite this proposed deviation, Figure 59 shows that most of the leucogranite compositions appear quite undisturbed, falling into a tight group at the low pressure granitic minima. This group suggests a crystallization pressure range of 0.5-1.0 kb. This represents a depth of 2-4 km which would be a rather shallow estimate of the depth at which the pegmatitic granites consolidated. If crystallization had in fact proceeded at these estimated pressures the pegmatitic granites would have either formed as miarolitic pegmatites with abundant gem quality minerals in cavities or more likely as explosive, highly fractionated ash flows. (Recent fluid inclusion work on TANCO minerals indicates crystallization pressures of 3 kilobars; Černý, written comm. 1984).

D. PETROGENESIS - DERIVATION OF THE PARENTAL MAGMA

Generation of the pegmatitic granites by short range igneous "lateral secretion" (Jahns, 1955) is not possible because of the following observations.

a) No textural features similar to textures in a migmatite terrain suggesting an "in-situ" or "sweating-out" process of these pegmatitic intrusions are evident.

Clark (1975) in Nova Scotia, and Anderson and Cullers (1978) in an anorogenic setting in Wisconsin. All these authors provide sufficient documentation to suggest that granitic differentiation can attain bulk compositions and trace element fractionation levels of the Winnipeg River pegmatitic granites.

Several mechanisms may be suggested for the formation of the Winnipeg River pegmatitic granites that could be fitted into the above categories of anatexis or igneous differentiation. They include:

a) Differentiation of batholithic tonalites and biotite granites exposed in the Bird River greenstone belt.

b) Differentiation from juvenile granitoid melts not exposed on the surface.

c) Partial melting of deep-seated sources being either sialic crust or greenstone belt metasediments/ metavolcanics, and subsequent crystallization.

d) Partial melting of different deep-seated sources (as above), followed by igneous and fluid fractionation.

Igneous differentiation of the batholithic tonalites and/or biotite granites within the Bird River greenstone belt is not suggested by the data in Černý et al. (1981). The most likely source would be the Lac du Bonnet, Maskwa Lake, or Marijane biotite granite; however, the pegmatitic

granites are more highly fractionated than these biotite granites and the trace element and REE distributions in the pegmatitic granites cannot be derived by igneous differentiation from the batholithic rocks. The same applies to any possible relationship to tonalites. (The Osis Lake biotite granite is the only rock type obviously linked to the pegmatitic granites, which has the modal and major element compositional characteristics close to those of the batholithic pegmatitic granites. However, it is significant that its trace element, REE, and $\delta^{18}O$ signatures are substantially different.)

A single stage partial melting process of deep-seated sialic crust has been discussed by several authors (Ewart et al., 1968; Condie et al., 1976) for several rhyolite sequences; however, all these rocks show a high Ce_N/Yb_N ratio in their REE abundances despite their relatively high HREE content. The Winnipeg River pegmatitic granites, however, have lower Ce_N/Yb_N ratios, higher HREE content, and a deeper negative Eu anomaly. The REE abundances of the pegmatitic granites could possibly approach those in the literature only after extensive fractionation of the original melt but this would change the trace element characteristics. Also, the extreme fractionation level of the pegmatitic granites would require extremely low melt percentage, with consequent mechanical problems of melt segregation from vast volumes of the metamorphic parent.

A direct partial melting of the metasediments and metavolcanics of the greenstone belt is impossible since REE data from all greenstone belt lithologies do not agree with that of the pegmatitic granites (Figures 73, 105). According to Arth and Hanson (1975) partial melting of greenstone belt rocks should produce residual plagioclase and hornblende and possibly garnet. This would result in a depletion in HREE and a negligible Eu anomaly in the melt fraction and this is definitely not observed in the pegmatitic granites (Figure 72).

The following two mechanisms conform with the data and as such, are more likely to illustrate the path of formation of the pegmatitic granites:

1. Model A - Partial melting of greenstone belt metasediments and acid metavolcanics followed by igneous and fluid fractionation (differentiated S-type magma).
2. Model B - Igneous and fluid fractionation from a juvenile source modified by interaction with greenstone belt rocks (contaminated I-type magma).

Both of these hypotheses suggest processes that are compatible with constant bulk composition of the pegmatitic granites, erratic accessory mineralogy, erratic trace element content, REE abundances, oxygen isotope ratios, and other data collected during this study.

In Model A the melts would be generated from green-

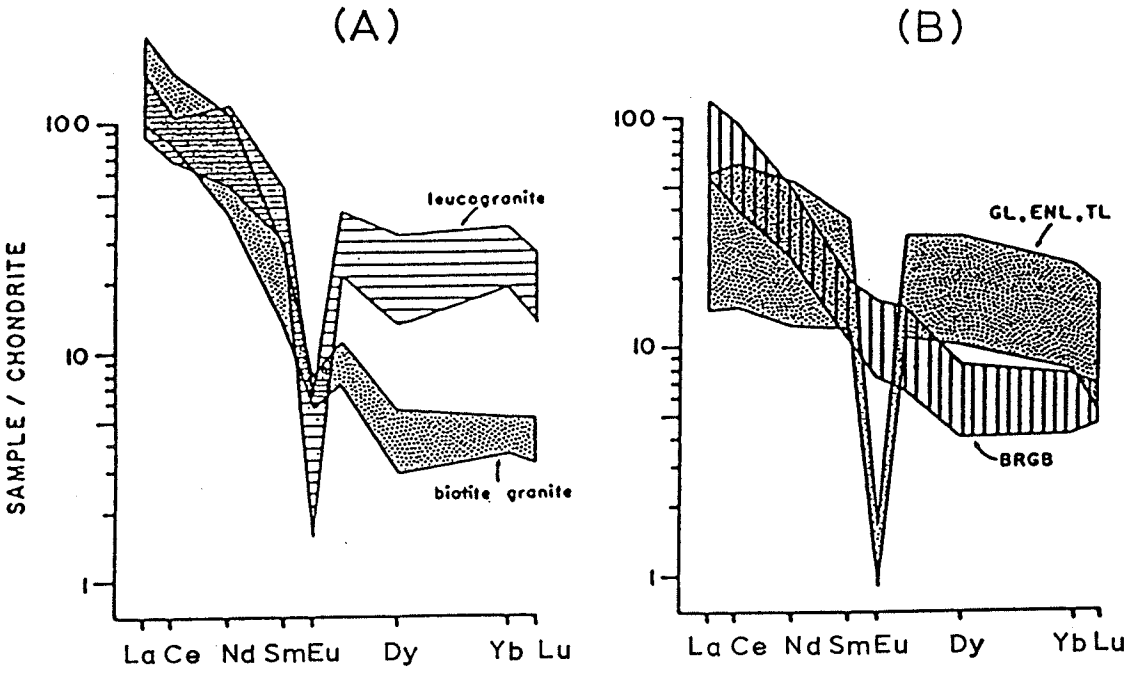

Figure 105. A comparison of the REE data of the early leucogranite, the late biotite granite (both from the Lac du Bonnet batholith, Figure 105-A), the Eaglenest Lake (ENL), Tin Lake (TNL), and Greer Lake (GL) pegmatitic granites and the metaturbidites of the Booster Lake formation of the Bird River greenstone belt (BRGB, Figure 105-B). The abundances suggest that there is no genetic relationship among the rock types within Figures 105-A and B. Data from the OL intrusion is suspected to be contaminated due to assimilation and are not included in Figure 105-B (Goad and Černý, 1981).

stone belt metasediments and/or volcanics. The northern TNL and OL intrusions could be generated at depth, from rocks similar to those which host the intrusions. The southern GL and ENL intrusions could also be derived from metamorphosed equivalents of greenstone belt sediments, mafic volcanics, and rhyolites, but they would have to be modified by reaction with the hosting metabasalts. This model better agrees with the restricted mobility of wet granitic magmas than does model B; however, the apparent rhyolite-leucogranite-pegmatitic suite (discussed below) would have to be dismissed as coincidental.

Model B explains the regional distribution of accessory minerals and the deviation of the minor and trace elements from ideal fractionation trends. Equilibration of juvenile melts with different host rocks explains the variations in oxygen isotopes among the four intrusions. Compositional data suggest a genetic link among the Peterson Creek metarhyolites, the early Lac du Bonnet leucogranite and the pegmatitic granites (Černý et al., 1981). These rocks appear to constitute a fractionation series.

1. Model A

Anatectic melting of specific suitable lithologies within the Bird River greenstone belt (e.g. metapelites and/or metarhyolites) followed by a process of igneous fractionation is a possibility. The REE abundances of the original

melts would be controlled by residual phases and modified by magmatic fractionation. The normative corundum values of the pegmatitic granites of 2 to 5 percent (CIPW) are typical of S-type granites. The oxygen isotope ratios could have been inherited from the parental lithologies in the OL and TNL intrusions; however, alteration of original $\delta^{18}O$ by isotopic exchange with the hosting metabasalts could be responsible for the present results in the southern (GL, ENL) intrusions (Figure 73).

The variations in mineralogy and trace elements between the northern (OL, TNL) and the southern (GL, ENL) groups would be explained by derivation of each group from different source lithologies. The biotite leucogranite plug in the centre of the OL intrusion could represent the magma close in composition to the initial anatectic melt from which the pegmatitic granites fractionated. It is significant that the Osis Lake biotite granite has a geochemical signiture substantially different from those of the diapiric tonalites and batholithic biotite granites.

2. Model B

It is possible that the pegmatitic granites differentiated from juvenile granitoid melts not exposed on the surface. This hypothesis agrees with the compositional characteristics of the pegmatitic granites. A link between the Lac du Bonnet leucogranite and the leucogranite phase of

the pegmatitic granites is suggested by similar geochemistry (Černý et al., 1981). This geochemistry also suggests a similarity of these two granite phases to the metarhyolites of the Peterson Creek formation (Černý et al., 1981). Table 26 is a compilation of the data that collectively illustrates a possible fractionation relationship among the three siliceous and potassic rock types and suggests that they become more fractionated with decreasing age.

REE abundances support the hypothesis of a common source. All phases of the pegmatitic granites have similar REE pattern types as the Lac du Bonnet leucogranite and the Peterson Creek metarhyolites (Černý et al., 1981). These REE patterns are distinctly different from and genetically incompatible with any other granitoids examined in the Winnipeg River pegmatite field (Černý et al., 1981). This type of flat pattern with low Ce_N/Yb_N values is considered typical of differentiation sequences derived from basaltic parents (Ewart et al., 1977; Bruhn et al., 1978).

Within the Winnipeg River pegmatitic granites, overall REE abundances decrease and negative Eu anomaly increases with decreasing K/Rb, K/Cs and other indicators of progressive fractionation. Koljonen and Rosenberg (1974), and Emmerman et al. (1975) recognized a general decrease in REE abundances in the final stages of granitic differentiation. Plagioclase fractionation causes deepening of the negative Eu anomaly, and the co-existing flattening

Table 26. Compositional characteristics of the Peterson Creek formation metarhyolites, Lac du Bonnet leucogranites, and fine-grained leucogranites of the pegmatitic granite intrusion

	Metarhyolites (3 anal.)	Leucogranites (18 anal., 2 intrus.)	Pegm. granites (22 anal., 4 intrus.)
K/Rb	198* (167-254)	190 ±51 (286-113)	117 ±46 (176-75)
K/Cs	27,433 (14,000-38,300)	18,397 ±10,812 (45,375-5,094)	4,798 ±1,645 (6,800-2,823)
K/Ba	142 (65,219)	222 ±221 (27,825)	1,696 ±2,480 (279-5,402)
Rb/Sr	10.2 (18.7-2.2)	17.3 ±42.2 (185-2.76)	25.4 ±21.5 (52.8-6)
Ca/Sr	19.9 (1.9-33.3)	139.1 ±49.1 (86-280)	147.6 ±50.2 (103.7-204.7)
Mg/Li	50.4 (100-11.2)	27.6 ±18.5 (66.7-2.9)	17.7 ±20.8 (48.6-6)
Al/Ga	7,024 (11,920-2,128)	2,156 ±333 (2,764-1,568)	1,695 ±466 (2,351-1,258)
Zr/Hf	22.9 (20-26.7)	27.5 ±5.8 (18.3-34.3)	34 ±10 (24.3-48.3)
Th/U**	4.2	2.6	0.4

* Arithmetic mean, ± 1σ, (range)

** ratios of average Th and U contents

of the REE pattern (i.e. LREE are depleted faster than the HREE) suggests residual biotite and apatite (Puchelt and Emmerman, 1976; Hanson, 1978). The abundances of these two minerals decreases in the pegmatitic granite intrusions simultaneously with decreasing total REE abundance.

Assuming a juvenile origin of the pegmatitic granites, other lines of compositional evidence which appear slightly contradictory can be accommodated by the highly probable possibility of melt contamination during its ascent through the greenstone belt. Longstaffe et al. (1981) explain variances in the oxygen isotope values of the four pegmatitic granites as a result of a thorough equilibration of the intrusions with the host metasediments in the Osis Lake and Tin Lake intrusions, and a lesser degree of equilibration of the southern Greer Lake and Eaglenest Lake intrusions with the hosting metabasalts.

Evidence of intense assimilation and hybridization of original melts is visible in the Osis Lake, and to a lesser extent, the Tin Lake intrusion. These two intrusions exhibit boron and phosphorus concentrations elevated over the southern intrusions. The Osis Lake intrusion has the highest B and P concentrations and it is also located closest to the phosphorus-enriched and tourmaline (boron)-bearing conglomerate of the Flanders Lake formation. Both the TNL and OL intrusions intrude into the phosphorus-rich metapelites of the Booster Lake formation (Černý et al., 1981).

Hybridization and a loss of alkalis to the country rock through a fluid phase would account for at least some of the corundum-normative compositions. However, peraluminous chemistry is not specific for S-type granites alone but can be generated by hornblende fractionation in sequences that are diopside-normative in their pre-granitic members (Cawthorn and Brown, 1976).

As shown above, both A and B models are qualitatively possible and seem to be equally applicable to the examined pegmatitic granites. However, there are several factors that have obviously influenced the chemistry and the course of crystallization of these rocks, which are so far beyond the reach of experimental modelling and prevent application of straight-forward crystal/melt processes.

The predominantly pegmatitic character of the intrusions suggests large volumes of volatiles and separation of a supercritical fluid early during crystallization. Water undoubtedly predominated, but fluorine, boron and phosphorus have also played a major role in at least some of the four intrusions.

The peraluminous nature of the pegmatitic granites apparently has been enhanced by a loss of alkalis through a vapour phase to the host rock. The coarse-grained facies of the pegmatitic granites (i.e. the pegmatitic leucogranite and the potassic pegmatite) in all four intrusions are the more peraluminous phases. Of the four intrusions, the Osis

Lake intrusion, which shows the most conspicuous exocontact effects, is the most peraluminous intrusion as a whole.

Crystal-melt fractionation by itself cannot be solely responsible for the high enrichment in Li, Rb, Cs, Be, Ga, Sn, and depletion in Ba and Sr when compared to the relative uniformity of the bulk rock compositions of the leucogranites and pegmatitic leucogranites of all four intrusions. This process could have been supplemented by liquid state differentiation, depolymerization (effective in volatile-saturated melts) and enrichment of apical parts of each intrusion in rare elements and HREE, transported as complex ions (Mahood, 1979; Crecraft et al., 1979; Miller and Mittlefehldt, 1979; Muecke and Clarke, 1981).

The above discussion of two models and three complicating factors demonstrates that the origin of the Winnipeg River pegmatitic granites cannot be solved with any certainty. The partial melting of greenstone belt metasediments modified by igneous fractionation (model A) agrees with the other studies of pegmatitic granites in the English River subprovince in Ontario (Breaks et al., 1978) and also in the Yellowknife area of the North West Territories (Drury, 1979).

Alternately, the petrochemical similarity of the three potassic suites in the area of the pegmatitic granites (i.e. the pegmatitic leucogranites, the Lac du Bonnet leucogranite and the Peterson Creek metarhyolites) is

striking. An anatectic or igneous juvenile source with subsequent hybridization in the greenstone belt (model B) fits the available data. However, a long-term survival of a differentiating igneous reservoir during the diapiric rise of tonalitic domes (which separates the metarhyolite extrusive from the intrusion of leucogranites) is questionable. Thus model A seems to be more compatible with the regional geologic evolution.

E. RELATIONSHIP TO THE ADJACENT PEGMATITES

Each intrusion of pegmatitic granite is flanked or partly surrounded by, a swarm of pegmatitic dikes (Figure 106). In addition to a close spatial relationship, several other features common to the individual pegmatitic granites and their adjacent pegmatite aureole suggest a common link.

a) A common accessory mineral assemblage can be observed (Table 27).

b) Bands and schlieren of mineralized potassic pegmatite facies that occur within the pegmatitic granite display similar zonal sequences and textural relationships to individual intrusions in adjacent pegmatite swarms. This is particularly true in the Greer Lake intrusions where the pegmatitic granite is becoming progressively enriched, mineralogically and chemically, as illustrated through a sequence of locations: GL-4, AC-1, AC-2, AC-3 to final enrichment

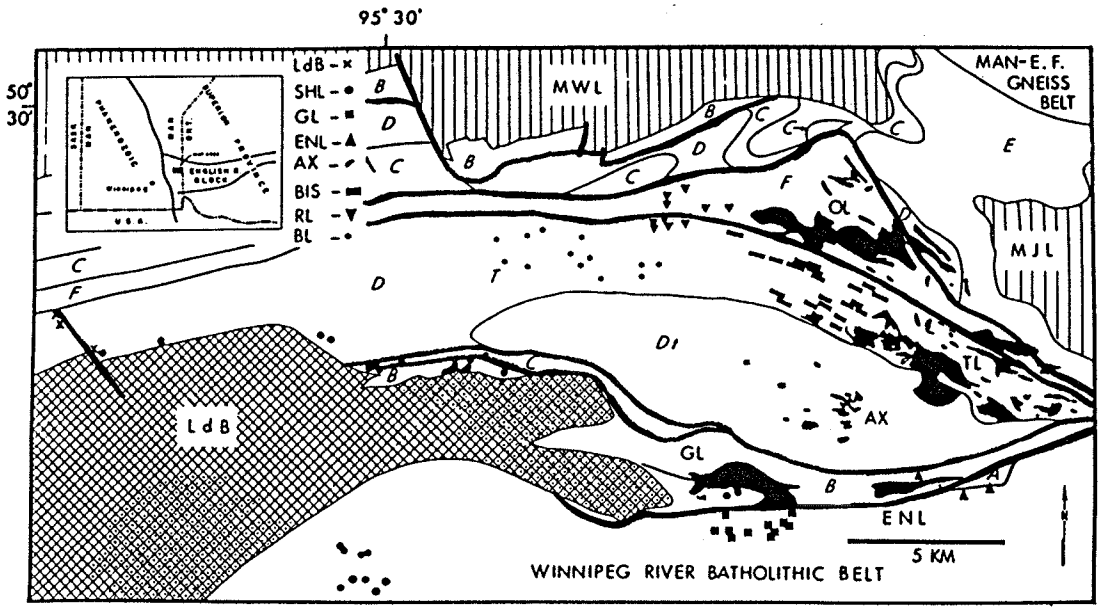

Figure 106. Location map (insert) and geological sketch of the Winnipeg River pegmatite district. (1) unsubdivided gneisses of the Winnipeg River batholithic belt and the Manigotagan - Ear Falls gneiss belt, and the schists of the Bird River greenstone belt: A Eaglenest formation, B Lamprey Falls formation, C Peterson Creek formation, D Bernic Lake formation, Dt subvolcanic tonalite, E Flanders Lake formation, F Booster Lake formation; (2) composite diapiric batholiths (MWL Maskwa Lake intrusion, MJL Marijane Lake intrusion); (3) early leucogranite and (4) late biotite granite of the Lac du Bonnet (LdB) batholith; (5) pegmatitic granites (GL Greer Lake, ENL Eaglenest Lake, AX Axial, TL Tin Lake, and OL Osis Lake intrusions); pegmatite groups: LdB Lac du Bonnet, SHL Shatford Lake, GL Greer Lake, BIS Birse Lake, RL Rush Lake, ENL Eaglenest Lake, AX Axial, BL Bernic Lake; T the Tanco pegmatite; heavy lines represent faults, light lines, lithological boundaries. (Goad and Černy, 1981).

1 

2 

3 

4 

5 

Table 27. Correlation of accessory mineral content and
of parent intrusions and their pegmatitic aur

Parent intrusion				
Typical accessory minerals	Local mineralization	Avg. whole rock K/Rb,K/Cs Mg/Li		Typical min
LAC DU BONNET LEUCOGRANITE(LdB)				
zircon, allanite, monazite, ((garnet))	((Be))	190; 28	18,400	beryl, garn monazite, z uraninite, euxenite, y gadolinite,
TIN LAKE PEGMATITIC GRANITE(TL)				
garnet((tourmaline))	((Mo))	176; 49	6,800	tourmaline,
GREER LAKE PEGMATITIC GRANITE(GL)				
garnet, cordierite, (gahnite, beryl) ((columbite-tantalite, monazite))	Be,Nb,Ta(Li,Rb, Cs,Zn)	87; 4.7	5,110	garnet, cor columbite-t monazite, z ((Li-micas)
EAGLENEST LAKE PEGMATITIC GRANITE(ENL)				
garnet		75; 6	4,460	garnet, ber
OSIS LAKE PEGMATITIC GRANITE(OL)				
garnet, tourmaline apatite, (triphylite, arsenopyrite)	(Li,P,As)	131; 11.5	2,800	tourmaline, petalite, an lite, (Nb,Ta cassiterite, ((polucite))
(unexposed; presumed pegmatitic granite)				tourmaline, (spodumene, lite, polluc Nb,Ta-oxide triphylite

( ) subordinate; (( )) rare.

cal characteristics

ated pegmatites

	Rare-element association	Avg. K/Rb,Cs (ppm) in blocky K-feldspars	
LAKE GROUP(SHL) lanite, e, talite, ,	Be,Nb-Ta,Sn, REE,Y,U,Th, Zr-Hf	66;	61
LAKE GROUP(BIS)	Be((Li,Nb-Ta))	119;	52
LAKE GROUP(GL) l, nite, erite)	Be,Nb,Ta (Sn,Zn)((Li))	42;	250
T LAKE GROUP(ENL)	Be	38;	53
LAKE GROUP(RL) mene, riphy- als	Li,Rb,(Cs),Be, Sn,Nb,Ta,F,B,P	50;	265
LAKE GROUP(BL) ite lepido- rite, blygonite,	Li,Rb,Cs,Be Sn,Nb,Ta,F,B,P.	9.5;	1262

at the Silverleaf pegmatitic intrusion. These Li, Rb, Cs, Be, Nb, Ta, and F-rich pegmatitic nodules that represent local, gradual evolution of potassic pegmatitic facies in the GL pegmatitic granite could be petrologic and paragenetic analogs to the most complexly zoned and mineralized pegmatite types in the area - the Rush Lake and Bernic Lake groups of Černý et al. (1981). Similarly the TNL intrusion is transitional into the Birse Lake pegmatite group in such a gradual manner that only an arbitrary boundary can be defined between the fingering out of the pegmatitic granite into the Birse Lake pegmatite group. This gradual change in form is accompanied by an equally gradual change in mineralogy. As the Birse Lake pegmatite group is approached, the beryl, tourmaline, and rose quartz content of the Tin Lake pegmatitic granite increases. These types of zonation characteristics are not as apparent, but they do exist in the remaining two pegmatitic granites and associated pegmatite swarms.

c) The most significant data that strongly suggests the existence of petrogenetic links between pegmatitic granites and their adjacent pegmatite swarms is the geochemistry. Gross chemical differences existing among intrusions of pegmatitic granites do not exist between individual intrusions of pegmatitic granite

(and specifically, their potassic pegmatite facies) and associated pegmatite swarms. For example, the pegmatitic granites south of the Winnipeg River (ENL, GL) carry extremely low amounts of boron and phosphorus-bearing minerals as do their respective pegmatite aureoles; however, north of the river these elements are enriched in the TNL and OL intrusions and this enrichment is also reflected in the abundance of tourmaline and phosphate-bearing minerals (apatite, triphylite, ferrisicklerite) in the adjacent pegmatite groups.

Plots of elements sensitive to fractionation (e.g. K/Rb, K/Cs, etc.) from rock-forming minerals (muscovite, potassium feldspar) in pegmatitic granites (this study) and the adjacent pegmatites (Černý et al., 1981) indicate a continuous common fractionation relationship (Figures 107-109). Rough parallelism in average geochemical characteristics of the pegmatitic granites and adjacent pegmatite swarms is summarized in Table 27.

Two pegmatite groups in Figure 108 appear to have no exposed source. The Lac du Bonnet group (Černý et al., 1981) located along the northern contact of the Lac du Bonnet batholith contains primary zonal spodumene and is injected into shear fractures along a late fault which displaces the margin of the late biotite-granite phase of the Lac du Bonnet batholith (Černý et al., 1981) and adjacent metasediments.

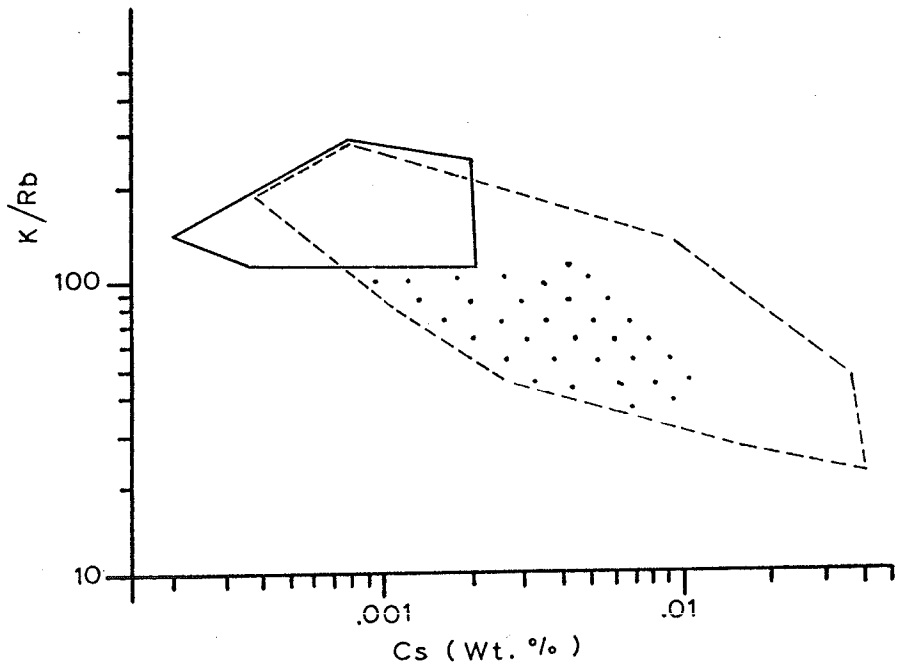

Figure 107. K/Rb vs. Cs values in blocky K-feldspar from the Tin Lake intrusion of pegmatitic granite (——) and the adjacent Birse Lake pegmatite group (---). The Li and Nb,Ta-bearing members of this group fall in the area illustrated by the dots.

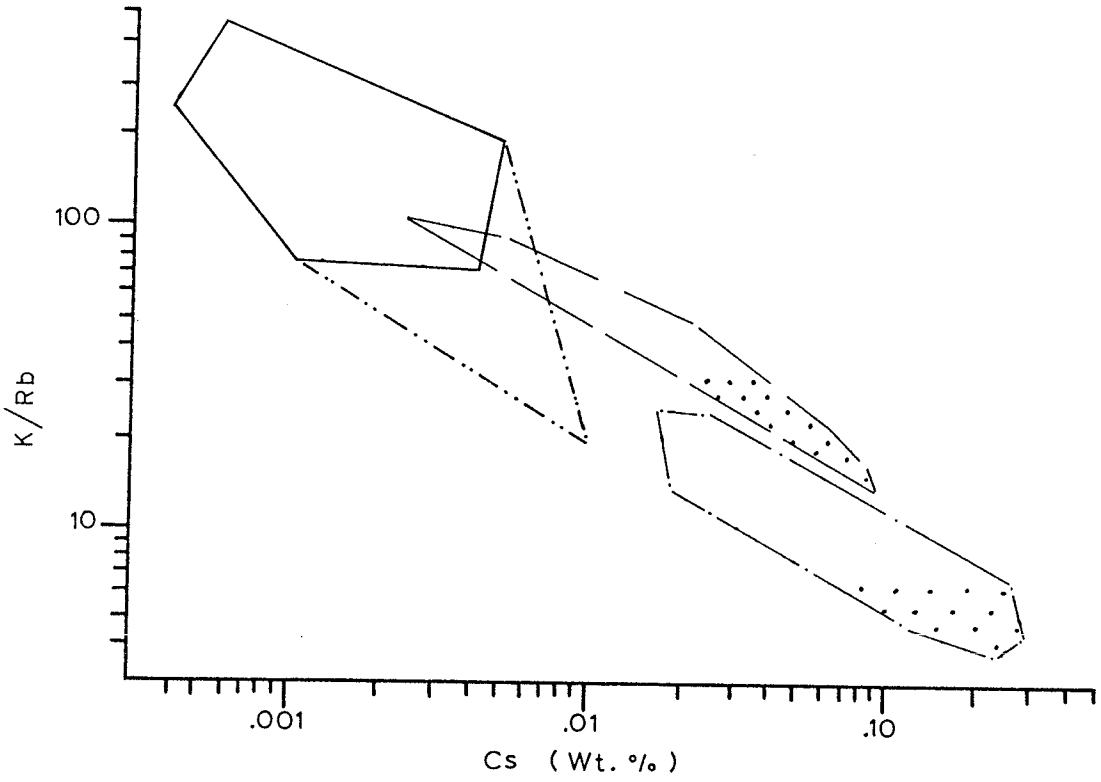

Figure 108. K/Rb vs. Cs values in blocky K-feldspar from the potassic pegmatite facies of the Osis Lake intrusion of pegmatitic granite (——). (-·-·-) is the extension of the Osis Lake field to cover a lone sample which has an anomalously low K/Rb value and a high Cs value (Figure 81). The Rush Lake pegmatite group (— —) and the Bernic Lake pegmatite group (-·-·) are also indicated. The Li-bearing members of the Rush Lake group are indicated by the dotted area. The TANCO pegmatite is the most mineralogically enriched member of the Bernic Lake pegmatite group.

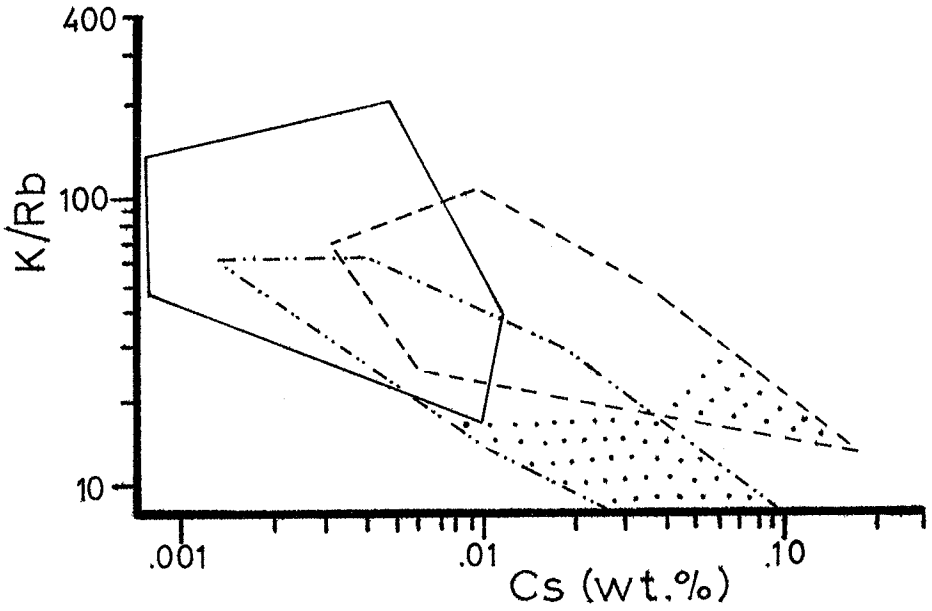

Figure 109. K/Rb vs. Cs values in blocky K-feldspar from the potassic pegmatite facies of the main body of the Greer Lake pegmatitic granite (——). The internal mineralized pods of potassic pegmatite located mostly along the southern margin (mineralized pods) including the Silverleaf Claim are marked by (-·-·-). The field of the Greer Lake pegmatite group is marked by (----). Samples from the Li-bearing (Li micas, amblygonite, lithiophylite etc.) areas are marked by the dotted zones.

The Bernic Lake pegmatite group is the other swarm with no apparent source. It is the most fractionated, complex, mineralogically diversified, and economically important group known in the Bird River greenstone belt. The TANCO pegmatite (Crouse et al., 1979) is included in this group. This group is not included as a western extension of the Osis Lake pegmatitic granite and the adjacent Rush Lake pegmatites for two main reasons. The distance spanned between the Osis Lake pegmatitic granite in the east to the TANCO pegmatite at the western extremity (approximately 8 km) is greater than the 2 km distance (Beus et al., 1968) established as an empirical maximum between parental granites and derived pegmatites. In addition, the geochemistry of the feldspars in Figure 108 suggests a parallel, but not continuous, fractionation in the Rush Lake and Bernic Lake groups.

Speculation by Černý et al. (1981) suggests that a pegmatitic granite source hidden beneath the central parts of the area occupied by the Bernic Lake pegmatites is indicated by the directions of lateral fractionation trends within individual pegmatite dikes. Such a hypothetical source would fit the extreme fractionation and enrichment in rare elements attained by this group: in an idealized 3-dimensional pegmatite aureole flanking and topping its parental intrusion extreme enrichment in volatile components and associated rare elements should be expected in its

uppermost part. A pegmatitic granite of the Greer Lake type may be envisaged as a parental intrusion. The Silverleaf and Annie Claim pods in the Greer Lake intrusion are not as fractionated as the Bernic Lake pegmatite group but they exhibit the same low pressure assemblage (petalite as the primary Li-aluminosilicate) and similar paragenesis.

REFERENCES

Ahrens, L.H., Pinson, W.H., and Kearns, M.M.
1952 Association of Rb and K and their abundance in common igneous rocks and meteorites. Geochimica et Cosmochimica Acta, v. 2, p. 229-242.

Albuquerque, C.A.R. de,
1971 Petrochemistry of a series of granitic rocks from northern Portugal. Geological Society of America Bulletin, v. 82, p. 2783-2798.

Anderson, J.L. and Cullers, R.L.
1978 Geochemistry and evolution of the Wolf River batholith, a late Precambrian rapakavi massif in north Wisconsin, U.S.A. Precambrian Research, v. 7, p. 287-324.

Appleman, D.E. and Evans, H.T. Jr.
1973 Job 9214. Indexing and least-squares refinement of powder diffraction data. United States Geological Survey Comp. Contra., v. 20.

Arth, J.G. and Hanson, G.N.
1975 Geochemistry and origin of the early Precambrian crust of north-eastern Minnesota. Geochimica et Cosmochimica Acta, v. 39, p. 325-362.

Bailey, J.C.
1977 Fluorine in granitic rocks and melts, A review. Chemical Geology, v. 19, p. 1-42.

Barth, T.F.W.
1959 Principles of classification and norm calculations of metamorphic rocks. Journal of Geology, v. 67, p. 135-152.

1962 A final proposal for calculating the mesonorm of metamorphic rocks. Journal of Geology, v. 70, p. 497-498.

1966 Aspects of the crystallization of quartzo-feldspathic plutonic rocks. Tschmaks Mineral. und Petrog., v. 11, p. 209-222.

Bateman, J.D.
1943 Tin in Manitoba. Canadian Mining Journal, v. 64, p. 273-278.

Beakhouse, G.P.
1977 A subdivision of the Western English River subprovince. Canadian Journal of Earth Sciences, v. 14, p. 1481-1489.

Beus, A.A.
1961 Acid-alkali conditions in metasomatism as a factor in the transportation and concentration of rare elements, Fiz.-Khem. Problemy Formweovan Goin. Porod. i Rud. Akad. Nauk S.S.S.R., Inst. Geol. Rudnykh Mestorozhden. Petrograd. Mineral. Geokhem., v. 1, p. 149-160 (in Russian).

Beus, A.A., Berengilova, V.V., Grabovskaya, L.I., Kotchemasov, G.G., Leontyeva, L.A., and Sitnin, A.A.
1968 Geochemical exploration for endogenic deposits of rare elements: on the example of tantalum. Nedra, Moscow. (English translation, Geological Survey of Canada, Library, Ottawa) 263 p.

Breaks, F.W., Bond, W.D., and Stone, D.
1978 Preliminary geological synthesis of the English River subprovince, northwestern Ontario and its bearing upon mineral exploration. Ontario Geological Survey, Miscellaneous Paper 72, 55 p.

Bruhn, R.L., Stern, C.R., and DeWitt, M.J.
1978 Field and geochemical data bearing on the development of a mesozoic volcano-tectonic rift zone and back-arc basin in southernmost South America. Earth and Planetary Science Letters, v. 14, p. 32-46.

Castle, R.O. and Theodore, T.G.
1972 Some genetic implications of the phase composition of a simple New England pegmatite. United States Geological Survey, Professional Paper 800B, p. B105-B117.

Cawthorn, R.G. and Brown, P.A.
1976 A model for the formation and crystallization of corundum-normative calc-alkaline magmas through amphibolite fractionation. Journal of Geology, v. 84, p. 467-476.

Černá, I., Černý, P., and Ferguson, R.B.
1973 The fluorine content and some physical properties of the amblygonite-montebrasite minerals. American Mineralogist, v. 58, p. 291-301.

Černý, P. and Ferguson, R.B.
1972 The TANCO pegmatite at Bernic Lake, Manitoba. IV Petalite and spodumene relations. Canadian Mineralogist, v. 11, p. 660-678.

Černý, P. and Hawthorne, F.C.
1976 Refractive indices versus alkali content in beryl: general limitations and applications to some pegmatite types. Canadian Mineralogist, v. 14, p. 491-497.

Černý, P. and Simpson, F.M.
1977 The TANCO pegmatite at Bernic Lake, Manitoba. IX, Beryl. Canadian Mineralogist, v. 15, p. 489-499.

Černý, P. and Trueman, D.L.
1977 Petrogenesis of pegmatites in the Cat Lake-Winnipeg River area. Centre for Precambrian Studies, University of Manitoba. Annual Report, 1976, p. 26-32.

1978 The distribution and petrogenesis of lithium pegmatites in the Western Archean of Canada. Energy. v. 3, p. 365-377.

Černý, P., Trueman, D.L., Zielke, D.V., Goad, B.E., and Paul, B.J.
1981 The Cat Lake-Winnipeg River and the Wekusko Lake pegmatitic fields, Manitoba. Manitoba Mineral Resources Division Geology Report ER80-1, 205 p.

Černý, P. and Turnock, A.C.
1971 Pegmatites of southeastern Manitoba. Geological Association of Canada, Special Paper 9, p. 119-127.

Chappell, B.W. and White, A.J.R.
1974 Two contrasting granite types. Pacific Geology, v. 8, p. 173-174.

Chorlton, L.D. and Martin, R.F.
1978 The effect of boron on the granite solidus. Canadian Mineralogist, v. 16, p. 239-244.

Chou, C. L., Hamud, A.J., Harris, N.B.W. and Goodwin, A.M.
1977 Geochemistry and origin of the eastern Lac Seul area, English River gneiss belt. Proceedings of the Geotraverse Conference, University of Toronto 1977, p. 80-93.

Clayton, R.N. and Mayeda, T.D.
1963 The use of bromine pentafluoride in the extraction of oxygen from oxides and silicates for isotopic analysis. Geochimica et Cosmochimica Acta, v. 27, p. 43-52.

Condie, K.C.
1976 Trace-element models for the origin of Archean volcanic rocks. in: The Early History of the Earth, ed. B.F. Windley, 1976, Wiley and Sons, New York, p. 419-426.

Cooke, H.C.
1922 Geology and mineral resources of the Rice Lake and Oiseau River areas, Manitoba. Geological Survey of Canada, Summary Report 1921, Part C, p. 120-142.

Crecraft, H.R., Nash, W.P., and Evans, S.H. Jr.
1979 Chemical evolution and development of compositional gradients in a silicic magma. G.S.A.-M.S.A. Annual Meeting, San Diego, 452 p.

Crouse, R.A., Černý, P. Trueman, D.L., and Burt, R.O.
1979 The TANCO pegmatite, southeastern Manitoba. Canadian Institute of Mining and Metallurgy Bulletin, 1979, No. 2, p. 1-10.

Cummings, G.L., Wilson, J.T., Farquhar, R.M., and Russell, R.D.
1955 Some dates and subdivisions of the Canadian Shield. Proceedings of the Geological Association of Canada, v. 7, Part 2.

Davies, J.F.
1952 Geology of the Oiseau (Bird) River area, Lac du Bonnet Mining Division. Manitoba Mines Branch. Publication 51-3, 24 p.

1954 Geology of the West Hawk Lake-Falcon Lake area, Lac du Bonnet Mining Division. Manitoba Mines Branch, Publication 53-4, 28 p.

1955 Geology and mineral deposits of the Bird Lake area. Manitoba Mines Branch, Publication 54-1, 44 p.

1956a Manitoba lithium deposits. Canadian Mining Journal, v. 77, April No. 4, 78-79.

1956b Geology of the Booster Lake area, Lac du Bonnet Mining Division. Manitoba Mines Branch, Publication 55-1, 15 p.

1957 Geology of the Winnipeg River area (Shatford Lake-Ryerson Lake), Lac du Bonnet Mining Division, Manitoba. Manitoba Mines Branch, Publication 56-1, 27 p.

1958 The lithium and beryllium pegmatites of south-eastern Manitoba. Canadian Institute of Mining and Metallurgy Transactions. v. 61, p. 230-236.

Davies, J.F., Bannatyne, B.B., Barry, G.S., and McCabe, H.R.
1962 Geology and mineral resources of Manitoba. Manitoba Mines Branch, 190 p.

De Lury, J.S.
1926 Pegmatites of southeastern Manitoba. Canadian Mining Journal, v. 47, p. 695-697.

1930 Beryl in Manitoba. Canadian Mining Journal, v. 51, p. 1017.

De Lury, J.S. and Ellsworth, H.V.
1931 Uraninite from the Huron Claim, Winnipeg River area, southeastern Manitoba. American Mineralogist v. 12, p. 569-575.

Derry, D.R.
1931 The genetic relationships of pegmatites, aplites, and tin veins. Geological Magazine, v. 68, p. 454-475.

Dickson, W.L.
1974 General geology and geochemistry of the granitoid rocks of the northern Gander Lake belt, Newfoundland. Unpublished M.Sc. thesis, Memorial University of Newfoundland, St. John's, 122 p.

Didier, J. and Lameyre, T.
1969 Les granites du Massif Central francais: etude comparee des leucogranites et granodiorites. Contributions to Mineralogy and Petrology, v. 24, p. 219-238.

Dostal, T.
1975 The origin of garnet-cordierite-sillimanite-bearing rocks from Chandos Township, Ontario. Contributions to Mineralogy and Petrology, v. 49, p. 163-175.

Drury, S.A.
1979 Rare-earth and other trace element data bearing on the origin of Archaean granitic rocks from Yellowknife, Northwest Territories. Canadian Journal of Earth Sciences, v. 16, p. 809-815.

Eckelmann, F.D., Long, L.E., and Olsen, E.A.
1958 Origin and occurrence of extensively developed layered structures in leucogranite-granite pegmatite, Huron Claim, Johnston Lake areas, southeast Manitoba, Canada. G.S.A.-M.S.A. Annual Meeting, Program and Abstracts, p. 48.

El Bouseily, A.M. and El Sokkary, A.A.
1975 The relation between Rb, Ba and Sr in granitic rocks. Chemical Geology, v. 16, p. 207-219.

Ellsworth, H.V.
1932 Rare-element minerals of Canada. Canadian Department of Mines, Geological Survey, Economic Geology Series 11, 272 p.

Emmerman, R., Daieva, L., and Schneider, J.
1975 Petrologic significance of rare earths distribution in granites. Contributions to Mineralogy and Petrology, v. 52, p. 267-283.

Evans, H.T. Jr., Appleman, D.E., and Handwerker, S.S.
1963 The least-squares refinement of crystal unit cells with powder diffraction data by an automatic computer indexing method. Program and Abstracts, American Crystallographic Association Meeting, Cambridge, Mass., 42 p.

Ewart, A., Mateen, A., and Ross, J.A.
1976 Review of mineralogy and chemistry of Tertiary central volcanic complexes in southeast Queensland and northeast New South Wales. in: Volcanism in Australia, ed. R.W. Johnston, Elsevier, Amsterdam.

Ewart, A., Oversby, V.M., and Mateen, A.
1977 Petrology and isotopic geochemistry of Tertiary lavas from the northern flank of the Tweed volcano-southeastern Queensland. Journal of Petrology, v. 18, p. 73-113.

Farquharson, R.B.
1975 Revised Rb-Sr age of the Lac du Bonnet quartz monzonite, southeastern Manitoba. Canadian Journal of Earth Sciences, v. 12, p. 115-118.

Farquharson, R.B. and Clark, G.S.
1971 Rb-Sr geochronology of some granitic rocks in southeastern Manitoba. Geological Association of Canada. Special Paper 9, p. 111-117.

Foord, E.E.
1976 Mineralogy and petrogenesis of layered pegmatite-aplite dikes in the Mesa Grande district, San Diego County, California. Unpublished Ph.D. dissertation, Stanford University, 326 p.

1982 Minerals of tin, titanium, niobium, and tantalum in granitic pegmatites. Mineralogical Association of Canada Short Course Handbook, 1982, p. 187-238.

Frondel, C.
1962 Dana's system of mineralogy. 7th edition, Silica Minerals, Wiley and Sons. New York, v. 3.

Frost, I.C.
1959 An elutriation tube for the specific gravity separation of minerals. American Mineralogist, v. 44, p. 886-890.

Fryer, B.J. and Jenner, G.A.
1978 Geochemistry and origin of the Archean Prince Albert group volcanics, western Melville Penninsula, Northwest Territories. Geochimica et Cosmochimica Acta, v. 42, p. 1645-1654.

Goad, B.E. and Černý, P.
1981 Peraluminous pegmatitic granites and their pegmatite aureoles in the Winnipeg River district, southeastern Manitoba. Canadian Mineralogist, v. 19, p. 177-194.

Gouder de Beauregard, C., Dubois, J., and Bourguigon, P.
1967 Comportement thermique des columbo-tantalites. Ann. Soc. Geol. Belgique, v. 90, p. 8501-8518.

Hancock, R.G.V.
1976 Low flux multielement instrumental neutron activation analysis in archaeometry. Analytical Chemistry. v. 48, p. 1443-1445.

Hanson, G.N.
1978 The application of trace elements to the petrogenesis of igneous rocks of granitic composition. in: Trace Elements in Igneous Petrology, ed. C.J. Alligre and S.R. Hart, Developments in Petrology, v. 5. Esevier, p. 26-43.

Harris, N.B.W.
1974 The petrology and petrogenesis of some msucovite granite sills from the Barousse massif, Central Pyrenees. Contributions to Mineralogy and Petrology, v. 45, p. 215-230.

Hauseux, M.A.
1977 Mode of uranium occurrence in a migmatitic granite terrain, Baie Johan Beetz, Quebec. Canadian Institute of Mining and Metallurgy, v. 70, p. 110-116.

Heaman, L.M.
1982 Isotropic and trace element study of the Loon Lake pluton, Grenville Province, Ontario. Canadian Journal of Earth Sciences, v. 19, p. 1045-1054.

Heier, K.S. and Taylor, S.R.
1959a Distribution of Li, Na, K, Rb, Cs, Pb, and Tl in southern Norweigan pre-Cambrian alkali feldspars. Geochimica et Cosmochimica Acta, v. 15, p. 284-304.

1959b Distribution of Ca, Sr, and Ba in southern Norweigan pre-Cambrian alkali feldspars. Geochimica et Cosmochimica Acta, v. 17, p. 286-304.

Jahns, R.H.
1955 The study of pegmatites. Economic Geology, v. 50, p. 1025-1130.

Jahns, R.H. and Burnham, C.W.
1969 Experimental studies of pegmatite genesis: I. A model for the derivation and crystallization of granitic pegmatites. Economic Geology, v. 64, p. 843-864.

Janes, D.A.
in prep. Southeastern Manitoba. Manitoba Mineral Resources Division, Geological Report.

Kleeman, A.W.
1965 The origin of granitic magmas. Journal of the Geological Society of Australia, v. 12, p. 35-52.

Kolbe, P. and Taylor, S.R.
1966 Major and trace element relationships in granodiorites and granites from Australia and South Africa. Contributions to Mineralogy and Petrology, v. 12, p. 202-222.

Koljonen, T. and Rosenberg, R.J.
1974 Rare earth elements in granitic rocks. Lithos, v. 7, p. 249-261.

Komkov, A.I.
1970 Relationship between the X-ray constants of columbites and composition. Doklady of the Academy of Sciences, Union of Soviet Socialistic Republics, v. 195, p. 434-436.

Longstaffe, F.J., Černý, P., and Muehlenbachs, K.
1981 Oxygen isotope geochemistry of the granitoid rocks in the Winnipeg River pegmatite district, southeastern Manitoba. Canadian Mineralogist, v. 19, p. 195-204.

Mackie, B.W.
1978 Petrogenesis of the Lac Turgeon granite and uranium occurrences near Baie Johan Beetz, Quebec. Unpublished M.Sc. thesis, Department of Earth Sciences, University of Manitoba, Winnipeg, 84 p.

Mahood, G.
1979 Contrasting trace element behavior in rhyolitic ash flows and lavas, Sierra da Primavera (SLP), Mexico. Geological Society of America, Abstract and Programs, v. 11, p. 471.

Masuda, A.
1975 Abundances of monoisotopic REE, consistent with the Leedey chondrite values. Geochemical Journal, v. 9, p. 183-184.

Madusa, A., Nakamura, N., and Tanaka, T.
1973 Fine structure of mutually normalized rare-earth patterns of chondrites. Geochimica et Cosmochimica Acta, v. 37, p. 239-248.

McKenzie, C.B. and Clarke, D.B.
1975 Petrology of the South Mountain batholith. Canadian Journal of Earth Sciences, v. 12, p. 1209-1218.

McRitchie, W.D.
1971 The petrology and environment of the acidic plutonic rocks of the Wanipigow-Winnipeg Rivers region, southeastern Manitoba. Manitoba Mines Branch, Publication 71-1, Report 2, p. 7-61.

Miller, C.F. and Mittlefehldt, D.W.
1979 Rare earth element depletion accompanying differentiation of felsic plutonic rocks. G.S.A.-M.S.A. Annual Meeting, San Diego, 1979, p. 479-480.

Moore, E.S.
1913 Region east of the south end of Lake Winnipeg. Geological Survey of Canada, Summary Report 1912, p. 78-81.

Muecke, G.K. and Clarke, D.B.
1981 Geochemical evolution of the South Mountain batholith, Nova Scotia: rare earth element evidence. Canadian Mineralogist, v. 19, p. 133-145.

Mulligan, R.
1957 Lithium deposits of Manitoba, Ontario, and Quebec, 1956. Geological Survey of Canada, Paper 57-3, 26 p.

1961 Pollucite (caesium) in Canada. Geological Survey of Canada, Paper 61-4, 4 p.

1965 Geology of Canadian lithium deposits. Geological Survey of Canada, Economic Geology Report 21, 131 p.

1968 Geology of Canadian beryllium occurrences. Geological Survey of Canada, Economic Geology Report 23, 109 p.

1975 Geology of Canadian tin occurrences. Geological Survey of Canada, Economic Report 28, 155 p.

Nickel, E.H., Rowland, J.F., and McAdam, R.C.
1963 Wodginite - a new tin-manganese tantalite from Wodgina, Australia, and Bernic Lake, Manitoba. Canadian Mineralogist, v. 7, p. 390-402.

Nockolds, S.R. and Allen, R.
1953 The geochemistry of some igneous rock series. Geochimica et Cosmochimica Acta, v. 4, p. 105-142.

Nuffield, E.W.
1966 X-ray diffraction methods. Wiley and Sons, New York.

Orville, P.M.
1960 Petrology of several pegmatites in the Keystone district, Black Hills, South Dakota. Geological Society of America Bulletin, v. 71, p. 1467-1490.

1967 Unit cell parameters of the microcline-low albite and the sanidine-high albite solid solution series. American Mineralogist, v. 52, p. 55-86.

Paul, B.J.
in prep. Mineralogy, geochemistry, and petrology of the Huron Claim pegmatite, southeastern Manitoba. Department of Earth Sciences, University of Manitoba, M.Sc. thesis.

Penner, A.P. and Clark, G.S.
1971 Rb-Sr age determinations from the Bird River area southeastern Manitoba. in: Geoscience Studies in Manitoba, ed. A.C. Turnock, Geological Association of Canada, Special Paper 9, p. 105-109.

Proctor, P.D. and El-Etr, H.A.
1968 Layered pegmatites, southern Wind River Mountains, Fremont County, Wyoming. Economic Geology, v. 63, p. 595-611.

Puchelt, H. and Emmermann, R.
1976 Bearing of rare earth patterns of apatites from igneous and metamorphic rocks. Earth and Planetary Science Letters, v. 31, p. 279-286.

Ramlal, K.
1979 The chemical analysis of silicate rocks. Centre for Precambrian Studies, University of Manitoba Annual Report 1978, p. 56-59.

Ribbe, P.H. and Roesenberg, P.E.
1971 Optical and X-ray determinative methods for fluorine in topaz. American Mineralogist, v. 42, p. 635-647.

Rinaldi, R., Černý, P., and Ferguson, R.B.
1972 The TANCO pegmatite at Bernic Lake, Manitoba. VI. Lithium-rubidium-cesium micas. Canadian Mineralogist, v. 11, p. 690-707.

Rowe, R.B.
1956 Lithium deposits in Manitoba. Geological Survey of Canada, Paper 55-26, 23 p.

Rucklidge, J.C. and Gasparrini, E.L.
1969 EMPADR VII, a computer program for processing electron microprobe data. University of Toronto.

Siedner, G.
1968 Distribution of alkali metals and thallium in some South-West African granites. Geochimica et Cosmochimica Acta, v. 32, p. 1303-1315.

Springer, G.D.
1949 Geology of the Cat Lake-Winnipeg River area. Manitoba Mines Branch, Preliminary Report 48-7, 28 p.

1950 Mineral deposits of the Cat Lake-Winnipeg River area, Lac du Bonnet Mining Division. Manitoba Mines Branch, Publication 49-7, 14 p.

Stockwell, C.H.
1933 The genesis of pegmatites of southeast Manitoba. Transactions of the Royal Society of Canada. v. 27, Section IV, p. 37-51.

Taylor, S.R., Emeleus, C.H., and Exley, C.S.
1956 Some anomalous K/Rb rations in igneous rocks and their petrological significance. Geochimica et Cosmochimica Acta, v. 10, p. 224-229.

Taylor, S.R., Ewart, A., and Capp, A.C.
1968 Leucogranites and rhyolite: trace element evidence for fractional crystallization and partial melting. Lithos, v. 1, p. 179-186.

Trueman, D.L.
1976 Evidence in support of a meteorite impact crater at Poplar Bay, Lac du Bonnet, southeastern Manitoba. Canadian Journal of Earth Sciences, v. 13, p. 1608-1612.

1980 Stratigraphic, structural, and metamorphic petrology of the Archean greenstone belt at Bird River, Manitoba. Ph.D. Thesis, Department of Earth Sciences, University of Manitoba, 155 p.

Trueman, D.L., Posehn, G.A., and Stoetterau, W.
1976 Metamorphism, structure, and stratigraphy in the Rice Lake-Manigotagan gneiss belt, Bird Lake area of southeastern Manitoba and northwestern Ontario, Centre for Precambrian Studies, University of Manitoba, 1975 Annual Report, p. 67-84.

Tyrrell, J.B.
1900 East Shore, Lake Winnipeg. Geological Survey of Canada, Annual Report, v. 11, Pt. G.

Winkler, H.G.F.
1965 Petrogenesis of metamorphic rocks. 1st edition. Springer-Verlag. New York, 237 p.

1976 Petrogenesis of metamorphic rocks. 4th edition, Springer-Verlag, New York, 334 p.

Winkler, H.G.F. and Von Platen, H.
1961 Experimentelle Gesteinsmetamorphose. V. Experimentelle Anatektische Schmelzen und ihre petrogenetische Bedeutungi. Geochimica et Cosmochimica Act, v. 24, p. 250-259.

Winkler, H.G.B., Boese, M., and Marcopoulos, T.
1975 Low-temperature granitic melts. Neues Jahrbuch für Mineralogists, Monatsheffe, p. 245-268.

Wright, J.F.
1926 Geology and mineral deposits of Oiseau River map area, Manitoba. Geological Survey of Canada, Summary Report, 1924, Part B, p. 74-138.

1932 Geology and mineral deposits of a part of southeastern Manitoba. Department of Mines and Resources, Mines and Geology Branch, Mem. 169, 150 p.

Wyllie, P.J.
1979 Magmas and volatile components. American Mineralogist, v. 64, p. 469-500.

Wyllie, P.J. and Tuttle, O.F.
1964 Experimental investigation of silicate systems containing two volatile components, Part III. The effects of SO_3, P_2O_5, HCl, and Li_2O, in addition to H_2O on the melting temperatures of albite and granite. American Journal of Science, v. 262, p. 930-939.

Yoder, H.S. and Eugster, H.P.
1955 Synthetic and natural muscovites, Geochimica et Cosmochimica Acta, v. 8, p. 225-236.

A. Major Minor and Trace Elements

Appendix 1. Whole Rock Analyses

Sample No.	SiO_2	TiO_2	Al_2O_3	Fe_2O_3	FeO	MnO	MgO	CaO	Na_2O	K_2O	P_2O_5	CO_2	H_2O	F_2	Total	Li	Rb	Cs	Be	Sr	Ba	Pb	Ga	U	Th	Zr	Sn	Y	Hf
TNL-2	78.60	0.02	12.10	0.18	0.20	0.02	0.10	0.46	3.93	3.89	0.09	0.03	0.34		99.96	29	161	9.4	2	29	183	26	22	29	N.D.	61	N.D.	N.D.	
TNL-21	76.10	0.01	13.29	0.10	0.52	0.11	0.05	0.45	3.90	5.35	0.04	0.07	0.28		100.27	196	28												
TNL-27	76.40	0.05	12.61	0.58	0.76	0.02	0.11	0.37	3.22	5.41	0.04	0.04	0.42		100.03	52	327	2.9	1.3	41	132	56	29	29	30	95	14	46	
TNL-31	77.10	0.03	12.28	0.31	0.68	0.01	0.20	0.42	3.23	5.24	0.06	0.02	0.52	0.01	100.11	42	168	4	1	3	244	30	27	36	15	130	3	61	4.35
TNL-34	77.05	0.04	12.38	0.30	0.64	0.02	0.14	0.45	3.52	4.71	0.04	0.08	0.49		99.86	54	220	4.6	1.1	28	31	24	25	33	15	67	13	44	
TNL-39	71.40	0.01	16.28	0.27	0.82	0.20	0.13	1.19	6.50	2.64	0.07	0.05	0.36		99.92	19	318	5.2	3	31	165	17	46	13	N.D.	65	7	22	
TNL-43	76.60	0.02	12.80	0.24	0.78	0.04	0.15	0.46	3.33	5.04	0.09	0.04	0.50	0.01	100.10	59	128	10.4	2	24	155	29	32	32	14	111	10	53	3.55
TNL-54(c)	75.70	0.07	13.04	0.81	0.88	0.03	0.23	0.37	3.25	4.96	0.04	0.20	0.57		100.15	49	338	9.4	2.3	40	169	43		38	5	106	10	6	
TNL-58	78.90	0.02	11.60	0.47	0.30	0.04	0.15	0.35	3.33	5.04	0.09	0.040	0.50		100.30	23	310	11.2	3	32	202	32	28	19	3	135	11	45	
TNL-61	78.40	0.05	12.05	0.34	0.18	0.01	0.19	0.34	2.30	5.79	0.07	0.03	0.41		100.16	11	306	9.3	2	55	413	25	22	13	2	140	9	34	
TNL-65(a)	75.95	0.03	13.18	0.69	0.28	0.03	0.16	0.37	3.55	5.22	0.08	0.10	0.48		100.12	11	261	3.4	1.5	40	202	41	40	27	11	80	10	54	
TNL-67	75.40	0.04	12.98	0.92	0.56	0.03	0.23	0.47	3.22	5.38	0.04	0.17	0.51		99.95	11	231	11.4	2.4	49	295	36		40	17	114	12	82	
TNL-68	76.90	0.02	13.42	0.71	0.30	0.12	0.21	0.57	3.02	3.76	0.03	0.17	0.74		99.97	22	168	5.7	2.2	53	416	23	29	27	12	131	6	44	
OL-8	74.80	0.00	14.62	0.96	0.30	0.15	0.11	0.55	3.73	3.49	0.22	0.10	0.70	0.02	99.73	69	193	17	0.8	28	3	9	41	52	4	24	15	12	
OL-10	76.00	0.00	14.05	0.49	0.26	0.02	0.16	0.89	4.45	2.18	0.10	0.06	0.64		99.3	47	116	3.9	0.3	36	3	15	46	8	4	17	10	30	
OL-23	73.55	0.13	14.34	0.45	0.86	0.03	0.46	0.81	3.10	5.21	0.15	0.05	0.88		100.20	87	196	20	1	105	315	27	32	71	N.D.	79	9	N.D.	
OL-23(a)	73.45	0.11	14.25	0.55	1.06	0.03	0.49	0.74	2.97	5.67	0.15	0.03	0.79	0.01	100.30	72	196	15.5	1	101	347	34	29	18	N.D.	82	5	N.D.	1.75
OL-23(b)	74.05	0.09	14.33	0.24	0.90	0.04	0.40	0.62	3.16	5.03	0.17	0.06	0.85		99.94	64	179	15	0.6	65	284	22	26	20	N.D.	78	2	N.D.	
OL-23(c)	72.75	0.11	14.46	0.47	1.24	0.03	0.50	0.71	3.14	5.64	0.15	0.01	0.88		100.09	63	179	11.8	0.3	63	203	23	25	12	N.D.	73	3	N.D.	1.5
GL-13(a)	73.55	0.02	13.82	0.04	0.16	0.02	0.01	0.04	2.62	8.81	0.08	0.02	0.27		99.46	29	1050	9.5	2	17	122	23	32	17	N.D.	38	10	18	
GL-33(e)	76.60	0.01	13.66	0.46	0.36	0.03	0.09	0.26	3.72	3.88	0.05	0.04	0.71		99.87	58	375	9.3	10	15	150	28	73	11	9	58	25	32	
GL-35(a)	74.35	0.01	14.23	0.45	0.32	0.02	0.07	0.40	4.97	4.55	0.06	0.03	0.32	0.01	99.79	60	353	7.0	3	11	136	28	44	30	1	55	5	45	
GL-38(a)	75.90	0.01	13.48	0.35	0.26	0.01	0.03	0.31	3.68	5.41	0.08	0.03	0.34	0.01	99.90	57	340	13.7	3	20	142	33	45	9	25	58	8	40	1.2
GL-1002	75.50	0.06	14.24	0.33	0.94	0.26	0.03	0.10	4.28	3.50	0.04	0.07	0.53		99.88	86	695	5.1	1.2	28	12	5	71	8	2	11	20	17	
ENL-6(b)	75.55	0.00	13.68	0.51	0.50	0.35	0.04	0.15	4.02	4.65	0.11	0.03	0.48	0.02	100.09	140	817	24	3	15	110	10	59	6	3	71	11	56	3.4
ENL-29(c)	76.60	0.01	13.59	0.29	0.46	0.09	0.05	0.21	4.00	3.91	0.05	0.02	0.62	0.03	99.93	72	499	10.4	13	11	100	18	56	8	N.D.	51	13	17	0.8
ENL-2(a)	77.35	0.01	13.02	0.70	0.24	0.11	0.05	0.26	4.40	3.02	0.05	0.03	0.54		99.78	224	506	67	34	22	96	25	50	6	13	58	13	26	
ENL-26(b)	76.55	0.00	14.20	0.30	0.36	0.10	0.03	0.33	4.77	2.56	0.07	0.01	0.53		99.81	63	254	7.5	4	12	153	16	66	3	1	76	11	42	
GL-33(c)	76.90	0.01	13.47	0.30	0.36	0.02	0.09	0.30	4.05	3.85	0.06	0.02	0.62		100.05	50	359	6.3	7	20	162	24	69	44	4	58	19	29	

Appendix 1 Continued..

Sample No.	SiO_2	TiO_2	Al_2O_3	Fe_2O_3	FeO	MnO	MgO	CaO	Na_2O	K_2O	P_2O_5	CO_2	H_2O	F_2	Total	Li	Rb	Cs	Be	Sr	Ba	Pb	Ga	U	Th	Zr	Sn	Y	Hf
OL-12	75.50	0.00	14.64	0.56	0.80	0.33	0.08	0.53	5.78	1.10	0.13	0.07	0.51	0.03	100.06	74	103	4.3	1.2	13	18	10	51	9	12	74	14	14	
GL-19(c)	77.80	0.01	14.04	0.11	0.59	0.02	0.06	0.22	5.32	1.22	0.08	0.02	0.63		100.15	324	418	15.5	4	16	113	10	71	13	10	93	21	82	
GL-25(a)	76.10	0.01	14.27	0.49	0.48	0.11	0.03	0.27	6.70	1.14	0.07	0.01	0.28		99.97	19	306	2.9	2	10	107	8	55	2	N.D.	66	8	14	
ENL-25(c)-A	78.00	0.01	12.40	0.33	1.68	0.32	0.06	0.34	4.77	1.08	0.03	0.13	0.59	0.03	99.77	133	245	3.7	1.9	14	19	9	57	14	32	16	19	56	
TNL-37	72.70	0.02	15.04	0.58	0.92	0.19	0.06	0.37	3.37	6.62	0.12	0.04	0.17	0.01	100.21														
OL-11	75.80	0.00	14.64	0.98	0.42	0.16	0.13	0.47	4.78	1.56	0.17	0.10	0.50	0.03	99.74														
GL-6(a)-A	77.50	0.06	12.79	0.76	0.80	0.21	0.03	0.40	6.22	0.66	0.04	0.10	0.39	0.01	99.97	45	138	1.5	2.0	5	N.D.	4	51	6	12	14	13	34	
GL-6(d)-A	74.55	0.01	14.54	0.56	1.16	0.33	0.05	0.22	4.55	3.25	0.03	0.04	1.56	0.03	100.88	78	559	21	1.6	21	2	5	69	5	7	27	20	32	
SL-1-95	73.55	0.04	14.85	0.73	1.48	0.81	0.04	0.36	7.27	0.60	0.06	0.06	0.28	0.01	100.14	66	90	2.1	2.8	6	N.D.	9	53	43	26	156	16	199	
SL-2-18	72.30	0.03	16.30	0.26	0.42	0.25	0.02	0.21	9.65	0.40	0.48	0.03	0.18		100.53	143	96	20	5.1	5	N.D.	3	60	1	10	50	11	4	
Lobe-12	69.90	0.00	15.05	1.35	3.32	2.55	0.07	0.17	6.73	0.36	0.06	0.04	0.21		99.81	14	9	0.2	2.2	11	57	4	48	21	12	144	5	135	
ENL-10-1	71.50	0.04	16.76	0.59	0.36	0.18	0.01	0.32	9.40	0.35	0.05	0.10	0.20		99.86	18	32	1.7	1.3	23	N.D.	6	58	1	30	69	13	62	
ENL-11(a)	73.40	0.02	16.33	0.24	0.24	0.22	0.01	0.32	9.18	0.14	0.12	0.08	0.21	0.01	100.52	7	11	0.9	5.6	17	N.D.	3	56	4	4	49	9	2	
ENL-20(c)	74.10	0.05	14.15	0.69	1.04	0.42	0.04	0.27	4.72	3.41	0.03	0.10	0.60		99.62														
GL-6(a)-P	75.55	0.04	15.01	0.56	0.20	0.01	0.05	0.18	2.90	4.65	0.02	0.22	1.15	0.06	100.60	107	735	4.6	1.7	13	N.D.	5	102	5	3	2	20	N.D.	
GL-6(a)-P	76.70	0.01	14.48	0.60	0.40	0.06	0.07	0.30	3.95	2.38	0.02	0.10	1.04	0.07	100.18	120	453	8.5	2.5	6	N.D.	4	107	5	6	1	25	14	
ENL-25(c)-P	77.90	0.06	13.20	0.65	0.80	0.13	0.06	0.43	4.13	1.60	0.04	0.11	0.77	0.04	99.92	177	405	5.4	2.4	15	N.D.	19	77	10	8	31	29	20	
OL-13(P+SA)	75.30	0.00	14.82	0.92	0.16	0.03	0.11	0.33	4.80	2.04	0.31	0.12	0.90		99.84														
TNL-1006	73.50	0.03	14.40	0.47	0.88	0.03	0.09	0.36	3.98	5.63	0.05	0.09	0.23	0.01	99.75	28	275	3.2	0.5	43	50	20	62	3	N.D.	5	13	17	
OL-1004	72.05	0.03	15.92	0.79	0.68	0.10	0.08	0.24	4.08	4.98	0.42	0.10	0.53	0.02	100.02	10	318	11	0.7	37	3	11	43	5	N.D.	25	22	N.D.	
OL-1005	73.40	0.06	14.80	0.44	0.68	0.02	0.03	0.33	4.80	4.59	0.56	0.11	0.39	0.02	100.23	10	366	6.2	0.9	52	26	10	43	2	N.D.	2	18	N.D.	0.35
GL-1002	75.00	0.03	14.80	0.21	0.92	0.09	0.03	0.06	2.75	5.32	0.03	0.09	0.71	0.06	100.10	119	1001	5.6	1.8	25	9	5	65	9	2	N.D.	33	N.D.	
GL-1003	75.30	0.04	14.30	0.86	0.92	0.08	0.03	0.22	5.20	2.19	0.06	0.08	0.55	0.03	99.86	76	442	2.3	1.7	31	1	11	64	8	5	16	23	32	1.25
ENL-1001	76.00	0.00	13.98	0.59	1.10	0.09	0.04	0.32	4.25	2.92	0.04	0.09	0.56	0.03	100.01	118	391	15	12	23	1	17	48	25	14	5	13	32	0.95
SR-54(e)-2	74.00	0.00	14.30	0.32	1.32	0.34	0.06	0.28	4.75	3.96	0.12	0.08	0.44		99.97	27	293	3.8	0.7	5	N.D.	7	60	4	18	38	15	9	2.7

Appendix 1 Continued..

B. Rare Earth Elements

Sample No.	La	Ce	Nd	Sm	Eu	Tb	Dy	Yb	Lu
TNL-31	19.70	46.0	5.5	7.245	0.180	0.985	8.90	4.7	0.560
TNL-43	19.60	45.5	33.0	6.65	0.140	0.830	8.25	4.6	0.510
OL-23(a)	8.60	18.0	(3.0)	2.580	0.465	0.250	2.05	0.85	0.190
OL-23(c)	8.80	17.0	11.5	2.415	0.270	0.360	2.15	1.15	0.180
OL-1005	1.75	3.0	(3.0)	0.365	0.070	(0.070)	(0.04)	(0.03)	(0.020)
GL-38(a)	5.50	16.5	(3.0)	2.950	(0.050)	0.730	7.15	3.35	0.320
GL-1003	7.50	18.5	6.5	4.685	(0.050)	0.585	5.85	2.70	0.260
ENL-6(b)	11.90	31.0	14.5	8.145	0.090	0.860	6.10	5.25	0.545
ENL-29(c)	5.95	14.5	7.0	2.840	(0.050)	0.384	4.00	2.00	0.190
ENL-1001	10.40	29.0	(3.0)	5.770	0.090	0.790	6.05	3.15	0.385
SR-54(e)-2	3.85	12.0	6.0	2.010	0.08	0.460	6.70	3.10	0.325

Appendix 2. Blocky K-feldspar Analyses

Sample No.	K_2O	Na_2O	CaO	Rb_2O	Cs_2O	Li_2O	PbO	K	Na	Ca	Rb	Cs	Li	Pb	Or	Ab	An	Rb-F	K/Rb	Rb/Cs	K/Cs
OL-1	11.80	2.51	0.13	0.046	0.0009	0.0006	0.0046	9.80	1.87	0.09	0.042	0.0008	0.0003	0.0043	75.6	23.4	0.6	0.3	233	53	12250
OL-2	2.90	10.90	0.56	0.015	0.0005	0.0004	0.0023	2.41	8.09	0.40	0.014	0.0005	0.0003	0.0021	15.4	82.2	2.4	0.03	172	28	4820
OL-4	12.70	2.73	0.10	0.027	0.0006	0.0024	0.0085	10.54	2.03	0.07	0.025	0.0006	0.0011	0.0079	76.0	23.4	0.5	0.11	422	42	17567
OL-5	12.40	2.72	0.11	0.032	0.0004	0.0011	0.0123	10.29	2.02	0.079	0.029	0.0004	0.0005	0.0114	75.5	23.9	0.5	0.14	355	73	25725
OL-6	13.20	2.36	0.081	0.045	0.0008	0.0013	0.0059	10.96	1.75	0.058	0.041	0.0008	0.0006	0.0055	79.8	19.6	0.4	0.19	267	51	13700
OL-7	12.70	2.59	0.076	0.046	0.0007	0.0004	0.0053	10.54	1.92	0.054	0.042	0.0007	0.0002	0.0049	77.0	22.4	0.4	0.19	251	60	15057
OL-8	13.50	2.63	0.11	0.069	0.0019	0.0017	0.0044	11.21	1.95	0.079	0.063	0.0018	0.0008	0.0041	77.6	21.6	0.6	0.24	178	35	6228
OL-9	12.90	2.20	0.14	0.069	0.0033	0.0009	0.0038	10.71	1.63	0.10	0.063	0.0031	0.0004	0.0035	79.6	19.6	0.6	0.24	170	20	3455
OL-11	12.55	3.43	0.05	0.081	0.0015	0.0062	0.0015	10.42	2.57	0.04	0.074	0.0014	0.0029	0.0014	71.7	27.7	0.3	0.28	141	53	7443
OL-12	12.50	3.34	0.069	0.089	0.0027	0.0033	0.0024	10.38	2.48	0.049	0.081	0.0025	0.0015	0.0022	70.1	29.3	0.4	0.34	128	32	4152
OL-13	11.00	4.05	0.10	0.114	0.0011	0.0084	0.0009	9.13	3.00	0.07	0.104	0.0010	0.0039	0.0008	64.8	34.3	0.5	0.36	88	104	9130
OL-14	11.65	3.32	0.23	0.106	0.0032	0.0120	0.0006	9.67	2.46	0.16	0.097	0.0030	0.0056	0.0006	70.1	28.6	0.9	0.36	100	32	3223
OL-15	11.50	3.25	0.054	0.085	0.0010	0.0013	0.0013	9.55	2.37	0.039	0.078	0.0009	0.0006	0.0012	71.0	28.4	0.3	0.33	122	87	10611
OL-16	11.70	3.02	0.035	0.35	0.0180	0.0024	0.0012	9.71	2.24	0.025	0.32	0.0170	0.0011	0.0011	72.1	26.4	0.2	1.3	30	19	571
OL-17	12.25	3.07	0.06	0.063	0.0010	0.0062	0.0022	10.17	2.28	0.04	0.058	0.0009	0.0029	0.0020	73.5	26.0	0.3	0.24	175	64	11300
OL-18	10.75	3.63	0.056	0.072	0.0007	0.0030	0.0016	8.92	2.66	0.040	0.066	0.0007	0.0014	0.0015	67.2	32.3	0.3	0.3	135	94	12743
OL-19	13.45	2.53	0.11	0.052	0.0014	0.0047	0.0023	11.17	1.88	0.08	0.048	0.0013	0.0022	0.0021	78.1	21.3	0.4	0.2	233	37	8592
OL-20	11.60	3.08	0.059	0.058	0.0012	0.0185	0.0030	9.63	2.23	0.042	0.053	0.0011	0.0086	0.0028	72.9	27.1	0.3	0.2	182	48	8755
OL-21	11.80	2.90	0.091	0.072	0.0008	0.0009	0.0010	9.80	2.09	0.065	0.066	0.0008	0.0004	0.0009	73.5	25.8	0.4	0.3	148	83	12250
OL-22	12.92	2.99	0.008	0.047	0.0012	0.0019	0.0046	10.71	2.22	0.063	0.043	0.0011	0.0009	0.0043	74.9	24.6	0.4	0.2	249	39	9736
OL-24	12.60	2.97	0.082	0.037	0.0009	0.0039	0.0040	10.46	2.20	0.059	0.034	0.0008	0.0018	0.0037	74.6	24.8	0.4	0.15	308	43	13075
OL-25	12.20	2.99	0.060	0.092	0.0017	0.0045	0.0010	10.13	2.22	0.043	0.084	0.0016	0.0021	0.0009	73.7	25.5	0.3	0.4	121	53	6331
OL-27	14.70	1.56	0.092	0.072	0.0044	0.0028	0.0025	12.20	1.16	0.066	0.066	0.0042	0.0013	0.0023	86.3	13.0	0.4	0.3	185	16	2905
OL-28	12.10	3.06	0.22	0.073	0.0043	0.0028	0.0015	10.04	2.27	0.16	0.067	0.0041	0.0013	0.0014	73.3	25.7	0.7	0.3	150	16	2449
OL-30	12.90	2.78	0.09	0.035	0.0012	0.0009	0.0039	10.71	2.06	0.06	0.032	0.0011	0.0004	0.0036	75.9	23.5	0.4	0.2	335	29	9736
OL-31	11.45	3.30	0.12	0.057	0.0010	0.0006	0.0028	9.51	2.45	0.085	0.052	0.0009	0.0003	0.0026	70.4	28.9	0.4	0.2	183	58	10567
OL-32	11.00	3.64	0.11	0.057	0.0008	0.0028	0.0036	9.13	2.70	0.079	0.052	0.0007	0.0013	0.0033	67.5	31.8	0.4	0.2	176	74	13043
OL-33	13.15	2.61	0.05	0.143	0.0033	0.0015	0.0016	10.92	1.94	0.04	0.131	0.0031	0.0007	0.0015	77.5	21.7	0.3	0.5	83	42	3523
OL-34	11.45	3.48	0.092	0.055	0.0010	0.0045	0.0025	9.51	2.58	0.066	0.050	0.0009	0.0021	0.0023	69.4	30.0	0.4	0.2	190	56	10567
OL-35	12.00	2.91	0.060	0.083	0.0012	0.0011	0.0016	9.96	2.16	0.043	0.076	0.0011	0.0005	0.0015	73.8	25.6	0.3	0.3	131	69	9055
OL-36	11.25	3.08	0.13	0.069	0.0013	0.0047	0.0012	9.34	2.28	0.093	0.063	0.0012	0.0022	0.0011	71.8	27.5	0.7	0.32	148	53	7783
OL-37	11.05	3.42	0.05	0.066	0.0016	0.0045	0.0010	9.17	2.57	0.036	0.060	0.0015	0.0021	0.0009	69.4	30.05	0.3	0.21	153	40	6113

Appendix 2 Continued..

Sample No.	K_2O	Na_2O	CaO	Rb_2O	Cs_2O	Li_2O	PbO	K	Na	Ca	Rb	Cs	Li	Pb	Or	Ab	An	Rb-F	K/Rb	Rb/Cs	K/Cs
OL-38	11.10	3.43	0.051	0.106	0.0025	0.0030	0.0008	9.21	2.54	0.04	0.097	0.0024	0.0014	0.0007	69.4	30.0	0.3	0.4	95	40	3838
OL-39	11.25	2.45	0.040	0.12	0.0034	0.0047	0.0010	9.34	1.82	0.029	0.11	0.0032	0.0022	0.0009	76.3	23.0	0.2	0.46	849	34	2919
GL-6(c)	11.80	3.31	0.016	0.15	0.0027	0.0039	0.0043	9.80	2.46	0.012	0.14	0.0026	0.0018	0.0040	71	28.4	0.1	0.5	70	54	3769
GL-9(c)	10.50	4.02	0.13	0.16	0.0010	0.0022	0.0028	8.72	2.98	0.093	0.15	0.0009	0.0010	0.0026	64.4	34.3	0.6	0.6	58	167	9767
GL-10-3	11.58	3.36	0.047	0.248	0.0047	0.0065		9.61	2.49	0.034	0.227	0.0044	0.0030	0.0018	69.4	29.0	0.3	0.9	42	52	2184
GL-10-6	12.55	2.89	0.051	0.265	0.0075	0.0124		10.42	2.14	0.036	0.242	0.0071	0.0058	0.0017	74.5	24.1	0.3	1.0	43	34	1468
GL-10-9	11.25	3.37	0.036	0.244	0.0105	0.0121	0.0033	9.34	2.50	0.026	0.223	0.0099	0.0056	0.0031	69.0	29.8	0.2	0.93	42	23	943
GL-11-1	11.10	3.67	0.06	0.0199	0.0027	0.0043	0.0015	9.21	2.72	0.043	0.182	0.0027	0.0020	0.0014					51	67	3411
GL-11-2	11.23	3.38	0.02	0.267	0.0073	0.0075	0.0010	9.32	2.51	0.014	0.244	0.0069	0.0035	0.0009					38	35	1351
GL-11(e)	11.48	3.75	0.014	0.25	0.0057	0.0034	0.0016	9.53	2.78	0.0098	0.23	0.0054	0.0016	0.0015	67.9	31.1	0.1	0.85	41	43	1765
GL-12(g)	11.30	3.32	0.042	0.17	0.0032	0.0028	0.0039	9.38	2.46	0.030	0.16	0.0030	0.0013	0.0036	69.6	29.5	0.2	0.6	59	53	3127
GL-13(c)	11.06	2.58	0.045	0.14	0.0011	0.0024	0.0031	9.18	1.91	0.032	0.13	0.0010	0.0011	0.0029	75.3	24.5	0.2		71	130	9180
GL-14(b)	10.80	3.76	0.038	0.14	0.0007	0.0026	0.0030	8.97	2.79	0.027	0.13	0.0007	0.0012	0.0028	66.8	32.4	0.2	0.5	69	186	12814
GL-15(c)	12.0	2.84	0.048	0.19	0.0036	0.0026	0.0047	9.96	2.11	0.034	0.17	0.0034	0.0012	0.0044	74.4	24.6	0.2	0.7	59	50	2929
GL-17(b)	12.01	2.99	0.043	0.24	0.0050	0.0062	0.0022	9.98	2.22	0.031	0.22	0.0047	0.0029	0.0020	74.2	25.6	0.2		45	47	2123
GL-19	11.90	2.94	0.026	0.27	0.0046	0.0054	0.0018	9.88	2.18	0.019	0.25	0.0042	0.0025	0.0017	73.4	25.5	0.1	0.95	40	60	2352
GL-19-1	12.32	2.90	0.011	0.26	0.0075	0.0067	0.0011	10.23	2.15	0.0076	0.24	0.0071	0.0031	0.0010	74.1	24.9	0.1	0.9	43	34	1441
GL-19-2	13.00	1.98	0.022	0.32	0.0108	0.0045	0.0025	10.79	1.47	0.016	0.29	0.0102	0.0021	0.0023	81.7	17	0.1	1.2	37	28	1058
GL-19-3	11.94	3.36	0.0091	0.18	0.0057	0.0062	0.0018	9.91	2.49	0.0065	0.16	0.0054	0.0029	0.0017	71	28.2	0.1	0.7	62	30	1835
GL-20(a)	12.40	2.60	0.033	0.31	0.0108	0.0108	0.0027	10.29	1.93	0.024	0.28	0.0102	0.0048	0.0025	76.6	22	0.2	1.2	37	27	1009
GL-21(a)	10.70	3.60	0.022	0.20	0.0053	0.0054	0.0018	8.88	2.67	0.016	0.18	0.0050	0.0025	0.0017	67.1	32	0.1	0.75	49	36	1776
GL-22(a)	11.90	2.88	0.011	0.21	0.0061	0.017	0.0039	9.88	2.14	0.0076	0.19	0.0057	0.0080	0.0036	74.1	24.9	0.1	0.8	52	33	1733
GL-24	12.14	2.76	0.023	0.36	0.0072	0.0052	0.0018	10.08	2.05	0.016	0.33	0.0068	0.0024	0.0017	74.8	23.9	0.1	1.2	31	49	1482
GL-26(b)	11.58	3.76	0.011	0.21	0.0008	0.0039	0.0034	9.61	2.79	0.0080	0.19	0.0007	0.0018	0.0032	68.1	31	0.1	0.8	51	271	13729
GL-28	11.30	3.34	0.034	0.14	0.0013	0.0032	0.0034	9.38	2.48	0.024	0.13	0.0012	0.0015	0.0032	70	29.2	0.2	0.5	72	108	7817
GL-30-1	12.60	2.80	0.036	0.451	0.0057	0.0074	0.0012	10.46	2.08	0.026	0.412	0.0054	0.0035	0.0011	74.6	23.6	0.2	1.57	25	76	1937
GL-30-2	13.60	2.19	0.045	0.477	0.0064	0.0073	0.0017	11.29	1.62	0.032	0.436	0.0060	0.0034	0.0016	80.8	17.4	0.2	1.65	26	73	1882
GL-32(d)	12.02	3.36	0.025	0.078	0.0012	0.0067	0.0072	9.98	2.49	0.018	0.071	0.0011	0.0031	0.0067	71.4	28.1	0.1	0.3	141	65	9073
GL-35(c)	12.60	2.87	0.022	0.082	0.0011	0.0045	0.0074	10.46	2.13	0.016	0.075	0.0011	0.0021	0.0069	75.7	23.8	0.1	0.3	139	68	9509
GL-36(b)	11.50	3.60	0.018	0.051	0.0039	0.0067	0.0051	9.50	2.67	0.013	0.047	0.0037	0.0031	0.0047	69.1	30.5	0.1	0.2	202	13	2568
GL-37(d)	10.96	3.64	0.059	0.11	0.0030	0.0075	0.0040	9.10	2.70	0.042	0.10	0.028	0.0035	0.0037	68	31.2	0.3	0.4	91	36	3250
GL-38(d)	13.48	1.79	0.017	0.098	0.0024	0.0088	0.0068	11.61	1.33	0.011	0.090	0.0023	0.0041	0.0063	83.7	15.7	0.1	0.4	129	39	5048

Appendix 2 Continued..

Sample No.	K_2O	Na_2O	CaO	Rb_2O	Cs_2O	Li_2O	PbO	K	Na	Ca	Rb	Cs	Li	Pb	Or	Ab	An	Rb-F	K/Rb	Rb/Cs	K/Cs
GL-41(a)	13.70	2.04	0.012	0.21	0.0071	0.014	0.0042	11.37	1.51	0.0089	0.19	0.0067	0.0053	0.0039	81.5	17.1	0.1	0.8	60	28	1697
GL-46(b)	12.74	2.28	0.033	0.60	0.0109	0.0017	0.0014	10.58	1.69	0.024	0.55	0.0103	0.0008	0.0013	78	19.8	0.2	2	19	53	1027
TNL-1	12.10	2.98	0.055	0.075	0.0009	0.0026	0.0031	10.04	2.21	0.039	0.069	0.0008	0.0012	0.0029	74	25.4	0.3	0.3	146	86	12550
TNL-4	12.30	2.84	0.110	0.060	0.0019	0.0019	0.0034	10.21	2.11	0.079	0.055	0.0018	0.0009	0.0032	75.1	24.1	0.5	0.2	186	31	5672
TNL-6	12.00	2.80	0.048	0.050	0.0009	0.0028	0.0025	9.96	2.08	0.034	0.046	0.0008	0.0013	0.0023	75.1	24.3	0.3	0.2	217	58	12450
TNL-8	12.00	3.00	0.115	0.061	0.0009	0.0032	0.0032	9.96	2.23	0.082	0.056	0.0008	0.0015	0.0030	73.4	25.8	0.5	0.2	178	70	12450
TNL-10	11.90	3.24	0.069	0.045	0.0008	0.0015	0.0034	9.88	2.40	0.049	0.041	0.0008	0.0007	0.0032	71.8	27.7	0.3	0.2	241	51	12350
TNL-12	12.20	2.96	0.104	0.068	0.0011	0.0058	0.0029	10.13	2.20	0.074	0.062	0.0010	0.0027	0.0027	73.6	25.5	0.5	0.3	163	62	10130
TNL-14	11.60	3.28	0.094	0.045	0.0006	0.0075	0.0036	9.63	2.43	0.067	0.041	0.0006	0.0035	0.0033	71.4	27.9	0.5	0.2	235	68	16050
TNL-16	12.80	2.50	0.105	0.085	0.0013	0.0037	0.0043	10.63	1.85	0.075	0.078	0.0012	0.0017	0.0040	77.5	21.5	0.5	0.3	136	65	8858
TNL-18	11.70	3.30	0.080	0.040	0.0010	0.0039	0.0044	9.71	2.45	0.057	0.037	0.0009	0.0018	0.0041	70.9	28.4	0.4	0.2	262	41	10789
TNL-23	11.10	3.58	0.056	0.059	0.0008	0.0024	0.0026	9.21	2.66	0.040	0.054	0.0008	0.0011	0.0024	68.3	31.2	0.2	0.2	171	68	11513
TNL-26	11.00	3.74	0.065	0.073	0.0002	0.0028	0.0031	9.13	2.77	0.046	0.067	0.0002	0.0013	0.0029	67.2	32	0.3	0.3	136	335	45650
TNL-29	11.92	3.26	0.058	0.095	0.0003	0.0028	0.0037	9.90	2.42	0.041	0.087	0.0003	0.0013	0.0034	71.6	27.6	0.3	0.4	114	290	33000
TNL-30	12.72	2.68	0.071	0.106	0.0018	0.0026	0.0034	10.54	1.99	0.051	0.097	0.0017	0.0012	0.0032	76.2	22.8	0.4	0.4	109	57	6200
TNL-32	11.90	3.08	0.059	0.044	0.0024	0.0043	0.0039	9.88	2.28	0.042	0.040	0.0023	0.0020	0.0036	72.9	26.5	0.3	0.2	247	17	4296
TNL-35	12.54	2.66	0.108	0.080	0.0024	0.0093	0.0036	10.41	1.97	0.077	0.073	0.0023	0.0043	0.0033	76.4	22.7	0.5	0.3	143	32	2421
TNL-37	13.80	1.12	0.194	0.166	0.0248	0.0062	0.0034	11.46	0.83	0.139	0.152	0.0234	0.0029	0.0032	88.3	10.3	0.7	0.6	75	7	490
TNL-38	11.38	3.36	0.035	0.091	0.0019	0.0082	0.0030	9.45	2.49	0.025	0.083	0.0018	0.0038	0.0028	70.2	29.1	0.2	0.4	114	46	5250
TNL-40	12.20	2.88	0.054	0.060	0.0016	0.0019	0.0034	10.13	2.14	0.039	0.055	0.0015	0.0009	0.0032	75	24.5	0.2	0.2	184	37	6753
SR-151	12.83	3.02	0.023	0.091	0.0029	0.0034	0.0024	10.65	2.24	0.016	0.083	0.0027	0.00155	0.0022	74.2	24.7	0.2	0.35	128	31	3944
SR-155	12.35	3.22	0.063	0.030	0.0024	0.0004	0.0027	10.25	2.39	0.045	0.027	0.0023	0.00019	0.0025	72.7	26.7	0.4	0.14	380	12	4457
SR-156	14.33	1.67	0.054	0.047	0.0047	0.0027	0.0040	11.90	1.24	0.039	0.043	0.0044	0.00127	0.0037	85.3	14.1	0.4	0.2	277	10	2705
SR-157	12.40	2.85	0.052	0.037	0.0023	0.0020	0.0048	10.29	2.11	0.037	0.034	0.0022	0.0009	0.0045	75.0	24.4	0.4	0.19	303	15	4677
SR-158	12.85	2.93	0.015	0.180	0.0022	0.0048	0.0043	10.67	2.17	0.011	0.165	0.0021	0.0022	0.0040	75.3	24.0	0.1	0.67	65	79	5081
SR-159	12.50	3.12	0.053	0.174	0.0057	0.0039	0.0029	10.38	2.31	0.038	0.159	0.0054	0.0018	0.0027	73.7	25.3	0.4	0.63	65	29	1922
SR-160	12.05	3.15	0.086	0.081	0.0024	0.0014	0.0067	10.00	2.34	0.061	0.074	0.0023	0.0006	0.0062	72.9	26.1	0.7	0.33	135	32	4348
SR-161	12.18	3.37	0.084	0.038	0.0013	0.0013	0.0054	10.11	2.50	0.060	0.035	0.0012	0.0006	0.0050	71.4	27.7	0.7	0.19	289	29	8425
SR-162	12.85	2.95	0.016	0.072	0.0022	0.0039	0.9952	10.67	2.19	0.011	0.066	0.0021	0.0018	0.0048	75.4	24.3	0.1	0.23	162	31	5081
SR-115-A-1	11.70	3.60	0.058	0.075	0.0015	0.0013	0.0010	9.71	2.67	0.041	0.069	0.0014	0.0006	0.0009	69.6	30.1	0.2		141	49	6936
SR-115-A-2	11.80	3.24	0.088	0.080	0.0022	0.0010	0.0008	9.80	2.40	0.063	0.073	0.0021	0.0005	0.0007	71.7	27.8	0.5		134	35	4667

Appendix 2 Continued..

Sample No.	K_2O	Na_2O	CaO	Rb_2O	Cs_2O	Li_2O	PbO	K	Na	Ca	Rb	Cs	Li	Pb	Or	Ab	An	Rb-F	K/Rb	Rb/Cs	K/Cs
SR-116-A-1	11.45	3.76	0.041	0.074	0.0013	0.0012	0.0011	9.51	2.79	0.029	0.068	0.0012	0.0006	0.0010	68.0	31.8	0.2		140	57	7925
SR-117-A-1	12.05	3.20	0.205	0.124	0.0045	0.0069	0.0009	10.00	2.37	0.147	0.113	0.0042	0.0032	0.0008	72.1	27.2	0.7		89	27	2381
SR-118-A-1	11.25	3.70	0.121	0.090	0.0017	0.0027	0.0011	9.34	2.74	0.086	0.082	0.0016	0.0013	0.0010	69.3	30.3	0.4		114	51	5838
SR-118-A-2	0.90	10.45	0.504	0.007	0.0011	0.0501	0.0005	0.75	7.75	0.360	0.006	0.0010	0.0233	0.0005					125	6	750
ENL-1	13.00	2.51	0.070	0.23	0.014	0.0064	0.0030	10.79	1.86	0.050	0.21	0.013	0.0030	0.0028	77.2	21.6	0.4	0.8	51	16	830
ENL-2	12.50	2.74	0.057	0.22	0.0080	0.0114	0.0044	10.38	2.03	0.041	0.20	0.0076	0.0053	0.0041	75.7	23.2	0.3	0.8	52	26	2540
ENL-3(a)-1	11.40	3.52	0.054	0.12	0.0033	0.015	0.0052	9.46	2.61	0.039	0.11	0.0031	0.0049	0.0048	68.8	30.8	0.4		86	36	3052
ENL-5	12.24	3.23	0.035	0.29	0.0043	0.0071	0.0022	10.16	2.40	0.025	0.27	0.0040	0.0033	0.0020	71.8	26.9	0.2	1.0	38	68	2540
ENL-6	11.46	3.93	0.079	0.26	0.0089	0.0052	0.0026	9.51	2.92	0.056	0.24	0.0084	0.0024	0.0024	66.5	32.2	0.4	0.9	40	29	1132
ENL-7	11.94	3.23	0.041	0.31	0.0072	0.0069	0.0059	9.91	2.40	0.029	0.28	0.0067	0.0032	0.0055	71.5	27.2	0.2	1.1	35	42	1479
ENL-9	12.06	3.21	0.053	0.24	0.0064	0.0090	0.0029	10.01	2.38	0.038	0.22	0.0060	0.0042	0.0027	72	27	0.2	0.9	46	37	1668
ENL-10-3	11.58	3.36	0.047	0.248	0.0047	0.0065		9.61	2.49	0.034	0.227	0.0044	0.0030	0.0018	69.4	29.0	0.3	0.9	42	52	2184
ENL-10-6	12.55	2.89	0.051	0.265	0.0075	0.0124		10.42	2.14	0.036	0.242	0.0071	0.0058	0.0017	74.5	24.1	0.3	1.0	43	34	1468
ENL-10-9	11.25	3.37	0.036	0.244	0.0105	0.0121	0.0033	9.34	2.50	0.026	0.223	0.0099	0.0056	0.0031	69.0	29.8	0.2	0.93	42	23	943
ENL-22(d)	12.44	3.17	0.071	0.11	0.0026	0.0071	0.0054	10.33	2.35	0.051	0.10	0.0025	0.0033	0.0050	73.3	26	0.4	0.4	103	40	4132
ENL-23(d)	11.26	3.92	0.089	0.11	0.0026	0.0052	0.0054	9.35	2.91	0.064	0.099	0.0025	0.0024	0.0050	66.5	32.7	0.4	0.4	94	40	3740
ENL-27(a)	13.50	2.11	0.068	0.26	0.011	0.0039	0.0047	11.21	1.57	0.049	0.23	0.0010	0.0018	0.0044	81	17.9	0.3	0.9	49	23	1121
ENL-31(a)	11.06	2.58	0.069	0.18	0.011	0.0062	0.0043	9.18	1.91	0.049	0.16	0.010	0.0029	0.0044	74.6	24.3	0.3	0.7	57	16	918
Zone-5-4	12.20	3.39	0.053	0.50	0.0078	0.0073	0.0011	10.13	2.52	0.038	0.46	0.0074	0.0034	0.0010	70.4	27.3	0.3	0.2	22	62	1369
Zone-5-5	13.14	2.64	0.028	0.84	0.012	0.0073	0.0004	10.91	1.96	0.020	0.77	0.011	0.0034	0.0004	75.5	21.4	0.1	3	14	70	992
AC-1	12.88	2.49	0.036	0.45	0.014	0.0034	0.0012	10.69	1.85	0.026	0.41	0.013	0.0016	0.0011	76.5	21.6	0.2	1.6	26	32	822
AC-2(a)	13.18	2.37	0.024	0.86	0.017	0.0047	0.0006	10.94	1.76	0.017	0.79	0.016	0.0022	0.0006	77.4	19.5	0.1	3	14	49	684
AC-2(b)	13.10	2.51	0.024	0.65	0.017	0.016	0.0009	10.88	1.86	0.017	0.59	0.016	0.0072	0.0008	76.5	21.3	0.1	2	18	37	680
AC-2(c)	13.68	2.51	0.016	0.67	0.013	0.0081	0.0009	11.36	1.86	0.011	0.61	0.012	0.0038	0.0008	77.4	20.6	0.1	2	19	51	947
AC-2(d)	12.88	2.70	0.019	0.65	0.013	0.0075	0.0006	10.69	2.00	0.014	0.59	0.012	0.0035	0.0006	75.1	22.7	0.1	2	18	49	891
AC-3(a)	11.64	3.69	0.046	0.38	0.019	0.0088	0.0012	9.66	2.74	0.033	0.35	0.018	0.0041	0.0011	68	30.3	0.2	1.4	28	19	537
AC-3(b)	14.80	1.10	0.046	0.82	0.033	0.0043	0.0008	12.29	0.82	0.033	0.75	0.031	0.0020	0.0007	87.3	9.5	0.2	3	16	24	396
Lobe-5	11.66	3.82	0.036	0.20	0.0021	0.0034	0.0016	9.68	2.83	0.026	0.18	0.0020	0.0016	0.0015	67.5	31.5	0.2	0.75	54	90	4840
Lobe-11	11.78	3.77	0.032	0.18	0.0017	0.0037	0.0018	9.78	2.80	0.023	0.17	0.0016	0.0017	0.0017	68.7	30.4	0.2	0.7	58	106	6113
Lobe-13	11.44	3.73	0.038	0.18	0.0021	0.0037	0.0015	9.50	2.77	0.027	0.16	0.0020	0.0017	0.0014	67.9	31.1	0.2	0.7	59	80	4750
Lobe-17	14.62	1.42	0.042	0.24	0.0044	0.0037	0.0027	12.14	1.05	0.030	0.22	0.0042	0.0017	0.0025	87.3	11.6	0.2	0.85	55	55	2890

Appendix 2 Continued..

Sample No.	K_2O	Na_2O	CaO	Rb_2O	Cs_2O	Li_2O	PbO	K	Na	Ca	Rb	Cs	Li	Pb	Or	Ab	An	Rb-F	K/Rb	Rb/Cs	K/Ca
GL-4(f)	12.68	3.07	0.044	0.31	0.0088	0.0028	0.0015	10.53	2.28	0.031	0.28	0.0083	0.0013	0.0014	73.4	25.3	0.2	1.1	38	38	1269
SF-7	12.55	2.45	0.003	1.12	0.029		0.005	10.58	1.82	0.002	1.024	0.027		0.0046	75	21	0.3	3.7	10	38	392
SF-8	13.20	1.98	0.003	1.14	0.030		0.003	11.12	1.97	0.002	1.092	0.028		0.0028	79	17	0.2	3.8	11	37	397
SF-10	12.77	2.43	0.0005	1.20	0.082		0.003	10.68	1.80	0.0036	1.097	0.077		0.0028	76	20	0.0	4.0	10	14	139

Appendix 3. Graphic K-Feldspar Analyses

A. Graphic K-Feldspar + Quartz

Sample No.	K_2O	Na_2O	CaO	Rb_2O	Cs_2O	Li_2O	PbO	K	Na	Ca	Rb	Cs	Li	Pb
GL-12(c)	8.45	2.88	0.048	0.12	0.0016	0.0037	0.0029	7.01	2.14	0.034	0.11	0.0015	0.0017	0.0027
GL-22(b)	9.15	2.32	0.030	0.19	0.0063	0.0179	0.0020	7.60	1.72	0.021	0.17	0.0059	0.0083	0.0019
GL-23(b)	7.75	3.26	0.050	0.13	0.0006	0.0047	0.0012	6.43	2.42	0.036	0.12	0.0006	0.0022	0.0011
GL-24(b)	8.85	2.54	0.040	0.15	0.0056	0.0054	0.0016	7.35	1.88	0.029	0.14	0.0053	0.0025	0.0015
GL-26(b)	9.00	2.92	0.042	0.14	0.0017	0.0032	0.0017	7.47	2.17	0.030	0.13	0.0016	0.0015	0.0016
GL-32(b)	8.75	2.72	0.070	0.065	0.0012	0.0054	0.0062	7.26	2.02	0.050	0.059	0.0011	0.0025	0.0058
GL-34(c)	9.25	2.18	0.068	0.084	0.0020	0.0011	0.0045	7.68	1.62	0.049	0.077	0.0019	0.0005	0.0042
GL-37(a)	10.50	1.93	0.095	0.077	0.0018	0.0103	0.0065	8.72	1.43	0.068	0.070	0.0017	0.0048	0.0060
GL-38(c)	10.30	2.39	0.080	0.073	0.0014	0.0050	0.0059	8.55	1.77	0.057	0.067	0.0013	0.0023	0.0055
ENL-2	8.10	2.85	0.040	0.12	0.0029	0.0071	0.0020	6.72	2.11	0.029	0.11	0.0027	0.0033	0.0019
ENL-3(b)	9.00	2.45	0.048	0.091	0.0020	0.0086	0.0044	7.47	1.82	0.034	0.083	0.0019	0.0040	0.0041
ENL-21(e)	11.25	2.16	0.065	0.15	0.0041	0.0056	0.0051	9.34	1.60	0.046	0.14	0.0039	0.0026	0.0047
ENL-23(d)	9.25	2.46	0.062	0.091	0.0021	0.0050	0.0054	7.68	1.82	0.044	0.083	0.0020	0.0023	0.0050
ENL-10-3	7.68	3.65	0.064	0.168	0.0085	0.0263		6.38	2.71	0.046	0.154	0.0080	0.0122	
ENL-10-6	9.15	2.68	0.040	0.197	0.0095	0.0114		7.60	1.99	0.029	0.180	0.0090	0.053	
TNL-1	8.60	2.22	0.085	0.035	0.0010	0.0039	0.0093	7.14	1.65	0.061	0.032	0.0009	0.0081	0.0086
TNL-4	9.05	2.22	0.070	0.039	0.0016	0.0009	0.0033	7.51	1.65	0.050	0.036	0.0015	0.0004	0.0031
TNL-18	9.70	2.77	0.074	0.049	0.0027	0.0028	0.0045	8.05	2.05	0.053	0.045	0.0025	0.0013	0.0042
TNL-24	10.10	3.28	0.071	0.51	0.0099	0.0037	0.0026	8.38	2.43	0.051	0.14	0.0093	0.0017	0.0024
TNL-26	8.80	2.93	0.062	0.069	0.0017	0.0015	0.0023	7.31	2.17	0.044	0.063	0.0016	0.0007	0.0021
OL-2	9.05	2.11	0.11	0.040	0.0009	0.0013	0.0047	7.51	1.57	0.079	0.037	0.0008	0.0006	0.0044
OL-6	9.85	2.35	0.092	0.036	0.0008	0.0009	0.0043	8.18	1.74	0.066	0.033	0.0008	0.0004	0.0040
OL-10	8.90	2.52	0.10	0.039	0.0006	0.0017	0.0031	7.39	1.87	0.071	0.036	0.0006	0.0008	0.0029
OL-13	8.55	2.40	0.024	0.086	0.0019	0.0030	0.0009	7.10	1.78	0.017	0.039	0.0018	0.0014	0.0008
OL-22	8.55	2.32	0.071	0.034	0.0024	0.0043	0.0027	7.10	1.72	0.051	0.031	0.0023	0.0020	0.0025
OL-28	9.05	2.01	0.19	0.043	0.0017	0.0004	0.0010	7.51	1.49	0.14	0.039	0.0016	0.0002	0.0009
OL-36	7.80	2.63	0.066	0.049	0.0018	0.0043	0.0012	6.48	1.95	0.047	0.035	0.0017	0.0020	0.0011
OL-40	9.30	3.12	0.036	0.055	0.0014	0.0019	0.0011	7.72	2.31	0.026	0.050	0.0013	0.0009	0.0010

Appendix 3 Continued..

B. Graphic K-Feldspar + Quartz Recalculated to 100 Percent

Sample No.	K_2O	Na_2O	CaO	Rb_2O	Cs_2O	Li_2O	PbO	K	Na	Ca	Rb	Cs	Li	Pb	Or	Ab	An	Rb-F	% Quartz	K/Rb	Rb/Cs	K/Cs
GL-12(c)	11.49	3.92	0.653	0.163	0.0022	0.0050	0.0039	9.53	2.91	0.046	0.150	0.0020	0.0023	0.0037	66.78	32.38	0.32	0.53	25.87	64	25	4765
GL-22(b)	12.54	3.18	0.041	0.260	0.0086	0.0245	0.0027	10.41	2.36	0.0288	0.233	0.0081	0.0114	0.0026	73.03	25.84	0.19	0.94	26.47	45	29	1285
GL-23(b)	10.62	4.47	0.069	0.178	0.0008	0.0064	0.0016	8.81	3.32	0.049	0.164	0.0008	0.0030	0.0015	62.47	36.66	0.33	0.54	26.36	54	205	11013
GL-24(b)	12.04	3.45	0.054	0.204	0.0076	0.0073	0.0022	10.00	2.56	0.039	0.190	0.0072	0.0034	0.0020	70.68	28.32	0.30	0.70	25.86	53	26	1388
GL-26(a)	11.61	3.77	0.054	0.181	0.0022	0.0041	0.0022	9.64	2.80	0.039	0.168	0.0021	0.0019	0.0021	68.01	31.05	0.28	0.65	22.07	57	80	4290
GL-32(b)	11.64	3.62	0.093	0.087	0.0016	0.0072	0.0083	9.66	2.69	0.067	0.079	0.0015	0.0033	0.0077	68.85	30.45	0.44	0.26	24.47	122	53	6440
GL-34(c)	12.77	3.01	0.094	0.116	0.0028	0.0015	0.0062	10.60	2.24	0.068	0.106	0.0026	0.0007	0.0058	75.74	23.41	0.45	0.40	27.38	100	41	4077
GL-37(a)	13.44	2.47	0.122	0.099	0.0023	0.0132	0.0083	11.16	1.83	0.087	0.090	0.0022	0.0061	0.0077	79.27	19.82	0.58	0.33	21.79	125	41	5073
GL-38(c)	12.57	2.92	0.098	0.089	0.0017	0.0061	0.0072	10.43	2.16	0.070	0.082	0.0016	0.0028	0.0067	74.88	24.35	0.46	0.30	17.87	127	51	6519
ENL-2	11.26	3.96	0.056	0.167	0.0040	0.0099	0.0028	9.34	2.93	0.040	0.153	0.0038	0.0046	0.0026	65.87	33.28	0.31	0.54	27.89	61	40	2458
ENL-3(b)	12.24	3.33	0.065	0.124	0.0027	0.0117	0.0060	10.16	2.48	0.046	0.113	0.0026	0.0054	0.0056	71.83	27.37	0.33	0.47	26.21	90	43	3908
ENL-21(e)	13.39	2.57	0.077	0.179	0.0049	0.0067	0.0061	11.12	1.90	0.055	0.167	0.0046	0.0031	0.0056	78.87	20.16	0.36	0.62	15.68	67	36	2417
ENL-23(d)	12.21	3.25	0.082	0.120	0.0028	0.0066	0.0071	10.14	2.40	0.058	0.110	0.0026	0.0030	0.0066	72.51	26.63	0.40	0.46	24.15	92	42	3900
ENL-10-3	10.21	4.86	0.085	0.223	0.0113	0.0350	0.0021	8.49	3.60	0.061	0.205	0.0106	0.0162	0.0019	59.10	39.67	0.44	0.79	24.37	41	19	801
ENL-10-6	11.99	3.51	0.052	0.258	0.0125	0.0149	0.0015	9.97	2.61	0.038	0.236	0.0118	0.0069	0.0014	69.65	29.16	0.29	0.90	23.19	42	20	845
TNL-1	12.56	3.24	0.124	0.051	0.0015	0.0057	0.0136	10.42	2.41	0.089	0.047	0.0013	0.0026	0.0126	73.72	25.55	0.55	0.18	31.50	222	36	8016
TNL-4	12.67	3.11	0.098	0.055	0.0022	0.0013	0.0046	10.51	2.31	0.070	0.050	0.0021	0.0006	0.0043	74.81	24.52	0.46	0.21	28.62	210	24	5005
TNL-18	11.93	3.41	0.091	0.060	0.0033	0.0034	0.0055	9.90	2.52	0.065	0.055	0.0031	0.0016	0.0052	70.79	28.56	0.43	0.22	18.77	180	18	3194
TNL-24	11.72	3.81	0.082	0.174	0.0115	0.0043	0.0030	9.72	2.82	0.059	0.162	0.0108	0.0020	0.0028	67.93	31.09	0.38	0.60	13.15	60	15	900
TNL-26	11.44	3.81	0.081	0.090	0.0022	0.0020	0.0030	9.50	2.82	0.057	0.082	0.0021	0.0009	0.0027	67.83	31.44	0.39	0.34	23.04	116	39	4524
OL-2	12.76	2.98	0.155	0.056	0.0013	0.0018	0.0066	10.59	2.21	0.111	0.052	0.0011	0.0009	0.0062	75.12	23.96	0.69	0.23	29.05	204	47	9627
OL-6	12.71	3.03	0.119	0.046	0.0010	0.0012	0.0056	10.55	2.25	0.085	0.043	0.0010	0.0005	0.0052	74.83	24.43	0.59	0.15	22.22	245	43	10550
OL-10	12.02	3.40	0.135	0.053	0.0008	0.0023	0.0042	9.98	2.53	0.096	0.047	0.0008	0.0011	0.0039	91.05	28.10	0.65	0.20	25.97	212	59	12475
OL-13	12.23	3.43	0.034	0.123	0.0027	0.0043	0.0013	10.15	2.55	0.024	0.113	0.0026	0.0020	0.0011	71.74	27.70	0.14	0.41	29.61	90	43	3904
OL-22	12.23	3.32	0.102	0.049	0.0034	0.0062	0.0039	10.15	2.46	0.073	0.044	0.0033	0.0029	0.0038	72.19	27.16	0.47	0.17	30.05	231	13	3076
OL-28	12.76	2.83	0.268	0.061	0.0024	0.0006	0.0014	10.59	2.10	0.197	0.055	0.0023	0.0003	0.0013	74.85	23.55	1.36	0.24	28.66	193	24	4604
OL-36	11.47	3.87	0.097	0.072	0.0027	0.0063	0.0018	9.53	2.87	0.069	0.066	0.0025	0.0030	0.0016	67.98	31.27	0.48	0.26	31.89	144	26	3812
OL-40	11.53	3.87	0.045	0.068	0.0017	0.0024	0.0014	9.57	2.86	0.032	0.062	0.0016	0.0011	0.0012	68.79	31.29	0.19	0.24	19.46	154	39	5981

A. Platy Muscovite

Appendix 4. Muscovite Analyses

Sample No.	K_2O	Na_2O	Li_2O	Rb_2O	Cs_2O	CaO	MgO	K	Na	Li	Rb	Cs	Ca	Mg	Be	Fe	F	K/Rb	K/Cs	Rb/Li	Rb/Cs	Mg/Li
GL-17(b)	8.20	0.81	0.12	0.46	0.0088	0.020	0.07	6.81	0.60	0.057	0.42	0.0083	0.014	0.04	8.3	2.29	0.238	16	820	7.37	50.60	0.70
GL-26(c)	8.60	0.81	0.13	0.50	0.0097	0.017	0.12	7.14	0.60	0.060	0.46	0.0091	0.012	0.07	8.1	2.57	0.335	16	785	7.67	50.55	1.17
GL-30(a)	8.40	0.76	0.13	0.36	0.0051	0.023	0.20	6.97	0.56	0.059	0.33	0.0048	0.016	0.12	8.7	1.87	0.217	21	1452	5.59	68.75	2.03
GL-36(c)	9.05	0.99	0.24	0.35	0.0084	0.015	0.18	7.51	0.73	0.11	0.32	0.0079	0.011	0.11	7.3	3.03	0.331	23	951	2.91	40.51	1.00
ENL-2	8.95	0.96	0.24	0.35	0.017	0.027	0.13	7.43	0.71	0.11	0.32	0.016	0.019	0.08	6.3	2.34	0.406	23	464	2.91	20.00	0.73
ENL-10-3	8.95	0.63	0.26	0.39	0.0095	0.019	0.20	7.43	0.47	0.12	0.36	0.0090	0.014	0.12	21.9	2.06	0.382	21	826	3.00	40.00	1.00
ENL-23(b)	9.05	0.79	0.24	0.25	0.0070	0.020	0.16	7.51	0.59	0.11	0.23	0.0066	0.014	0.096	3.7	2.69	0.333	33	1138	2.09	34.85	0.87
ENL-25(c)	8.65	0.57	0.19	0.36	0.0050	0.022	0.25	7.18	0.42	0.089	0.33	0.0052	0.016	0.15	6.9	2.20		22	1381	3.71	63.46	1.69
ENL-31(b)	8.80	0.67	0.26	0.28	0.0081	0.042	0.24	7.31	0.50	0.12	0.26	0.0076	0.030	0.14	16.2	2.04	0.338	28	962	2.17	34.21	1.17
TNL-2	8.90	0.73	0.12	0.087	0.0095	0.023	0.48	7.39	0.54	0.055	0.08	0.0090	0.016	0.29	6.6	3.35	0.169	93	821	1.45	8.89	5.27
TNL-9	8.50	0.67	0.11	0.12	0.0068	0.048	0.38	7.06	0.50	0.052	0.11	0.0064	0.034	0.23	9.7	3.26		64	1103	2.12	17.19	4.42
TNL-18	8.70	0.66	0.15	0.10	0.0057	0.025	0.49	7.22	0.49	0.069	0.094	0.0054	0.018	0.28	5.8	3.15	0.262	77	1337	1.36	17.41	4.06
TNL-25	9.25	0.68	0.069	0.16	0.031	0.013	0.38	7.68	0.50	0.332	0.15	0.029	0.009	0.23	6.1	2.57	0.256	51	265	4.69	5.17	7.19
OL-BP	9.40	0.91	0.030	0.17	0.0073	0.019	0.34	7.80	0.68	0.014	0.16	0.0069	0.014	0.21	5.5	1.36	0.241	49	1130	11.43	23.19	5.00
OL-GRID	8.90	0.91	0.024	0.17	0.0076	0.012	0.31	7.39	0.68	0.011	0.16	0.0072	0.009	0.19	6.4	1.46	0.210	46	1026	14.55	22.22	17.27
OL-2(p)	8.60	0.73	0.032	0.12	0.016	0.15	0.47	7.14	0.54	0.015	0.11	0.015	0.11	0.28	3.0	1.94		65	476	7.33	7.33	18.67
OL-14(p)	9.00	0.81	0.069	0.11	0.0045	0.015	0.41	7.47	0.60	0.032	0.10	0.0042	0.011	0.25	2.1	1.24		75	1779	3.13	23.81	7.81
OL-39	9.25	0.88	0.052	0.098	0.0031	0.036	0.44	7.68	0.65	0.024	0.09	0.0029	0.026	0.27	1.8	1.46	0.233	85	2648	3.75	31.03	11.25
SR-123(c)-1	10.20	1.07	0.12	0.17	0.007	0.015	0.557	8.47	0.79	0.057	0.159	0.0066	0.011	0.336	4.7	1.44		53			24	5.9
GL-4(f)	8.35	0.66	0.24	0.71	0.044	0.022	0.08	6.93	0.49	0.11	0.65	0.042	0.016	0.05	16.9	3.53		11	165	5.91	15.48	0.45
GL-19-3	8.90	0.78	0.39	0.84	0.033	0.009	0.032	7.39	0.58	0.18	0.77	0.031	0.006	0.019	40.1	3.57		10	238	4.00	25	0.11
GL-HT	8.90	0.65	0.13	0.28	0.0068	0.013	0.21	7.39	0.48	0.060	0.26	0.0064	0.0009	0.13	10.8	2.66		28	1155	4.33	40.63	2.17
Lobe-1	8.65	0.89	0.19	0.33	0.0035	0.024	0.21	7.18	0.66	0.089	0.30	0.0033	0.017	0.13	7.2	2.44	0.568	24	2176	3.37	90.91	1.46
Lobe-7&10	8.95	0.75	0.18	0.47	0.013	0.019	0.19	7.43	0.56	0.083	0.43	0.012	0.014	0.11	11.8	3.07	0.365	17	619	5.18	35.83	1.33
Lobe-17	8.80	0.82	0.16	0.33	0.0037	0.021	0.18	7.31	0.61	0.076	0.30	0.0035	0.015	0.11	8.8	2.59		24	2089	3.95	85.71	1.45
AC-2(i)	9.05	0.71	0.28	0.51	0.032	0.020	0.16	7.51	0.53	0.13	0.47	0.030	0.014	0.10	18.3	3.42		16	250	3.62	15.67	0.77
AC-2(k)	8.55	0.44	0.47	1.60	0.11	0.025	0.014	7.10	0.33	0.22	1.46	0.10	0.018	0.008	19.5	2.72	0.786	5	71	6.64	14.60	0.036
AC-3(k)	8.85	0.62	0.39	0.79	0.018	0.024	0.064	7.35	0.46	0.18	0.72	0.17	0.17	0.39	14.3	3.76		10	430	4.00	42.35	0.22
Zone-5-1	9.00	0.32	0.30	1.14	0.046	0.020	0.014	7.47	0.24	0.14	1.04	0.043	0.014	0.008	12.6	5.38		7	174	7.43	24.19	0.057
Zone-5-6	9.35	0.39	0.26	0.56	0.047	0.020	0.046	7.76	0.29	0.12	0.51	0.044	0.014	0.028	18.5	2.99		15	176	4.25	11.59	0.23
Zone-5-9	8.50	0.81	0.41	0.61	0.014	0.027	0.150	7.06	0.60	0.19	0.56	0.013	0.019	0.090	8.6	3.39		13	543	2.95	43.08	0.47
SF-1-64.5	8.80	0.68	0.30	0.48	0.010	0.017	0.190	7.31	0.50	0.14	0.44	0.0094	0.012	0.110	20.8	2.50		17	778	3.14	46.81	0.79
SF-2-14.3	9.10	0.50	0.73	0.69	0.023	0.031	0.120	7.55	0.37	0.34	0.63	0.022	0.022	0.070	27.7	3.13	0.680	12	343	1.85	28.64	0.21
SF-2-28	9.10	0.65	0.37	0.37	0.0046	0.018	0.160	7.55	0.48	0.17	0.34	0.0043	0.013	0.100	23.5	2.26		22	1756	2.00	79.07	0.59

Appendix 4 Continued..

B. Radial Muscovite

Sample No.	K_2O	Na_2O	Li_2O	Rb_2O	Cs_2O	Cao	MgO	K	Na	Li	Rb	Cs	Ca	Mg	Be	Fe	F	K/Rb	K/Cs	Rb/Li	Rb/Cs	Mg/Li
GL-9(c)	8.90	0.72	0.10	0.28	0.0030	0.024	0.15	7.39	0.53	0.046	0.26	0.0028	0.017	0.09	7.4	2.49		28	2639	5.65	93	1.96
GL-13(b)	8.70	0.64	0.12	0.25	0.0028	0.014	0.21	7.22	0.47	0.057	0.23	0.0026	0.010	0.13	39.2	2.26		31	2777	4.04	88	2.28
GL-27(c)	8.95	0.66	0.10	0.17	0.0012	0.022	0.25	7.43	0.49	0.048	0.16	0.0011	0.016	0.15	7.2	1.94		46	6755	3.33	145	3.13
GL-31(a)	8.70	0.61	0.16	0.19	0.0140	0.035	0.30	7.22	0.45	0.073	0.17	0.0130	0.025	0.18	9.1	2.95		43	5554	2.33	13	2.47
GL-34(b)	8.75	0.51	0.12	0.14	0.0021	0.024	0.32	7.26	0.38	0.054	0.13	0.0020	0.017	0.19	5.0	2.86		56	3630	2.41	65	3.52
ENL-1	9.00	0.76	0.20	0.22	0.0044	0.016	0.15	7.47	0.56	0.091	0.20	0.0042	0.011	0.09	8.2	2.26		37	1779	2.20	48	0.99
ENL-3	3.90	0.21	0.08	0.11	0.0040	0.010	0.07	3.24	0.16	0.038	0.10	0.0038	0.007	0.04		1.06		32	853	2.63	26	
ENL-22(a)	9.30	0.51	0.19	0.15	0.0051	0.023	0.18	7.72	0.38	0.088	0.14	0.0048	0.016	0.11	8.4	2.33		55	1608	1.59	29	1.25
OL-10	9.20	0.63	0.40	0.07	0.0016	0.026	0.43	7.64	0.47	0.018	0.06	0.0015	0.019	0.26	1.3	1.36		127	5093	3.33	40	14.44
OL-14	9.25	0.66	0.07	0.10	0.0021	0.025	0.42	7.68	0.49	0.033	0.09	0.0020	0.018	0.25	1.4	1.42		85	3840	2.73	45	7.58

Appendix 4 Continued..

C. Mineralized Pods

Sample No.	K_2O	Na_2O	Li_2O	Rb_2O	Cs_2O	CaO	MgO	K	Na	Li	Rb	Cs	Ca	Mg	Be	Fe	F	K/Rb	K/Cs	Rb/Li	Rb/Cs	Mg/Li
SF-2-8.10	9.25	0.40	3.06	1.94	0.44	0.014	0.02	8.09	0.30	1.42	1.77	0.42	0.010	0.01	67.7	0.51	3.33	5	19	1.25	4.21	0.01
AC-3(r)	9.40	0.26	0.58	1.45	0.073	0.051	0.016	7.80	0.19	0.27	1.33	0.069	0.036	0.0097	32.1	3.16		6	113	4.93	19.28	0.04
AC-3(s)	9.50	0.18	0.24	1.03	0.068	0.180	0.014	7.89	0.13	0.11	0.94	0.064	0.130	0.0084	27.1	1.63		8	123	8.55	14.69	0.03
AC-2(m)	10.00	0.17	0.69	1.29	0.056	0.014	0.015	8.30	0.13	0.32	1.18	0.053	0.010	0.0090	33.0	4.26		7	157	3.69	22.26	0.03
SF-1	9.78	0.50	3.40	2.12	0.120			8.12	0.371	1.58	1.94	0.113						4	72	1.23	17.15	
SF-1(a)	9.40	0.51	3.44	2.49	0.138	0.004		7.80	0.378	1.60	2.28	0.130	0.0029					3	60	1.42	17.52	
SF-4	9.90	0.34	2.32	2.26	0.099	0.001		8.22	0.252	1.08	2.07	0.093	0.0007					4	88	1.91	22.12	
SF-5	9.40	0.33	3.91	1.49	0.140			7.80	0.245	1.82	1.34	0.132						6	59	0.74	10.18	
AC-2(k)-1	10.05	0.17	0.82	1.38	0.058	0.011	0.013	8.34	0.13	0.38	1.26	0.055	0.008	0.0078	34.9	4.20		7	152	3.32	22.91	0.021
AC-2(m)-1	9.95	0.20	0.78	1.43	0.064	0.011	0.013	8.26	0.15	0.36	1.31	0.060	0.008	0.0078	32.7	4.29		6	138	3.64	21.83	0.022
AC-3(n)	9.70	0.14	2.73	2.08	0.16	0.036	0.0082	8.05	0.10	1.27	1.90	0.15	0.026	0.0049	39.6	0.99		4	54	1.50	12.67	0.0039
AC-3(o)	9.25	0.24	3.77	2.14	0.24	0.022	0.0091	7.68	0.18	1.75	1.96	0.23	0.016	0.0055	27.4	0.036	2.41	4	33	1.12	8.52	0.0031
Zone-5-4	9.85	0.22	0.67	1.24	0.047	0.020	0.012	8.18	0.16	0.31	1.18	0.044	0.014	0.0072		4.16		7	186	3.65	25.68	0.023

Appendix 4 Continued..

D. Matrix Muscovite

Sample No.	K_2O	Na_2O	Li_2O	Rb_2O	Cs_2O	CaO	MgO	K	Na	Li	Rb	Cs	Ca	Mg	Be	Fe	F	K/Rb	K/Cs	Rb/Li	Rb/Cs	Mg/Li
GL-14(d)	8.50	0.70	0.14	0.31	0.0025	0.010	0.18	7.06	0.52	0.066	0.28	0.0024	0.007	0.11	16.9	2.24		25	2942	4.24	116.67	1.67
GL-25(d)	10.00	0.59	0.15	0.30	0.005	0.015	0.25	8.30	0.44	0.071	0.27	0.005	0.011	0.15	21.0	2.62		31	1660	3.80	54.00	2.11
ENL-8(a)	9.15	0.60	0.26	0.26	0.0074	0.015	0.23	7.60	0.45	0.012	0.24	0.00	0.011	0.14	23.0	2.43		32	1086	2.00	34.29	1.17
ENL-20(d)	9.10	0.61	0.22	0.42	0.0084	0.013	0.24	7.55	0.45	0.10	0.38	0.0079	0.009	0.14	19.4	1.96		20	956	3.80	48.10	1.40
OL-2	10.10	0.67	0.03	0.098	0.012	0.016	0.54	8.38	0.50	0.014	0.09	0.011	0.011	0.33	9.4	1.90		93	762	6.43	8.18	23.57
OL-16	9.30	0.75	0.028	0.11	0.0026	0.020	0.43	7.72	0.56	0.013	0.10	0.0025	0.014	0.26	5.8	1.73		77	3088	7.69	40.00	20.00

Appendix 4 Continued..

E. Secondary Muscovite

Sample No.	K_2O	Na_2O	Li_2O	Rb_2O	Cs_2O	CaO	MgO	K	Na	Li	Rb	Cs	Ca	Mg	Be	Fe	F	K/Rb	K/Cs	Rb/Li	Rb/Cs	Mg/Li
OL-16	8.80	0.78	0.0034	0.11	0.0035	0.015	0.034	7.31	0.58	0.0016	0.10	0.0033	0.011	0.021	22.2	0.2		73	2215	62.50	30.30	13.13
ENL-9	8.65	0.61	0.26	0.36	0.028	0.026	0.32	7.18	0.45	0.12	0.33	0.026	0.019	0.19	22.4	2.02		22	276	2.75	12.69	1.58

Appendix 5. Garnet Analyses

A. Microprobe Analyses

Sample No.	SiO_2	TiO_2	ZrO_2	Al_2O_3	Sc_2O_3	Y_2O_3	FeO	MnO	MgO	CaO	$\frac{Mn}{Mn+Fe}$ x 100	Total
Leucogranite												
TNL-4	35.76	0.00	0.00	20.33	0.11	0.00	32.72	8.69	0.76	0.47	21.00	98.84
TNL-21	36.90	0.01	0.02	20.05	0.00	0.00	34.87	6.52	1.82	0.38	15.80	100.57
TNL-30	36.81	0.02	0.01	20.76	0.00	0.00	35.76	4.83	1.34	0.37	11.90	99.92
TNL-32	36.93	0.00	0.00	20.56	0.13	0.00	35.15	5.39	1.61	0.68	13.30	100.46
TNL-41	36.95	0.04	0.04	20.58	0.05	0.00	35.92	5.47	1.30	0.27	13.20	100.62
Sodic Aplite												
TNL-17-2	36.77	0.02	0.00	20.18	0.05	0.00	35.47	6.02	1.36	0.45	14.50	100.31
TNL-29	36.04	0.01	0.04	20.53	0.04	0.00	36.87	3.89	0.80	0.59	9.50	98.80
TNL-37	36.94	0.00	0.28	20.71	0.10	0.00	35.38	6.37	0.84	0.05	15.30	100.66
TNL-44	36.54	0.01	0.00	20.56	0.00	0.02	38.39	3.16	1.02	0.06	7.60	99.76
Pegmatitic Leucogranite												
TNL-14	36.80	0.00	0.12	20.77	0.06	0.00	33.33	7.86	1.44	0.22	19.10	100.61
TNL-15-1-e	36.33	0.00	0.00	20.07	0.05	0.00	35.51	6.41	0.68	0.69	15.30	99.73
TNL-15-1-c	36.39	0.00	0.00	20.33	0.04	0.00	35.86	5.88	1.01	0.21	14.10	99.71
TNL-17-1	36.95	0.02	0.00	20.74	0.09	0.00	34.48	6.62	1.57	0.19	16.10	100.65
TNL-19-e	36.29	0.00	0.00	20.31	0.10	0.00	33.59	7.82	1.31	0.30	18.90	99.71
TNL-19-c	36.14	0.00	0.00	20.87	0.05	0.00	32.97	7.39	1.63	0.31	18.30	99.36
Late Variety												
TNL-36	36.01	0.00	0.03	20.60	0.04	0.00	35.03	7.26	0.72	0.06	17.20	99.74
TNL-38	36.49	0.00	0.00	20.61	0.02	0.00	34.49	6.40	1.51	0.15	15.60	99.87
Leucogranite												
OL-8-2	35.99	0.03	0.12	19.89	0.06	0.00	31.02	10.96	0.93	0.31	26.10	99.31
OL-20	36.47	0.08	0.00	20.76	0.03	0.00	32.48	7.51	1.84	0.27	18.80	99.44
OL-33	36.44	0.04	0.00	20.31	0.07	0.00	29.68	13.02	0.58	0.25	39.50	100.38
Sodic Aplite												
OL-11	36.16	0.00	0.00	20.15	0.00	0.00	33.57	8.53	0.89	0.10	20.30	99.40
OL-34	35.96	0.02	0.00	20.99	0.08	0.00	30.45	10.76	1.23	0.20	26.10	99.67
OL-34-1	36.33	0.00	0.00	20.84	0.10	0.00	33.08	8.44	1.11	0.18	20.30	100.09
OL-38-1	36.55	0.02	0.00	20.60	0.11	0.00	28.64	12.59	0.80	0.12	30.50	99.43
Pegmatitic Leucogranite												
OL-2-e	36.39	0.00	0.00	20.84	0.00	0.00	25.17	15.99	1.15	0.47	38.80	100.01
OL-2-c	35.99	0.00	0.00	20.86	0.00	0.00	23.32	18.48	0.67	0.32	44.20	99.65
OL-11	36.11	0.05	0.09	19.95	0.03	0.00	34.67	7.40	0.86	0.18	17.60	99.35
OL-12-c	35.73	0.00	0.00	20.60	0.06	0.00	33.09	8.99	0.56	0.19	21.40	99.22
OL-12-e	36.26	0.02	0.00	20.91	0.07	0.00	34.85	7.62	0.48	0.18	17.90	100.40
OL-13-1	36.32	0.01	0.00	20.32	0.05	0.00	33.50	9.29	0.65	0.17	21.70	100.32
OL-14-1	36.61	0.03	0.00	21.05	0.07	0.00	31.23	10.24	1.19	0.15	24.70	100.58
OL-17	36.10	0.00	0.00	20.35	0.00	0.00	33.90	7.28	1.12	0.25	16.80	99.00
OL-24	36.91	0.09	0.00	20.22	0.00	0.00	32.44	9.09	1.75	0.23	21.90	100.72
OL-25-1	36.72	0.02	0.00	20.50	0.07	0.00	31.85	8.87	1.63	0.14	21.80	99.79
OL-26	36.60	0.00	0.00	20.57	0.02	0.00	30.50	10.64	1.50	0.11	25.90	99.93
OL-32	36.66	0.02	0.00	20.61	0.10	0.00	31.46	9.92	1.73	0.29	24.00	100.80
OL-34-1	37.25	0.00	0.01	20.96	0.00	0.00	33.02	8.78	1.08	0.25	21.00	101.33
OL-35	36.45	0.00	0.00	20.92	0.13	0.00	33.37	7.81	1.35	0.19	18.90	100.22
OL-36-1	36.88	0.00	0.00	20.80	0.07	0.00	32.24	8.86	1.36	0.16	21.60	100.37
OL-38	35.76	0.04	0.00	20.53	0.04	0.00	29.57	12.05	0.77	0.15	28.90	98.90
OL-38-1	36.60	0.00	0.00	20.30	0.04	0.00	28.49	13.89	0.55	0.16	32.80	100.04
OL-40-1	36.16	0.02	0.03	20.47	0.00	0.00	32.11	9.98	0.59	0.21	23.70	99.58
Leucogranite												
ENL-29(b)	36.60	0.00	0.13	20.27	0.09	0.00	36.40	6.11	0.65	0.18	14.40	100.43

Sample No.	SiO_2	TiO_2	ZrO_2	Al_2O_3	Sc_2O_3	Y_2O_3	FeO	MnO	MgO	CaO	$\frac{Mn}{Mn+Fe} \times 100$	Total
Sodic Aplite												
ENL-9	36.06	0.00	0.00	20.72	0.06	0.43	28.31	11.89	1.60	0.56	29.60	99.64
ENL-11(a)-1	36.46	0.07	0.03	20,72	0.00	0.00	5.58	36.82	0.18	0.18	86.80	99.95
ENL-20(c)	36.43	0.03	0.00	20.85	0.13	0.00	31.73	10.95	0.40	0.21	25.60	100.72
ENL-25(b)	36.67	0.04	0.00	20.60	0.06	0.00	34.97	7.11	0.87	0.23	16.90	100.54
Pegmatitic Leucogranite												
ENL-10-6	36.14	0.07	0.06	20.46	0.00	0.00	30.25	12.07	0.40	0.03	28.50	99.50
Radial												
ENL-1(a)	36.24	0.00	0.01	19.98	0.00	0.00	33.28	10.05	0.40	0.03	23.20	99.99
ENL-3	36.50	0.00	0.00	20.38	0.00	0.00	33.91	9.40	0.41	0.00	21.70	100.60
ENL-22(a)	36.35	0.00	0.22	20.48	0.03	0.00	34.27	7.42	1.08	0.30	17.80	100.15
Leucogranite												
GL-4(a)	36.57	0.01	0.00	20.72	0.04	0.00	35.58	7.18	0.31	0.08	16.70	100.47
GL-31(b)	36.29	0.05	0.00	20.40	0.00	0.02	34.90	7.31	0.80	0.04	17.30	99.81
GL-41(b)-1	36.37	0.01	0.00	20.20	0.07	0.00	33.32	9.94	0.57	0.23	21.50	99.90
Sodic Aplite												
GL-6(a)	36.15	0.00	0.00	20.42	0.08	0.00	34.08	8.07	0.31	0.15	19.10	99.27
GL-11(c)	35.54	0.03	0.00	20.52	0.02	0.00	35.03	6.98	0.41	0.14	16.60	98.66
GL-18(b)	35.91	0.01	0.00	20.48	0.08	0.00	29.45	13.13	0.13	0.14	30.80	99.32
GL-20(a)	36.73	0.03	0.00	20.31	0.00	0.00	33.13	10.26	0.15	0.14	23.60	100.75
Pegmatitic Leucogranite												
GL-6(a)	36.18	0.04	0.00	19.98	0.00	0.00	23.92	19.59	0.04	0.13	45.00	99.88
GL-16(b)	36.54	0.04	0.00	20.70	0.00	0.00	30.54	12.90	0.14	0.01	29.70	100.89
GL-38(b)	35.79	0.02	0.11	20.19	0.00	0.11	35.13	6.72	0.70	0.05	16.10	98.84
Late Variety												
GL-4(e)-IV-1	36.54	0.00	0.00	20.35	0.01	0.00	34.95	8.36	0.18	0.13	19.30	100.52
GL-4(e)-IV-2	36.42	0.00	0.00	20.52	0.00	0.00	34.57	8.13	0.33	0.14	19.00	100.12
GL-41(b)-e	36.28	0.03	0.00	20.14	0.12	0.00	34.24	8.22	0.55	0.22	19.40	99.80
GL-41(b)-c	36.69	0.05	0.00	20.62	0.15	0.00	33.59	8.88	0.61	0.24	20.90	100.84
Enriched Pegmatitic Pods												
Lobe-6	36.33	0.00	0.02	20.57	0.03	0.00	27.89	14.25	0.66	0.13	33.80	99.87
Lobe-8	36.47	0.00	0.32	20.61	0.01	0.00	32.96	9.41	0.48	0.16	22.20	100.42
Lobe-9	36.74	0.00	0.30	20.75	0.03	0.00	33.25	9.58	0.43	0.15	22.40	101.23
Lobe-12	36.68	0.00	0.00	20.59	0.03	0.00	26.07	16.41	0.57	0.13	38.60	100.46
Lobe-e pseudomorph	36.97	0.00	0.00	20.36	0.00	0.00	13.63	28.59	0.00	0.24	67.72	98.80
Lobe-c pseudomorph	36.58	0.00	0.00	20.31	0.00	0.00	13.57	29.43	0.00	0.24	68.44	100.16
AC-2(p)-c	36.86	0.01	0.00	20.22	0.14	0.00	36.33	5.27	1.56	0.26	12.70	100.75
AC-2(p)-e	36.15	0.00	0.00	20.03	0.07	0.00	33.29	8.20	0.90	0.35	19.80	99.00
AC-3(a)	36.44	0.00	0.00	20.31	0.06	0.00	28.98	13.90	0.47	0.12	32.40	100.30
AC-3(j)	36.54	0.00	0.00	20.57	0.05	0.00	14.36	28.19	0.41	0.12	66.30	100.24
SL-1-57	36.22	0.01	0.00	20.32	0.05	0.00	26.44	16.79	0.03	0.15	38.80	100.00
SL-1-76.6	35.88	0.02	0.00	20.00	0.07	0.00	30.24	12.93	0.24	0.11	29.90	99.48
SL-1-86	36.18	0.03	0.00	20.34	0.04	0.00	29.38	14.08	0.14	0.10	32.40	100.30
SL-1-95	36.12	0.00	0.00	20.39	0.10	0.00	28.73	13.80	0.15	0.17	32.40	99.47
SL-2-14.6	35.89	0.02	0.00	20.42	0.04	0.00	27.54	15.73	0.01	0.12	36.40	99.77
SL-2-27.0	36.43	0.02	0.00	20.61	0.02	0.00	26.84	15.99	0.00	0.11	37.30	100.01
SL-2-35.6	36.54	0.01	0.00	20.28	0.04	0.00	30.66	12.99	0.28	0.12	29.80	100.92

For samples with two analyses taken, one analysis was taken at the centre (c) of the crystal and one analysis was taken at the edge (e).

Appendix 5 Continued..

B. Wet Chemical Analyses

Sample No.	SiO_2	Al_2O_3	Fe_2O_3	FeO	Mgo	CaO	Na_2O	K_2O	P_2O_5	MnO	Y_2O_3	$\frac{Mn}{Mn+Fe} \times 100$	Total
Leucogranite													
TNL-20	36.15	20.35	1.13	34.56	1.21	0.39	0.03	0.02	0.04	6.00	0.11	14.4	99.99
TNL-39	36.10	20.40	0.00	33.88	0.96	0.19	0.03	0.01	0.13	8.30	0.03	19.7	100.07
Sodic Aplite													
TNL-17	36.55	20.50	0.34	33.60	1.08	0.24	0.03	0.02	0.08	7.10	0.06	17.3	99.60
TNL-37	36.15	20.28	0.69	33.12	0.85	0.20	0.04	0.01	0.15	8.40	0.03	19.9	99.92
Pegmatitic Leucogranite													
TNL-1	36.85	20.45	0.05	34.28	1.11	0.19	0.03	0.06	0.10	6.80	0.09	16.5	100.01
TNL-15	36.60	20.40	0.19	34.60	0.85	0.28	0.02	0.00	0.12	6.30	0.06	15.3	99.42
Leucogranite													
GL-4(a)	36.40	20.40		32.20	0.34	0.05	0.02	0.09	0.00	9.70	0.15	23.2	99.35
GL-36(a)	36.30	20.35		34.33	0.64	0.11	0.02	0.01	0.07	7.50	0.09	17.9	99.42
GL-41(b)	36.00	20.42	0.27	32.64	0.53	0.15	0.04	0.07	0.09	9.30	0.21	22.0	99.72
Sodic Aplite													
GL-9(d)	36.80	20.08	0.18	31.92	0.33	0.06	0.02	0.06	0.09	10.20	0.10	24.1	99.84
GL-11(c)	36.35	20.42	0.18	35.20	0.48	0.06	0.01	0.02	0.06	7.20	0.10	16.9	100.06
Pegmatitic Leucogranite													
GL-25	36.00	20.46		36.40	0.46	0.05	0.02	0.10	0.27	6.00	0.13	14.2	99.79
Leucogranite													
OL-18	36.05	22.22	0.48	32.84	1.28	0.08	0.03	0.02	0.26	8.90	0.02	21.1	100.18
Pegmatitic Leucogranite													
OL-2	36.30	20.50		25.21	0.88	0.16	0.03	0.08	0.23	16.20		39.1	99.59
OL-16	36.10	20.26	0.84	33.48	1.00	0.10	0.05	0.01	0.20	8.50	0.02	19.9	100.56
Leucogranite													
ENL-1(a)	38.15	20.16	0.96	30.08	0.28	0.07	0.09	0.51	0.03	9.05	0.25	22.6	99.63
ENL-6(b)	41.00	19.26	0.95	29.16	0.30	0.17	0.10	0.32	0.07	8.60	0.22	22.2	100.15
Sodic Aplite													
ENL-8(b)	36.40	20.52	1.20	30.00	0.26	0.07	0.03	0.08	0.08	11.50	0.18	26.9	100.32
ENL-10-1	36.20	20.54	0.10	29.20	0.41	0.06	0.03	0.01	0.00	13.10	0.21	30.9	99.86
Pegmatitic Leucogranite													
ENL-2	36.15	20.64	0.03	28.56	0.12	0.06	0.01	0.10	0.12	14.60	0.11	33.8	100.50
Sodic Aplite													
Lobe-6	36.20	20.48		26.91	0.28	0.04	0.01	0.00	0.05	15.70	0.07	36.8	99.75
Pegmatitic Leucogranite													
AC-3(j)	35.50	21.22		14.26	0.01	0.03	0.01	0.02	0.13	28.44	0.10	66.6	99.72

Appendix 6. Nb,Ta Oxide Mineral Analyses

Sample No.	Ta_2O_5	Nb_2O_5	TiO_2	ZrO_2	SnO_2	Al_2O_3	Sb_2O_3	Sc_2O_3	FeO	MgO	MnO	CaO	Na_2O	WO_3	Total	Mn/ Mn+Fe	Ta/ Ta+Nb
GL-30-1	21.87	57.49	0.62	0.00	0.00	0.02	0.00	0.00	12.65	0.01	6.08	0.02			98.75	0.33	0.19
GL-30-2	15.47	66.16	0.59	0.00	0.12	0.03	0.10	0.00	11.77	0.00	5.73	0.01	0.01		99.99	0.33	0.12
GL-30-3	20.94	59.11	0.45	0.00	0.17	0.05	0.10	0.00	12.19	0.00	6.02	0.06	0.01		99.10	0.33	0.18
GL-30-4	19.37	59.75	0.54	0.00	0.18	0.01	0.13	0.00	12.50	0.03	6.20	0.07	0.01		98.79	0.33	0.16
GL-30(a)-1	20.65	59.22	0.81	0.00	0.00	0.03	0.00	0.00	16.62	0.00	2.33	0.05			99.70	0.12	0.17
GL-HT	15.51	63.00	0.37	0.00	0.05	0.03	0.09	0.00	12.16	0.00	7.78	0.06	0.01		99.04	0.39	0.13
AC-1(a)-dark	61.90	21.51	0.56	0.00	0.39	0.00	0.02	0.00	10.11	0.00	5.02	0.05	0.00		99.57	0.33	0.63
AC-1(a)-light	57.16	23.88	0.94	0.00	0.47	0.00	0.09	0.00	11.22	0.00	4.73	0.04	0.00		98.52	0.30	0.59
AC-1(b)-dark	78.64	0.27	0.44	0.00	1.26	0.15	0.12	0.00	0.17	0.00	0.01	9.45	2.05		92.56	0.07	0.99
AC-1(b)-light	66.05	17.85	0.15	0.00	0.23	0.06	0.10	0.00	4.45	0.00	10.31	0.00	0.00		99.20	0.70	0.69
AC-2-79-1	70.16	2.85	0.18		14.86			0.59	0.74	0.08	11.11	0.16			100.72	0.94	0.94
SF-14(a)	58.40	24.84	0.30	0.00	1.35				3.04		12.46				100.39	0.81	0.59
SF-16	47.77	31.48	0.17	0.00	3.44		0.54		0.49		14.47	1.23			99.59	0.94	0.48
SF-17	47.40	29.90	0.00	0.00	0.01				1.00		19.80				98.21	0.95	0.49
SF-18	41.77	34.55	0.41	0.00	4.16		1.18		2.16		13.14	1.58			98.94	0.86	0.42
SF-19	48.33	34.13	0.33	0.00	0.51	0.00	0.16		1.85		14.73	0.08			100.12	0.89	0.46
SF-21	45.40	34.90	0.21	0.00	1.50		0.00		1.80	0.00	16.50	0.00			100.31	0.90	0.44
SF-22	37.85	40.83	0.20	0.00	4.58		0.00		1.49	0.00	15.43	0.00			100.38	0.91	0.36
SF-BM-E	48.10	34.73	0.21		0.00		0.00		0.51		16.54	0.00	0.00		100.10	0.97	0.45
SF-BM-M	47.53	34.98	0.21		0.00		0.06		0.78		15.87	0.00	0.00		99.43	0.95	0.45
SF-T-E	62.87	21.25	0.02		0.00		0.00		0.05		15.47	0.00	0.00		99.66	0.997	0.64
SF-T-M	62.89	20.41	0.02		0.69		0.00		0.05		15.56	0.25	0.00		99.86	0.997	0.65
A-5-dark(a)	25.82	50.15	0.32		0.04				15.62	0.06	2.79	0.01		1.25	99.05	0.15	0.26
A-5-dark(b)	28.85	49.92	0.32		0.04			0.53	15.61	0.06	2.80	0.01			98.14	0.15	0.26
A-5-light(a)	26.15	53.46	0.43		0.03				12.91	0.08	6.24	0.00		0.83	100.12	0.33	0.23
A-5-light(b)	26.16	53.27	0.43		0.03			0.62	12.90	0.08	6.25	0.00			99.73	0.33	0.23
A-6-dark(a)	67.57	15.90	0.16		0.07				1.94	0.09	13.06	0.04		0.32	99.15	0.87	0.72
A-6-dark(b)	66.73	15.86	0.16		0.07			0.81	1.95	0.09	13.11	0.04			98.83	0.87	0.72
A-6-light(a)	68.10	16.00	0.20		0.15				1.70	0.00	13.00	0.05		0.3	99.50	0.89	0.72
A-6-light(b)	68.13	15.68	0.22		0.15			0.87	1.65	0.01	12.69	0.05			99.45	0.89	0.72
AC-2	70.27	2.85	0.18		14.89				0.05	0.00	11.12	0.16			99.52	0.996	0.94
AC-2(a)	70.25	2.85	0.18		14.87				0.05	0.00	11.11	0.16		0.27	99.75	0.995	0.94

Appendix 7. Beryl Analyses

Sample No.	K_2O	Na_2O	Li_2O	Rb_2O	Cs_2O	Total Fe	MgO	CaO	K	Na	Li	Rb	Cs	Mg	Ca	Na/Li	Li/Cs	Na/Cs	N	Density
GL-19-1	0.024	0.34	0.130	0.0081	0.100	0.3100	0.0250	0.0032	0.020	0.25	0.062	0.0074	0.094	0.015	0.0023	4.03	0.660	2.66		
GL-19-2	0.22	0.87	0.45	0.0280	0.200	0.39	0.026	0.0100	0.180	0.65	0.210	0.026	0.19	0.016	0.0071	3.10	1.11	3.42	1.5807	
GL-19-3	0.014	0.44	0.22	0.0130	0.170	0.31	0.0019	0.0022	0.012	0.33	0.100	0.012	0.16	0.0011	0.0016	3.30	0.625	2.06	1.5804	
GL-30-1	0.12	0.46	0.24	0.0096	0.029	0.34	0.0290	0.0069	0.10	0.34	0.110	0.0088	0.027	0.017	0.0049	3.09	4.07	12.59	1.5721	
GL-37-1(a)	0.024	0.45	0.116	0.0030	0.066	0.466	0.0670	0.0090	0.017	0.33	0.056	0.0027	0.062	0.0404	0.0064	5.89	0.903	5.32	1.5772	
GL-HT	0.036	0.64	0.26	0.0037	0.051	0.37	0.0280	0.0050	0.030	0.47	0.12	0.0034	0.048	0.0169	0.0036	3.92	2.50	9.79	1.5752	
Lobe-(7&10)	0.074	0.40	0.14	0.0083	0.047	0.66	0.0440	0.0032	0.061	0.30	0.064	0.0076	0.044	0.0265	0.0023	4.69	1.45	6.82	1.5755	
AC-1	0.024	0.67	0.34	0.014	0.32	0.26	0.0032	0.0058	0.020	0.50	0.16	0.013	0.30	0.0019	0.0041	3.12	0.533	1.64	1.5803	
AC-2(g)	0.028	0.58	0.34	0.035	0.31	0.16	0.0021	0.0044	0.023	0.43	0.16	0.032	0.29	0.013	0.0031	2.69	0.522	1.48	1.5784	
AC-3(e)	0.036	1.14	0.80	0.059	1.66	0.017	0.0030	0.0065	0.030	0.85	0.37	0.054	1.57	0.0018	0.0046	2.30	0.236	0.541	1.5845	
AC-3(g)	0.030	1.32	0.75	0.035	0.68	0.057	0.0051	0.013	0.025	0.98	0.35	0.032	0.63	0.0031	0.0093	2.80	0.556	1.56	1.5897	
AC-3(h)	0.045	0.91	0.67	0.066	1.50	0.019	0.0031	0.0062	0.037	0.68	0.31	0.060	1.41	0.0019	0.0044	2.19	0.220	0.482	1.5862	
AC-3(m)	0.032	0.97	0.71	0.075	1.62	0.011	0.0028	0.0054	0.027	0.72	0.33	0.069	1.53	0.0017	0.0039	2.18	0.216	0.471	1.5866	
AC-3(n)	0.026	1.23	0.84	0.052	1.67	0.029	0.0021	0.0046	0.022	0.91	0.39	0.048	1.58	0.0013	0.0033	2.33	0.247	0.576		
AC-3(n)-1	0.034	1.13	0.80	0.059	1.88	0.020	0.0033	0.0094	0.028	0.84	0.37	0.054	1.77	0.0020	0.0067	2.27	0.209	0.475	1.5873	
AC-3(r)	0.031	1.00	0.56	0.048	0.29	0.066	0.0040	0.0019	0.026	0.74	0.26	0.044	0.27	0.0024	0.0014	2.85	0.963	2.74		
AC-3(r)-1	0.034	0.77	0.43	0.048	0.22	0.092	0.0032	0.0024	0.028	0.57	0.20	0.044	0.21	0.0019	0.0017	2.85	0.952	2.71	1.5850	
AC-3(x)	0.032	1.00	0.82	0.083	2.30	0.0089	0.0020	0.0013	0.027	0.74	0.38	0.076	2.17	0.0012	0.0009	1.95	0.175	0.341	1.5856	
AC-3(y)-1	0.058	1.71	1.05	0.038	1.34	0.023	0.0057	0.0039	0.048	1.27	0.49	0.035	1.26	0.0034	0.0028	2.59	0.389	1.01	1.5880	
SF-27	0.038	0.97	0.62	0.069	0.70	0.009	0.0020	0.0010	0.032	0.720	0.288	0.063	0.660	0.0012	0.0007	2.50	0.436	1.09	1.583	2.725
SF-28	0.066	1.12	0.69	0.062	0.78	0.033	0.0040	0.0080	0.055	0.831	0.320	0.057	0.736	0.0024	0.0057	2.60	0.435	1.13	1.5835	2.735

Appendix 8. Miscellaneous Analyses

Spodumene

	SiO_2	Al_2O_3	Na_2O	Li_2O	K_2O	Total Fe	Total
SF-1	74.50	19.01	0.085	5.84		0.379	99.81
SF-2	78.25	15.96	0.59	4.50		0.369	99.67
SF-1(Fe)			0.119	5.89		0.029	
SF-2-7.4	74.50	18.44	0.103	5.58	0.10	0.033	98.72

Inmenite

Fe_2O_3	Al_2O_3	MnO	TiO_2	Cr_2O_3	Total	Density
46.3	0.01	1.41	51.82	0.02	99.40	4.581

Cassiterite

	SnO_2	Fe_2O_3	Ta_2O_5	MnO	Total
SF-14	94.41	0.71	4.72	0.19	100.03
SF-15	93.99	0.99	4.91	0.06	99.95

Appendix 9. Certificate of Analysis for ENL-11

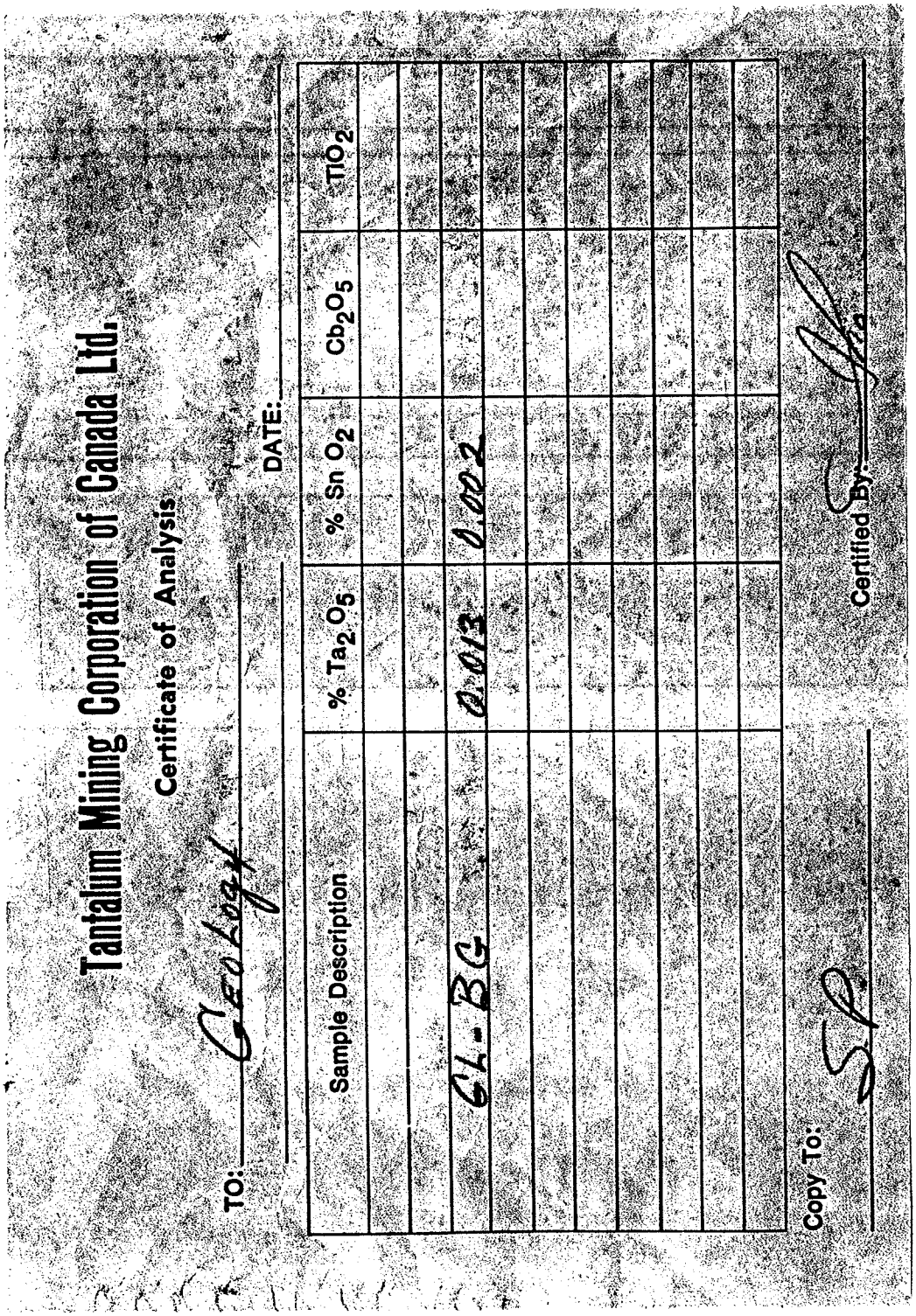

Tantalum Mining Corporation of Canada Ltd.

Certificate of Analysis

TO: Geology DATE:

Sample Description	% Ta_2O_5	% $Sn O_2$	Cb_2O_5	TiO_2
EL-BG	0.013	0.002		

Copy To: SP

Certified By:

Appendix 10. Sample Locations of TNL
(Eastern Extension)